DISSERTATION

MODELING STREAM EVOLUTION AND ITS CONSEQUENCES FOR WATERSHED SCALE POLLUTANT LOADING

Submitted by

Roderick W. Lammers

Department of Civil and Environmental Engineering

In partial fulfillment of the requirements

For the Degree of Doctor of Philosophy

Colorado State University

Fort Collins, Colorado

Summer 2018

Doctoral Committee:

Advisor: Brian P. Bledsoe

Mazdak Arabi
Peter Nelson
Sara Rathburn

ABSTRACT

MODELING STREAM EVOLUTION AND ITS CONSEQUENCES FOR WATERSHED SCALE POLLUTANT LOADING

Throughout the world, streams are degraded due to impaired water quality and erosion and sedimentation caused by hydrologic and sediment imbalances. These two issues are linked. Channel erosion not only damages stream habitat but can be a significant source of fine sediment and nutrient pollution in watersheds. Phosphorus in particular is common in streambanks and when these soils are mobilized — for example during amplified high flows in urban streams — they can contribute to eutrophication of downstream water bodies. Understanding these dynamics is important for reversing these impairments and sustainably managing our water resources.

In this dissertation, I provide a new tool to quantify the magnitude of channel erosion as a pollutant source. First, I put this issue in context by reviewing recent literature on stream restoration and its ability to either reduce nutrient loading or enhance natural nutrient removal processes. Results suggest that stream restoration can help reduce nutrient pollution, but quantifying these benefits remains challenging. Despite the rapid growth of the stream restoration industry, there is still insufficient monitoring and assessment of project success. Perhaps this is due to a lack of standardized tools and methodologies. The remainder of this dissertation attempts to fill part of this gap — providing a new tool to predict watershed sediment and phosphorus loading from channel erosion.

I develop a new model to simulate stream channel evolution at the watershed scale. This model is built around specific stream power, a variable that is straightforward to calculate using easily quantified parameters: discharge, slope, and width. I first develop new sediment transport equations based on specific stream power. These are used by the model to

simulate channel bed aggradation and degradation. I link these processes with a simplified version of a bank erosion model to account for lateral channel adjustment. Model simulations match physical understanding of channel evolution in response to disturbance as well as field datasets of rivers adjusting to both human and natural perturbations. Importantly, the model is structured to quantify uncertainty in model projections. This is essential for understanding both model limitations and more generally for simulating complex systems in a stochastic world.

Finally, I apply this new model to estimate sediment and phosphorus loading from bank erosion in two watersheds: Big Dry Creek, Colorado and Lick Creek, North Carolina. Despite their many differences and their unique simulated responses to disturbance, results for both watersheds suggest that channel erosion may be responsible for nearly all of the suspended sediment pollution, but very little of the phosphorus. This new model has a number of applications in both the scientific and management communities — exploring river behavior in more detail while also answering relevant management questions as we try to more effectively steward our water resources.

ACKNOWLEDGEMENTS

First, I would like to thank my advisor, Brian Bledsoe, for his constant support throughout my time at CSU. Despite moving to Georgia halfway through my Ph.D., Brian always made time to talk over the phone or in person on those lucky occasions our paths crossed. It was almost like you never left. Your expert guidance, entertaining stories, and genuine interest in my life always helped to re-motivate me for the work ahead. Thank you and I look forward to continuing to work together at UGA.

To the rest of my committee, Mazdak Arabi, Peter Nelson, and Sara Rathburn, thank you for your support and guidance. Peter was especially helpful in ironing out issues during model development. Much of this dissertation would not have been possible without data collected by others. I would especially like to thank Richard McDowell, Robert Walter, Dorothy Merritts, Gary Fox, Ron Miller, Keith Schilling, John Kovar, Eric Young, and Don Ross for sharing their streambank phosphorus data. Mike Church and Chris Parker sent me their compiled and curated bedload transport databases which saved me many hours of scouring the literature. Adam Mosbrucker at the USGS provided helpful data and advice for the North Fork Toutle River modeling. Eddy Langendoen from the USDA provided expertise and access to the BSTEM code. Sandi Wilbur and others at the City of Durham were excellent resources for information about Lick Creek. Jane Clary provided wonderful support for my work on Big Dry Creek and was a major impetus for the broader project from which Chapter 2 was born.

I did collect *some* of my own data. Travis Hardee and Travis Stroth both helped me explore Big Dry Creek and Lick Creek — including hauling soil samples back to the lab. They were both amiable assistances and have been good friends. Joel Sholtes, Dan Baker, Tim Stephens, Jacob Morgan, Dan Brogan, Stephen Adams, Tyler Rosburg, and Johannes Beeby also provided valuable advice and camaraderie throughout my time at CSU.

I of course would have been unable to complete any of this work without the funding support of numerous groups. I was partially funded through the EPA CLEAN center (grant RD835570), an NSF IGERT grant (DGE-0966346) for the 'I-WATER' program at CSU, a Water Environment & Reuse Foundation grant, and funding from the Urban Drainage and Flood Control District and members of the Big Dry Creek Watershed Association.

Finally, I wish to thank my family. My parents have given me a great life, and supported me even when I moved so far from home. Thank you also to Charlotte, Elle, Matt, and Ryan. I could not ask for better siblings. To Lindsay, you are the best person I know. Every time I struggled, you cheered me up. Every time I succeeded, you made sure we celebrated. Thank you for your patience and love. I look forward to finding our farm together.

DEDICATION

To Lindsay

TABLE OF CONTENTS

LIST OF TABLES

LIST OF FIGURES

Chapter 1

Introduction

Humanity does not have a good record of environmental stewardship. As early as the 1860's, George Perkins Marsh described the magnitude and consequences of our environmental modifications in *Man and Nature* [*Marsh*, 1864]. It has even been suggested that environmental degradation has historically been a leading cause of the demise of civilizations [*Montgomery*, 2007; *Diamond*, 2005]. While our recognition of environmental issues has certainly improved in the century and a half since Marsh's book, we may be no closer to a solution. We are still eroding our topsoil, are polluting our waterways, and are paving over our natural landscape to house exploding urban populations. Rivers are not immune to these changes. In fact, rivers are often the most affected natural features because — as integrators of their environment — they are impacted by every change on the landscape.

Our uncontrolled growth has altered the water cycle. By building cities and subdivisions, we prevent precipitation from infiltrating into the ground, instead funneling it directly to streams. This pulse of water overwhelms stream channels, causing them to erode in response [*Booth*, 1990]. This eroded sediment can pollute downstream rivers and lakes directly, but can also carry other contaminants, including the nutrient phosphorus.

Like the water cycle, we have irreversibly altered the natural cycles of phosphorus and its companion nutrient, nitrogen. We mine phosphorus from rock — and nitrogen from the air — fertilizing our crops with these products. While this technological advance has enabled us to feed a growing world population, the huge input of nutrients to the environment has radically altered the natural function of ecosystems. Across the world, water quality is impaired by high concentrations of phosphorus and nitrogen. These nutrients stimulate algal growth and the resulting "blooms" kill fish, contaminate drinking water, and limit human enjoyment of rivers, lakes, and oceans [*Smith et al.*, 1999]. Phosphorus pollution comes

from many sources, including farms, wastewater treatment facilities, and urban stormwater runoff. An additional source — erosion of stream channels — has been largely overlooked. River erosion may be a large source of pollution [*Fox et al.*, 2016], but it is unclear just how widespread the problem is. In this dissertation, I describe a new method for estimating phosphorus loading from stream erosion, and more broadly examine the role of functioning stream ecosystems in managing altered nutrient cycles.

River erosion may be a significant — and even the largest — source of phosphorus in some watersheds [*Fox et al.*, 2016; *Sekely et al.*, 2002; *Howe et al.*, 2011; *Miller et al.*, 2014; *Walter et al.*, 2007]. Quantifying phosphorus loading from stream erosion, however, requires intensive data collection, modeling, or both. This can be prohibitively expensive and time consuming for water quality managers looking to identify the dominant phosphorus sources in a watershed. A simpler approach is needed to help answer the question: is river erosion a major source of phosphorus in my watershed? And, if so, what can be done about it? I first address the latter question by reviewing the effectiveness of stream restoration for mitigating nutrient pollution. To help managers answer the first question, I developed a new, simple, watershed-scale model for simulating phosphorus loading from river erosion.

The significant erosion in rivers caused by land use modification (e.g. urbanization) and channelization spurred initial research into river channel change. Based on observations in the loess hills of Mississippi and channelized streams of western Tennessee, two similar conceptual channel evolution models (CEMs) were developed [*Schumm et al.*, 1984; *Simon*, 1989]. These CEMs predict that channels respond to disturbance first by incising, followed by rapid widening as banks become unstable. As widening continues, the power of the flow is reduced and aggradation begins. As the channels begin to stabilize, vegetation colonizes this deposited sediment and an inset floodplain is established (Figure 1.1). While this sequence of channel change is based on field observations, many exceptions have been observed. In southern California, for example, channels may respond to disturbance by transitioning from a single thread to braided planform [*Hawley et al.*, 2012]. *Cluer and Thorne* [2014] made

additional modifications to the classic CEMs to account for the formation of anastomosing channels and arrested degradation (i.e. incision is halted before significant widening occurs). Recently, a CEM for urban channels was developed which also accounts for bank and bed stabilization which can impact trajectories of channel change [*Booth and Fischenich*, 2015]. The increasing complexity of these proposed CEMs illustrates the difficulty of developing a universal model — even conceptually — that describes the wide variety of potential stream types and responses.

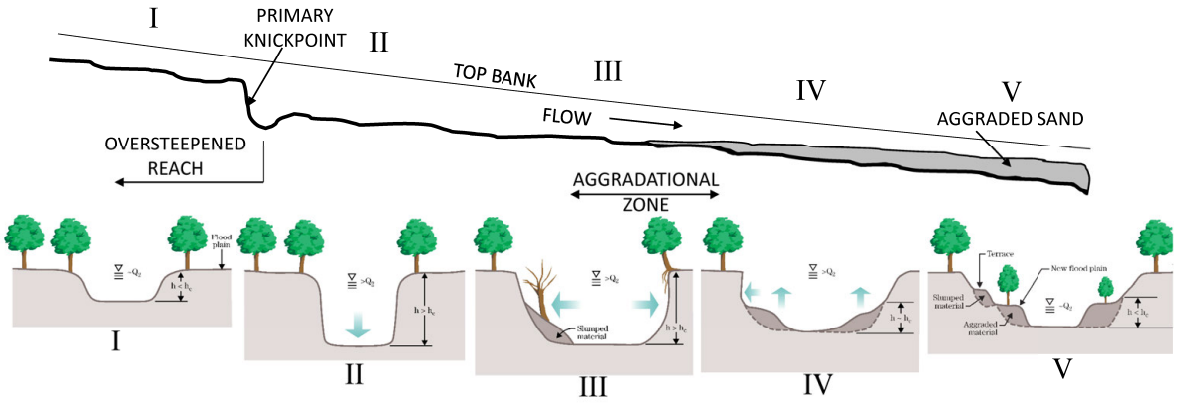

Figure 1.1: Conceptual channel evolution model. Redrawn from *Schumm et al.* [1984] and *NRCS* [2007].

Despite the significant interest in developing conceptual models for channel evolution, quantitative prediction of these changes has proven more difficult. Several mechanistic models have been developed, primarily with a focus on bank erosion [*Osman and Thorne*, 1988; *Simon et al.*, 2000; *Darby et al.*, 2007]. Other models link bank and bed erosion to more realistically simulate channel change [*Darby and Thorne*, 1996a; *Langendoen and Simon*, 2008; *Langendoen and Alonso*, 2008]. While these models may accurately predict channel evolution over time [e.g. *Darby et al.*, 1996], they have significant data requirements and can only be applied at the reach or bank scale. This is a significant limitation. Stream evolution should be modeled at the watershed scale to effectively simulate channel response and

quantify phosphorus loading. The model I have developed is easily applied at this scale by relying on stream power — a physically based variable that is relatively simple to calculate.

Stream power is the power available to do work in a stream [*Bagnold*, 1966]. Stream power per unit width — which I will call specific stream stream power [after *Knighton*, 1999] (but which has also been labeled unit stream power [*Rhoads*, 1987]) — is defined as:

$$\omega = \frac{\Omega}{w} = \frac{\gamma Q S}{w} \tag{1.1}$$

where ω is specific stream power [W m^{-2}], Ω is total stream power [W m^{-1}], Q is discharge [m^3 s^{-1}], S is slope [m m^{-1}], w is flow width [m], and γ is the specific weight of water [9810 N m^{-3}].

Discharge data are often available from gaging stations, regional regression equations, or hydrologic modeling. Channel slope and width can be calculated throughout a drainage basin using increasingly available, high resolution digital elevation models (DEMs), often constructed from aerial LiDAR (Light Detection and Ranging) data. Stream power is therefore relatively easy to calculate throughout a stream network. Because of this, stream power has been used to determine large scale erosion and deposition potential [*Vocal Ferencevic and Ashmore*, 2012; *Bizzi and Lerner*, 2015; *Parker et al.*, 2015; *Orr et al.*, 2008; *Soar et al.*, 2017]. Often, these analyses assume a single "geomorphically effective discharge" in their calculations, neglecting the importance of flow variability and timing [but see *Soar et al.*, 2017]. Stream power has also been used as the basis of sediment transport equations [e.g. *Bagnold*, 1980] (see Chapter 3 for more details). I am not aware, however, of any study using stream power as the physical driver of a morphodynamic model. This dissertation builds upon the rich history of stream power river research, but extends it further to mechanistically model channel change — accounting for both incision and bank erosion. This model is a useful tool to assess the magnitude of pollutant loading from channel erosion, and can be used to test the effectiveness of different mitigation strategies.

In Chapter 2, I summarize the state of the science on the effectiveness of stream restoration for reducing nutrient pollution. This review addresses the second question posed above: if channel erosion is a significant phosphorus source, what can be done to mitigate this pollution? Rather than focus solely on phosphorus and river erosion, I broadened the scope to include nitrogen and stream restoration strategies that target other sources of nutrient pollution (e.g. riparian buffers to mitigate high nitrate loading in groundwater).

In Chapter 3, I develop new bedload and total load sediment transport equations based on specific stream power. These equations use only slope, width, discharge, and grain size — making them straightforward to apply at the watershed scale.

In Chapter 4, I describe the development of the River Erosion Model (REM), a mechanistic computer model to simulate stream channel evolution. This model uses the sediment transport equations described in Chapter 3 to simulate bed incision and aggradation. It also uses a modified version of the Bank Stability and Toe Erosion Model (BSTEM) [*Simon et al.*, 2000, 2011] to simulate bank erosion and widening.

In Chapter 5, I use REM to estimate future sediment and phosphorus loading from channel erosion in two watersheds: Big Dry Creek, Colorado and Lick Creek, North Carolina. Finally, I synthesize the results of this work, describe how REM can be a useful tool for watershed management and research, and provide an outlook for future advances in understanding stream evolution, stream restoration, and their implications for sustainably managing our river resources.

Chapter 2

What role does stream restoration play in nutrient management?

Summary

Nutrient pollution is a pervasive water quality problem. Stream restoration has been proposed as a novel approach to reduce loading and increase nutrient processing within streams. I summarize evidence from the literature on the efficacy of stream restoration for reducing nutrient loading and increasing nutrient removal in stream ecosystems. I also analyze published data on streambank phosphorus concentrations and riparian and stream denitrification rates to improve understanding of the potential benefits of stream restoration for phosphorus retention and nitrogen removal. Finally, I discuss the role of stream restoration in nutrient management and provide recommendations for practice and future research.

2.1 Introduction

Eutrophication of aquatic systems — excessive nutrient concentrations and subsequent accelerated primary production — is a pressing water quality problem in the U.S. and around the world [*Smith et al.*, 1999; *Smith*, 2003]. Nitrogen and phosphorus, nutrients required for plant and animal growth, are often limiting in these ecosystems [*Elser et al.*, 2007], meaning that small increases in the availability of one or both of these compounds can lead to large increases in biomass. Although necessary for proper ecological function, excessive nitrogen

Lammers, R. W. and B. P. Bledsoe (2017), What role does stream restoration play in nutrient management?, Critical Reviews in Environmental Science and Technology, 47, 335–371. doi: 10.1080/10643389.2017.1318618.

Roderick W. Lammers reviewed the necessary literature, compiled and analyzed the data, and wrote the manuscript. Brian P. Bledsoe contributed to the discussion and edited the manuscript.

and/or phosphorus can lead to algal blooms, depleting dissolved oxygen (potentially lethal to aquatic life), producing harmful toxins, impairing aesthetics and recreation, and fouling water infrastructure. This eutrophication significantly degrades water quality, harming aquatic organisms and beneficial human use of water resources. According to the U.S. Environmental Protection Agency (EPA), nutrient pollution is the third largest source of water quality impairment in rivers and streams and the second largest for lakes, ponds, and reservoirs [*EPA*, 2015].

Significant effort has been made to improve water quality by reducing nutrient loading to streams from upland sources; however, in-stream nutrient removal and retention may be significant [*Peterson et al.*, 2001; *Reisinger et al.*, 2015], leading to the suggestion that enhancing natural removal and sequestration mechanisms may be a viable strategy to improve water quality. Stream restoration is a booming enterprise in the U.S. (>$1 billion per year industry), and the majority of these projects list water quality improvement as one of their objectives [*Bernhardt et al.*, 2005]. Despite the rapid growth of stream restoration as a management tool over the last two decades, there is a notably limited set of studies that examine the efficacy of stream restoration for nutrient removal, processing, and retention.

The purpose of this review is to synthesize existing evidence for the ability of stream restoration to reduce nutrient loads and concentrations in aquatic systems. Furthermore, I provide a quantitative analysis of streambank phosphorus concentrations and stream and riparian denitrification rates, issues of concern for both nutrient loading and removal. I focus on denitrification as a permanent removal pathway for nitrogen. Phosphorus has no analogous removal processes but stream restoration may decrease phosphorus inputs by reducing streambank erosion. This analysis will aid in future quantification of nutrient-related benefits of restoration, and may support development of crediting programs which can spur additional investment in restoration as a nutrient management strategy.

2.2 Background

2.2.1 Phosphorus

The chemical partitioning of phosphorus is important for understanding its transport. Phosphorus species are relatively insoluble and are typically adsorbed to soil particles. They have a high affinity for the large specific surface area of clay and silt particles and are also found bound in various metal oxyhydroxides including Fe-OH, Al-OH, and Ca-OH [*Brady and Weil*, 2002]. The partitioning of phosphorus among its various states determines its bioavailability for uptake by organisms, which is directly tied to its importance as a limiting nutrient. The relative abundance of bioavailable phosphorus in stream sediment has been shown to vary markedly within single study sites (1–55%; *Veihe et al.* [2011]) and between study areas (averaging 0.5–22% of total phosphorus; *Nellesen et al.* [2011]; *Howe et al.* [2011]; *Hubbard et al.* [2003]; *McDowell and Sharpley* [2001]; *McDowell and Wilcock* [2007]; *Thompson and McFarland* [2007]).

Phosphorus speciation and subsequent bioavailability is a dynamic process; therefore, there may be a lag from when phosphorus is introduced to a stream and when the effects of this loading are manifested [*Meals et al.*, 2010]. Additionally, sediment may serve as either a sink or a source of phosphorus depending on whether the sediment sorptive capacity is higher or lower than the in-stream dissolved phosphorus concentrations [*Hoffman et al.*, 2009; *McDaniel et al.*, 2009]. The bioavailability of phosphorus has important implications for its effects on water quality. However, most water quality monitoring programs focus only on total phosphorus because of the difficulty in both quantifying bioavailability and predicting how the forms of phosphorus will change over time. Unlike denitrification of nitrate, there is no biotic or abiotic process that effectively removes phosphorus from an ecosystem. Therefore, phosphorus removal is likely only temporary biotic uptake, although burial and storage in floodplain or lacustrine sediment may be a longer-term removal mechanism [*Records et al.*, 2016].

Recent evidence has made it increasingly clear that bank and bed erosion may be a significant source of particulate phosphorus loading to streams [*Fox et al.*, 2016], typically accounting for between 10% [*Sekely et al.*, 2002] and 40% [*Howe et al.*, 2011] of the total phosphorus load in an individual watershed. However, phosphorus and sediment loading rates from bank erosion are highly variable both within and among watersheds, ranging from <1 to 1,000s of kg/km/yr (Table 2.1). Nitrogen loading from bank erosion is commonly neglected (but see *Walter et al.* [2007]), likely because phosphorus is more commonly found adsorbed to soil particles than nitrogen, and most nitrogen studies focus on dissolved, inorganic forms. Despite increasing recognition of the role of bank erosion a phosphorus source, quantifying this contribution remains difficult, in part because of uncertainty in bank phosphorus concentrations. I addressed this uncertainty by analyzing available data on bank phosphorus content to help practitioners quantify the magnitude of this potentially potent nutrient source.

Table 2.1: Summary of bank sediment and phosphorus loading rates from select studies. *Ton is a metric ton (1,000 kg). †Reported nitrogen concentrations of 400–2,100 mg/kg and nitrogen loading rates of 447–6,113 kg/km/yr.

Study	**Location**	**Bank P Concentrations [mg/kg]**	**Sediment Loading Rate [ton/km/yr]***	**Phosphorus Loading Rate [kg/km/yr]**
DeWolfe et al. [2004]	Vermont, USA	369 – 740	10 – 1,333	10 – 840
Hubbard et al. [2003]	Mississippi, USA	168 – 273	7,574 – 17,604	1,170 – 2,719
Kronvang et al. [2012]	Funen, Denmark	400 – 1,400	–	4.2 – 167
Langendoen et al. [2012]	Vermont, USA	422 – 973	0.1 – 3,266	0.1 – 2,970
Miller et al. [2014]	Oklahoma, USA	239 – 427	300 – 12,857	320 – 4,104
Nellesen et al. [2011]	Iowa, USA	184 – 347	–	3.4 – 20.7
Peacher [2011]	Missouri, USA	197 – 637	9.2 – 447.5	2.9 – 114
Thoma et al. [2005]	Minnesota, USA	249 – 452	9,147	3,589
Tufekcioglu [2010]	Iowa, USA	246 – 349	58 – 664	20 – 183
Walter et al. [2007]†	Pennsylvania, USA	339 – 958	510 – 2,800	298 – 2,680
Zaimes et al. [2008b]	Iowa, USA	303 – 555	5 – 304	2 – 123

2.2.2 Nitrogen

In aquatic systems, nitrogen cycles between organic and inorganic forms through plant uptake, organic material decomposition, mineralization, and microbially-mediated nitrification (formation of nitrate from ammonia) and denitrification. Denitrification is the anaerobic reduction of nitrate by heterotrophic bacteria under anoxic conditions, leading to the production of N_2O or N_2 gas [*Hill*, 1996]. Denitrification completely removes nitrate from a system, making it a desirable target for restoration as opposed to biotic assimilation which only temporarily alters nitrogen availability (e.g. plants use nitrogen but release it back to the stream when they die and decompose). Denitrification rates are highest in saturated soils and streambeds (water providing a source of dissolved nitrate and anoxic conditions) and when organic carbon is available (to serve as an energy source). However, denitrification is rarely a constant process. High rates of denitrification may occur in discrete locations ("hot spots") and at discrete points in time ("hot moments") when conditions are right [*McClain et al.*, 2003]. Although, it remains unclear just how significant these hot spots and hot moments are for controlling ecosystem function [*Bernhardt et al.*, 2017].

Encouraging denitrification through stream restoration is desirable; however, denitrification rates may remain high even in impacted streams. Forested and urban riparian soils have similar denitrification potential [*Groffman et al.*, 2003], suggesting that under the right conditions, namely high water tables, riparian denitrification will occur even in developed areas. On the other hand, suburban and agricultural riparian areas may have lower organic carbon availability compared with forested sites, a potential constraint on denitrification [*Watson et al.*, 2010]. Stream restoration may also fail to encourage denitrification, and rates may not be significantly different between restored and unrestored reaches [*Groffman et al.*, 2005; *Harrison et al.*, 2012; *Tuttle et al.*, 2014]. In fact, restored reaches may have lower denitrification rates due to coarser streambed sediment [*Weigelhofer et al.*, 2013] and lower organic carbon availability [*Gift et al.*, 2010], side effects of construction activities. Focusing on denitrification for nitrogen removal is commendable but it is a difficult goal to

achieve in practice. I conducted an analysis of in-stream and riparian denitrification rates to help determine what controls this important nitrogen removal process and provide guidance for restoration.

2.2.3 Stream Restoration

Stream or river restoration is a broad topic with varying definitions [*National Research Council*, 1992; *Society for Ecological Restoration*, 2004; *Wohl et al.*, 2005]. Studies included in this review fit the definition of stream restoration broadly by incorporating modifications to streams, riparian areas, and/or the watershed with the intent of providing some ecological and/or human benefit. The studies incorporated within this review use a variety of stream restoration strategies, including Natural Channel Design (NCD) [*Rosgen*, 1996, 2006]. NCD attempts to restore a degraded reach to match the geomorphic form of some nearby reference reach that is considered representative of natural and stable conditions. This approach has been criticized for failing to account for differences in watershed condition and processes (e.g. hydrology and sediment flux) between degraded and reference sites and the focus on stability, rather than ecological improvement, as a restoration goal [*Simon et al.*, 2007; *Lave*, 2009]. Nutrient removal and retention in aquatic systems is a dynamic process and therefore restoration that focuses specifically on relevant biotic and abiotic processes is likely to be the most successful [*Wohl et al.*, 2005, 2015b].

While the most commonly stated objective of stream restoration projects is water quality management, fewer than 10% of projects have any kind of post-restoration monitoring [*Bernhardt et al.*, 2005]. Even fewer projects have published data on changes in water quality, making it difficult to assess whether these projects achieved their stated goals. Recent reviews have assessed stream restoration success broadly [*Palmer et al.*, 2014b; *Newcomer Johnson et al.*, 2016] and with a focus on specific processes (e.g. denitrification in restored hyporheic zones; *Merill and Tonjes* [2014]). However, to date there has been no comprehensive assessment of the ability of specific restoration strategies to improve nutrient retention

and processing. The purpose of this review is to synthesize the current state of the science on stream restoration as a strategy for nutrient removal and retention.

2.3 Methods

2.3.1 Streambank Phosphorus Concentrations

A number of studies have quantified streambank phosphorus concentrations in diverse locations. These studies focused on a variety of aspects of bank erosion and phosphorus loading including the influence of adjacent land use, variability between stream reaches and between bed, bank, and upland areas, relative abundance of various forms of phosphorus, and quantification of total watershed phosphorus loading from bank erosion. However, there has been no large-scale analysis of the available bank phosphorus data to determine whether observed trends are consistent between studied geographic areas. I collected bank phosphorus data from the literature and supplemented this dataset with my own field data from Big Dry Creek, Westminster, CO and Lick Creek, Durham, NC. These bank samples were analyzed for both total phosphorus (EPA Method 3051a) and bioavailable phosphorus (Mehlich-3).

Bank sampling and laboratory analysis of phosphorus content is expensive. I assessed the feasibility of using regional soil phosphorus data as a more cost-effective approach to estimate bank phosphorus concentrations. I obtained coarse-scale soil phosphorus data for the conterminous U.S. from a recent U.S. Geological Survey publication [*Smith et al.*, 2013]. I compared bank total phosphorus concentrations from various studies to upland soil (surface, A, and C horizons) phosphorus concentrations within a 50 mile radius (chosen to yield $\sim$10 upland data points). For some studies, bank phosphorus data were separated by study stream if they were geographically distant. Weighted least squares (WLS) regression was used to relate mean bank phosphorus concentration to upland phosphorus concentrations for each location, incorporating a pseudo R^2 value to account for the applied weights [*Willett and Singer*, 1988]. Each point was weighted by the inverse of its squared residual from ordinary least squares regression (giving points closer the line higher weight). I quantified

uncertainty using 1000 bootstrap replicates with data resampling (with replacement) for each site, yielding new mean concentrations with which regression was performed. This allowed for the quantification of a nonparametric 95% confidence interval (CI) for the pseudo R^2 values.

Phosphorus bioavailability is important for understanding its effect on water quality, but it remains an elusive parameter to quantify. I assessed variability in streambank phosphorus bioavailability using data from eight sources. In each case, Mehlich-3 phosphorus was assumed to represent bioavailable phosphorus. Although various extraction methods may be used to estimate bioavailable phosphorus (e.g. water extraction), Mehlich-3 is most widely used and therefore provided the largest dataset.

Individual laboratory methods differ in their ability to extract adsorbed phosphorus from soils, leading to potentially different results and complicating direct comparison of data from various sites [*Kleinman et al.*, 2001]. Analytical methods for determining total phosphorus concentrations of bank soils were divided into four major categories to test their relative influence on observed data. The *aqua regia* approach utilizes a combination of nitric and hydrochloric acid in conjunction with microwave heating [*Crosland et al.*, 1995; *U.S. EPA*, 2007]. Others use only hydrochloric acid, also with heat [*Pardo et al.*, 2004]. Alternative methods include sulfuric acid digestion [*U.S. EPA*, 1983] (method 365.4 colorimetric, automated) and alkaline oxidation [*Dick and Tabatabai*, 1977].

2.3.2 Stream and Riparian Denitrification Rates

Reviews have examined denitrification in freshwater and marine ecosystems [*Seitzinger*, 1988] and riparian zones [*Martin et al.*, 1999], and have even attempted to quantify effects of various controlling variables on denitrification rates [*Saunders and Kalff*, 2001; *Piña-Ochoa and Álvarez-Cobelas*, 2006]. However, numerous studies on stream and riparian denitrification have been published since these reviews were conducted, and no review has collected stream and riparian denitrification data for concurrent analysis.

Data on stream and riparian denitrification rates were obtained from 98 peer-reviewed studies (69 stream and 38 riparian with some overlap, data in supplemental material). Actual denitrification rates were collected from text, tables, and figures. If potential denitrification rates (i.e. measured rates after adding abundant nitrate and carbon) were available, these data were obtained as well (data in supplemental material). Information was collected on quantification approach, including specific method, spatial scale (i.e. core or reach), temporal scale (i.e. days, months, or years), and whether the analysis was performed in the lab or field. Other variables of interest include dominant watershed land use, riparian vegetation type, Köppen-Geiger climate classification [*Kottek et al.*, 2006], and average streamwater nitrate concentration. Since riparian nitrate levels were not consistently reported (e.g. soil concentration versus groundwater concentration), these data were not included in the analysis.

The collected data are meant to be representative rates from streams and riparian zones. I either used mean rates reported by the authors or I averaged point measurements across space and time for each site. Different methods measure rates at different scales. In streams, reach scale rates can be measured directly using tracers; however, many stream data (and all riparian data) are obtained as point measurements and averaged across the sample area to obtain denitrification rates on a per area basis. This analysis accounts for differences in method and scale, and direct comparison of riparian and stream denitrification rates should be appropriate.

Denitrification in natural systems is notoriously difficult to measure. A variety of methods have been developed; however, they each have their drawbacks [*Groffman et al.*, 2006]. Details on the benefits and shortcomings of various methods are provided by *Groffman et al.* [2006], and therefore will not be repeated here. However, I do include a brief description of the major methods used by studies included in this analysis (Table 2.2).

I used several approaches to quantify the influence of selected variables on denitrification rates: linear regression, regression tree, and random forest. Regression trees are similar to

Table 2.2: Summary of common denitrification methods. See *Groffman et al.* [2006] for more detailed descriptions.

Method	Description
Acetylene Inhibition	Acetylene (C_2H_2) blocks the conversion of nitrous oxide (N_2O) to dinitrogen gas (N_2), leaving the easier to measure N_2O as the terminal product of denitrification. This method is inexpensive and lends itself to large numbers of samples. However, it may underestimate actual denitrification rates.
^{15}N Tracer	Use of a nitrogen isotope tracer allows for quantification of denitrification by tracking isotopically-labeled nitrogen gas production. Complications with this method may arise if adequate mixing of the added tracer is not achieved.
Direct N_2 or N_2:Ar Measurement	Direct measurement of N_2 produced from denitrification is difficult because of the high background concentrations in the atmosphere. However, it is more suitable in aquatic systems where gas exchange is limited. Use of mass spectrometry to quantify denitrification via the ratio of N_2:Ar in produced gas is also increasing in use.
Mass Balance	Quantitative nitrogen mass balance can allow for estimation of denitrification in aquatic systems. To be effective, all other nitrogen fluxes must be quantified, with the discrepancy attributed to denitrification. This is obviously prone to significant error.

linear regression techniques in that the response variable can be predicted based on a set of predictor variables. However, while linear regression treats the entire predictor space the same, tree-based approaches stratify the predictor space into regions. Instead of a linear regression model, the output is a "tree" with binary splits based on predictor variable values or categories. A random forest approach extends this idea by creating a large number of regression trees and averaging the result. I assessed variable importance by these three methods using R (version 3.2.2; *R Core Team* [2018]). I used the "rpart" package [*Therneau et al.*, 2015] for regression tree analysis and the "party" package [*Hothorn et al.*, 2006; *Strobl et al.*, 2007, 2008] for random forest. Each of these approaches yielded variable importance metrics which were normalized to their sum for comparison between methods. The average of these normalized metrics was used as an overall indicator of variable importance. Climate types were consolidated by main climate group (e.g. tropical, temperate, arid) if there were

fewer than five observations. The exception was the sole study in a polar climate [*Gooseff et al.*, 2004] which was left independent. I retained this data point because removing it did not significantly influence results.

2.3.3 Restoration Assessment

Different restoration practices target different nutrient removal pathways and are therefore likely to have different levels of impact on nutrient loading in stream and riparian ecosystems. I performed simple Monte Carlo simulations to compute the mean nutrient removal potential, along with associated uncertainty, of four restoration strategies: bank stabilization, floodplain reconnection, riparian buffer restoration, and hyporheic zone restoration. Simulations assumed a conceptual 1 km long, 10 m wide restored reach with a 20 m buffer on one bank and a 20 m reconnected floodplain on the other. Bank and bed stabilization and floodplain reconnection were analyzed for phosphorus removal (avoided loading from erosion and increased deposition on floodplains). I used representative bank erosion rates (Table 2.1), bank phosphorus concentrations (Figure 2.1), and floodplain phosphorus retention rates [*Kronvang et al.*, 2007]. Hyporheic zone restoration, riparian buffer restoration, and floodplain reconnection were assessed for their effect on removing nitrate via denitrification. I used stream and riparian denitrification rates collected from the literature (Section 2.3.2).

2.4 Results

2.4.1 Streambank Phosphorus Concentrations

Figure 2.1 shows the variability in bank total phosphorus concentrations reported in 17 studies from around the U.S. and the world (overall mean 337 mg/kg, 5th percentile 72.5 mg/kg, 95th percentile 707 mg/kg). This variability can lead to significant uncertainty in estimated phosphorus loading rates from bank erosion. Streambank phosphorus concentrations are well correlated with upland surface soil data (Figure 2.2; slope = 0.505; $R^2 = 0.447$, 95% CI: 0.136–0.583). Regression results using data from the A- and C-horizons have higher

slopes but weaker relationships (data not shown; A: slope = 0.674; R^2 = 0.336, 95% CI: 0.056–0.537; C: slope = 0.878; R^2 = 0.314, 95% CI: 0.066–0.487). Dominant land use of the upland data does not appear to significantly influence the regression results.

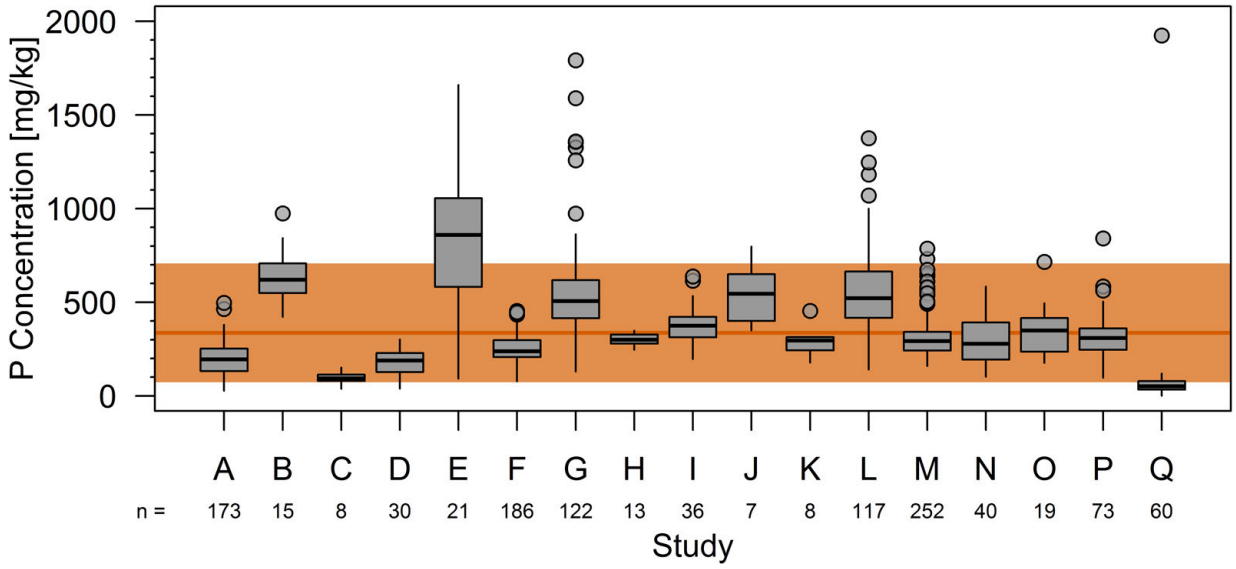

Figure 2.1: Box plot of bank phosphorus concentrations for 17 studies from the U.S. and the world. Box plots indicate the median, quartiles, and non-outlier maximum and minimums (1.5 times the interquartile range). Points are outliers. The horizontal line is the mean of the composite dataset and the shaded area represents the 90% confidence interval. [A] *Bledsoe et al.* [2000]; [B] *Howe et al.* [2011]; [C] *Thompson and McFarland* [2007]; [D] *Hubbard et al.* [2003]; [E] *Veihe et al.* [2011]; [F] *Nellesen et al.* [2011]; [G] *Schilling et al.* [2009]; [H] *Tufekcioglu* [2010]; [I] *Peacher* [2011]; [J] *Kerr et al.* [2011]; [K] *Hongthanat* [2010]; [L] *Walter et al.* [2007]; [M] *Miller et al.* [2014]; [N] *McDowell et al.* [2003]; [O] *McDowell* [2003]; [P] unpublished data from Big Dry Creek, Westminster, CO, and [Q] Lick Creek, Durham, NC.

Bioavailable phosphorus accounts for, on average, 11.7% of total streambank phosphorus in the available studies (Figure 2.3). These data are variable but suggest bioavailable phosphorus is usually less than one quarter of total phosphorus (90% CI: 2.7–23.6%). Percent bioavailability is negatively correlated with total phosphorus (TP; Spearman ρ = -0.20, p $<$ 1e-6) suggesting that the bioavailable phosphorus fraction decreases as TP increases and it may be inappropriate to assume a constant percent bioavailability for any value of TP. However, this negative correlation is relatively weak and more data are needed at TP values greater than ∼600 mg/kg to yield more definitive results.

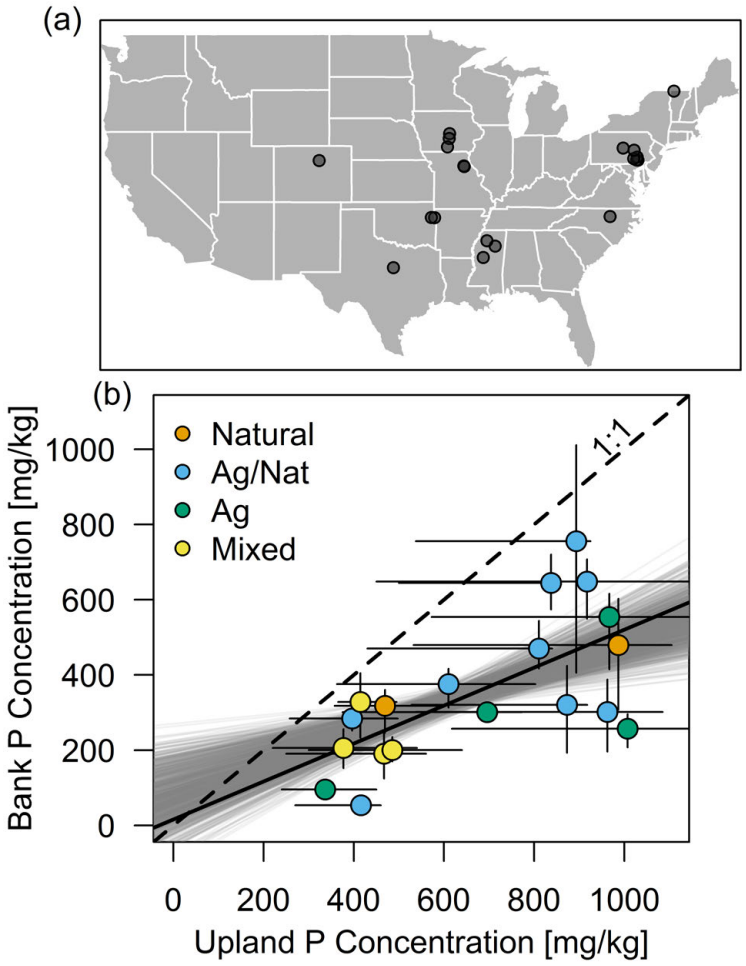

Figure 2.2: (A) Locations of studies used in this analysis [*Bledsoe et al.*, 2000; *Hubbard et al.*, 2003; *McDowell et al.*, 2003; *Walter et al.*, 2007; *Thompson and McFarland*, 2007; *Schilling et al.*, 2009; *Hongthanat*, 2010; *Tufekcioglu*, 2010; *Howe et al.*, 2011; *Nellesen et al.*, 2011; *Peacher*, 2011; *Miller et al.*, 2014] and unpublished data from Big Dry Creek, Westminster, CO and Lick Creek, Durham, NC. (B) Mean bank phosphorus concentrations versus mean surface soil (top 5 cm) phosphorus concentrations. Solid line is a weighted least squares linear regression (Bank P [mg/kg] = 15.6 + 0.505 × Upland P [mg/kg]). Error bars are the interquartile range of individual points. Gray lines are bootstrap-estimated regression lines, indicating the range of uncertainty. Points are colored based on major land use type from the upland dataset.

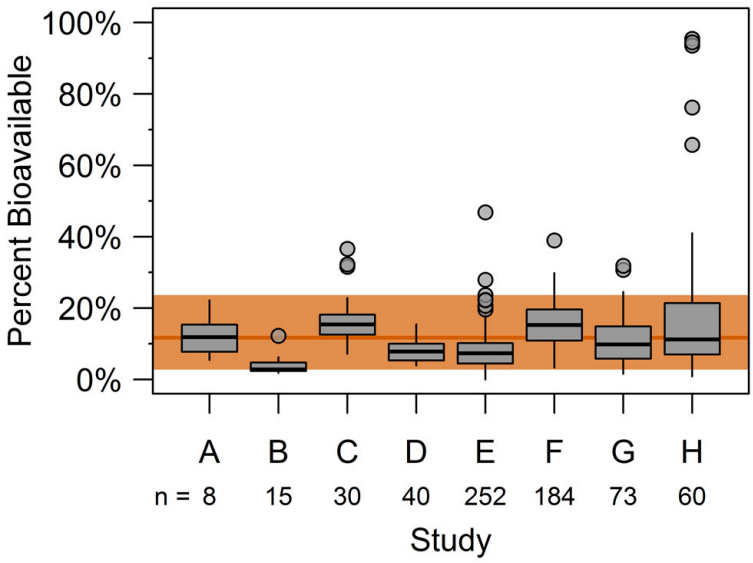

Figure 2.3: Percent of total phosphorus that is bioavailable (Mehlich-3 extraction) from a variety of sources. Box plots indicate the median, quartiles, and non-outlier maximum and minimums (1.5 times the interquartile range).Points are outliers. The horizontal line is the mean of the composite dataset and the shaded area represents the 90% confidence interval. [A] *Hongthanat* [2010]; [B] *Howe et al.* [2011]; [C] *Hubbard et al.* [2003]; [D] *McDowell et al.* [2003]; [E] *Miller et al.* [2014]; [F] *Nellesen et al.* [2011]; [G] unpublished data from Big Dry Creek, Westminster, CO and [H] Lick Creek, Durham, NC.

Statistically significant differences were observed between different phosphorus extraction methods based on a non-parametric, rank-based pairwise comparison [*Siegel and Castellan*, 1988] (Figure 2.4). However, these differences pale in comparison to inter-study variability. Multiple linear regression results suggest that differences between studies explain an order of magnitude greater variability in total phosphorus concentrations than the analytical method.

2.4.2 Stream and Riparian Denitrification Rates

Areal denitrification rates in stream and riparian systems are shown in Figure 2.5. A two-sided Wilcoxon Rank Sum test suggests that stream denitrification rates are significantly different than riparian rates at the 95% confidence level ($p = 0.016$). However, the difference in the medians of these two datasets is only 0.84 mg N m^{-2} h^{-1} (1.85 and 1.01 mg N m^{-2} h^{-1} for stream and riparian, respectively). Given the several orders of magnitude range in both datasets, this difference may not be practically meaningful.

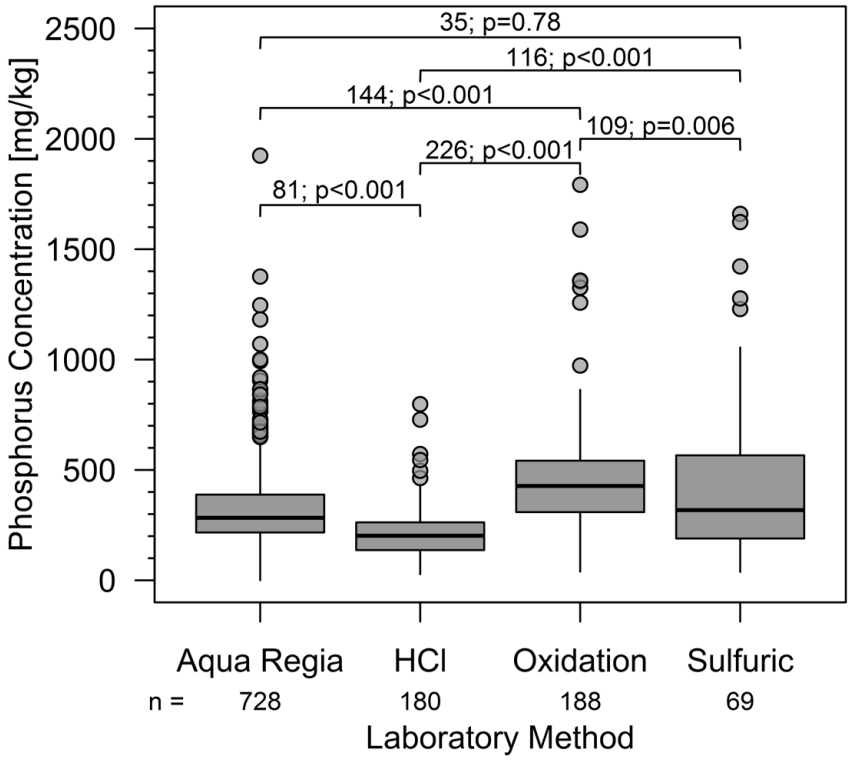

Figure 2.4: Comparison of bank total phosphorus concentration by extraction method. Box plots indicate the median, quartiles, and non-outlier maximum and minimums (1.5 times the interquartile range). Points are outliers. Brackets show differences in medians and p-values from a rank-based pairwise comparison [*Siegel and Castellan*, 1988]. See Section 2.3.1 for details on laboratory methods.

Streamwater nitrate concentration is generally considered one of the most significant controls on stream denitrification rates. Our compiled dataset shows a similarly strong relationship between these two variables (Figure 2.6). A fitted power regression has a larger exponent than previous studies (Table 2.3; 0.72 compared to 0.51, *Mulholland et al.* [2009], 0.44, [*Böhlke et al.*, 2009], and 0.62, *Roley et al.* [2012a]). However, using just data collected using a ^{15}N tracer method, the calculated exponent (0.56) is more similar to those found by others using ^{15}N tracer data [*Mulholland et al.*, 2009]. Fitted exponents for data collected using the other methods are all substantially higher (0.71 – 0.75), suggesting a greater increase in denitrification rate per unit increase in nitrate concentration.

The Michaelis-Menten equation is commonly used to model the saturation effects of enzyme-substrate reactions:

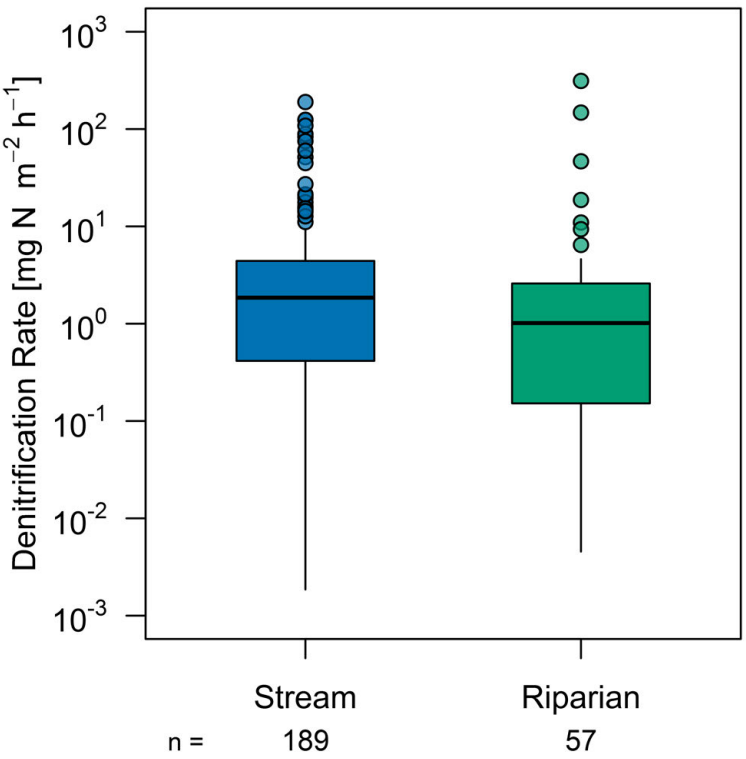

Figure 2.5: Summary of published denitrification rates in stream and riparian ecosystems. Box plots indicate the median, quartiles, and non-outlier maximum and minimums (1.5 times the interquartile range). Points are outliers.

$$Den = (NO_3^- \times V_{max})/(NO_3^- + K_s) \tag{2.1}$$

where Den is the denitrification rate [mg N m^{-2} h^{-1}], NO_3^- is the stream nitrate concentration [μg L^{-1}], V_{max} is the maximum obtainable value of Den [mg N m^{-2} h^{-1}], and K_s is the nitrate concentration at which Den is half of V_{max} [μg L^{-1}]. Fitted values of V_{max} and K_s were 31.8 mg N m^{-2} h^{-1} and 3,466 μg L^{-1}, an order of magnitude higher than those reported by *Mulholland et al.* [2009] (3.9 and 422, respectively) but only 2–3 times higher those of *Böhlke et al.* [2009]. Fitted values were more similar to these previous studies when I used only ^{15}N tracer data from our compiled dataset (Table 2.3). The power regression model appears to fit the data better (Akaike information criterion, AIC = 405) than the Michaelis-Menten model (AIC = 1708). This corresponds with previous conclusions that a

saturation-law model may not be appropriate when comparing denitrification data across streams [*Böhlke et al.*, 2009; *Mulholland et al.*, 2009].

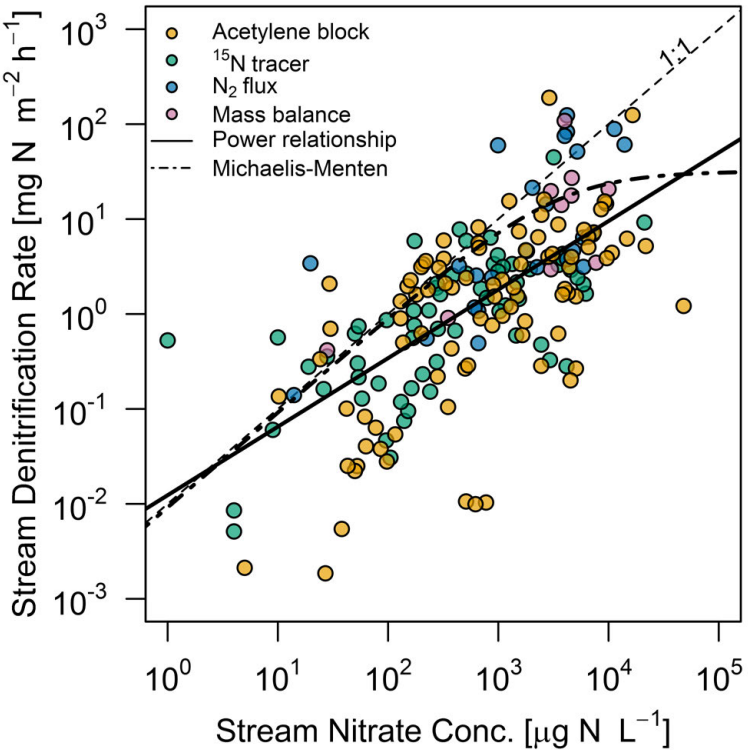

Figure 2.6: Stream denitrification rate versus in-stream nitrate concentration. Solid line is a power regression equation fit to the data ($\log_{10}$(Den) = -1.91 + 0.72 × $\log_{10}$(Nitrate) or, alternatively, Den = 0.012 × Nitrate$^{0.722}$; R^2 = 0.45). Dash-dot line is fitted Michaelis-Menten model (V_{max} = 31.8 mg N m^{-2} h^{-1}, K_s = 3,466 μg L^{-1}). Points are colored to indicate differences in denitrification quantification methods.

Actual denitrification as a percent of denitrification potential was significantly different for riparian versus stream data (medians = 15.6% and 3.5%, respectively; two-sided Wilcoxon Ranked Sign Test; p = 0.014). Given that streams overall tend to have slightly higher denitrification rates, this suggests that streams have greater denitrification potential than riparian areas, although a smaller proportion of this potential is being utilized. Denitrification potential and rates were reported on either a per-mass or per-area basis. The percentages reported above incorporate both datasets, but additional analysis required separating these two datasets. There was a positive correlation between percent of potential and

Table 2.3: Fitted models for denitrification rate versus nitrate for this and previous studies. Various units were used in development of power relationships. While coefficients (a) are not directly comparable between units, exponents (b) are. Michaelis-Menten models for the acetylene block, N_2 flux, and mass balance methods were not statistically significant. †Coefficient not statistically significant at $\alpha = 0.05$.

Model Parameters			Den Method	Source
Power Relationship $\text{Den} = \text{a}(\text{NO}_3^{-1})^b$				
Den [mg N m^{-2} h^{-1}]; NO_3^{-1} [μg L^{-1}]	Den [μmol N m^{-2} h^{-1}]; NO_3^{-1} [μmol L^{-1}]	R^2		
a = 0.012; b = 0.72	a = 5.9; b = 0.72	0.45	Various	This Study
a = 0.01; b = 0.51	–	0.37	^{15}N Tracer	*Mulholland et al.* [2009]
–	a = 26; b = 0.44	0.44	Various	*Böhlke et al.* [2009]
a = NA; b = 0.62	–	–	Various	*Roley et al.* [2012a]
a = 0.031; b = 0.56	a = 9.5; b = 0.56	0.44	^{15}N Tracer	This Study
a = 0.007; b = 0.75	a = 3.7; b = 0.75	0.41	Acetylene Block	This Study
a = 0.036; b = 0.71	a = 17.1; b = 0.71	0.45	N_2 Flux	This Study
a = 0.03; b = 0.73	a = 14.5; b = 0.73	0.58	Mass Balance	This Study
Michaelis-Menten Relationship $\text{Den} = (\text{NO}_3^{-1} \times \text{V}_{max}) \,/\, (\text{NO}_3^{-1} + \text{K}_s)$				
V_{max} [mg N m^{-2} h^{-1}]; K_s [μg L^{-1}]	V_{max} [μmol N m^{-2} h^{-1}]; K_s [μmol L^{-1}]			
V_{max} = 31.8; K_s = 3,466	V_{max} = 2,274; K_s = 248		Various	This Study
V_{max} = 3.9; K_s = 422	–		^{15}N Tracer	*Mulholland et al.* [2009]
–	V_{max} = 640; K_s = 180		^{15}N Tracer	*Böhlke et al.* [2009]
V_{max} = 6.8; K_s = 962†	V_{max} = 483; K_s = 69†		^{15}N Tracer	This Study

per-mass actual rates (Spearman $\rho = 0.64$, p = 0.012, n = 15) but no correlation with per-area actual rates (Spearman ρ = -0.09, p = 0.783, n = 12). The reason for this discrepancy is unclear. However, there is a greater frequency of low potential percentages for the per-mass dataset which could affect results. The first analysis suggests that as actual denitrification rates increase, they are approaching the potential of the system. However, the second analysis suggests that percent of potential is relatively consistent across systems regardless of the in-situ denitrification rate. More data are needed to analyze these relationships in more detail.

The variable importance analysis (Figure 2.7) suggests that stream nitrate concentration is the dominant predictor of stream denitrification rates. However, land use, method, and climate are also important. Agricultural and urban streams had higher rates than reference systems. Temperate and continental climates without noticeable dry seasons tended to have higher denitrification than other climate types. For the riparian dataset, climate was by far the most important predictor, followed by method, temporal scale, and riparian vegetation type. Climate types Cfa (temperate, no dry season, hot summer) and Dfb (continental, no dry season, warm summer) had the highest denitrification rates. However, these results may be somewhat skewed because only agricultural and urban sites (no reference sites) were represented in these climate types. Bare riparian buffers tended to have slightly higher denitrification than vegetated types (grass and forested buffers did not have significantly different rates). The results from the three methods (linear regression, regression tree, and random forest) agreed well, increasing confidence in the results.

The influence of method on denitrification rate was examined in more detail using a Tukey-adjusted pairwise comparison of the means for the log-transformed denitrification data. For the stream data, the two most common methods, ^{15}N tracers and acetylene block, were not significantly different (p = 0.89). Neither were the mass balance and N_2 flux methods (p = 0.99); however, all remaining differences were significant, with mass balance and N_2 flux yielding higher denitrification rates than ^{15}N tracer and acetylene block

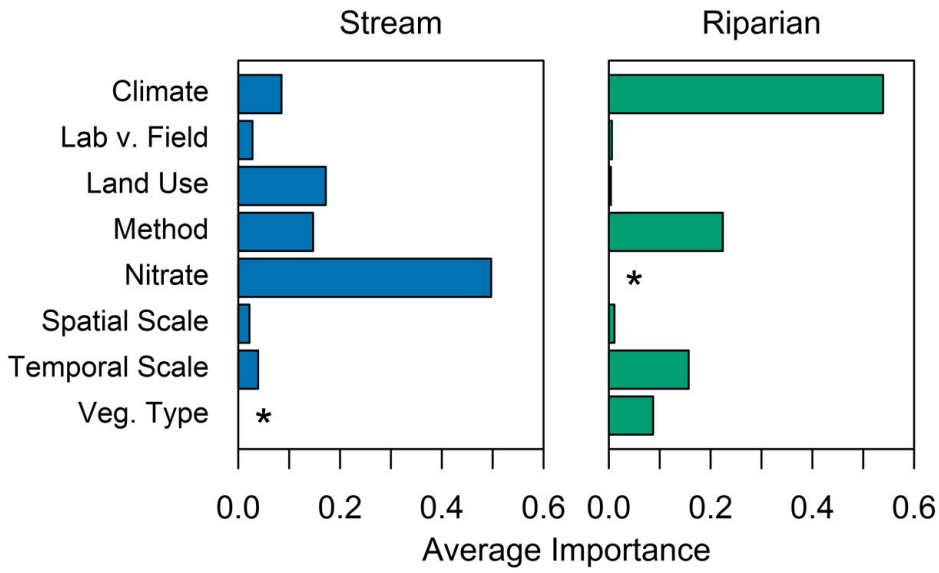

Figure 2.7: Average normalized importance metric from the regression tree, random forest, and multiple linear regression results for the stream and riparian denitrification rate datasets. *Variables not available for these datasets.

results (all p-values < 0.05). Higher rates from mass balance results are expected because this method accounts for all forms of nitrate uptake, not just denitrification. This could also explain why the Michaelis-Menten parameters were higher than others reported in the literature — the mass balance data may skew the results. N_2 flux rates are not expected to be higher since this method only accounts for net denitrification (gross denitrification minus nitrogen fixation, *Groffman et al.* [2006]). Differences among methods were not statistically significant for the riparian dataset, despite method appearing as the second most important explanatory variable (Figure 2.7).

2.4.3 Restoration Assessment

Our simple simulations quantified the relative efficacy of various stream restoration practices for nutrient reduction and removal (Figure 2.8). Bank stabilization had much greater potential to remove phosphorus from the system (609 ± 1,175 kg P/km/yr; mean ± sd) compared to floodplain reconnection (25 ± 15 kg P/km/yr). Riparian restoration had the greatest nitrogen removal potential (1,086 ± 4,973 kg N /km/yr), followed by hyporheic

restoration (226 ± 692 kg N/km/yr) and floodplain reconnection (86 ± 402 kg N/km/yr). High removal potential for riparian restoration is largely a result of larger surface area compared to the streambed. These simple calculations assume the maximum possible benefits of restoration (e.g. complete bank stabilization, no denitrification prior to restoration). The goal is to provide estimates of relative removal potential of various strategies, and these results should not be more broadly interpreted.

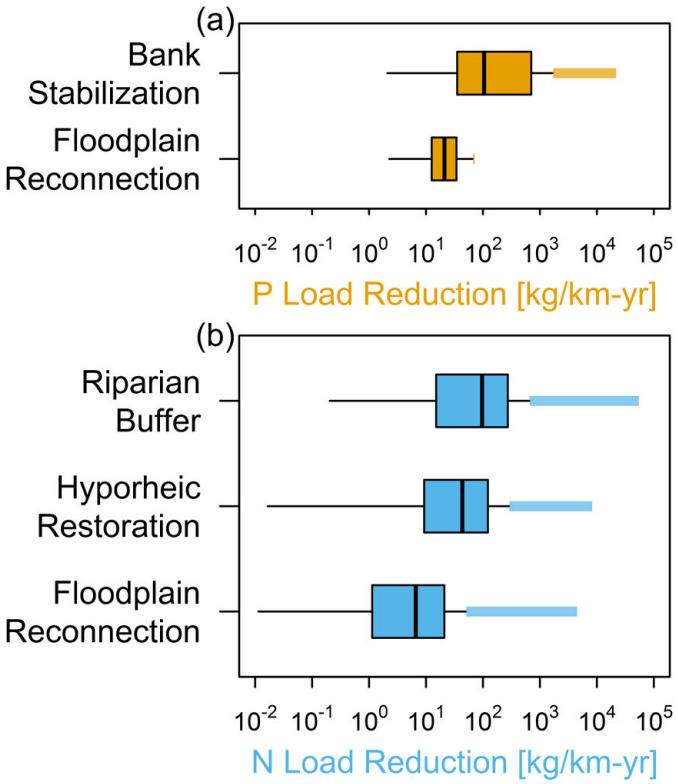

Figure 2.8: Results of Monte Carlo simulations of nutrient load reduction potential for phosphorus (a) and nitrogen (b). Box plots indicate the median, quartiles, and non-outlier maximum and minimums (1.5 times the interquartile range). The shaded rectangle indicates the range of outliers for each boxplot.

2.5 Discussion

2.5.1 Stream Restoration for Phosphorus Reduction

Phosphorus and bank erosion

As discussed previously, bank erosion in unstable streams can be a significant source of particulate phosphorus. Empirical evidence suggests that bank stabilization (e.g. bioengineering, bendway weirs, rip-rap), often in conjunction with other restoration techniques, can significantly reduce pollutant loading [*Meals*, 2001; *Carline and Walsh*, 2007]. However, post-restoration monitoring of a stream where bank stabilization and grade control structures were installed showed no change in nutrient concentrations [*Selvakumar et al.*, 2010]. Bank erosion is clearly an important phosphorus source in some watersheds (Table 2.1), but quantifying potential benefits of bank stabilization for phosphorous retention is difficult.

Estimating historic bank erosion rates is only the first step to assessing the potential for bank stabilization to reduce phosphorus loading since these rates may not be representative of future channel evolution. Conceptual channel evolution models (CEMs) predict eroding channels will at some point adjust to a new, stable state [*Schumm et al.*, 1984; *Simon*, 1989; *Hawley et al.*, 2012; *Cluer and Thorne*, 2014; *Booth and Fischenich*, 2015], assuming no further disturbances to the sediment and hydrologic regime. Therefore, current or historic erosion rates cannot simply be extrapolated for actively evolving channels as these systems should eventually stabilize on their own; although, the time scale may range from years to decades. In addition, deposition of eroded sediment on banks and floodplains may be a significant sink in some watersheds [*Hupp et al.*, 2013; *Kronvang et al.*, 2013], meaning loading estimates from bank erosion alone without accounting for sediment storage processes may overestimate total export. An additional source of uncertainty in estimating loading rates is variability in bank phosphorus content. Bank phosphorus concentrations are associated with a number of factors (soil texture, pH, metals concentrations, and the geology of the soil parent material; *Brady and Weil* [2002]) and are often highly variable, even in a single reach [*Bledsoe et al.*, 2000; *Nellesen et al.*, 2011; *Schilling et al.*, 2009]. Streambank phos-

phorus concentrations may also be higher in intensively farmed catchments [*Palmer-Felgate et al.*, 2009] or in deforested areas [*Haggard et al.*, 2007], although others have shown little correlation to land use [*Zaimes et al.*, 2008a; *Tufekcioglu*, 2010; *Nellesen et al.*, 2011].

In some cases, streambank phosphorus concentrations have been found to be positively correlated with silt-clay content [*Cooper and Gilliam*, 1987; *Bledsoe et al.*, 2000; *Agudelo et al.*, 2011; *Kerr et al.*, 2011; *Young et al.*, 2012, 2013] while others have found no correlation [*Schilling et al.*, 2009; *Hongthanat*, 2010; *Howe et al.*, 2011; *Veihe et al.*, 2011]. The reason for this discrepancy is likely rooted in differences in the types of clays in each of these regions. Phosphorus binds strongly to iron and aluminum oxides in soil. Therefore, soils with high concentrations of these compounds (especially in amorphous form) will likely have higher sorbed total phosphorus concentrations. These oxides are common in Ultisols and Oxisols, while Mollisols and other soil types dominated by silicate clays likely have low phosphorus binding capabilities [*Brady and Weil*, 2002, p. 617]. Studies in areas where silicate clays are dominant do not show a correlation between silt-clay content and TP [*Schilling et al.*, 2009; *Hongthanat*, 2010] while those with high oxide clays do demonstrate this positive correlation [*Bledsoe et al.*, 2000; *Young et al.*, 2012]. In these cases, silt-clay content may just be a proxy for metal oxide abundance. Several studies found positive correlations between metal oxide concentrations and TP, independent of the silt-clay:TP relationship [*Hongthanat*, 2010; *Kerr et al.*, 2011; *Young et al.*, 2012].

While direct quantification of bank phosphorus content through field sampling and analysis is the best approach, coarse estimates may be obtained based on regional soil phosphorus data (Figure 2.2). There appears to be a strong correlation between these two datasets, although uncertainty analysis indicates high variability. Points on Figure 2.2 fall below the 1:1 line, indicating that while the two datasets are correlated, upland phosphorus concentrations tend to be higher than streambank concentrations. While estimating actual streambank phosphorus concentrations based on this relationship is not advisable, this correlation can

at least be used to assess relative bank phosphorus levels in a preliminary assessment of phosphorus loading potential.

Differences in laboratory analysis are generally thought to have a significant influence on soil phosphorus data; however, my results suggest that differences between common total phosphorus extraction methods has a smaller effect than may have been previously thought. Nevertheless, it is still advisable to consider differences in laboratory techniques when comparing soil phosphorus data between studies. Additionally, using alternative extraction methods to estimate bioavailable phosphorus (e.g. Mehlich-3 or water extraction) is recommended to better understand potential impacts of phosphorus loading on water quality [*Fox et al.*, 2016]. Bioavailable phosphorus may be only about 10% of the total (Figure 2.3), meaning that phosphorus loading estimates from bank erosion could differ by an order of magnitude, depending on the type of phosphorus considered.

Phosphorus and other restoration techniques

Other restoration techniques, including riparian and floodplain restoration, also influence phosphorus dynamics. Phosphorus retention in riparian buffers is complex. Although buffers may trap particulate and dissolved phosphate in surface runoff [*Lee et al.*, 2003; *Newbold et al.*, 2010], groundwater phosphate concentrations often increase through buffers [*Peterjohn and Correll*, 1984; *Spruill*, 2000], potentially due to phosphate release from the reduction of iron oxyhydroxides [*Jordan et al.*, 1993]. These offsetting processes can result in little or no net retention of phosphorus in buffers [*Newbold et al.*, 2010]. Similarly, restored floodplains can be net phosphorus sources, even if they are effective nitrogen sinks [*Jones et al.*, 2015]. However, the type of restored floodplain may have an impact. A restored wetland-channel complex and two-stage ditch — a popular form of floodplain reconnection in agricultural areas — both reduced phosphorus export [*Richardson et al.*, 2011; *Davis et al.*, 2015; *Mahl et al.*, 2015].

Despite the potential for riparian buffers to be net phosphorus sources to streams, they may affect stream dynamics and reduce phosphorus loading indirectly. Vegetated stream-

banks tend to have lower erosion rates than non-vegetated banks [*Smith*, 1976; *Simon and Collison*, 2002; *Miller et al.*, 2014]. Additionally, riparian buffers may be significant sources of in-stream wood and organic carbon to streams [*Stanley et al.*, 2012], both of which can increase in-stream nutrient uptake [*Bernhardt and Likens*, 2002; *Roberts et al.*, 2007].

2.5.2 Stream Restoration for Nitrogen Reduction

Stream restoration typically targets nitrogen removal by increasing lateral and vertical hydrologic connectivity to encourage biochemical nitrogen removal, typically via denitrification. Hydrologic connectivity can be lost in degraded streams for a number of reasons. For example, channel incision lowers riparian groundwater tables, reducing denitrification potential by disconnecting the relatively anoxic, nitrate-laden groundwater with available organic carbon in the upper soil horizons. This incision results in higher nitrate loading to streams [*Schilling and Spooner*, 2006] and higher in-stream nitrate concentrations [*Groffman et al.*, 2002; *Böhlke et al.*, 2007], but not in all cases [*Schilling and Jacobson*, 2014]. Channel incision can also reduce overbank flooding, disconnecting the stream from its floodplain, an important nutrient sink. Degraded streams often become geomorphically simple, losing the complex bedforms and bed sediment heterogeneity that are important aquatic organism habitat and drive vertical hydrologic connectivity with the hyporheic zone. The hyporheic zone may be small, but it is a vitally important area for biochemical processing and nutrient removal [*Hester and Gooseff*, 2010]. Strategies to restore hydrologic connectivity and provide conditions suitable to denitrification have the greatest potential for addressing nitrogen loading.

Nitrogen and lateral connectivity

Riparian buffers have long been recognized for their potential to remove pollutants in surface and subsurface flow before they reach the stream. Under the right conditions, properly functioning riparian buffers (typically consisting of intact forest) can remove >90% of inflowing nitrate [*Peterjohn and Correll*, 1984; *Jordan et al.*, 1993; *Pinay et al.*, 1993; *Spruill*,

2000; *Liu et al.*, 2014]. A comprehensive review of published nitrate removal rates found an average removal effectiveness of $74.2 \pm 4.0\%$ (mean $\pm$ SE, *Mayer et al.* [2005]). The majority of this removal takes place in the subsurface [*Peterjohn and Correll*, 1984; *Hill*, 1996] where conditions amenable for denitrification are often found (low dissolved oxygen and available organic carbon).

Generally, nutrient removal effectiveness increases with buffer width and age [*Mayer et al.*, 2007; *Orzetti et al.*, 2010; *King et al.*, 2016]. The consensus seems to be that wider is better, although just how wide is up for debate. Effective buffer width is dependent upon a number of site specific factors including slope, soil type, incoming nutrient load, and buffer age. As buffers mature, root depth, root density, and organic carbon availability are expected to increase, leading to more conducive conditions for denitrification.

Floodplain reconnection promotes similar removal mechanisms as riparian buffers; encouraging subsurface denitrification in the riparian zone while retaining particulate and dissolved nutrients in surface flow. Floodplain reconnection aims to restore optimal conditions for denitrification and nutrient retention by raising the channel bed, removing or breaching levees, and/or re-grading and lowering banks. Natural floodplains have been demonstrated to be important areas for nitrate removal [*Forshay and Stanley*, 2005] and reconnected floodplains have the potential to be effective nutrient sinks [*Valett et al.*, 2005; *Fink and Mitsch*, 2007], removing small but potentially significant (0.6 – 23.7%) portions of a riverine nutrient load [*Sheibley et al.*, 2006; *Kronvang et al.*, 2007; *Roley et al.*, 2012a]. Floodplain reconnection can increase riparian groundwater residence time which can result in a measurable decrease in in-stream nitrate concentrations [*Kaushal et al.*, 2008]. Enhancing lateral connectivity and increasing hydraulic retention time with in-stream and floodplain wetlands can result in significant nitrogen load retention [*Browning*, 2008; *Filoso and Palmer*, 2011; *Sivirichi et al.*, 2011]. A recent comprehensive review suggested that restoring hydrologic connectivity (e.g. lowering floodplain, raising stream bottom, increasing sinuosity) has generally positive out-

comes for nutrient processing and retention (42 – 83% success rate, depending on practice) [*Newcomer Johnson et al.*, 2016].

Nitrogen and vertical connectivity

Although lateral connectivity is an important and visible linkage, vertical connectivity between the stream and subsurface can also influence nutrient retention and removal. In-channel structures (e.g. riffles, cross vanes, weirs, etc.) can increase nutrient uptake by enhancing in-stream transient storage [*Ensign and Doyle*, 2005; *Baker et al.*, 2012] and hyporheic exchange [*Kasahara and Hill*, 2006b; *Hester and Doyle*, 2008; *Crispell and Endreny*, 2009; *Azinheira et al.*, 2014]. Hyporheic exchange and subsurface nitrate removal may be significant at constructed riffles [*Kasahara and Hill*, 2006a, b; *Knust and Warwick*, 2009], cross-vanes [*Daniluk et al.*, 2013], and other in-channel structures [*Hester and Doyle*, 2008]. In addition, these installed structures can create secondary geomorphic features (e.g. pools and riffles) which can induce greater hyporheic exchange than the structures themselves [*Fanelli and Lautz*, 2008; *Gordon et al.*, 2013]. Direct modification of subsurface hydraulic conductivity has also been suggested as a potential strategy to enhance hyporheic exchange [*Vaux*, 1968; *Hester and Gooseff*, 2010; *Hester and Cranmer*, 2014]. Modeling suggests that these types of features would function similarly to natural geomorphic features in driving subsurface flux [*Ward et al.*, 2011].

Other, more natural restoration techniques can also enhance in-stream nutrient removal. In-stream wood can reduce flow velocities [*Elosegi et al.*, 2016], enhance surface transient storage, and provide similar nitrate uptake benefits as more construction-intensive structures [*Mueller Price et al.*, 2016]. Installed or natural log jams trap organic matter [*Wallace et al.*, 1995; *Quinn et al.*, 2007] and these organic debris dams have higher denitrification potential compared to other geomorphic features such as gravel bars, pools, and riffles [*Groffman et al.*, 2005; *Harrison et al.*, 2012]. Since in-stream wood abundance has often been significantly reduced in urban and degraded streams [*Booth et al.*, 1996; *Segura and Booth*, 2010], riparian planting may be an appropriate restoration strategy to restore sustainable organic carbon

fluxes to streams [*Stanley et al.*, 2012]. However, in-stream wood may not be retained in flashy urban streams [*Larson et al.*, 2001], and can be hazardous to infrastructure and boaters.

Beaver reintroduction has been proposed as a viable and cost-effective stream restoration technique [*Roni and Beechie*, 2013; *Pollock et al.*, 2014]. Beaver dams can achieve many restoration objectives including increase geomorphic complexity, serve as grade control, and increase nutrient retention, and have the added benefit of being more resilient than engineered structures. Beaver dams can induce significant hyporheic flux [*Fanelli and Lautz*, 2008] and beaver ponds can be significant nutrient sinks [*Law et al.*, 2016], especially at high flows [*Maret et al.*, 1987]. Furthermore, denitrification in beaver ponds is significant and they may be important watershed-scale nitrate sinks [*Lazar et al.*, 2015].

On the other hand, removal of anthropogenic dams is an increasingly common restoration practice for increasing longitudinal connectivity and restoring natural flow regimes; however, this may have unintended consequences for nutrient dynamics. Dams create conditions conducive to nutrient retention (e.g. deposition and biotic processing in anoxic bed sediments) and dam removal can decrease nutrient uptake and increase concentrations [*Doyle et al.*, 2003]. Dams may also be important watershed scale nitrogen sinks. Luckily, many nitrogen retaining dams are on smaller order streams and removal of dams on larger rivers may have fewer detrimental effects on nitrogen storage, and greater benefits for fish passage [*Gold et al.*, 2016].

Despite the promise of direct in-channel modifications for increasing hydraulic residence time and hyporheic exchange, significant limitations exist. Only a small fraction (<1%) of the total stream discharge may be exchanged at a given structure [*Gordon et al.*, 2013; *Azinheira et al.*, 2014] and subsurface hydraulic residence times and organic carbon availability may be insufficient for adequate nutrient removal to occur [*Gordon et al.*, 2013; *Smidt et al.*, 2014]. Furthermore, bed compaction and use of large footer boulders for structure installation can result in significantly lower hyporheic exchange compared with reference reaches [*Becker*

et al., 2013] . Similar limitations exist for floodplains and other forms of lateral connectivity. Nitrate removal in floodplains may be limited due to infrequent inundation [*Azinheira et al.*, 2014; *Jones et al.*, 2015]. Furthermore, increased hydrologic connectivity may be insufficient for nutrient retention in areas with very high nitrogen loads [*Roley et al.*, 2012b; *Davis et al.*, 2015; *Mahl et al.*, 2015]. Due to small removal rates in the hyporheic zone and floodplains, unreasonably long reaches of stream need to be restored to meet nutrient removal goals [*Hester et al.*, 2016]. Finally, floodplains, riparian areas, and the hyporheic zone can all be net sources of nutrients — and more toxic compounds (e.g. mercury) — depending on oxygen availability and redox conditions [*Vidon et al.*, 2010; *Jones et al.*, 2015].

Factors controlling denitrification rates

Stream denitrification rates have been shown to be influenced by stream nitrate concentrations [*Piña-Ochoa and Álvarez-Cobelas*, 2006; *Seitzinger et al.*, 2006; *Böhlke et al.*, 2009; *Mulholland et al.*, 2009; *Roley et al.*, 2012a], land use [*Mulholland et al.*, 2008, 2009], and measurement method [*Groffman et al.*, 2006; *Böhlke et al.*, 2009]. My results confirm the importance of these variables, but is the first study that quantifies the relative magnitude of their effects. I found that nitrate is by far the most influential, while land use and method are of similar importance (Figure 2.7). This aligns with previous conclusions that higher denitrification rates in disturbed systems is primarily due to higher nitrate loading [*Mulholland et al.*, 2008].

Climate emerges as the most important variable for riparian denitrification rates, but is only moderately important for streams. Using latitude as a coarse estimate of climate, *Piña-Ochoa and Álvarez-Cobelas* [2006] found no correlation with stream denitrification. For European riparian sites, denitrification has also been shown to be invariant with climate [*Hefting et al.*, 2004] while others demonstrated some correlation with temperature [*Pinay et al.*, 2007]. The difference in the influence of climate on denitrification rates could be due to fundamental process differences between streams and riparian sites; however, other factors may also have influenced the results. For example, the vast majority of the data are from

Cf- and Df- climates, temperate and continental climates with no dry seasons. Additionally, stream sites encompass nine climate types compared to five for riparian sites which could help explain the relative importance of climate between these two datasets.

The influence of vegetation type on nutrient removal in riparian buffers has been subject to some debate. Our analysis suggests that bare riparian sites tended to have higher denitrification rates than vegetated sites, although the small size of the bare subset (n = 3) makes the significance of this difference suspect. Although riparian vegetation type overall was somewhat influential, it had less of an effect than climate, method, or temporal scale. Others have suggested that total nitrate removal [*Groffman et al.*, 2003; *Schoonover and Williard*, 2003; *Mayer et al.*, 2007; *King et al.*, 2016] and denitrification rates [*Hefting et al.*, 2004] are not significantly different in buffers with different vegetation types. Similarly, I found no significant difference between denitrification rates in forested and grassed buffers.

Carbon limitation may be a significant factor influencing denitrification in degraded streams, especially those with high nitrogen loading [*Lefebvre et al.*, 2004; *Johnson et al.*, 2009; *Newcomer et al.*, 2012]. Although only a limited number of studies in my database examined what was limiting denitrification (carbon, nitrate, or both), there appears to be some correlation with land use. Impacted sites (urban and/or agriculture) had stream denitrification rates that were more often limited by carbon or carbon and nitrate than reference sites (Table 2.4; chi-squared goodness-of-fit test, p = 0.035). This is a tentative conclusion using a limited dataset but the importance of carbon limitation is supported by empirical studies. Carbon deficits in historically disconnected floodplains can lead to lower denitrification potential than hydrologically connected floodplains [*Theriot et al.*, 2013] and experimental carbon addition can increase denitrification rates to levels observed in reference sites [*Ullah and Faulkner*, 2006]. Restored stream reaches may also have lower denitrification rates due to lower organic carbon availability [*Gift et al.*, 2010].

Short term organic carbon additions, whether experimental or natural (i.e. leaf litter), can enhance removal of both nitrate and phosphorus [*Mulholland et al.*, 1985; *Bernhardt and*

Table 2.4: Contingency table of number of studies with various limiting factors for in-stream denitrification rates by watershed land use type.

	Limiting Factor		
Land Use	Both	Carbon	Nitrate
Impacted (Ag or Urban)	9	4	5
Reference	1	0	6

Likens, 2002; *Argerich et al.*, 2008; *Aldridge et al.*, 2009] and enhance subsurface denitrification [*Robertson and Merkley*, 2009; *Zarnetske et al.*, 2011]. More labile forms of carbon (e.g. leaf litter; *Aldridge et al.* [2010]) are likely to be a more important control on in-stream nutrient removal than coarser in-stream wood [*Wallace et al.*, 1995]. However, while in-stream wood may not be a significant source of bioavailable carbon, it is effective at trapping other sources of more labile organic carbon [*Wallace et al.*, 1995; *Quinn et al.*, 2007].

2.5.3 Implications for Stream Restoration

The number of studies with sufficient data to confidently assess the performance of stream restoration projects is increasing, but there is still comparatively little information for quantitatively evaluating the relative efficacy of different restoration methods for achieving nutrient reduction goals. The complexity of stream ecosystems and the significant variability among regions, watersheds, and sites further complicates comparisons. Because of these issues, previous reviews of stream restoration used self-reported success of individual studies, rather than some objective measure of restoration benefits. Despite these concerns, *Palmer et al.* [2014b] found that riparian restoration had the highest success in increasing nutrient uptake rates and reducing fluxes (88%), followed by in-stream structure installation (63%), wetland creation (25%), and channel reconstruction (14%). However, sample sizes were small and reported improvements were not necessarily statistically significant. *Newcomer Johnson et al.* [2016] found positive nutrient retention results were reported in 42 – 83% of projects for restoration strategies that increased hydrologic connectivity (e.g. floodplain connection, increased sinuosity).

While some success has been observed, it is important to recognize the limitations of stream restoration. Degraded streams may have high nutrient uptake rates, comparable to or greater than reference systems [*Bernhardt and Palmer*, 2007; *Mulholland et al.*, 2008; *Johnson et al.*, 2009]. However, this is largely the result of higher nutrient loading to these streams, and removal efficiency is often lower than in undisturbed streams [*Mulholland et al.*, 2008], a conclusion supported by my compiled denitrification data. This has important implications for stream restoration in these disturbed streams. There is likely some maximum capacity for nutrient assimilation in streams and — at a certain point — stream restoration will be ineffective for improving water quality. It may be tempting to assume that degraded streams exhibit no nutrient removal and that any stream restoration will be an improvement, but this is unlikely. This is not to say that restoration of degraded streams is not beneficial, only that it is important to consider site-specific context in designing a restoration strategy. For example, a degraded stream with reduced geomorphic complexity may have significant denitrification potential but few active denitrification sites. Increasing the area of sites conducive to denitrification (e.g. hyporheic exchange sites, debris dams, bedforms) can increase total nitrate removal.

The potential constraint on in-stream nutrient processing has led to the suggestion that stream restoration alone may be insufficient for reducing nutrient concentrations to desired levels if no upland best management practices are incorporated [*Walsh et al.*, 2005; *Bernhardt and Palmer*, 2007; *Craig et al.*, 2008; *Selvakumar et al.*, 2010]. Properly designed stormwater controls and source reduction strategies (e.g. fixing leaky sewers, *Pennino et al.* [2016]) can reduce nutrient delivery to streams and potentially improve the success of in-channel restoration efforts [*Charbonneau and Resh*, 1992]. There is an increasing recognition that urban stream restoration requires a watershed-scale approach, addressing causes of degradation (e.g. altered water and sediment regimes) rather than applying the band-aids of reach-scale restoration projects [*Roni and Beechie*, 2013; *Vietz et al.*, 2016].

There is evidence for nutrient removal in restored streams at small spatial and short temporal scales, but it is uncertain how these observations translate into broader water quality benefits. Removal is limited by inadequate hyporheic exchange at individual in-stream structures, infrequent floodplain inundation, and groundwater bypassing or undercutting riparian zones. Stream restoration projects are generally small scale, and may not result in measurable in-stream benefits [*Sutton et al.*, 2010; *Collins et al.*, 2013; *Muller et al.*, 2016]. These results lead to a disconcerting conclusion. While stream restoration can successfully remove nutrients from the stream, the benefits are generally small relative to the scale of the problem and unreasonably large segments of streams would have to be modified to achieve desirable benefits from restoration alone [*Hester et al.*, 2016].

2.6 Conclusions and Recommendations

Despite the many limitations of existing data on the effects of stream restoration on nutrient dynamics, I can make some general conclusions and recommendations:

- Bank stabilization has the greatest potential to reduce phosphorus loading in highly unstable streams, but other restoration strategies have a much smaller effect on phosphorus fluxes.

- Structures that are already incorporated into stream restoration designs can be constructed to encourage hyporheic exchange and nutrient processing through enhanced geomorphic complexity and bedforms, especially during low flow. However, low surface-subsurface exchange rates limit removal potential. The largest nitrogen removal potential likely comes from large scale manipulations to increase hydraulic retention time (e.g. in-channel and floodplain wetlands and stormwater ponds).

- Riparian buffers remove groundwater nitrate, protect streambanks, supply in-stream wood and organic carbon to increase in-stream processing, and are generally less intru-

sive and more cost-effective than construction-heavy restoration techniques. However, it is still unclear how significantly buffers affect stream water quality.

- Managing flows of water and sediment and reducing nutrient loading through source controls remains an essential strategy for improving water quality. A combination of restoration strategies that reduce nutrient inputs to streams, re-establish riparian functions, provide balanced water and sediment regimes, and increase in-stream nutrient processing and retention will likely be most effective for improving water quality.

The increase in published stream restoration monitoring studies is encouraging, but the lack of consistent methodology and failure to measure the right metrics makes it difficult to draw conclusions about restoration success [*Rubin et al.*, 2017]. Measuring the benefits of restoration projects is also complicated by the variable nature of in-stream nutrient concentrations; it is difficult to separate the effects of restoration projects from the noise of water quality data. These shortcomings can be addressed by more formal and statistically rigorous monitoring designs. Restoration monitoring should focus on metrics that are specific to project objectives [*Palmer et al.*, 2005] and should follow accepted statistical designs (e.g. Before-After-Control-Impact), comparing restored and control (both impaired and reference) sites over years to decades. Long term monitoring is required since there may be significant lag time between completion of restoration projects and observed improvements [*Meals et al.*, 2010]. Furthermore, monitoring should be well planned and hypothesis driven (e.g. bank stabilization will reduce phosphorus loads by 10%), rather than an afterthought. The complexity of stream restoration lends itself to adaptive management. This is an active approach to resource management, requiring constant monitoring to test the effects of management interventions (e.g. restoration) and updating management approaches as new data are collected [*Walters*, 1986; *Allen et al.*, 2011]. Designing restoration projects as experiments and rigorously monitoring them would reduce uncertainty and increase our knowledge of the effects of restoration on nutrient dynamics.

Existing studies suggest that certain restoration strategies may enhance nutrient retention and removal in stream and riparian systems; however, this is still an emerging science with insufficient evidence to precisely quantify the effects of different restoration strategies across regions and various hydrologic, geologic, and land use contexts. Given the attention stream restoration has been receiving, an increasing emphasis on improved effectiveness monitoring, and the growing number of published studies on nutrient dynamics in restored systems, the future looks promising for improved understanding of the role of stream restoration in nutrient management.

Chapter 3

Parsimonious sediment transport equations based on Bagnold's stream power approach

Summary

It is increasingly recognized that effective river management requires a watershed scale approach. Sediment transport processes are relevant to a number of river functions but quantifying sediment fluxes at network scales is hampered by the difficulty of measuring the variables required for most sediment transport equations (e.g. shear stress, velocity, and flow depth). To address this issue, I developed new bedload and total load sediment transport equations based on specific stream power. These equations use data that are relatively easy to collect or estimate throughout stream networks using remote sensing and other available data: slope, discharge, channel width, and grain size. The new equations are parsimonious yet have similar accuracy to other, more established, alternatives. I further confirm previous findings that the dimensionless critical specific stream power for incipient particle motion is generally consistent across datasets, and that the uncertainty in this parameter has only a minor impact on calculated sediment transport rates. Finally, I test the new bedload transport equation by applying it in a simple channel incision model. These model results are in close agreement to flume observations and can predict incision rates better than a more complicated morphodynamic model. These new sediment transport equations are well

Lammers, R. W. and B. P. Bledsoe (2018), Parsimonious sediment transport equations based on Bagnold's stream power approach, *Earth Surface Processes and Landforms*, 43: 242 – 258. doi: 10.1002/esp.4237.

Roderick W. Lammers and Brian P. Bledsoe had the idea for a new set of sediment transport equations. Roderick W. Lammers collected the necessary data from the literature, performed the analyses, and wrote the manuscript. Brian P. Bledsoe contributed to the discussion and edited the manuscript.

suited for use at stream network scales, allowing quantification of this important process for river management applications.

3.1 Introduction

Geomorphologists and engineers spent the last century developing empirical and process-based formulas for modeling sediment transport in rivers. Unfortunately, these formulas are data intensive and difficult to apply at larger spatial scales and in data poor environments. Managers and researchers recognize the importance of understanding sediment dynamics at the watershed scale [*Owens*, 2005], but existing sediment transport formulas are not well suited for this type of application. This watershed scale approach is necessary for numerous management issues, including assessing channel erosion and deposition potential [*Lea and Legleiter*, 2016], estimating flood risk [*Stover and Montgomery*, 2001], protecting benthic habitat [*Newson and Newson*, 2000; *Rice et al.*, 2001], and restoring natural sediment regimes [*Wohl et al.*, 2015a]. In this chapter, I present new sediment transport equations that use readily collected and widely available data for application to these challenging problems.

Many sediment transport equations rely on shear stress (requiring flow depth) [*Meyer-Peter and Müller*, 1948; *Parker*, 1990] or velocity [*Brownlie*, 1982] or both [*Engelund and Hansen*, 1967]. Although these variables are physically linked to sediment transport processes, their temporal and spatial variability makes them difficult to measure or model. This difficulty in quantifying flow depth and velocity makes it challenging to apply equations based on these variables at the watershed scale.

An alternative variable is specific stream power:

$$\omega = \frac{\Omega}{w} = \frac{\rho g Q S}{w} \tag{3.1}$$

where Ω is unit-length stream power [W m^{-1}], w is channel width [m], Q is discharge [m^3 s^{-1}], and ω is specific stream power [W m^{-2} or equivalently N m^{-1} s^{-1}]. Specific stream

power is relatively straightforward to estimate throughout river basins using remote sensing data to quantify channel slope and width and stream gages, hydrologic models, or regional empirical relationships to quantify discharge [*Reinfelds et al.*, 2003; *Phillips and Desloges*, 2014]. Stream power mapping has been successfully used to identify erosional and depositional areas [*Bizzi and Lerner*, 2015; *Parker et al.*, 2015]; however, quantitative estimates of sediment transport capacity may be needed to answer river management questions. The sediment transport equations developed here address this gap.

Others have recognized the benefits of a stream power approach to sediment transport modeling and several existing sediment transport equations use specific stream power. The most widely used of these is the *Bagnold* [1980] empirical bedload equation; however, this equation also relies on flow depth — directly and indirectly through calculation of the critical specific stream power for incipient motion. This renders the equation impractical to apply throughout a stream network. I adapted the Bagnold bedload equation — eliminating its dependence on flow depth — and developed a total load equation using the same set of variables.

The proliferation of sediment transport equations has been criticized as excessive — "there appears to be more bed load formulas than there are reliable data sets by which to test them" [*Gomez and Church*, 1989] — and the development of yet another equation may be unwelcome. Sediment transport formulas, however, should be considered part of a toolbox, where each tool has its own purpose. While I add more equations to the toolbox, they have a specific role that is currently unfulfilled — to model sediment transport where only limited data are available.

This chapter has three objectives. First, I test several methods to estimate critical specific stream power for incipient motion. I show that a simple approach using only sediment grain size [*Parker et al.*, 2011] is as accurate as more data intensive methods. Second, I develop new bedload and total load formulas based on Bagnold's stream power approach but with no flow depth term. I examine the sensitivity of these new equations and show the most difficult

to quantify variables (grain size and dimensionless critical specific stream power) have the smallest influence on calculated transport rates. Third, I use the bedload equation in a simple channel incision model and show it is as accurate as a physically detailed morphodynamic model. These new transport equations are accurate and rely on variables that are easy to quantify at network scales, making them suitable for a wide array of watershed management applications.

3.2 Background

3.2.1 Limitations of Shear Stress-Based Transport Equations

Sediment transport equations generally follow a consistent pattern. Some measure of the excess available force or energy of the flowing water (i.e. total force less some critical force for incipient motion) is directly related to sediment transport rates. Many equations use excess shear stress [*Meyer-Peter and Müller*, 1948; *Parker et al.*, 1982; *Wilcock and Crowe*, 2003] where critical shear stress is often expressed in dimensionless form, also known as the Shields parameter (θ_c; *Shields* [1936]):

$$\theta_c = \frac{\tau_c}{((\rho_s - \rho)gD_s)} = \frac{hS}{((s-1)D_s)} \tag{3.2}$$

where τ_c is critical shear stress [Pa], ρ_s and ρ are sediment and fluid density [kg m^{-3}], g is gravitational acceleration [m s^{-2}], h is flow depth [m], S is water surface slope [m m^{-1}], D_s is a representative grain size [m], usually assumed to be the median grain size, D_{50}, and s is the sediment specific gravity (assumed to be 2.65). Shear stress and the Shields parameter rely on flow depth, a limitation for quantifying incipient motion in data poor areas or throughout stream networks. Depth may be calculated using discharge and a flow resistance equation, but this approach relies on assumptions of channel geometry which are not always applicable [*Recking*, 2013].

In addition to relying on flow depth, another downside of using the Shields parameter is its tendency to increase with channel slope [*Lamb et al.*, 2008; *Recking*, 2009; *Parker et al.*, 2011; *Camenen*, 2012; *Ferguson*, 2012] which could cause over-prediction of sediment transport rates in steep streams. Stream power based sediment transport equations may be more accurate in these cases because dimensionless critical specific stream power is uncorrelated with slope [*Ferguson*, 2005; *Parker et al.*, 2011].

Despite its popularity, shear stress may not be the most appropriate basis for sediment transport equations. In a comprehensive analysis, specific stream power was shown to be more correlated with bedload transport rates than either shear stress or velocity [*Parker*, 2010; *Parker et al.*, 2011]. Excess specific stream power to the 3/2 power — without any other variables — predicted bedload transport rates with an R^2 value of 0.656 [*Martin and Church*, 2000], further demonstrating the strength of this variable for sediment transport modeling. In a comparison study using data from a gravel-bed Austrian river, stream power equations were shown to perform markedly better than shear stress formulas [*Habersack and Laronne*, 2002]. Shear stress may be more physically representative of sediment transport mechanisms than specific stream power; however, the reach average shear stress is often used, which is not an accurate estimate of the force acting on individual grains.

3.2.2 Incipient Motion

Several methods have been proposed to quantify critical specific stream power (ω_c) for incipient motion, but most require additional data that are not easily quantified at the watershed scale. For example, the *Bagnold* [1980] formula for ω_c is dependent on flow depth to account for flow resistance (via relative roughness):

$$\omega_c = 5.75 \times \left(\frac{g}{\rho}\right)^{0.5} [0.04(\rho_s - \rho)D_{50}]^{3/2} \times \log \frac{12h}{D_{50}} \tag{3.3}$$

where ω_c is in units of kg m^{-1} s^{-1}. Note that the units here are different from in Equation (3.1) because Bagnold divided ω by gravitational acceleration to yield the same units as bedload transport rate [*Ferguson*, 2005; *Parker et al.*, 2011].

Camenen [2012] and *Ferguson* [2012] used theoretical approaches to develop equations to predict dimensionless critical specific stream power (ω_{c*}) as a function of grain size and grain sorting (D_{84}/D_{50}), respectively. Dimensionless specific stream power is defined as:

$$\omega_* = \frac{\omega}{\rho((s-1)gD_{50})^{3/2}} \tag{3.4}$$

where here, ω is in units of N m^{-1} s^{-1} (or W m^{-2}).

Because grain size and grain sorting are both correlated with channel slope, Camenen and Ferguson's equations both predict a non-linear relationship between slope and ω_{c*}. But, these equations predict ω_{c*} varies by only a factor of ~1.5 for a wide range of slopes (0.02 – 30%). *Eaton and Church* [2011] proposed another method for determining ω_{c*} using the Shields parameter and a flow resistance term. Since both parameters vary with slope, this approach also has an inherent slope dependence.

Parker et al. [2011] collected incipient motion data from field and flume studies and showed that dimensionless critical specific stream power (ω_{c*}) was not correlated with slope and had a mean value of ~0.1. Using this estimate, ω_c can be calculated from Equation (3.4) using only grain size.

The *Parker et al.* [2011] method for quantifying ω_c is attractive in its simplicity, but other approaches may be more robust [*Bagnold*, 1980; *Eaton and Church*, 2011; *Camenen*, 2012; *Ferguson*, 2012]. I compare the accuracy of all these methods to determine which is most appropriate for the new sediment transport equations.

3.2.3 Sediment Transport Equations

Bagnold [1966] defined stream power as the available power supply in a stream and used it to derive a theoretical bedload transport relationship [*Bagnold*, 1973]. Unfortunately, this

equation failed to match field observations, leading Bagnold to develop an empirical version [*Bagnold*, 1977, 1980]:

$$\begin{aligned} &\frac{q_b}{q_{b,ref}} = \frac{s}{s-1}\left[\frac{\omega-\omega_c}{(\omega-\omega_c)_{ref}}\right]^{3/2}\left(\frac{h}{h_{ref}}\right)^{-2/3}\left(\frac{D_{50}}{D_{50,ref}}\right)^{-1/2} \\ &q_{b,ref} = 0.1 \text{ kg m}^{-1} \text{ s}^{-1},\ (\omega-\omega_c)_{ref} = 0.5\text{kg m}^{-1} \text{ s}^{-1} \\ &h_{ref} = 0.1 \text{ m}, D_{50,ref} = 1.1\text{e}{-3} \text{ m} \end{aligned} \tag{3.5}$$

where q_b is the unit bedload transport rate (kg m^{-1} s^{-1} dry mass), and ω and ω_c are specific and critical specific stream power, respectively (also in kg m^{-1} s^{-1}). The term $s/(s-1)$ was added to convert from immersed to dry mass [*Gomez and Church*, 1989]. The subscript $_{ref}$ refers to reference values which Bagnold used to make this empirical equation dimensionless.

Martin and Church [2000] made this equation dimensionally consistent without relying on reference values:

$$q_b = [\omega-\omega_c]^{3/2}\frac{D_{50}^{1/4}}{h}\frac{1}{\rho_r^{1/2}g^{1/4}} \tag{3.6}$$

where ρ_r is submerged sediment density $(\rho_s - \rho)$. They determined that this equation outperformed all other variations they examined, including Bagnold's 1980 version. A more recent analysis using a comprehensive bedload transport dataset resulted in a purely empirical equation using only dimensionless specific stream power [*Parker*, 2010; *Parker et al.*, 2012]:

$$q_{b*} = \begin{cases} 100\omega_*^6, & \text{for } \omega_* < 0.25 \\ 0.2\omega_*^{1.5}, & \text{for } \omega_* \geq 0.25 \end{cases} \tag{3.7}$$

where q_{b*} is dimensionless unit bedload transport rate (analogous to Einstein's sediment transport parameter but with different units of bedload transport):

$$q_{b*} = \frac{q_b}{\rho((s-1)gD_{50})^{3/2}} \tag{3.8}$$

where q_b is in units of N m^{-1} s^{-1} (submerged weight of sediment). Another empirical relationship relates dimensionless specific stream power to a new dimensionless transport parameter, E^* [*Eaton and Church*, 2011]:

$$E^* = \left[0.92 - 0.25 \left[\frac{\omega_{c*}}{\omega_*}\right]^{1/2}\right]^9 \tag{3.9}$$

where ω_{c*} can be calculated using the Shields parameter and a flow roughness variable (see Section A). The dimensionless transport parameter is a function of transport rate, unit discharge, and slope:

$$E^* = \frac{(s-1)q_b}{qS} \tag{3.10}$$

where q_b is in units of m^3 m^{-1} s^{-1} and q is unit discharge (Q/w; m^2 s^{-1}).

Williams [1970] used flume data — accounting for the effects of wall roughness — to show that, all else being equal, sediment transport rate increased as depth decreased. Expanding this to field data, *Bagnold* [1977] confirmed that bedload transport rate was inversely related to relative roughness (h/D_{50}). While the *Bagnold* [1980] transport equation did not contain relative roughness explicitly, sediment transport rate is inversely related to flow depth (Equation (3.5)).

Since the purpose of simplifying the Bagnold sediment transport relationship is to eliminate the depth term without losing significant predictive power, I selected another variable that is proportional to depth — unit discharge ($q = Q/w$). From continuity, I can show that flow depth is related to unit discharge:

$$\begin{aligned} Q &= whV \\ \frac{Q}{wV} &= \frac{q}{V} = h \end{aligned} \tag{3.11}$$

where V is flow velocity [m s^{-1}], and q is unit discharge [m^2 s^{-1}]. Depth and unit discharge are only equal at constant velocity. Also, depth is influenced by roughness and I neglect roughness effects on sediment transport by using unit discharge instead. Despite this simpli-

fication, I will show that using q in place of depth does not substantially reduce the accuracy of the sediment transport equations. In this paper, I developed and tested new bedload and total load equations with a similar form as *Bagnold* [1980] and *Martin and Church* [2000], but using unit discharge in place of depth. These equations have the following structure:

$$q_s = a[\omega - \omega_c]^b {D_s}^c q^d \tag{3.12}$$

where a, b, c, and d are empirically fit values.

3.3 Methods

3.3.1 Data Collection

I collected flume data of incipient grain motion from the literature, including sources used by others in critical stream power analyses (Table 3.1; *Parker et al.* [2011]; *Camenen* [2012]; *Ferguson* [2012]). The definition of incipient motion varied among these datasets which may impact direct comparison among sources. The full incipient motion database is included in the supplemental material.

Sources of flume and field bedload transport data are summarized in Table 3.2. When testing bedload transport equations, it is important to use data at equilibrium transport [*Gomez and Church*, 1989]. Equilibrium transport assumes steady flow and constant sediment characteristics but may be practically achieved if the material in transport is representative of the material in the streambed. The data compiled by *Gomez and Church* [1988] meet the equilibrium transport standard by ensuring the bedload D_{50} is within one phi unit of the subsurface bed D_{50} (where phi $= -\log_2(D_s)$). Additionally, *Gomez and Church* [1988] excluded flume data if bedforms were observed, the Froude number was greater than one, or the width-depth ratio was less than ten.

Additional bedload transport data were obtained from other sources [*Yang*, 1979; *Williams and Rosgen*, 1989; *Bravo-Espinosa*, 1999; *Almedeij*, 2002; *King et al.*, 2004; *Parker*, 2010;

Hinton et al., 2016]. I assessed equilibrium transport conditions using two methods. If full bed material and bedload grain size distributions were available, I adjusted transport rates to include only the fraction of the bedload that was within one phi unit of the bed material D_{50} (after *Parker* [2010]). If these full grain size distributions were not available, I only included data where the bedload D_{50} was within one phi unit of the subsurface D_{50} (after *Gomez and Church* [1988]).

I obtained total load transport data from *Brownlie* [1981]. Only a subset of these data were used, consistent with Brownlie's criteria for the development of his total load equation [*Brownlie*, 1982]. I filtered data using the following restrictions: 0.062 mm $< D_{50} <$ 2 mm; $\sigma_g < 5$; $w/h > 4$; $R_h/D_{50} > 100$, and $Q_t > 10$ ppm. Despite using the same criteria, I kept more data points than Brownlie (1,463 compared to 999). I made sidewall corrections [*Vanoni*, 1975] to adjust hydraulic radius for the *Ackers and White* [1973], *Engelund and Hansen* [1967], and *Brownlie* [1982] total load equations. The full bedload and total load datasets are included in the supplemental material.

Table 3.1: Summary of data used in the incipient motion analysis. [1]This analysis used the full sediment transport dataset.

Study	Abbr.	Type	N	Slope [m m^{-1}]	ω [W m^{-2}]	D_{50} [mm]	Incipient Method
Bathurst et al. [1987]	Bathurst	Flume	12	0.005–0.09	7.6–55.6	11.5–44.3	Extrapolating graphical relationships between water discharge and sediment discharge
Bathurst [1979] cited in *Bathurst* [2013]	Bathurst 2	Flume	3	0.05–0.08	5.1–35.3	8.8–34	Extrapolating graphical relationships between water discharge and sediment discharge
Dey and Raju [2002]	Dey.Raju	Flume	33	0.0101–0.0169	1.2–4.6	4.89–9.47	All surface fractions showed movement
Ikeda [1983] cited in *Bathurst* [2013]	Ikeda	Flume	3	0.0025–0.009	2.7–4.6	6.4	Extrapolating graphical relationships between water discharge and sediment discharge
Johnson [1943] cited in *Parker et al.* [2011]	Johnson	Flume	21	0.0015–0.1	0.1–1.8	1.4–4.4	q_{b*} = 0.0001; extrapolated from sediment transport data[1]
Mizuyama [1977]	Mizuyama	Flume	12	0.01–0.2	2.1–22.4	6.4–22.5	Extrapolating graphical relationships between water discharge and sediment discharge
Meyer-Peter and Müller [1948] cited in *Bathurst* [2013]	MPM	Flume	7	0.00275–0.0065	1.2–62	3.3–28.65	Extrapolating graphical relationships between water discharge and sediment discharge
Parker et al. [2011]	Parker	Flume	14	0.0071–0.0167	3.3–8.6	6–11.5	q_{b*} = 0.0001; extrapolated from sediment transport data[1]
Prancevic and Lamb [2015] and *Prancevic et al.* [2014]	Prancevic	Flume	20	0.031–0.41	5.6–12.9	15	Extrapolating graphical relationships between water discharge and sediment discharge
Shvidchenko and Pender [2000] cited in *Parker et al.* [2011]	S.P	Flume	33	0.0019–0.0287	0.2–9.8	1.5–12	q_{b*} = 0.0001; extrapolated from sediment transport data[1]
Saad [1989]	Saad	Flume	21	0.0049–0.0253	0.2–29.8	7–40	W = 0.02 [*Taylor*, 1971]
King et al. [2004]	--	Field	45	0.0005–0.057	18.3–174.4	9–186	q_{b*} = 0.0001; extrapolated from sediment transport data[1]

Table 3.2: Summary of bedload transport data used in this analysis (excluding data where no transport was predicted). [1]Data used to fit Equation (3.15).

Source	Type	Site	N	D_{50} [m]	S [m m^{-1}]	q_b [kg m^{-1} s^{-1}]	ω [W m^{-2}]
Almedeij [2002]	Field	Goodwin Creek	92	0.0117	0.0024 - 0.0034	0.0057 - 2.98	25.5 - 45.1
Bravo-Espinosa [1999]	Field	Chippewa River at Durand	25	6.00E-04	3e-04 - 4e-04	0.00386 - 0.11059	0.9 - 11.4
		Chippewa River at Pepin	18	5.00E-04	2e-04 - 6e-04	0.00684 - 0.05307	1.3 - 5.3
		North Fork Toutle River	6	0.01	0.0032 - 0.0079	1.61224 - 5.72881	71.3 - 123.2
		Toutle River	13	0.008	0.0019 - 0.0055	0.14581 - 3.46269	17.1 - 412.3
		Wiconsin River	19	4.00E-04	2e-04 - 5e-04	0.00479 - 0.13881	0.8 - 17.9
		Yampa	29	6.00E-04	5e-04 - 9e-04	0.00812 - 0.85806	1.8 - 39.9
Gomez and Church [1988]	Field	Clearwater River[1]	5	0.032	4e-04 - 6e-04	0.0317 - 0.2581	47.2 - 129.2
		East Fork River[1]	38	0.0012	7.00E-04	0.0112 - 0.1268	3.2 - 15.1
		Elbow River[1]	19	0.027	0.0074	0.0385 - 0.9242	74.6 - 146.7
		Mountain Creek[1]	37	9.00E-04	0.0015 - 0.0016	0.00467 - 0.0262	0.6 - 1.6
		Snake River[1]	17	0.032	7e-04 - 0.0011	0.0161 - 0.3103	43.5 - 177.1
		Tanana River[1]	14	0.0076	5e-04 - 6e-04	0.0327 - 0.2482	13.1 - 27.3
	Flume	ETH: 2[1]	14	0.0015	0.0022 - 0.0029	0.0045 - 0.147	0.9 - 4.7
		ETH: 3[1]	6	0.0037	0.008 - 0.0083	0.059 - 0.332	4 - 8.8
		IIHR: 1	11	0.0044	0.0035 - 0.0048	0.00012 - 0.01844	1.1 - 3.2
		IIHR: 2	25	0.0034	0.0012 - 0.0095	4e-05 - 0.01976	0.5 - 2.5
		IIHR: 3	30	0.0023	0.0016 - 0.005	4e-05 - 0.02315	0.5 - 1.4
		IIHR: 4	37	0.0014	0.0014 - 0.01	5e-05 - 0.01978	0.2 - 0.9
		IIHR: 5	14	0.0036	0.0027 - 0.0054	5e-05 - 0.01724	0.9 - 2.9
		IIHR: 6	34	0.0018	0.0016 - 0.005	4e-05 - 0.01703	0.4 - 1
		Ikeda[1]	7	0.0065	0.0023 - 0.0052	3e-04 - 0.0779	3.7 - 9.2
		Paintal	75	0.0025 - 0.0222	0.0012 - 0.0092	0 - 0.04961	0.2 - 25.1
		Wilcock - 0.5Phi[1]	1	0.0018	0.001	1.00E-05	0.5
		Wilcock - 1.0Phi[1]	2	0.0018	0.001 - 0.0011	2e-05 - 3e-05	0.5 - 0.6
		Wilcock - CUNI[1]	4	0.0053	0.0026 - 0.0049	0 - 0.00096	1.6 - 4.4
		Wilcock - MUNI[1]	2	0.0019	0.001 - 0.0012	0 - 0.00036	0.5 - 0.7
		Williams[1]	19	0.0014	6e-04 - 0.0044	0.0014 - 0.0865	0.5 - 5.3

Table 3.2: Summary of bedload transport data used in this analysis (excluding data where no transport was predicted). [1]Data used to fit Equation (3.15).

Source	Type	Site	N	D_{50} [m]	S [m m^{-1}]	q_b [kg m^{-1} s^{-1}]	ω [W m^{-2}]
Hinton et al. [2016]	Field	Annie Creek	20	0.009	0.0026	0.00083 - 0.02889	6.3 - 12.7
		Cache Creek near Jackson	1	0.046	0.021	0.00096	106.7
		Cherry Creek	1	0.048	0.0051	0.00043	19.5
		East St. Louis Creek	10	0.051	0.054 - 0.0577	0.00038 - 0.0033	135.6 - 228.3
		Fall Creek	5	0.078	0.0349	0.00143 - 0.01462	75.3 - 109.6
		Fool Creek	3	0.038	0.055	8e-04 - 0.00255	74.5 - 130.3
		Goose Creek 2	2	0.092	0.01	0.01125 - 0.03109	22.4 - 47.1
		Little Granite Creek	3	0.058	0.02	0.04268 - 0.04946	167.8 - 319.3
		Oak Creek	19	0.063	0.0094 - 0.0126	0 - 0.10961	1 - 89.2
		Paradise Creek	6	0.021	0.0027	7e-05 - 0.00327	7.8 - 12.1
		Sagehen Creek	4	0.058	0.0095 - 0.011	0.01155 - 0.02228	66.8 - 112.3
		South Fork Sprague River	1	0.039	0.0067	0.00027	51.2
		St. Louis Creek Site 2	3	0.076	0.015 - 0.019	0.00179 - 0.00499	121.5 - 152.2
		St. Louis Creek Site 3	3	0.082	0.017 - 0.018	0.00111 - 0.00271	105.7 - 114.8
		Sycan River above Marsh	16	0.016	0.0012	0.00017 - 0.01563	3.5 - 10
		Tom McDonald Creek	4	0.015	0.006	0.00044 - 1.55556	16.8 - 75.9
		West Fork San Juan Lower	1	0.042	0.0029	0.00627	15.4
		Wolf Creek at Bridge	1	0.049	0.0163	0.01172	58.3
King et al. [2004]	Field	Big Wood River	27	0.119	0.0091	0.00081 - 0.05063	45 - 216.1
		Blackmare Creek	1	0.099	0.0299	0.00061	69.4
		Boise River	4	0.074	0.0038	0.00199 - 0.12124	83.6 - 187.8
		Bruneau River	42	0.034	0.0054	8e-05 - 0.00572	28 - 95.8
		Cat Spur Creek	9	0.027	0.0111	3e-05 - 0.00332	9.5 - 37.3
		Fourth of July Creek	8	0.051	0.0202	0.00015 - 0.00099	53.3 - 90.8
		Hawley Creek	21	0.04	0.0233	3e-05 - 0.00221	19 - 68.5
		Herd Creek	4	0.067	0.0077	0.00103 - 0.00202	21.5 - 48.9
		Jarbidge River	13	0.092	0.016	0.00033 - 0.00645	43.8 - 165.6
		Lolo Creek	5	0.068	0.0097	8e-05 - 0.00343	15.4 - 174.5
		Main Fork Red River	15	0.059	0.0059	7e-05 - 0.00429	13.7 - 105.3
		Marsh Creek	27	0.056	0.006	0.00015 - 0.00711	19.2 - 93.4
		Middle Fork Salmon River	9	0.146	0.0041	0.01214 - 0.03301	191.1 - 260.2
		North Fork Clearwater River	5	0.0775	5.00E-04	0.00259 - 0.12217	23.9 - 51.1

Table 3.2: Summary of bedload transport data used in this analysis (excluding data where no transport was predicted). [1]Data used to fit Equation (3.15).

Source	Type	Site	N	D_{50} [m]	S [m m^{-1}]	q_b [kg m^{-1} s^{-1}]	ω [W m^{-2}]
King et al. [2004]	Field	Rapid River	12	0.079	0.0108	0.00054 - 0.02664	68.1 - 213.4
		Salmon River near Obsidian	37	0.061	0.0066	8e-05 - 0.01887	55.5 - 94.6
		Salmon River near Shoup	43	0.096	0.0019	0.00213 - 0.22411	71.9 - 116.1
		Selway River	2	0.186	0.0021	0.00452 - 0.01599	220.7 - 224.9
		South Fork Payette River	34	0.0825	0.004	0.00038 - 0.04334	15.7 - 163
		South Fork Red River	2	0.096	0.0146	0.00064 - 0.00075	190.1 - 192.5
		South Fork Salmon River	16	0.038	0.0025	2e-05 - 0.00269	35.8 - 104.7
		Squaw Creek (USFS)	32	0.027	0.024	0 - 0.01621	21 - 105.7
		Squaw Creek (USGS)	24	0.0445	0.01	0.00013 - 0.00303	32.3 - 52.8
		Thompson Creek	15	0.062	0.0153	0.00014 - 0.00398	21.9 - 76.6
		Trapper Creek	1	0.076	0.0414	0.00102	149.9
		Valley Creek	51	0.04	0.004	3e-05 - 0.01489	13.3 - 86.3
Williams and Rosgen [1989]	Field	Black River	7	5.00E-04	1e-04 - 3e-04	0.01213 - 0.04134	0.4 - 3.4
		Chippewa River near Caryville	7	0.0044	2e-04 - 3e-04	8e-05 - 0.00874	1.6 - 7.7
		Chulitna River near Talkeetna	36	0.0106	4e-04 - 0.0026	0.00662 - 0.5567	8 - 253.2
		Muddy Creek	21	8.00E-04	0.0012	0.00018 - 0.10115	0.5 - 3.9
		Pony Creek	13	0.0021	0.005 - 0.006	1e-05 - 0.00111	3-Jan
		Rich Creek	2	0.0544	0.039	0.00106 - 0.00415	79.1 - 96.1
		Susitna River at Sunshine	24	0.0394	0.0012 - 0.0024	0.0022 - 0.21151	46.4 - 214
		Susitna River near Talkeetna	11	0.0535	0.0012 - 0.0018	0.00082 - 0.02006	35.2 - 86.3
		Tanana River at Fairbanks	30	0.0024	4e-04 - 0.0041	0.00232 - 0.18377	10.6 - 157.9
		Trail Creek	13	0.0025	0.018	7e-05 - 0.01548	6.3 - 28.8
Yang [1979]	Field	Niobrara River	25	3.00E-04	0.0011 - 0.0018	0.07127 - 1.05258	3.2 - 12.7
		Middle Loup River	15	3.00E-04	9e-04 - 0.0015	0.08205 - 0.42839	2.5 - 4.1
		Mississippi River	25	2e-04 - 8e-04	0 - 1e-04	0.00807 - 2.08758	1.9 - 20.5
		Rio Grande A	42	2e-04 - 4e-04	7e-04 - 9e-04	0.03777 - 5.0349	2 - 26.4
	Flume	Gilbert	630	3e-04 - 0.0017	0.0013 - 0.0296	0.00218 - 1.06545	0.2 - 11.3
		Guy	315	2e-04 - 9e-04	1e-04 - 0.0193	1e-05 - 12.00662	0.1 - 60.8
		Kennedy	41	2e-04 - 5e-04	0.0017 - 0.0272	0.00722 - 2.52413	0.6 - 14.4
		Nomicos	12	2.00E-04	0.002 - 0.0039	0.00348 - 0.21597	0.3 - 1.5
		Rio Grande B	31	1e-04 - 2e-04	1e-04 - 0.0043	0.00485 - 7.14127	0.4 - 23.2
		Shvidchenko and Pender	253	0.0015 - 0.012	0.0019 - 0.0287	0 - 0.02019	0.1 - 11.4

Table 3.2: Summary of bedload transport data used in this analysis (excluding data where no transport was predicted). [1]Data used to fit Equation (3.15).

Source	Type	Site	N	D_{50} [m]	S [m m^{-1}]	q_b [kg m^{-1} s^{-1}]	ω [W m^{-2}]
Yang [1979]	Flume	Shvidchenko	94	0.0026 - 0.0064	0.0041 - 0.0141	1e-05 - 0.03034	0.7 - 6.2
		Stein	42	4.00E-04	6e-04 - 0.0108	0.00771 - 4.74627	0.7 - 28.9
		Vaoni and Brooks	14	1.00E-04	7e-04 - 0.0028	0.00041 - 0.09522	0.2 - 0.9
		Wilcock	34	0.0053 - 0.0122	0.0032 - 0.0204	0 - 0.50444	1.8 - 24.6

3.3.2 Incipient Motion Analysis

Flume and field data were used to examine the relationship between ω_{c*} and channel slope. I also assessed the accuracy of five methods for computing critical specific stream power: *Bagnold* [1980]; *Eaton and Church* [2011]; *Parker et al.* [2011]; *Camenen* [2012]; *Ferguson* [2012] (see Appendix A for details on these methods). Only flume data were included in this analysis because field data did not include all the inputs required by these methods.

Critical specific stream power for field data and three flume studies [*Johnson*, 1943; *Shvidchenko and Pender*, 2000; *Parker et al.*, 2011] was computed indirectly. Dimensionless bedload transport rate (q_{b*}, Equation (3.8)) was plotted versus dimensionless specific stream power (ω_*, Equation (3.4)). A best fit line was computed as the bisector of the y-on-x and x-on-y least-squares regression lines using log10-transformed data. I adjusted the fitted coefficient for de-transformation bias after *Ferguson* [1986]:

$$c_{adj} = 10^{c_{orig}} \times e^{2.65s^2} \tag{3.13}$$

$$s^2 = \frac{1}{n-2} \sum_{i=1}^{n} \left(q_{b*i} - q_{b*,pred,i}\right)^2 \tag{3.14}$$

where c_{adj} is the adjusted coefficient (in normal space), c_{orig} is the original (in log space), s^2 is the estimated variance, and n is the total number of data points. Dimensionless critical specific stream power was calculated as the intersection of this best fit line and $q_{b*} = 0.0001$, a value corresponding to incipient motion of bed particles [*Parker et al.*, 2011; *Ferguson*, 2012]. I used best judgment to excluded field sites with insufficient data to develop an accurate best fit or if substantial extrapolation was required to reach $q_{b*} = 0.0001$.

I quantified how the uncertainty in ω_{c*} is translated into uncertainty in ω_c for a range of grain sizes. Monte Carlo simulations were run selecting ω_{c*} values from a lognormal

distribution that approximated the collected flume and field data (log-mean = -2.51, log-sd = 0.40) and computing ω_c using Equation (3.4).

3.3.3 Bedload Transport Equation

I developed a new version of the *Bagnold* [1980] empirical bedload transport equation using unit discharge in place of flow depth. I first created a dimensionally consistent equation following *Martin and Church* [2000]; however, the dimensionally consistent equation was relatively inaccurate and was therefore not included in further analysis. Instead, I developed empirical equations using a similar transport dataset as *Martin and Church* [2000], but using the *Parker et al.* [2011] equation for ω_c ($\omega_{c*} = 0.1$; Equation (3.4)). Only the subsurface D_{50} was available for these data, which may alter the empirical fits. I used multiple linear regression of the log10-transformed data, with coefficient bias correction after *Ferguson* [1986].

The initial fitted exponents were very close to rational fractions. These exponents were fixed and only the coefficient was allowed to vary yielding a new version of the *Bagnold* [1980] equation but with unit discharge in place of flow depth:

$$q_b = a\left[\omega - \omega_c\right]^{3/2} {D_s}^{-1/2} q^{-1/2} \tag{3.15}$$

where the coefficient a is 0.0044 if ω and ω_c are in units of kg m^{-1} s^{-1} (after Bagnold's original definition) but is 1.43e-4 if ω and ω_c are in units of W m^{-2}.

Despite the strong physical basis for including a threshold of motion (e.g. critical specific stream power) in bedload transport equations, inaccuracies in ω_c can cause transport equations to predict no sediment movement when movement occurs. To avoid this issue, I developed an alternative equation with no critical specific stream power. This equation, however, performed poorly (root-mean-square error (RMSE) = 2.81 and R^2 = 0.66). The *Parker* [2010] bedload equation is a more accurate option that does not rely on critical specific stream power.

I used the full bedload transport dataset to test the new empirical equation against four existing stream power based formulas: *Bagnold* [1980]; *Martin and Church* [2000]; *Parker* [2010]; *Eaton and Church* [2011]. I quantified equation accuracy using four metrics: RMSE (Equation (3.16)), root-mean-square-logarithmic-error (RMSLE; (Equation (3.17)), *Theil* [1958] measure of association (U; (Equation (3.18); *Smith and Rose* [1995]), and the adjusted coefficient of determination using log10-transformed data (R^2; (Equation (3.19)).

$$RMSE = \sqrt{\frac{1}{n}\sum_{i=1}^{n}\left(q_{b,i} - q_{b,pred,i}\right)^2} \tag{3.16}$$

$$RMSLE = \sqrt{\frac{1}{n}\sum_{i=1}^{n}\left(\log q_{b,i} - \log q_{b,pred,i}\right)^2} \tag{3.17}$$

$$U = \frac{\sqrt{\frac{1}{n}\sum_{i=1}^{n}\left(q_{b,i} - q_{b,pred,i}\right)^2}}{\sqrt{\frac{1}{n}\sum_{i=1}^{n} {q_{b,i}}^2} + \sqrt{\frac{1}{n}\sum_{i=1}^{n} {q_{b,pred,i}}^2}} \tag{3.18}$$

$$R^2 = 1 - \frac{1 - \frac{\sum_{i=1}^{n}\left(\log q_{b,i} - \log q_{b,pred,i}\right)^2}{\sum_{i=1}^{n}\left(\log q_{b,i} - \log mean(q_{b,i})\right)^2} \times (n-1)}{n-p-1} \tag{3.19}$$

where n is the sample size and p is the number of fitted model parameters.

Each of these error measures has benefits and drawbacks and it is useful to examine them collectively to assess model fit. RMSE is the average error across all observations and is in the same units as sediment transport (kg m^{-1} s^{-1} or ppm); however, high transport values have a larger influence on estimating model accuracy due to the orders of magnitude variation in transport data. I therefore used log-transformed data for the RMSLE and adjusted R^2 value to obtain a more balanced error estimate. Similar to R^2, Theil's measure of association estimates relative error (on a 0 to 1 scale), but it also accounts for how close predictions are to the 1:1 line [*Smith and Rose*, 1995]. Smaller values indicate a better fit for RMSE,

Table 3.3: Summary of distributions used in the bedload sensitivity analysis.

Variable	Distribution	Min	Max
D_{50} [m]	Log-Uniform	0.0001	0.2
ω_{c*}	Lognormal (mean = -2.4, sd = 0.46)	0.03	0.3
Slope [m m^{-1}]	Lognormal (mean = -5.6, sd = 1.83)	5e-5	0.06
Discharge [m^3 s^{-1}]	Lognormal (mean = 1.45, sd = 3.50)	0.008	6000
Width [m]	Lognormal (mean = 2.2, sd = 1.96)	0.2	500

RMSLE, and U, while higher values do for R^2. Data were only used if all equations predicted transport to allow direct comparisons between formulas.

I used a density-based sensitivity analysis [*Plischke et al.*, 2013] to assess the relative importance of equation variables on calculated sediment transport rates. Briefly, conditional probability density functions (pdfs) for each input variable are compared to the full output pdf. Larger differences between the conditional and full pdfs indicate larger parameter influence on model output. I estimated input variable distributions based on observed distributions in the collected bedload transport data (Table 3.3).

3.3.4 Total Load Transport Equation

Because the dimensionally consistent bedload transport equation failed to predict observed transport rates, I opted for a purely empirical approach to develop a total load equation. The total load database was randomly split into a "training" set (N = 731) and a "testing" set (N = 732). I used the same parameter set as the bedload formula and fit the model using multiple linear regression on the log10 transformed training set, with bias correction. Like the empirical bedload equation, fitted exponents were close to rational fractions. Fixing these exponents and allowing only the coefficient to vary yielded:

$$Q_t = a\left[\omega - \omega_c\right]^{3/2} {D_s}^{-1} q^{-5/6} \tag{3.20}$$

Table 3.4: Summary of distributions used in the total load sensitivity analysis.

Variable	Distribution	Min	Max
D_{50} [m]	Lognormal (mean = -7.9, sd = 0.52)	0.00008	0.002
ω_{c*}	Lognormal (mean = -2.4, sd = 0.46)	0.03	0.3
Slope [m m^{-1}]	Lognormal (mean = -8.4, sd = 1.20)	9e-6	0.02
Discharge [m^3 s^{-1}]	Lognormal (mean = 4.4, sd = 3.33)	0.002	30000
Width [m]	Lognormal (mean = 6.0, sd = 1.34)	0.3	1200

Table 3.5: Ranges of values for which the new bedload (Equation (3.15)) and total load (Equation (3.20)) equations were tested.

	S [m m^{-1}]	**Q [m^3 s^{-1}]**	**w [m]**	**D_{50} [mm]**	**q [m^2 s^{-1}]**	**ω [W m^{-2}]**	**Transport Rate**
Bedload	4.28e-5–5.77e-2	3e-4–13,248	0.13–532	0.137–186	0.001–24.9	0.092–412	7e-9–12 kg m^{-1} s^{-1}
Total load	9.6e-6–1.7e-2	2e-3–28,825	0.27–1,110	0.085–1.5	0.005–40	0.2–161	11–47,300 ppm

where Q_t is the total load sediment concentration [ppm]. The coefficient a is 0.6568 if ω and ω_c are in units of kg m^{-1} s^{-1} but is 0.0214 if ω and ω_c are in units of W m^{-2}.

I used the testing dataset to compare Equation (3.20) with three existing total load equations: *Ackers and White* [1973]; *Engelund and Hansen* [1967]; *Brownlie* [1982] (see Appendix for formulas). The Ackers and White and Engelund and Hansen equations were chosen because they performed best among the equations examined by *Brownlie* [1982]. I also performed a sensitivity analysis of Equation (3.20). Input distributions were estimated based on observed distributions in the collected total load transport data (Table 3.4). Table 3.5 shows ranges of input values for which the bedload and total load equations were tested. All analyses were done in R version 3.2.5 [*R Core Team*, 2018].

3.3.5 Incision Modeling

I tested the applicability of the bedload transport relationship by modeling channel incision using the flume experiment of *Ashida and Michiue* [1971]. The total load equation was not used because the grain sizes in this experiment were much coarser than the grain sizes used to fit this equation. I used data from Run 6 of their experiments from a 20 m long, 0.8

m wide rectangular flume with an initial bed slope of 0.01 and a constant discharge of 0.0314 $m^3\ s^{-1}$. They used a graded sediment mixture with a mean of 2.47 mm and a standard deviation of 3.73 mm. The bed slope was initially stable and the sediment feed was cut off at the start of the experiment. The downstream bed elevation was controlled by a weir.

While the goal of this chapter was to develop sediment transport equations for application throughout a river network, I chose to test the bedload equation using a flume dataset for two reasons. First, there are limited field data describing network-scale channel incision. Second, flume studies generally have more accurate data and simpler conditions (e.g. constant discharge and fixed width) which allowed me to examine the uncertainty in the bedload transport equation while minimizing confounding factors. Ashida and Michiue's data have the added benefit of being used to test a complex morphodynamic channel degradation model: CONservational Channel Evolution and Pollutant Transport System (CONCEPTS) [*Langendoen and Alonso*, 2008]. I compared the incision model output to the experimental results and the CONCEPTS results.

In the *Ashida and Michiue* [1971] experiments, the flume incised while the bed armored, which controlled the extent and rate of channel degradation. To account for this armoring process, I modeled sediment transport by grain size fraction. Since no stream power based hiding function exists, I adjusted each representative grain size to calculate ω_c [*Garbrecht et al.*, 1995; *Langendoen and Alonso*, 2008]:

$$D_{c,k} = D_k \left(\frac{D_m}{D_k} \right)^{\eta} \tag{3.21}$$

where $D_{c,k}$ is the adjusted critical grain size of size class k, D_k is the actual grain size, D_m is the geometric mean grain size of the bed, and η is a hiding coefficient. Following *Langendoen and Alonso* [2008], I set η equal to 0.7. Channel incision was modeled using the Exner equation:

$$\frac{\partial z}{\partial t} = -\frac{1}{1-\lambda} \frac{\partial q_s}{\partial x} \tag{3.22}$$

where z is the bed elevation, q_s is the volumetric sediment transport rate per unit width, and λ is the bed porosity. Numerically, the sediment transport rate was estimated using the Quick scheme [*Hirsch*, 2007]:

$$q_{s,i+1/2} = q_{s,i} + \frac{1}{8}\left(q_{s,i} - q_{s,i-1}\right) + \frac{3}{8}\left(q_{s,i+1} - q_{s,i}\right) \tag{3.23}$$

where the subscript i refers to the cross section (increasing in the downstream direction) and the value of $\partial q_s/\partial x$ from Equation (3.22) is calculated as:

$$\frac{\partial q_s}{\partial x} = q_{s,i+1/2} - q_{s,i-1/2} \tag{3.24}$$

The change in the bed grain size distribution was calculated using the following [*Langendoen and Alonso*, 2008]:

$$\frac{\partial p_{s,k} A_s}{\partial t} = (1-\lambda) w \frac{\partial z_k}{\partial t} + p_{sub,k} w \left(\frac{\partial z}{\partial t} - \frac{\partial \delta_s}{\partial t}\right) \tag{3.25}$$

where $p_{s,k}$ is the proportion of the bed surface for the k^{th} grain size, A_s is the cross sectional area of the surface layer, $\partial z_k/\partial t$ is the bed elevation change from the k^{th} grain size, $p_{sub,k}$ is the proportion of the subsurface for the k^{th} grain size, $\partial z/\partial t$ is the total bed elevation change, and $\partial \delta_s/\partial t$ is the change in the surface layer thickness with time (assumed to be zero). The model was run for 100 hours with $\Delta x = 1$ m, $\Delta t = 20$ s, and $\lambda = 0.4$.

Uncertainty in the bedload equation was incorporated into the incision model. I varied the equation coefficient and exponents uniformly across their 95% confidence intervals estimated as part of the regression fit. The incision model was run 1000 times, giving a range of potential channel incision results.

3.4 Results

3.4.1 Incipient Motion

Figure 3.1 shows ω_{c*} plotted versus slope for flume (a) and field (b) data. Lines show calculated values of ω_{c*} using the *Camenen* [2012] and *Ferguson* [2012] formulas. Dimensionless critical specific stream power is weakly correlated with slope for flume data but shows a significant positive correlation with slope for field data. Specifically, Spearman's rank-based correlation coefficient (ρ) for flume data is negative, but insignificant at the α = 0.05 confidence level (ρ = -0.14; p = 0.06). Of all the flume studies, only *Dey and Raju* [2002] and *Yang et al.* [2006] show a significant correlation between ω_{c*} and slope ($\rho = 0.63$; p < 1e-4 and $\rho = 0.56$; p = 0.008, respectively). Field data, however, show a significant positive correlation with slope ($\rho = 0.63$; p < 1e-5). Combined, the field and flume data are not correlated with slope ($\rho = 0.03$; p = 0.63). I found ω_{c*} values for flume (0.085 $\pm$ 0.030; mean $\pm$ SD) and field data (0.10 $\pm$ 0.065), similar to the average of 0.1 found by *Parker et al.* [2011], although some of the same data in Parker et al.'s dataset are included in this analysis.

Figure 3.2 shows observed values of ω_c versus values predicted using the methods of *Camenen* [2012]; *Ferguson* [2012]; *Bagnold* [1980]; *Parker et al.* [2011], and *Eaton and Church* [2011]. The first three methods were slightly more accurate than the latter two, although all approaches show similar levels of error.

Figure 3.3 shows how uncertainty varies with grain size for ω_c values calculated using Equation (3.4) and the observed distribution of ω_{c*}. While this uncertainty may be large for grain sizes greater than ~20 mm, uncertainty bounds are substantially smaller for finer grain sizes (95% confidence interval ~30 W m^{-2} for 20 mm gravel but ~0.3 W m^{-2} for 1 mm sand).

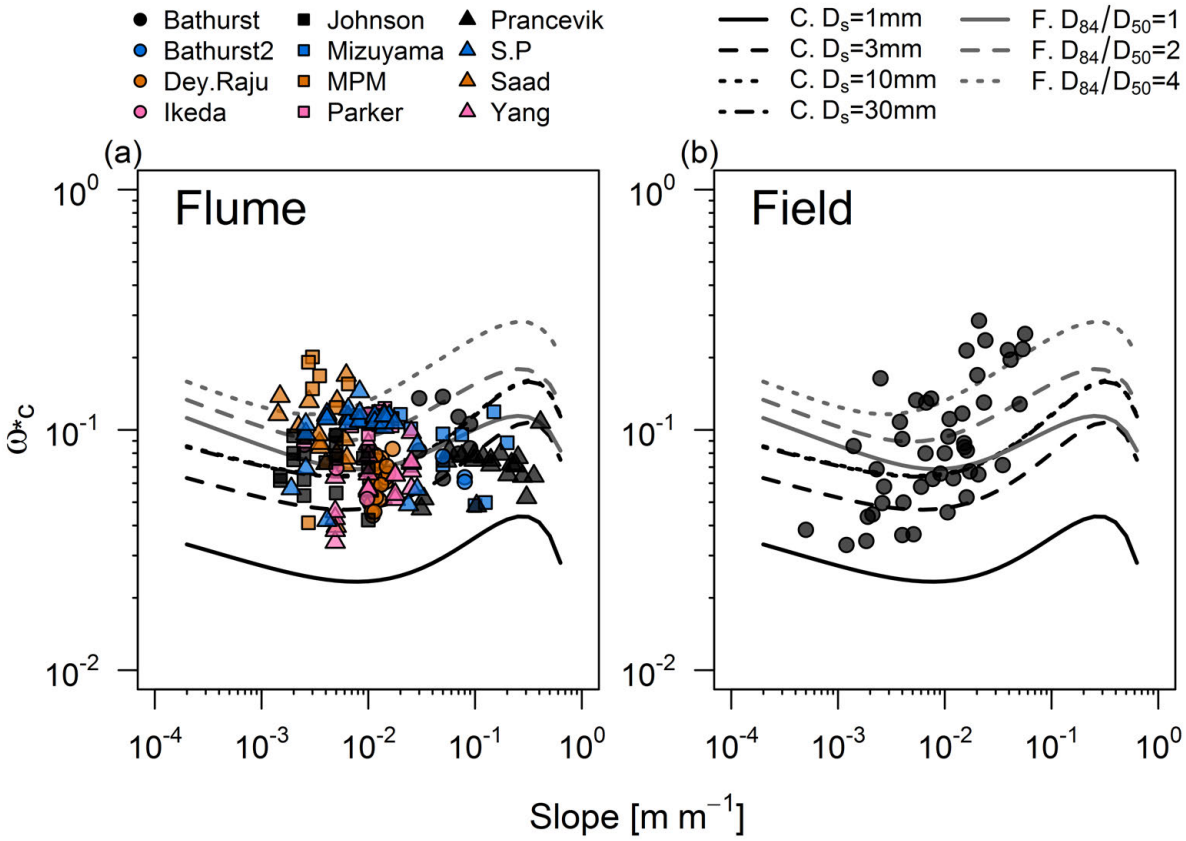

Figure 3.1: Relationships between dimensionless critical specific stream power (ω_{c*}) and channel slope for flume (a) and field (b) data. Lines correspond to theoretical relationships based on the models of *Camenen* [2012] (C.) and *Ferguson* [2012] (F.).

3.4.2 Bedload Transport Equation

Figure 3.4 compares predicted versus observed bedload transport rates for the new bedload equation (Equation (3.15)) and the four established alternatives. The *Bagnold* [1980] empirical bedload transport equation performed best, followed by the empirical equation (Equation (3.15)) and the *Parker* [2010] equation. The *Eaton and Church* [2011] and *Martin and Church* [2000] equations were generally the least accurate. In all cases, I used the *Parker et al.* [2011] approach for estimating critical specific stream power ($\omega_{c*} = 0.1$, Equation (3.4)) since my analysis suggests it is as accurate as other, more complicated alternatives. Equations with a critical specific stream power term (Bagnold, Martin and Church, and Equation (3.15)) predicted no motion for ~23% of the database (i.e. yielded a cal-

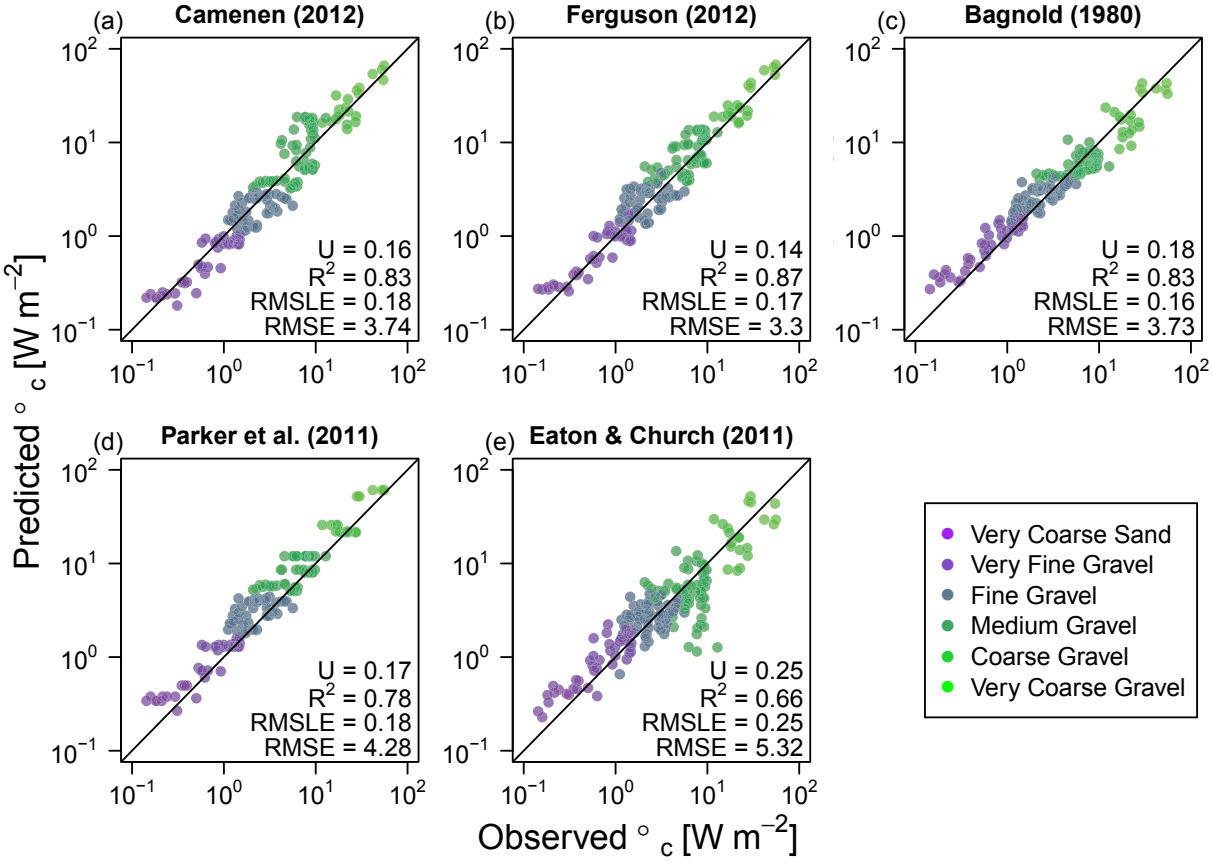

Figure 3.2: Predicted versus observed critical specific stream power for collected flume data using five different approaches.

culated transport rate of zero for sites with observed bedload transport). For consistency, I included only data points where all equations predicted transport. Testing with the full dataset (including zero transport predictions), did not change relative equation accuracy (RMSE decreased slightly for all equations and U was unchanged).

Figure 3.5 presents the results of the sensitivity analysis of Equation (3.15). These results suggest that discharge and slope have the largest influence on transport rates, while channel width, grain size, and ω_{c*} have only minor effects. This analysis, however, does not account for the threshold effect of ω_{c*} on determining whether transport is predicted; thus, this variable may be more important than the sensitivity results indicate.

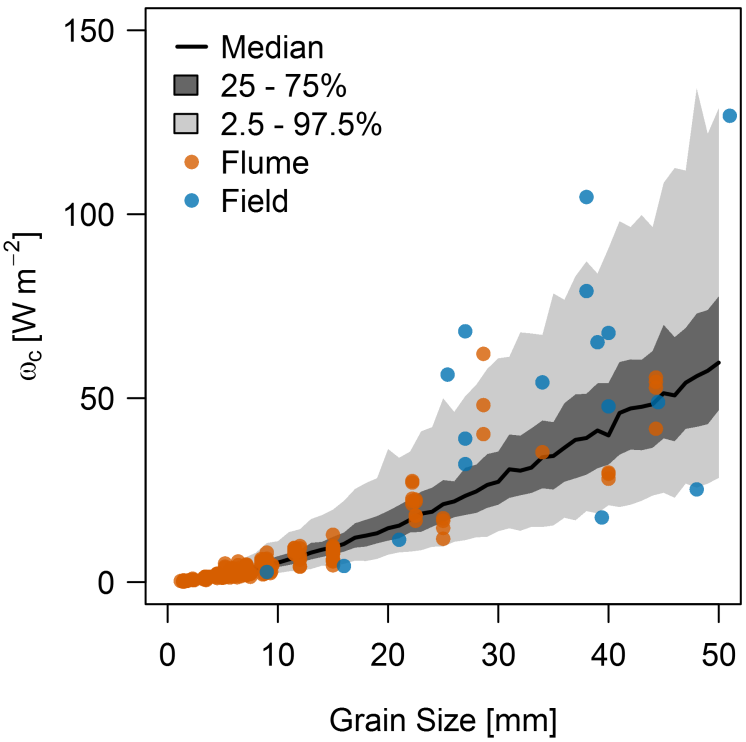

Figure 3.3: Uncertainty in critical specific stream power (ω_c) with grain size based on simulations using the observed distribution of ω_{c*}. Observed data points are also shown.

3.4.3 Total Load Transport Equation

Figure 3.6 compares predicted versus observed total load transport rates for Equation (3.20) and three commonly used total load formulas. The new equation is as accurate as these alternatives. Equation (3.20) is more parsimonious than *Brownlie* [1982] and *Ackers and White* [1973], and of similar complexity as *Engelund and Hansen* [1967]. Most importantly, Equation (3.20) relies on an easily quantified set of input variables, unlike the other equations which all require velocity and hydraulic radius.

Figure 3.7 shows the results of the sensitivity analysis of Equation (3.20). I converted total load transport rates from ppm to kg m^{-1} s^{-1} for this analysis to allow direct comparison with the bedload equation. The results show that discharge and slope are the most important variables, while width, grain size, and ω_{c*} have only a small effect.

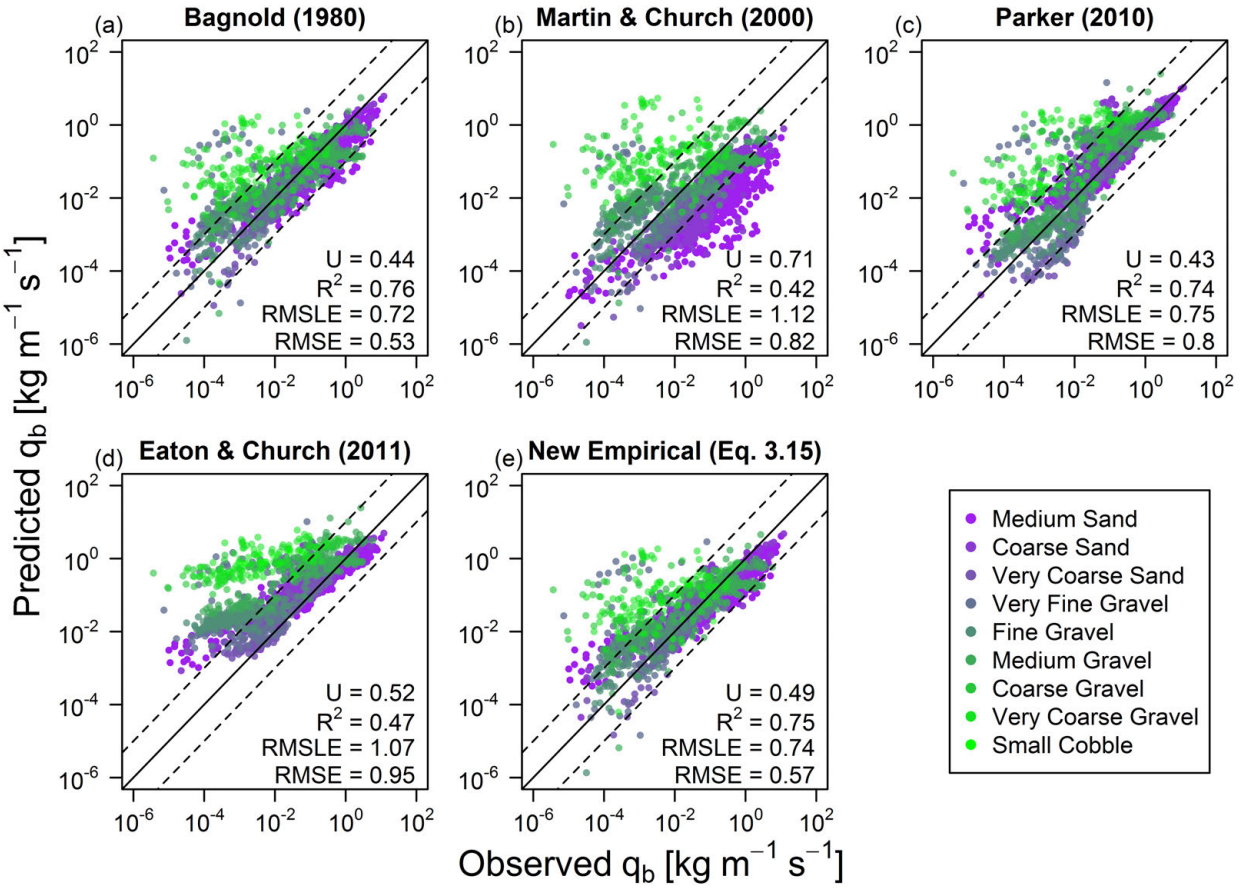

Figure 3.4: Predicted versus observed bedload transport rates for the five examined equations. The solid line is the line of perfect agreement and the dashed lines show ± one order of magnitude.

3.4.4 Incision Modeling

Figure 3.8 shows the results of the incision modeling using the new bedload equation. I included modeled and observed erosion depth over time for three different cross sections (Figure 3.8a), the modeled change in longitudinal profile (Figure 3.8b), and modeled and observed changes in bed grain size distribution for two cross sections (Figure 3.8c–d). Using the new bedload equation, the incision model agrees well (RMSE = 0.025 m) with *Ashida and Michiue* [1971] experimental data and matches the incision rate more closely than the CONCEPTS results (RMSE = 0.028 m). Uncertainty bands from the Monte Carlo analysis are shown for the erosion depth results (Figure 3.8a). Generally, there is significant uncertainty in the incision rate but much less in the predicted final erosion depth. Total

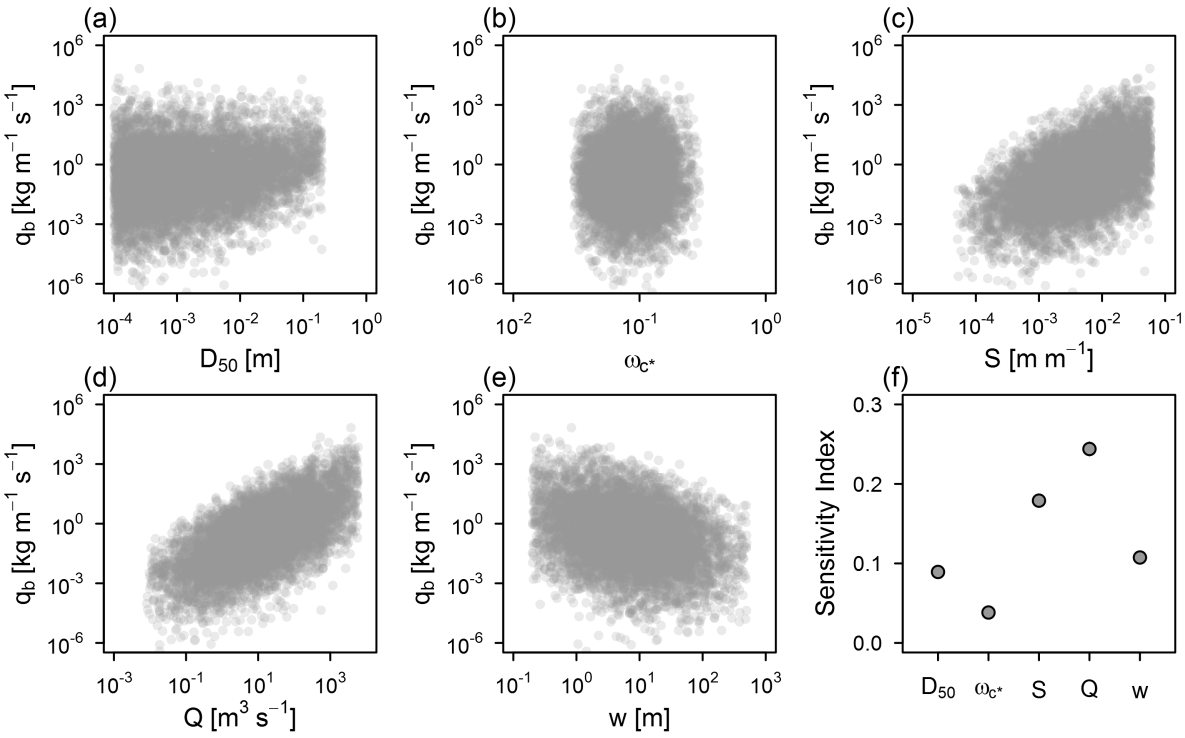

Figure 3.5: Scatterplots (a–e) show simple correlation between simulated bedload transport rates and each of the five equation variables (N = 6550). (f) shows bias corrected results of the formal sensitivity analysis of Equation (3.15). Uncertainty bounds of sensitivity estimates are smaller than the size of the points.

uncertainty, however, may be greater in systems that do not rapidly adjust to a new stable state (in this case an armored bed) as error in incision rates will continue to propagate.

3.5 Discussion

3.5.1 Incipient Motion

The *Parker et al.* [2011] approach to calculating critical specific stream power ($\omega_{c*} = 0.1$) has similar accuracy to more complicated and data demanding equations, despite its simplicity (Figure 3.2). Furthermore, their method is the only one that does not rely on flow depth or some measure of roughness. Assuming a constant value of ω_{c*} (or more realistically, a distribution of values) allows ω_c to be calculated using only grain size.

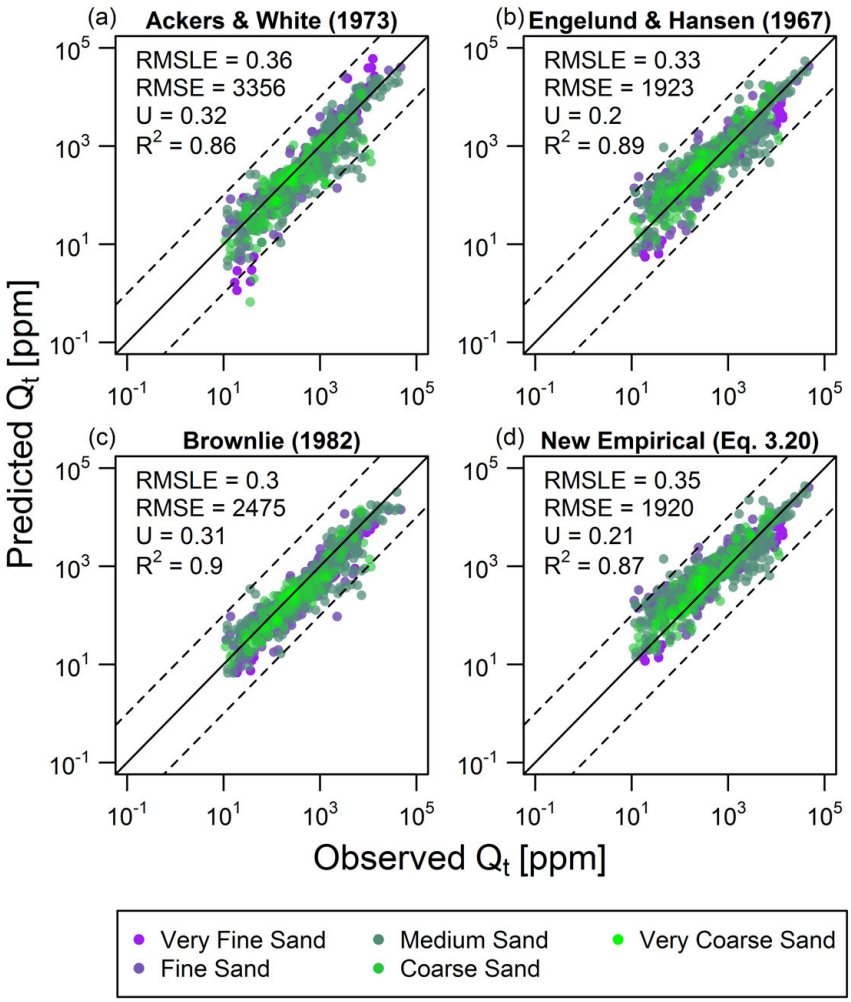

Figure 3.6: Predicted versus observed total transport rates for the four examined equations.

I found that ω_{c*} is not strongly correlated with slope in the flume dataset consistent with the findings of other studies [*Ferguson*, 2012; *Parker et al.*, 2011]. Field data, on the other hand, were positively correlated with slope. The difference between field and flume data could result from the larger grain sizes in field sites (mean diameter of 67 mm versus 10 mm for flume data). Additionally, steeper slopes in the field data may be associated with greater channel roughness, potentially leading to a correlation between ω_{c*} and slope. Finally, the field ω_{c*} values were all computed indirectly which could lead to greater uncertainty in these values compared to the flume data. Despite the apparent relationship between ω_{c*} and slope for field data, the *Parker et al.* [2011] model still had relatively low error rates for these data (RMSLE = 0.26, U = 0.26).

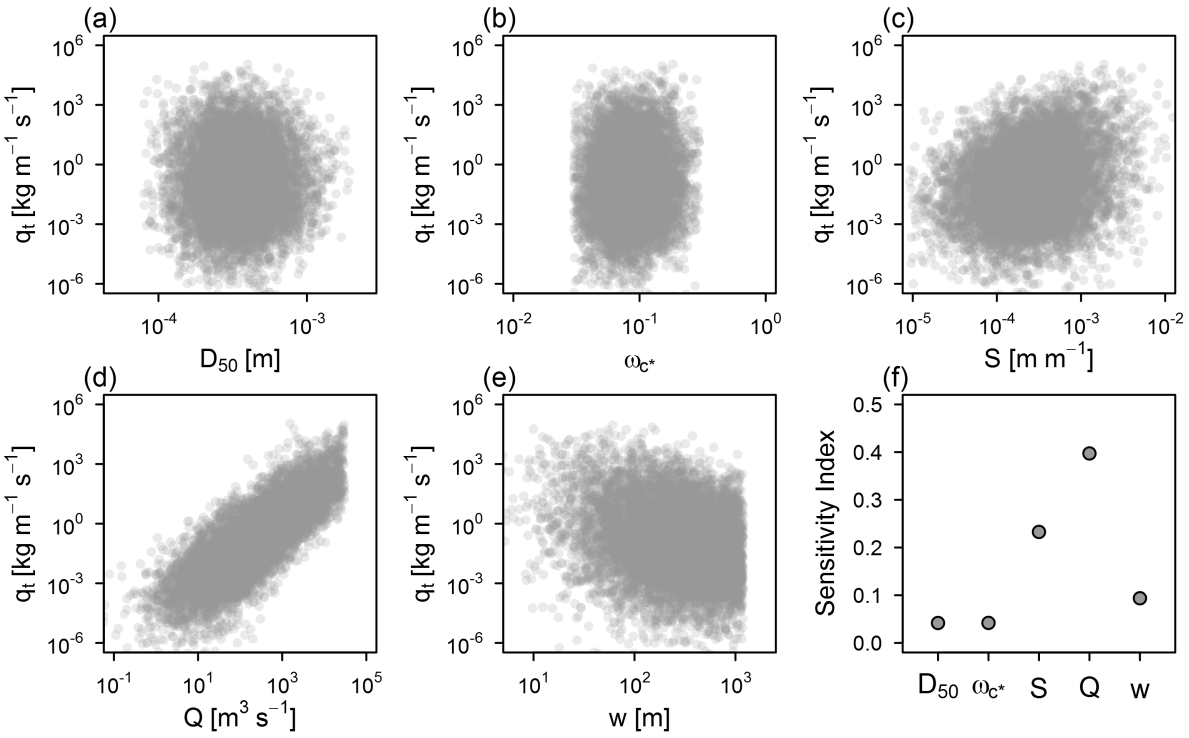

Figure 3.7: Scatterplots (a–e) show simple correlation between simulated total transport rates and each of the five equation variables (N = 7650). (f) shows bias corrected results of the formal sensitivity analysis of Equation (3.20). Uncertainty bounds of sensitivity estimates are smaller than the size of the points.

3.5.2 Sediment Transport Equations

The new empirical bedload (Equation (3.15)) and total load (Equation (3.20)) transport equations based on unit discharge instead of flow depth have similar accuracy to more established formulas (Figure 3.4 and Figure 3.6). The new bedload equation (Equation (3.15)) is nearly as accurate as the *Bagnold* [1980] empirical relationship and performs slightly better than other alternatives [*Martin and Church*, 2000; *Parker*, 2010; *Eaton and Church*, 2011]. Others have shown that the *Bagnold* [1980] equation and Martin and Church's version tend to underpredict transport rates [*Martin*, 2003; *Martin and Ham*, 2005], although they can overpredict rates in coarser bed streams [*Vázquez-Tarrío and Menéndez-Duarte*, 2015]. Our analysis also showed the *Martin and Church* [2000] equation underpredicted transport rates for finer grain sizes while all equations overpredicted rates for coarse sediment.

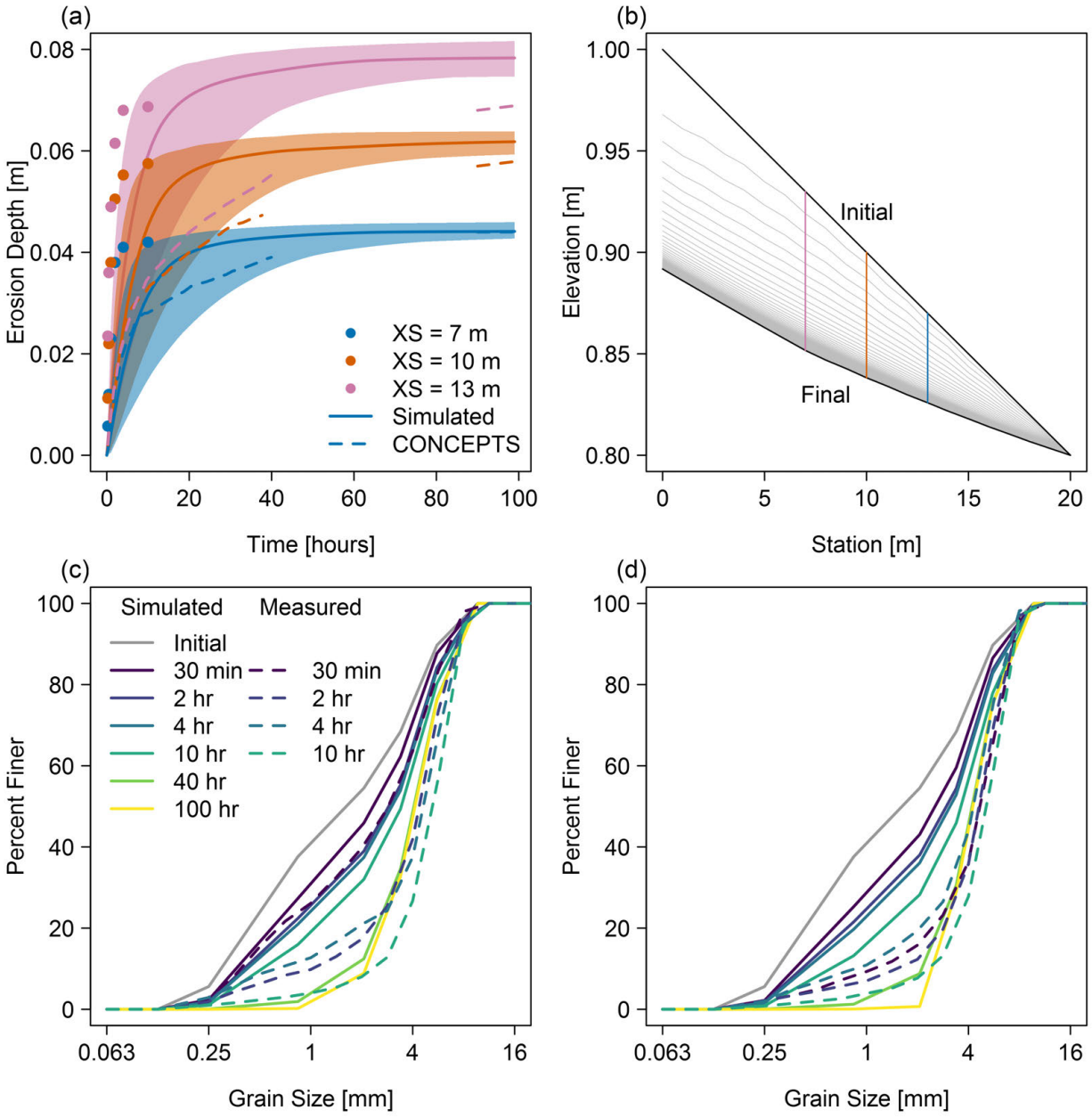

Figure 3.8: Results of incision modeling using the bedload equation (Equation (3.15)). (a) Observed erosion depths 7, 10, and 13 m from the downstream end compared to my simulations (with shaded uncertainty bounds) and those of CONCEPTS; (b) modeled evolution of the channel bed over time (with cross section locations shown); and observed and simulated changes in grain size distributions over time 10 m (c) and 13 m (d) from the downstream end.

Differences in equation accuracy may be tied to differences in structure. For example, the equations have different relationships between bedload transport rate and median bed grain size. The *Bagnold* [1980] formula and the new empirical equation (Equation (3.15)) both

have a negative exponent for grain size (-1/2) while the *Martin and Church* [2000] equation has a positive exponent (1/4). Due to the hidden positive correlation between ω_c and grain size, however, the net relationship between transport rate and grain size is positive for all equations. The former equations perform significantly better than the latter, although this cannot be attributed solely to grain size scaling.

Our new bedload equation is simple but — like all empirical sediment transport formulas — fails to account for some processes important in bedload transport. For example, size segregation on the channel bed can significantly affect transport rates [*Frey and Church*, 2011]. Our bedload formula can be used to model transport by grain size, using a hiding function to adjust ω_c — as in the incision modeling performed in this study (Equation (3.21)); however, it does not account for kinetic sorting mechanisms which may be a significant control on bedload transport and bed stability [*Bacchi et al.*, 2014].

Given their simplicity, the *Parker* [2010] and *Eaton and Church* [2011] equations are also suitable for network scale application. The *Parker* [2010] equation, however, has no incipient motion criterion, which may be beneficial or detrimental depending on the situation. There is no general guidance for when it is beneficial to include a critical stream power (or shear stress) criterion in sediment transport modeling, but Equation (3.15) and the *Parker* [2010] equation are two viable alternatives that can be applied in either case. Additionally, the new total load and bed load equations have the same structure and can be used in combination where bedload and suspended load transport are occurring at different times or for different grain sizes. The *Eaton and Church* [2011] formula relies on a dimensionless critical specific stream power that is dependent on flow roughness — an impediment to network scale application. For the dataset used in this study, assuming a constant ω_{c*} of 0.1 is just as accurate as their approach. Using this constant value of ω_{c*} makes it easier to apply the *Eaton and Church* [2011] bedload equation at the network scale.

3.5.3 Uncertainty in Sediment Transport Modeling

Much of the uncertainty in sediment transport modeling comes from uncertainty in the data used to parameterize transport formulas. The sensitivity results for both the new bedload and total load equations indicate that channel slope and discharge are the most important variables, while width, grain size, and ω_{c*} have only a small effect. This suggests that the accuracy of sediment flux predictions depends on a robust hydrologic foundation and accurate topographic data, but is less dependent on accurately quantifying grain size — a variable that is rarely well measured throughout a channel network. Despite this, improvements in estimating variability in grain size at network scales would improve the applicability of these equations in answering watershed management questions.

Sensitivity results are relatively consistent between the two equations, although grain size has a slightly higher influence in the bedload formula. This could be due to differences in equation structure as well as the much smaller range of grain sizes in the total load dataset. The relative unimportance of grain size suggests that observed uncertainty in ω_c (Figure 3.3) should have relatively little influence on calculated transport rates. Equation (3.15), however, was most accurate for finer grain sizes (sand and fine to medium gravel), suggesting that this equation may be better suited for finer grained streams. Additionally, coarse grained streams are more likely to be near threshold conditions where uncertainty in ω_c will produce greater uncertainty in transport rates.

Uncertainty in sediment transport rates translates directly to uncertainty in incision modeling. Quantifying this uncertainty is important, but is less feasible with complicated models that require long run times. Also, models which require hydraulic modeling are subject to additional sources of uncertainty (e.g. flow resistance equations and cross section geometry). Our simple stream power-based approach avoids these issues; however, morphodynamic models incorporating hydraulics are based on rigorous and physically-based principles and are likely to perform better in many situations if inputs, parameters, and boundary conditions can be specified with sufficient accuracy.

3.6 Conclusions

I developed new bedload (Equation (3.15)) and total load (Equation (3.20)) sediment transport equations based on specific stream power and with no flow depth term. These equations can be used with only limited data: channel slope, discharge, width, and bed grain size. Using a comprehensive dataset from the literature on bedload and total load transport rates, I show that these new transport equations perform well compared to other formulas and represent a viable alternative to more complex equations requiring flow depth, flow resistance equations, or grain sorting. In addition, my results for flume data are consistent with previous studies indicating that dimensionless critical specific stream power for incipient motion is not strongly correlated with slope and has a mean value of $\sim$0.1 [*Parker et al.*, 2011]. Using this mean value allows critical specific stream power to be calculated using only grain size.

This work expands upon a rich history of relating sediment transport rates to stream power, beginning with *Bagnold* [1966]. Others have built upon Bagnold's original approach, developing alternative bedload equations [*Martin and Church*, 2000; *Parker*, 2010; *Eaton and Church*, 2011] and exploring critical specific stream power as an alternative to critical shear stress [*Parker et al.*, 2011; *Camenen*, 2012; *Ferguson*, 2012]. I have contributed to this legacy, notably by developing a pair of bedload and total load equations that account for multiple modes of sediment transport. Still, much work remains to further test these equations and perhaps develop dimensionally consistent versions following *Martin and Church* [2000]. In addition, further investigation into the relationship between ω_{c*} and slope could be beneficial to better understand grain incipient motion within a specific stream power framework.

These new parsimonious equations can simplify sediment transport modeling at the stream network scale. A watershed scale approach to managing river sediment regimes is important [*Wohl et al.*, 2015a]; however, adequate tools are only now being developed. Our new transport equations can be added to this river management toolbox, enabling explicit

quantification of riverine sediment flux — a fundamental process affecting water quality, infrastructure operation, flood risk, habitat suitability, and channel morphodynamics.

Chapter 4

An intermediate complexity model for simulating channel evolution

Summary

Extreme river erosion and sedimentation threatens critical infrastructure, degrades aquatic habitat, and impairs water quality. Tools for predicting the magnitude and scale of erosion, sedimentation, and channel evolution processes are needed for effective mitigation and management. I present a new numerical model that simulates coupled river bed and bank erosion at the watershed scale (generally <1,000 km^2). The model uses modified versions of Bagnold's sediment transport equation to simulate bed erosion and aggradation, as well as a simplified Bank Stability and Toe Erosion Model (BSTEM) to simulate bank erosion processes. The model is mechanistic and intermediate complexity, accounting for the dominant channel evolution processes while limiting data requirements. I apply the model to a generic test case of channel network response following a disturbance and the results match physical understanding of channel evolution. The model was also tested on two field data sets: downstream from Parker Dam on the lower Colorado River and on the North Fork Toutle River (NFTR) which responded dramatically to the 1980 eruption of Mount St. Helens. It accurately predicts observed channel incision and bed material coarsening on the lower Colorado River, as well as observations for the upstream 18 km of the NFTR watershed. The model does not include algorithms for extensive lateral migration and avulsions and therefore did not perform well in the lower NFTR basin where the channel migrated across its valley bottom. Still, I am confident in the utility of the model for simulating channel network response to disturbance, while recognizing its mechanistic limitations.

4.1 Introduction

Excessive river erosion and sedimentation are triggered by a variety of watershed disturbances which alter natural flow and sediment dynamics. For example, urbanization increases discharge [*Hollis*, 1975; *Rosburg et al.*, 2017], channel straightening increases slope (and therefore stream power) [*Simon*, 1989], and dam construction decreases sediment supply and modifies flow regimes [*Williams and Wolman*, 1984]. Channel instability and sediment imbalance threatens critical infrastructure, degrades aquatic habitat, and impairs water quality. Landowners and environmental resource agencies often respond to these threats by attempting to stabilize channels, sometimes without success [e.g. *Miller and Kochel*, 2009]. Stream stabilization projects fail because designers do not account for the altered hydrology and sediment supply and because of the inherent uncertainty of channel response [*Simon et al.*, 2007; *Roni and Beechie*, 2013; *Wohl et al.*, 2005; *Bernhardt and Palmer*, 2007]. It is challenging to predict how streams will adjust and what new equilibrium state — if any — they will attain.

Numerical modeling can address this issue by providing a simple and reproducible way to (1) assess channel sensitivity to disturbance and (2) predict channel adjustment. While morphodynamic modeling has advanced in recent years, most of the research has focused on large spatial and temporal scales (e.g. landscape evolution models [*Lague*, 2014]) or individual processes (e.g. bar formation [*Nelson et al.*, 2015]). Models that predict channel changes at intermediate spatial and temporal scales (10s – 100s km^2 watersheds; 10s – 100s of years) are needed to help guide river restoration and management.

Recent research has attempted to fill this gap with regime-based models of river response [*Eaton and Millar*, 2017], watershed-scale accounting of sediment dynamics [*Parker et al.*, 2015; *Czuba and Foufoula-Georgiou*, 2014, 2015; *Schmitt et al.*, 2016; *Soar et al.*, 2017], and mechanistic bank erosion modeling [*Langendoen et al.*, 2012; *Stryker et al.*, 2017]. These approaches are useful but may not account for relevant erosion processes or tend to require significant amounts of data, making it difficult to assess uncertainty and provide results

useful to managers. The aim was to develop a network-scale model for simulating channel incision and bank erosion with limited data requirements. To achieve this goal, I built a morphodynamic model driven by specific stream power [*Bagnold*, 1966], allowing the modeling of channel erosion and deposition without simulating detailed flow hydraulics. Additionally, the model was intentionally designed to be transparent about uncertainty, explicitly translating variability in model inputs into probabilistic predictions of channel evolution.

This paper introduces this new stream power-based morphodynamic model — the River Erosion Model (REM). REM is designed primarily for modeling channel evolution in smaller watersheds (i.e. 10s - 100s km^2) with cohesive banks; unfortunately, watershed-scale data on channel response are rarely available for these types of systems. I therefore test REM on a generic watershed responding to base-level fall as well as two field datasets of rivers responding to different types of disturbance. The first is a reach of the lower Colorado River which incised and coarsened after Parker Dam was constructed in 1938. The second is the North Fork Toutle River (NFTR) which has followed a complex trajectory of channel change following massive sediment deposition from the eruption of Mount St. Helens in 1980. Applying REM to these complex systems tests the basic model processes, explores uncertainty and model sensitivity, and pushes the limits of model application, determining the range of conditions for which it is most suitable.

4.2 Model Description

4.2.1 Stream Power

Many models use the standard step method or a simple flow resistance relationship to compute flow depth, velocity, and shear stress [e.g. *El Kadi Abderrezzak et al.*, 2008; *Allen et al.*, 1999]. In contrast, I use specific stream power to directly model channel incision and bank erosion. Specific stream power is the power available to do work in the stream, normalized by bed area [*Bagnold*, 1966]:

$$\omega = \frac{\Omega}{w} = \frac{\gamma Q S}{w} \tag{4.1}$$

where ω is specific stream power [W m^{-2}], Ω is total stream power [W m^{-1}], γ is the specific weight of water [9810 N m^{-3}], Q is discharge [m^3 s^{-1}], S is the friction slope [m m^{-1}], and w is the water surface width [m].

Specific stream power is a useful variable because it is readily calculated throughout a stream network (assuming bed slope equals friction slope) but still represents the physical processes in rivers. Because of this, it has been used to determine erosion and deposition potential [*Parker et al.*, 2015; *Vocal Ferencevic and Ashmore*, 2012; *Bizzi and Lerner*, 2015; *Soar et al.*, 2017], explain dominant modes of channel adjustment [*Knighton*, 1999; *Bull*, 1979], model sediment transport processes [*Bagnold*, 1977, 1980; *Martin and Church*, 2000; *Eaton and Church*, 2011], and explain historic variability and future evolution of rivers [*Fryirs et al.*, 2012]. Discharge is available from gage data, regional regression equations, or hydrologic modeling (and can be scaled based on drainage area). Channel slope and width can be obtained from high resolution digital elevation models, often created from airborne LiDAR data.

Discharge

REM is driven by a user-supplied flow record with a given time step (e.g. daily, hourly, or 15 minute). To account for overbank flooding, the model uses the Manning equation to partition flow between the channel and floodplain using the sub-area method, similar to the approach used by HEC-RAS and others [e.g. *Soar et al.*, 2017]. The channel and two floodplains are treated as separate sections (j), each with their own Manning roughness coefficient (n_j). The discharge for each section is calculated using trial values of water surface elevation. This processes is repeated until the sum of these discharges equals the known total flow:

$$Q = \sum_{j=1}^{3} \left(\frac{A_j R_j^{2/3} S^{1/2}}{n_j} \right) \tag{4.2}$$

where A_j is the section area [m^2], R_j is the section hydraulic radius [m], and S is the channel slope. Only the discharge within the channel, and the corresponding flow width, are used to calculate specific stream power.

4.2.2 Channel Incision

The model simulates incision into non-cohesive and cohesive bed material, including a mix of both bed types as described below.

Non-cohesive incision

Fundamentally, the model uses the Exner equation to simulate bed elevation changes based on a sediment mass balance:

$$\frac{\partial \eta}{\partial t} = -\frac{1}{w_{avg}(1-\lambda)}\frac{\partial Q_b}{\partial x} \tag{4.3}$$

where η is the bed elevation [m], λ is the bed porosity (assumed to be 0.4), w_{avg} is the average bottom width of adjacent cross sections, Q_b is the volumetric sediment transport rate [m^3 s^{-1}], and t and x are time and downstream distance, respectively. REM models sediment transport by grain size and tracks changes in bed material composition:

$$\frac{\partial F_k}{\partial t} = -\frac{1}{L_a}(F_k - f_{lk})\frac{\partial L_a}{\partial t} + \frac{1}{L_a w_{avg}(1-\lambda)}\left(-\frac{\partial Q_{bk}}{\partial x} + f_{lk}\frac{\partial Q_b}{\partial x}\right) \tag{4.4}$$

where F_k is the bed surface fraction of the k^{th} grain size, L_a is the active layer thickness [m], Q_{bk} is the volumetric sediment transport rate of the k^{th} grain size [m^3 s^{-1}], and f_{lk} is the interface exchange fraction which depends on whether the bed is degrading or aggrading:

$$f_{lk} = \begin{cases} f_k, & \text{if } \frac{\partial \eta}{\partial t} < 0 \\ \alpha F_k + (1-\alpha)p_{bk}, & \text{if } \frac{\partial \eta}{\partial t} > 0 \end{cases} \tag{4.5}$$

where f_k is the bed subsurface fraction, p_{bk} is the bedload fraction of the k^{th} grain size, and α is a weighting parameter than ranges from 0 – 1 (I assume $\alpha = 0.5$). The model does not store bed stratigraphy, meaning information on buried sediment size is lost if the channel aggrades and then incises.

The active layer thickness L_a is calculated as three times the surface layer D_{90}. Sediment fluxes are discretized using the κ scheme with flux limiters [*Hirsch*, 2007]:

$$Q_{be} = Q_{bi} + \frac{1}{4}\left((1-\kappa)\psi(r_i) + (1+\kappa)r_i\psi\left(\frac{1}{r_i}\right)\right)(Q_{bi} - Q_{bi-1}) \tag{4.6}$$

where Q_{be} is the volumetric sediment flux out of the control volume centered on the i^{th} cross section [m^3 s^{-1}], Q_{bi-1} and Q_{bi} are the volumetric sediment fluxes at the $i^{th} - 1$ (upstream) and i^{th} cross sections [m^3 s^{-1}], and κ is a constant that controls the discretization scheme. I use second order upwinding ($\kappa = -1$) (other common options are the central difference scheme ($\kappa = 1$) and the Quick scheme ($\kappa = -0.5$) [*Hirsch*, 2007]). r_i is defined as:

$$r_i = \frac{Q_{bi+1} - Q_{bi}}{Q_{bi} - Q_{bi-1}} \tag{4.7}$$

Finally, REM uses the Superbee limiter function (ψ):

$$\psi = max(0, min(2 \times r_i, 1), min(r_i, 2)) \tag{4.8}$$

The model uses two new stream power based equations [*Bagnold*, 1980] for calculating bedload and total load sediment transport capacity (Chapter 3):

$$q_b = 1.43 \times 10^{-4}(\omega - \omega_c)^{3/2} D_s^{-1/2} q^{-1/2} \tag{4.9}$$

$$Q_t = 0.0214(\omega - \omega_c)^{3/2} D_s^{-1} q^{-5/6} \tag{4.10}$$

where q_b is the mass sediment transport rate per unit width [kg m^{-1} s^{-1}], Q_t is the total load [ppm], q is unit discharge [m^2 s^{-1}], D_s is the grain size [m], ω is specific stream power [W m^{-2}], and ω_c is the critical specific stream power for incipient motion [W m^{-2}]. This value is calculated for each grain size using a stream power based hiding function:

$$\frac{\omega_{ri}*}{\omega_{r50}*} = \left(\frac{D_i}{D_{50}}\right)^{-b} \tag{4.11}$$

where $\omega_{ri}*$ is the reference dimensionless specific stream power of the i^{th} grain size, $\omega_{r50}*$ is the reference dimensionless specific stream power of the median grain size, and b is an empirical exponent that varies from 0 (size independent mobilization) to 1.5 (equal threshold mobilization). Stream power is made dimensionless by:

$$\omega_* = \frac{\omega}{\rho(g(s-1)D_s)^{3/2}} \tag{4.12}$$

where ρ is water density [1000 kg m^{-3}], g is gravity [9.81 m s^{-2}], and s is sediment specific gravity (usually 2.65). Details of this hiding function are described in Appendix B.1.1.

Cohesive incision

The model uses a simple excess shear stress equation to model cohesive bed erosion [*Partheniades*, 1965]:

$$E = k\Delta t(\tau - \tau_c) \tag{4.13}$$

where E is the erosion distance [m], k is the erodibility coefficient [m^3 N^{-1} s^{-1}], Δt is the time step [s], τ is the applied shear stress [Pa], and τ_c is the critical shear stress of the bed material [Pa]. The erodibility coefficient can be supplied by the user, or it is calculated based on an empirical relationship developed by *Simon et al.* [2010] after work by *Hanson and Simon* [2001]:

$$k = 1.6 \times 10^{-6}\tau_c^{-0.826} \tag{4.14}$$

Equation 4.13 calculates erosion using excess shear stress, but this model is based on a stream power approach. Since data on τ_c of various soils are widely available in the literature, and there is no work that I am aware of defining critical stream power of cohesive material, I chose to use an empirical equation to calculate average bed shear stresses directly from ω (see Appendix B.1.2 for more information):

$$\tau = 1.96\omega^{0.72} \tag{4.15}$$

This estimated value of τ is then used to calculate cohesive erosion rates (Equation 4.13).

Mixed alluvial/cohesive incision

In streams with both non-cohesive and cohesive bed material, modeling bed elevation changes is more complicated. Sand and gravel can be deposited on top of cohesive material and sediment transport capacity may not be representative of actual sediment movement if the stream is supply limited (e.g. no alluvium on the bed). To account for these processes, I calculate the actual volume of sediment transported out of a cross section as the minimum of the sediment transport capacity (Q_{be}, Equation 4.6) and the sediment available for transport (sum of the incoming sediment from upstream and bank erosion and of the available non-cohesive alluvium on the channel bed). The available non-cohesive alluvium is calculated as:

$$Q_{bk,avail} = \frac{[(\eta - L_a - \eta_{cohesive})f_k + L_a F_k]\, w_{avg}(1-\lambda)\Delta x}{\Delta t} \tag{4.16}$$

where $Q_{bk,avail}$ is the volume of bed sediment of the k^{th} size class available for transport, converted to a rate [m^3 s^{-1}], $\eta_{cohesive}$ is the elevation of the cohesive layer [m], Δx is the distance to the next cross section [m], and Δt is the time step [s]. If $\eta_{cohesive} = \eta$ or F_k or $f_k = 0$, there is no available bed sediment.

4.2.3 Bank Erosion

The model simulates two fundamental bank erosion mechanisms: fluvial erosion and mass wasting. Bank erosion is calculated at the discharge time step (e.g. daily, hourly, 15-min, etc.), independent of the time step for bed aggradation and degradation.

Fluvial erosion

Fluvial erosion is the removal of bank soil by flowing water once the resistance threshold of the bank material has been exceeded. Similar to cohesive incision, REM models fluvial bank erosion using an excess shear stress approach (Equation 4.13). I use an empirical equation to calculate average wall (i.e. bank) shear stress directly from ω (see Appendix B.1.3 for more information):

$$\tau_w = 0.83\omega^{0.65} \tag{4.17}$$

where τ_w is the shear stress acting on the channel bank [Pa]. A user specified fraction of the eroded bank material is added to the bed material load (i.e. sand and coarser). The remainder is exported from the watershed as washload.

Mass failure

Planar mass failure is modeled using a modified version of the Bank Stability and Toe Erosion Model (BSTEM) [*Simon et al.*, 2000, 2011]. BSTEM estimates bank stability using a limit equilibrium analysis to calculate a factor of safety — the ratio of resisting to driving forces acting on the bank. The bank is predicted to be stable if the factor of safety is greater than one and unstable if it is less than one. BSTEM accounts for several processes that increase or decrease bank strength, including: (1) water pressure in soil pores (e.g. positive pressure decreasing stability and negative pressure increasing stability); (2) confining pressure of the streamflow; and (3) increased soil cohesion from plant roots. Although the simplified version of BSTEM accounts for the first two processes, I exclude vegetation effects since they have a negligible effect on BSTEM model output in sensitivity analyses [*Lammers*

et al., 2017] and increase computation time and data requirements. This gives the following factor of safety equation:

$$FS = \frac{cL + (\mu_a - \mu_w)L\tan\phi^b + [W\cos\beta - \mu_a L + P\cos(\alpha - \beta)]\tan\phi'}{W\sin\beta - P\sin(\alpha - \beta)} \tag{4.18}$$

where c is apparent cohesion [kPa], L is the length of the failure plane [m], W is the weight of the soil block per unit bank length [kN m^{-1}], P is the hydrostatic pressure force of the water in the stream [kN m^{-1}], β is the failure plane angle [degrees from horizontal], α is the bank angle [degrees from horizontal], μ_a is the pore-air pressure [kPa], μ_w is the pore-water pressure [kPa], ϕ' is the effective friction angle [degrees], and ϕ^b is an angle describing the rate of increase of shear strength from matric suction (assumed to be 15° [*Lammers et al.*, 2017]).

BSTEM uses a horizontal layer method to calculate a net factor of safety for the bank, accounting for different soil types. The simplified version of BSTEM follows this same basic approach but with these differences:

- Simplified bank geometry (based on a main bank height and angle, and a toe height and angle) rather than the complex geometry incorporated into BSTEM
- Two bank layers (the main bank and bank toe) rather than five distinct layers allowed by BSTEM
- Assumes failure planes intersect the bottom of the bank or the top of the bank toe rather than 50 locations evenly spaced across the bank profile (BSTEM method). This approach is significantly faster and simplifies updating the bank geometry after a failure while still accounting for the most likely failure plane locations.

For a more detailed description of BSTEM see *Midgley et al.* [2012]; *Daly et al.* [2015b]; *Lammers* [2015]; *Simon et al.* [2000, 2011].

Coupled bank erosion modeling

Fluvial erosion and mass failure are linked processes. Fluvial erosion is typically higher at the bank toe, which steepens the bank and makes it more susceptible to mass failure. After a bank fails, the collapsed soil is often deposited at the base of the bank toe. This protects the bank from further fluvial erosion until the collapsed soil blocks have been eroded [*Thorne*, 1982].

I account for these dynamic and coupled processes in two ways. First, fluvial erosion is assumed to be a maximum at the base of the bank toe. Therefore, this node is eroded the most, with zero erosion at the top of the toe, creating a steeper toe angle. If the new toe angle exceeds 90° (e.g. an undercut bank), the overhanging bank immediately collapses, and the upper bank angle is updated accordingly. This bank steepening, coupled with bank heightening from bed erosion, increases the chance of mass failure. If the bank fails, the collapsed soil block is deposited at the bank toe — narrowing the channel — and the toe angle is reduced to conserve the mass of the eroded block. If the failed soil block is too large for it all to fit at the base of the toe, any extra bank material is stored in "tank". No further erosion of the bank is allowed until the material in this "tank" is eroded [*Lai et al.*, 2015]. See Appendix B.1.4 for more details.

4.2.4 Meandering

In addition to incising, meandering channels can also reduce their slope via lateral migration. The model incorporates this process by simulating meander migration from fluvial erosion, allowing the channel to increase its length, thereby decreasing its slope.

Flow through bends is complex, creating unique distributions of shear stresses which directly influence bed and bank erosion. Generally, a primary helical flow cell directs water at the surface towards the outer bank, and drives eroded sediment along the bed towards the inner bank [*Markham and Thorne*, 1992]. This helical flow pattern and the effects of inner point bars forces flow to the outer bank where maximum shear stresses are often observed

[*Dietrich*, 1987]. Flume experiments suggest that the maximum shear stress on the outside of bends may be 2 – 3 times the boundary average shear stress [*Drinker*, 1961].

The effects of curvature on the flow field and shear stress distribution can be simulated by directly modeling flow mechanics, typically using a high resolution 1-D or 2-D model [*Crosato*, 2007; *Huang et al.*, 2014; *Darby et al.*, 2002]; however, REM does not directly calculate the flow field or boundary shear stress distribution, meaning it cannot mechanistically account for the effects of bend geometry on bank erosion. Instead, I use an empirical equation to find the maximum shear stress at the outer bank in bends [*Army Corps of Engineers*, 1970]:

$$\tau_{max} = 2.65\tau_w \left(\frac{R_c}{w}\right)^{-1/2} \tag{4.19}$$

where τ_{max} is the maximum bend shear stress [Pa], τ_w is the wall shear stress calculated using Equation 4.17 [Pa], R_c is the bend radius of curvature [m], and w is the channel bottom width [m].

This empirical equation is based on only five small flume datasets, and more recent analysis suggests that no single relationship adequately predicts maximum shear stress in bends [*Thornton et al.*, 2012]. Field studies, however, show that radius of curvature is a major control on channel migration rate [*Nanson and Hickin*, 1983, 1986; *Hooke*, 1997]. I therefore used Equation 4.19 — imperfect as it may be — to account for this process. Bend migration rates peak when R_c/w is between 2 and 3 [*Nanson and Hickin*, 1983, 1986] but drop significantly at values of $R_c/w < 2$, often near rates observed in mild curves ($R_c/w > 8-10$) [*Hooke*, 1997]. I therefore only use Equation 4.19 to adjust shear stress when $R_c/w > 2$.

Including meander dynamics in the model requires two new user inputs for each reach. Radius of curvature and sinuosity are both used to build and track changes in channel planform. To do this, I conceptualize the channel as a series of circular arc segments, where each arc is one bend. The number of bends between each cross section can be calculated from the user defined cross section spacing, radius of curvature, and sinuosity using equations describing circular arcs (see Appendix B.1.5 for more details).

4.2.5 Knickpoint Migration

Knickpoints or headcuts are small waterfalls or locally steep stream sections where bed erosion is especially pronounced. These vertical drops tend to migrate upstream as they erode, and can initiate substantial bank erosion [*Schumm et al.*, 1984]. I use a simple, empirical model to simulate headcut advance [*Allen et al.*, 2018]:

$$hc_m = 0.00126 \times Ehc \times Q_{cum}^{0.5} \times H_{hc}^{0.225} \tag{4.20}$$

where hc_m is the headcut migration distance [m], Q_{cum} is cumulative daily discharge [m^3], H_{hc} is headcut height [m], and Ehc is an erodibility resistance parameter that is a function of soil erodibility and vegetation cover:

$$Ehc = 17.8 + 16.5K_d - 15RCF \tag{4.21}$$

where K_d is soil erodibility [cm h^{-1} Pa^{-1}] and RCF is a root cover density factor (dimensionless, 0 – 1.4). While channel beds are usually unvegetated, using $RCF = 0$ sometimes requires a negative K_d value to accurately predict knickpoint migration rates; therefore, REM assumes $RCF = 1.4$ and requires users to calibrate K_d to match observed migration rates (see Appendix B.1.6 for more details). This sub-model requires the user to input the location, elevation, height, and K_d of each knickpoint. The position of each knickpoint is tracked as it migrates upstream (including into any tributaries) and bed elevations are adjusted accordingly.

4.2.6 Cross Section Geometry

REM assumes a prismatic channel, based on user-supplied bottom width, bank and toe heights and angles, and floodplain width and slope (Figure 4.1). All channel geometry variables are unique for the right and left banks. Bank soil parameters (e.g. cohesion) can be distinct for the bank toe and upper bank soil but are the same for the right and left banks

in a reach. For each cross section, a cohesive layer may be placed some distance below the channel bed. Aggradation and degradation only occur across the flat channel bottom.

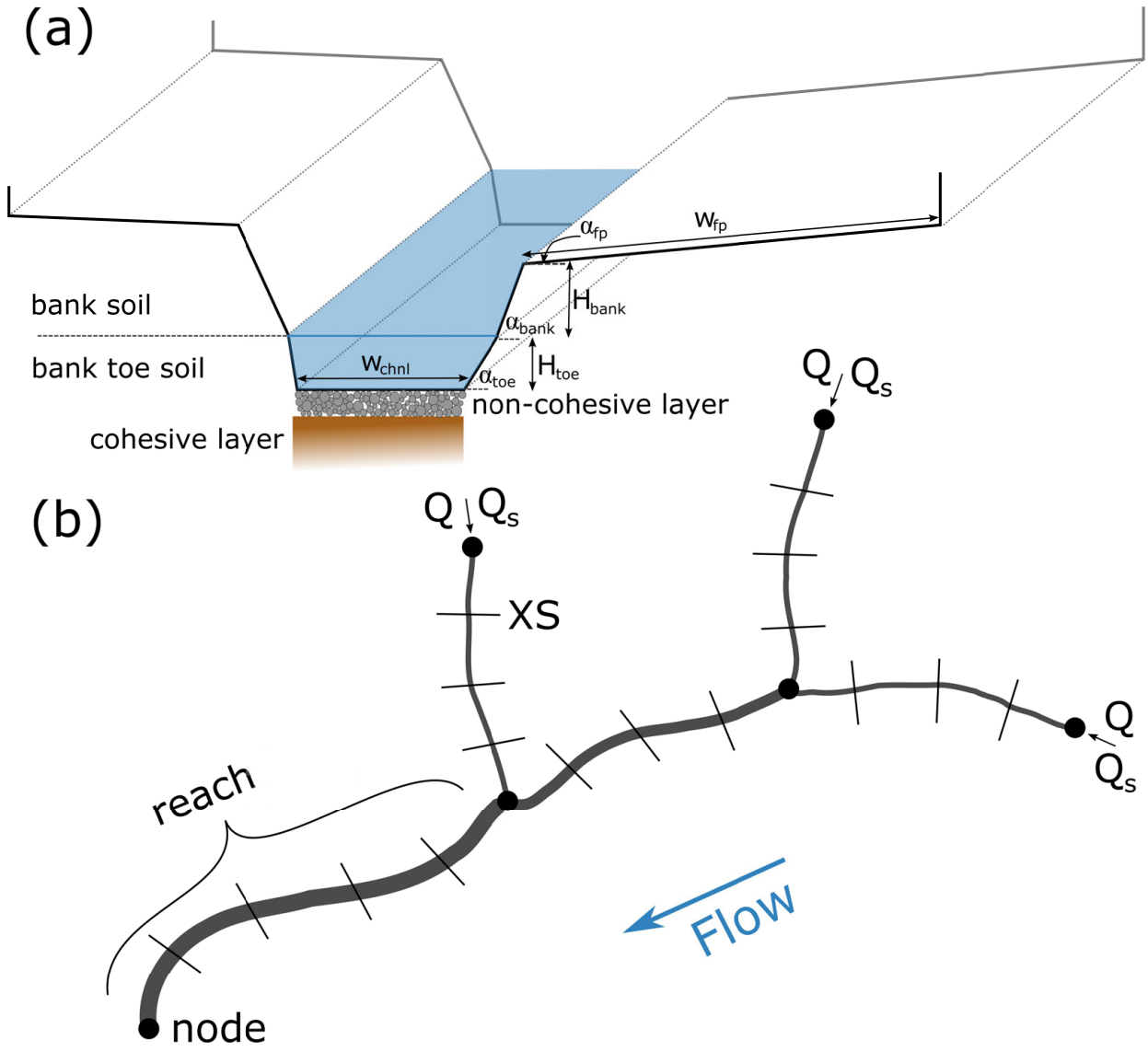

Figure 4.1: Schematic of cross section (a) and network (b) geometry included in REM. w = width; H = height, α = angle, Q = water discharge, and Q_s = sediment discharge. Cross section geometry can be unique for each side of the channel and the bank and bank toe can have unique soil properties (e.g. cohesion).

4.2.7 Network Structure and Sediment Routing

The model uses a simple reach-node network structure, where a series of channel reaches are connected by nodes (Figure 4.1) [*Schmitt et al.*, 2016; *Czuba and Foufoula-Georgiou*, 2015]. The user specifies inputs individually by reach, and each reach may have multiple cross sections. Incoming bed material load to each cross section is the sum of sediment supplied by the upstream cross section (or cross sections in the case of a tributary junction), sediment from local bank erosion, and any user-inputted upland sediment supply. Upland sediment supply and bed material load from eroded banks are assumed to be the same grain size distribution as the initial bed grain size distribution for that reach. The washload component of any bank, cohesive bed, or knickpoint erosion is immediately routed to the watershed outlet. The effects of grade controls or bank armoring can be incorporated by placing non-erodible cross sections within the channel network (i.e. cohesive soils with very high τ_c). All required and optional model inputs are summarized in Appendix B.2.

4.3 Model Testing

4.3.1 Generic Model Test

I simulated channel evolution in a generic watershed with six distinct reaches. The total channel length of 10.4 km corresponds to an approximate drainage area of 6.5 km^2 based on *Hack* [1957]. Initial grain size (2 mm), slope (0.003), and bank height (2 m) were constant throughout the watershed. Discharge was steady at a station but increased moving downstream. Upstream sediment supply was equal to the transport capacity of the undisturbed channel. A full table of model inputs is included in Appendix B.2. Beginning with an initially stable channel, I dropped the downstream elevation by 2.5 m, including a 1.5 m tall knickpoint. I modeled 20 years of resulting channel evolution.

4.3.2 Colorado River

Study area

Parker Dam, completed in 1938, is one of several large dams on the lower Colorado River built for water supply and power generation. Like most hydropower dams, Parker Dam altered flows and trapped sediment. The combined effects of these changes caused the Colorado River downstream from the dam to incise while the bed material coarsened [*Williams and Wolman*, 1984].

Data collection and modeling

Initial longitudinal profiles and grain size data for a 144 km reach downstream of Parker Dam were obtained from two U.S. Bureau of Reclamation reports [*U.S. Bureau of Reclamation*, 1948, 1950]. I used a single grain size distribution for the entire reach. The pre-dam grain size data were all finer than 2 mm; however, later observations included gravel up to 32 mm, presumably unearthed as the channel incised. Since the channel coarsened over time (and REM does not account for bed stratigraphy), I adjusted the initial grain size distribution to include a small amount of coarser material. Average channel widths were calculated from 1938 aerial photographs [*Norman et al.*, 2006] and contemporary satellite imagery [*Google Earth Pro*, 2017a].

I ran the model from 1938 – 1975 using daily discharge data from USGS gage 09427520 (CO River below Parker Dam, AZ-CA). Only bed elevation changes were modeled, bank erosion was not included. I used a cross section spacing of 2000 m and a time step of 2400 seconds. The total load sediment transport equation was used for all grain sizes < 4 mm and the bedload equation for all coarser grain sizes. I assumed no sediment inputs from upstream (e.g. the dam trapped all sediment) and a fixed downstream bed elevation. Model results were compared to measured longitudinal profiles for a 66 km subreach (from 27 – 93 km downstream of Parker Dam) [*Williams and Wolman*, 1984]. I also compared modeled

Table 4.1: Model inputs for the Colorado River downstream of Parker Dam.

Variable	Single Run Value	Monte Carlo Range	Source
Width [m]	220	170 – 270	Aerial Imagery
Floodplain width [m]	1000	500 – 1500	Aerial Imagery
Floodplain angle [degrees]	0	0 – 2	Assumed
Channel roughness (n)	0.04	0.03 - 0.05	Assumed
Floodplain roughness (n)	0.06	0.05 – 0.07	Assumed
Hiding function coefficient (ω_{c*})	0.1	lognormal; mean = -2.3, sd = 0.4	Chapter 3
Hiding function exponent (b)	0.8	0.3 – 1.2	Appendix B.1.1
Bank height [m]	4	–	Assumed
Bank angle [degrees]	90	–	Assumed

D_{50} to measured values from three cross sections (26, 64, and 130 km downstream of Parker Dam) [*Williams and Wolman*, 1984].

In additional to the single model run described above, I ran 5000 Monte Carlo simulations varying the initial grain size distribution, channel width, floodplain geometry, roughness values, and the exponent and coefficient of the hiding function. Sobol' quasi-random numbers (using the "gsl" R package; [*Hankin*, 2006]) were used to generate these variables since they provide more uniform coverage than simple random numbers [*Sobol'*, 1976].

4.3.3 North Fork Toutle River

Study area

The North Fork Toutle River (NFTR) was a typical gravel bed mountain river draining the northern slope of Mount St. Helens. On May 18, 1980, the volcano erupted following a massive debris avalanche on the north face. This deposited about 2.8 km^3 of sediment across the upper part of the NFTR, with depths averaging 45 m but reaching 140 m in some areas [*Simon et al.*, 1999]. Deposits were mostly sand (mean D_{50} = 1.6 mm) but ranged in size from silt to boulders [*Simon et al.*, 1999; *Voight et al.*, 1981]. This massive

sediment deposit buried the drainage network of the upper NFTR. Over the following months and years, channels reformed from surface runoff, emergency pumping from Spirit Lake to control water levels, and multiple lahars (volcanic debris or mudflows) [*Simon et al.*, 1999]. To prevent sedimentation in the downstream Cowlitz and Columbia Rivers, two sediment retention structures where built on the NFTR. The first (N1) was built in summer 1980 and operated until it was breached in 1982. A second, more permanent sediment retention structure (the "SRS"), was built in 1987 and was essentially filled by 1998 [*Simon et al.*, 1999; *Zheng et al.*, 2014]. To prevent overtopping of Spirit Lake, water was released into a NFTR tributary (Truman Channel; see TR065 and TR070 in Figure 4.2) at a constant rate of 5.1 m^3 s^{-1} from November 1982 to August 1983, causing extreme incision (up to 34 m) [*Paine*, 1984]. For more details on the eruption and its effects, see *Simon et al.* [1999], *Lipman and Mullineaux* [1981], and *Major et al.* [2018].

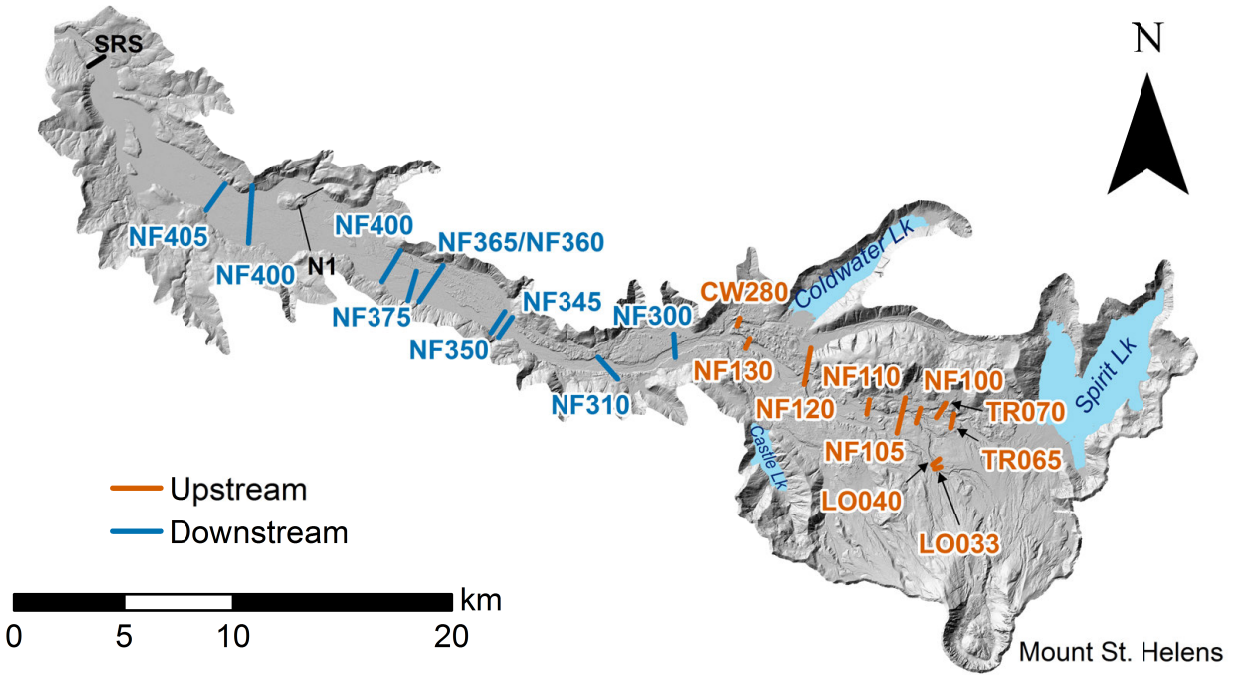

Figure 4.2: Overview of the North Fork Toutle River watershed upstream of the SRS. Shaded relief from 2009 LiDAR data [*Mosbrucker*, 2014]. Modeled cross sections are differentiated into "upstream" and "downstream" which will be referenced in certain result figures. Flow is from right to left.

Data collection and modeling

I modeled evolution of the upper NFTR and its tributaries from September 1983 – August 2011. I started the model nearly 3.5 years after the eruption because there were more cross section data and this avoided several lahars and pumping from Spirit Lake which had complicated effects on channel adjustment. Following the eruption, the USGS and Army Corps of Engineers established a monitoring program to document the response of the rivers draining Mount St. Helens. This monitoring included the establishment of several permanent cross sections which have been surveyed at irregular intervals since 1980. I used these data [*Mosbrucker et al.*, 2015] for 19 cross sections on the NFTR and its tributaries to estimate initial channel and floodplain geometry (Figure 4.2). Each of these cross sections defined a model reach with unique inputs. Initial bed grain sizes were estimated from data collected by the Army Corps of Engineers [*U.S. Army Corps of Engineers*, 1988] and others [*Paine*, 1984]. I used the daily discharge series at the SRS constructed by *Simon and Klimetz* [2012] from several nearby USGS gages. These values were scaled by drainage area to compute discharge in each reach. I also used bank sediment properties (τ_c, k, cohesion, unit weight, and ϕ') and Manning's n values estimated by *Simon and Klimetz* [2012]. I assumed no hillslope sediment supply since upland erosion peaked soon after the eruption and remained negligible compared to in-stream sediment sources [*Simon et al.*, 1999].

I used a model cross section spacing of 500 m, a time step of 2400 seconds, and the bedload sediment transport equation. Sediment specific gravity was adjusted to account for lighter volcanic material [*Simon and Klimetz*, 2012, Eq. 24]. Finally, I assumed that 100% of the eroded bank material consisted of bed material load. See Table 4.2 for all model inputs. I ran 5000 Monte Carlo simulations to quantify uncertainty, varying initial grain size, channel width, channel roughness, hiding function parameters, and bank soil properties. Model accuracy was assessed by comparing modeled bed elevations to observations (from survey data and a 1 m DEM from 2009 [*Mosbrucker*, 2014]). Other parameters (e.g. D_{50} and width)

were not used because only sparse grain size data were available and the simplified model cross sections could not adequately represent the complex observed channel geometries.

Table 4.2: Model inputs for the North Fork Toutle River. Each of the 19 cross sections have unique inputs so the median and range of the single model run and range of the Monte Carlo runs are shown.

Variable	Single Run Median	Single Run Range	Monte Carlo Range	Monte Carlo Method
Width [m][a]	11.6	4.0 – 263.1	2.0 – 394.6	±50% initial
D_{50} [mm][b]	2.26	0.79 – 2.95	0.24 – 7.20	25^{th} – 75^{th} %tile of all GSD
σ_g [mm][b]	7	6.4 – 10.1	6.0 – 9.3	25^{th} – 75^{th} %tile of all GSD
Bank τ_c [Pa][c]	12	5.5 – 32.1	2.8 – 48.1	±50% initial
Bank Erodibility [m^3 N^{-1} s^{-1}][c]	2.0e-07	9.1e-08 – 3.9e-07	4.6e-08 – 5.8e-07	±50% initial
Bank Cohesion [kPa][c]	0	0.0 – 0.0	0.0 – 1.0	0 – 1
Bank ϕ' [degrees][c]	30	25.2 – 34.0	12.6 – 51.0	±50% initial
Bank Soil unit weight [kN m^{-3}][c]	19.1	18.1 – 19.8	9.1 – 29.7	±50% initial
Channel roughness (n)[c]	0.04	0.030 – 0.065	0.015 – 0.065	50 – 100% initial
Hiding function coefficient (ω_{c*})[d]	0.1	–	0.025 – 0.4	lognormal; mean = -2.3, sd = 0.4
Hiding function exponent (b)[e]	0.8	–	0.3 – 1.2	Uniform

[a]XS Data [*Mosbrucker et al.*, 2015]
[b]Full grain size distribution. TR065 – NF120: *Paine* [1984]; others: *U.S. Army Corps of Engineers* [1988]
[c]*Simon and Klimetz* [2012]
[d]Chapter 3
[e]Appendix B.1.1

4.3.4 Sensitivity Analysis

For both case studies, I performed a sensitivity analysis of the model to determine which variables most influence model output. I used a density-based sensitivity analysis method that calculates differences between conditional and unconditional probability density functions of model output to estimate parameter sensitivity [*Plischke et al.*, 2013]. Variables

with a greater effect on model output have bigger differences between these conditional and unconditional probability density functions. This method has two advantages over other approaches: it requires no unique input parameter sampling design [e.g. *Saltelli et al.*, 2010] and it requires much fewer model runs [e.g. *Pianosi and Wagener*, 2015]. I therefore used the output from the uncertainty analysis directly to compute the sensitivity indices. Bootstrapping with 1000 replicates was used to correct for bias and calculate confidence bounds for the sensitivity indices. Finally, I incorporated a dummy variable to determine the threshold for influential variables. This dummy variable is a simple set of random numbers that has no influence on the model. Incorporating the dummy variable accounts for noise in the sensitivity analysis [*Plischke et al.*, 2013; *Khorashadi Zadeh et al.*, 2017].

These sensitivity analyses are only applicable for each individual case study. I did not account for variability in every input (e.g. discharge or initial longitudinal profile) and each case study has unique boundary conditions and relevant processes. Because of this, it is necessary to perform a sensitivity analysis separately for every model application to understand what variables are most influential in each case. Luckily, this is feasible using the *Plischke et al.* [2013] method and the output of simple Monte Carlo simulations.

For the Colorado River, I examined the sensitivity of two model outputs: bed elevation changes and changes in bed D_{50}. For the Toutle River, changes in channel width were also included. To give a single output value for each model run, I summed the absolute value of the total change in the variable (e.g. bed elevation) for each cross section. For the NFTR, a separate sensitivity analysis was performed for each reach because model inputs were varied independently for each. For comparison among reaches, I standardized the sensitivity indices by taking the difference between the index for each input variable and the "dummy" variable, divided by the dummy variable index. All analyses of model outputs were done using R version 3.4.1 [*R Core Team*, 2018].

4.4 Results

4.4.1 Generic Model Test

Figure 4.3 shows changes in bed elevation, channel width, and width-depth ratio for the modeled test case. The zone of disturbance migrated upstream through time, with changes in channel width lagging slightly behind changes in bed elevation. The greatest channel changes were at the far downstream end — the area with greatest disturbance.

Figure 4.4 shows changes in stream power, bed elevation, and channel width at two locations (indicated in Figure 4.3(a)). For both areas, stream power was relatively constant until the knickpoint passed, after which stream power spiked before slowly decreasing. Bed elevation and width show similar trends, with abrupt changes following passage of the knickpoint. After the initial drop in channel elevation, both cross sections showed a period of aggradation followed by renewed incision. Sediment export from the watershed peaked early in the simulation and then decreased exponentially.

4.4.2 Colorado River

Figure 4.5 shows the error in predicted bed elevation along the reach for three different years. The median of the Monte Carlo simulations generally has lower error than the single model run. Furthermore, model error decreases over the course of the simulation, although the uncertainty increases.

Figure 4.6 shows the error in predicted bed D_{50} over time at three different cross sections. The single model run and median of the Monte Carlo simulations generally have similar error, and uncertainty is high for all sites. At the more upstream site (XS 26), the modeled both over- and under-predicted bed D_{50} over the simulation period; however, at the lower two cross sections the model consistently over-predicted bed grain size.

Figure 4.7 shows the results of the sensitivity analysis for bed elevation and bed D_{50} outputs. Initial D_{50}, geometric standard deviation of the grain size distribution (σ_g), and channel width have the largest influence on predicted bed elevation changes. Initial D_{50} and

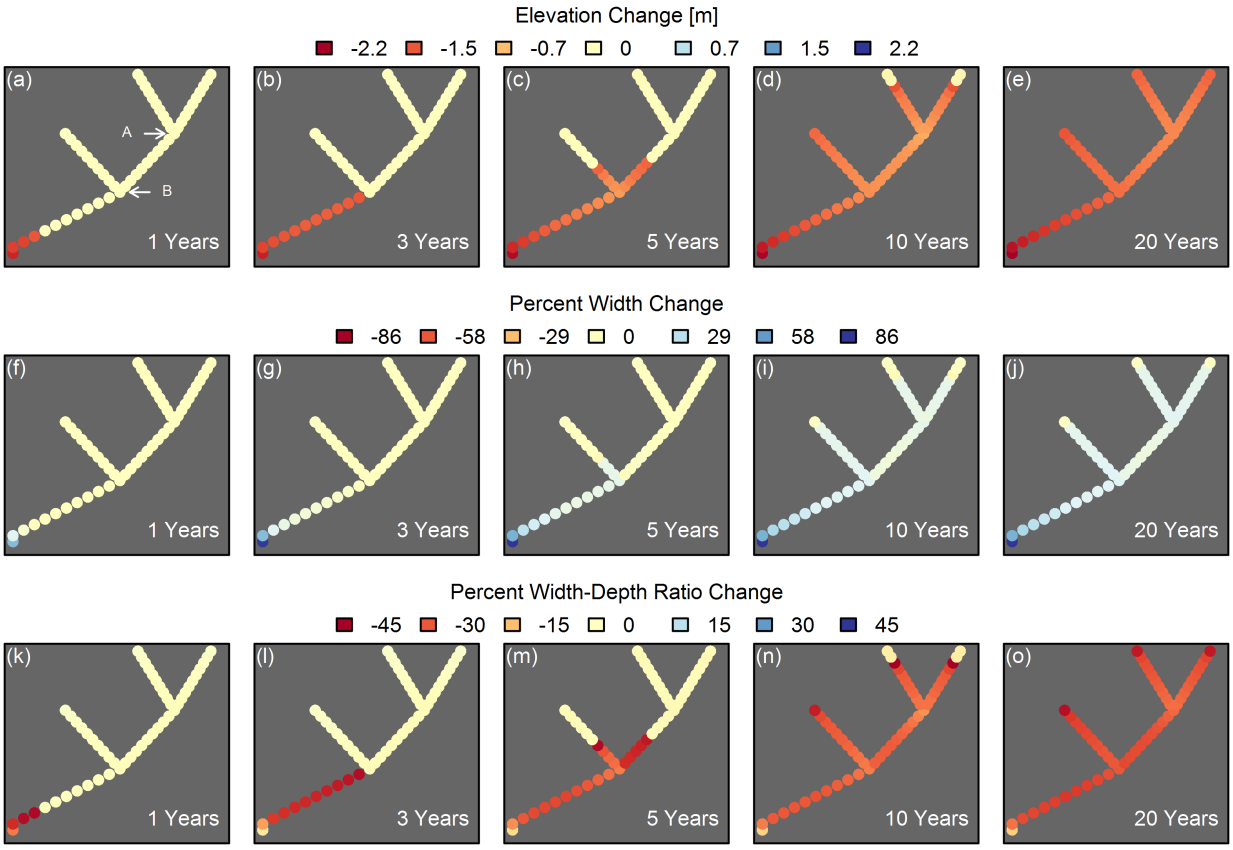

Figure 4.3: Modeled change in bed elevation (a–e), channel width width (f–j), and width-depth ratio (k–o) throughout the generic channel network for five of the simulation years. Each point represents one cross section.

σ_g have a significant effect on the final D_{50} while channel width and the hiding function parameters (ω_c and b) have only a small effect. Floodplain angle has a moderate impact on both outputs.

4.4.3 North Fork Toutle River

Figure 4.8 shows modeled and observed bed elevations for the NFTR. The model predicted channel change well at the majority of sites, mostly in the upper half of the watershed (CW280 – NF130, NF350, and NF405). These cross sections have generally low error in predicted final bed elevations normalized to the magnitude of total bed elevation change (Figure 4.9). Median normalized error is 43%, but is only 22% for reaches CW280 – NF130. For many of these cross sections, the single model run and median of the Monte Carlo sim-

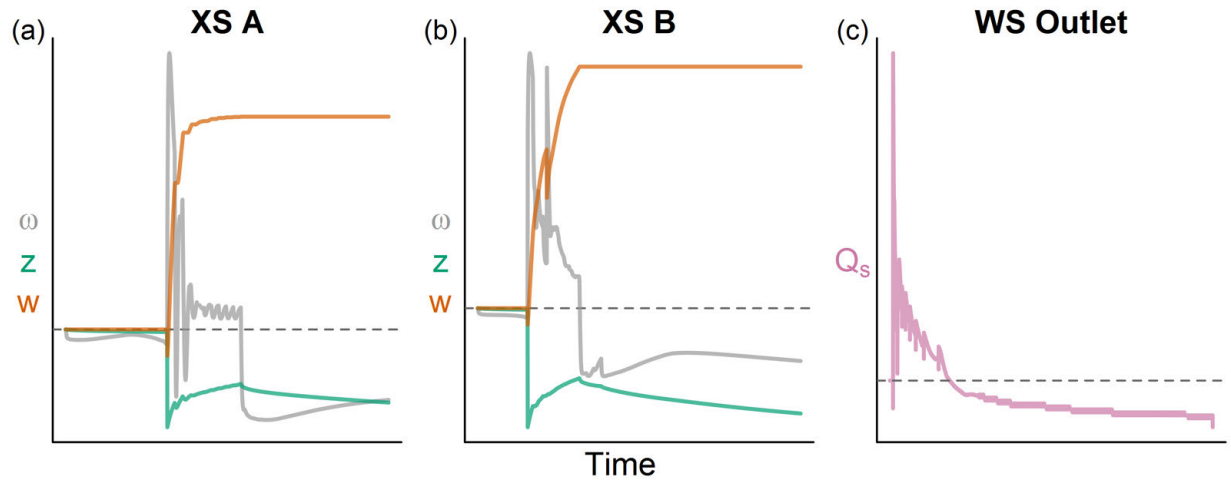

Figure 4.4: Changes over time in specific stream power (ω), bed elevation (z), and channel width (w) for two locations in the simulated drainage network (indicated in Figure 4.3(a)). Sediment discharge at the watershed outlet is also shown. All values are scaled to their starting value (horizontal lines).

ulations are very similar. For the remainder of the cross sections, the model did a relatively poor job of predicting changes in bed elevation.

There is substantial uncertainty for all sites, especially in the upper half of the watershed (e.g. $>$ 20 m wide 90% confidence interval). The magnitude of uncertainty is generally less in the lower portion of the watershed where the magnitude of aggradation and incision was smaller.

Figure 4.10 shows initial and final modeled cross sections along with surveyed geometry. Like the channel bed elevation results, the upstream half of the watershed matches observations much better than the lower half.

The sensitivity results for the NFTR model runs are summarized in Figure 4.11. Modeled bed elevation was influenced most by bank τ_c, bank cohesion, and hiding function parameters (ω_c and b). Channel width and initial bed grain size (D_{50} and σ_g) also had a minor effect. Modeled D_{50} was influenced by similar variables, but the hiding function parameters, initial grain size, and bank cohesion had a much larger effect. For modeled channel width, bank τ_c was by far the most influential but initial width and ω_c also contributed to some observed model uncertainty.

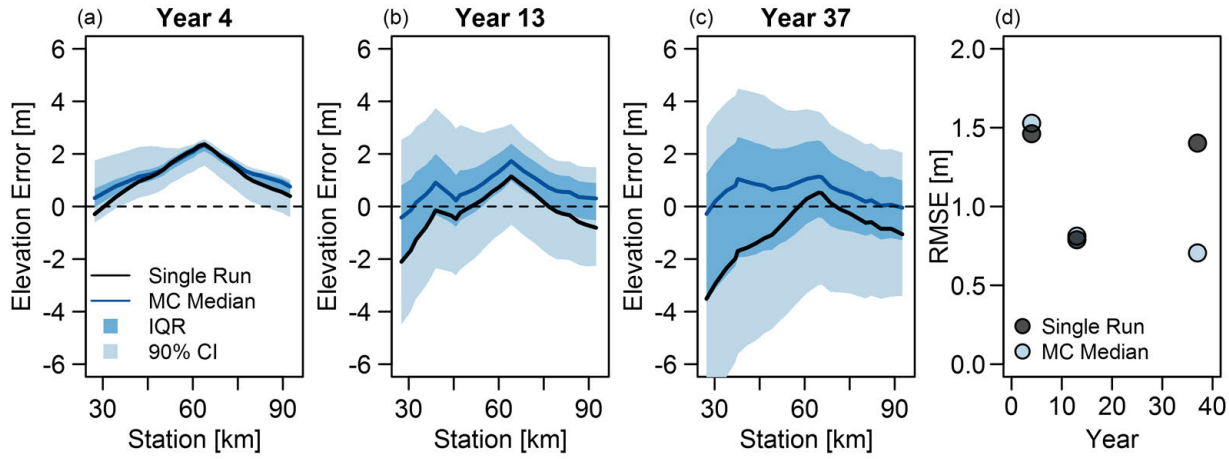

Figure 4.5: Error in modeled bed elevation along the Colorado River reach for three simulation years (a–c) for the single model run and summary of the Monte Carlo results (median, inter-quartile range (IQR) and 90% confidence interval). Part (d) shows the root mean squared error (RMSE) for the single model result compared to the median of the Monte Carlo simulation.

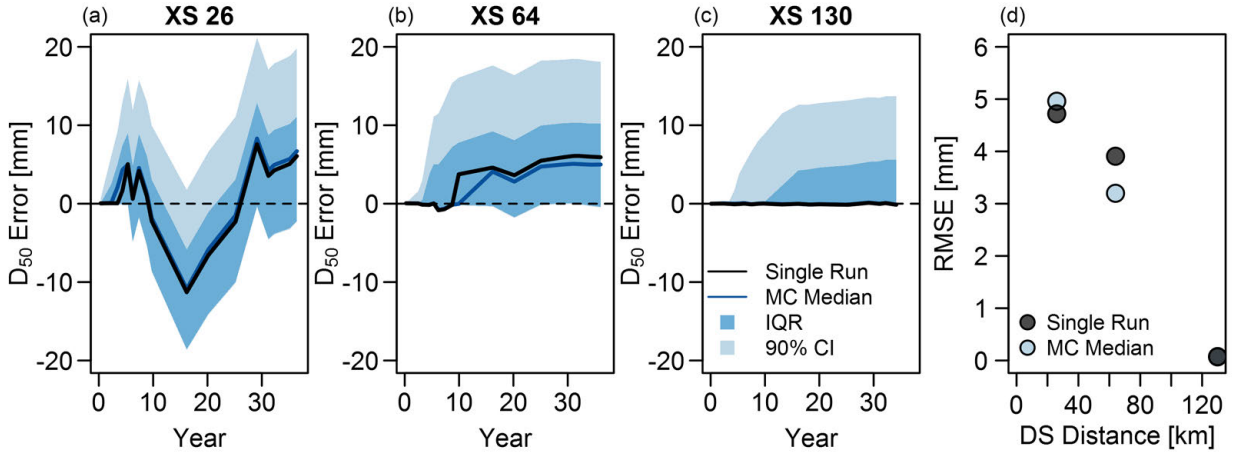

Figure 4.6: Error in modeled bed D_{50} over the course of the simulation for three cross sections along the Colorado River reach (a–c) for the single model run and summary of the Monte Carlo results (median, inter-quartile range (IQR) and 90% confidence interval). Part (d) shows the RMSE for the single model result compared to the median of the Monte Carlo simulation. For XS 130 the RMSE points for the single run and MC median overlap.

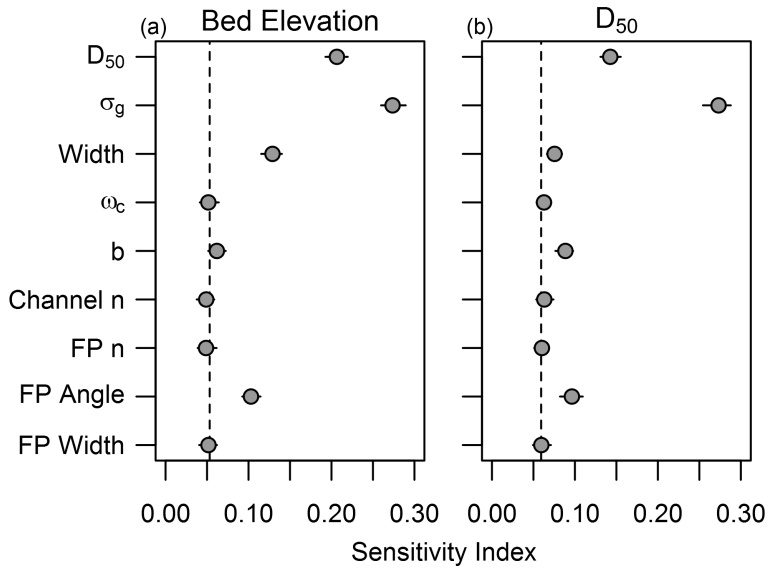

Figure 4.7: Sensitivity results from the Colorado River for the modeled bed elevation (a) and bed surface D_{50} (b). Points at or below the vertical dashed line had no influence on model output. Points are bias corrected sensitivity estimates with ranges of estimated value from bootstrapping.

4.5 Discussion

4.5.1 REM Accurately Predicts Channel Change

The generic test case and field applications show that REM can accurately simulate channel evolution. First, the model test case matches physical understanding of channel evolution in response to disturbance (in this case, base level drop). The greatest channel change is observed nearest the disturbance, and rates and magnitudes of erosion decline nonlinearly with time and distance upstream (Figure 4.3). This is consistent with conceptual models of channel evolution [*Schumm et al.*, 1984; *Simon*, 1989], and experimental [*Begin et al.*, 1981], numerical [*Simon and Darby*, 1997], and field studies [*Simon and Rinaldi*, 2006]. In general, the channel incises which destabilizes the banks, leading to rapid widening

Figure 4.8 ***(following page)*:** Observed and modeled bed elevations for 19 cross sections in the North Fork Toutle River (generally shown in order of upstream to downstream). Modeled results are shown for the single model run and median, interquartile range (IQR), and 90% confidence interval for the Monte Carlo simulations. Model results start to diverge significantly from observations at NF300.

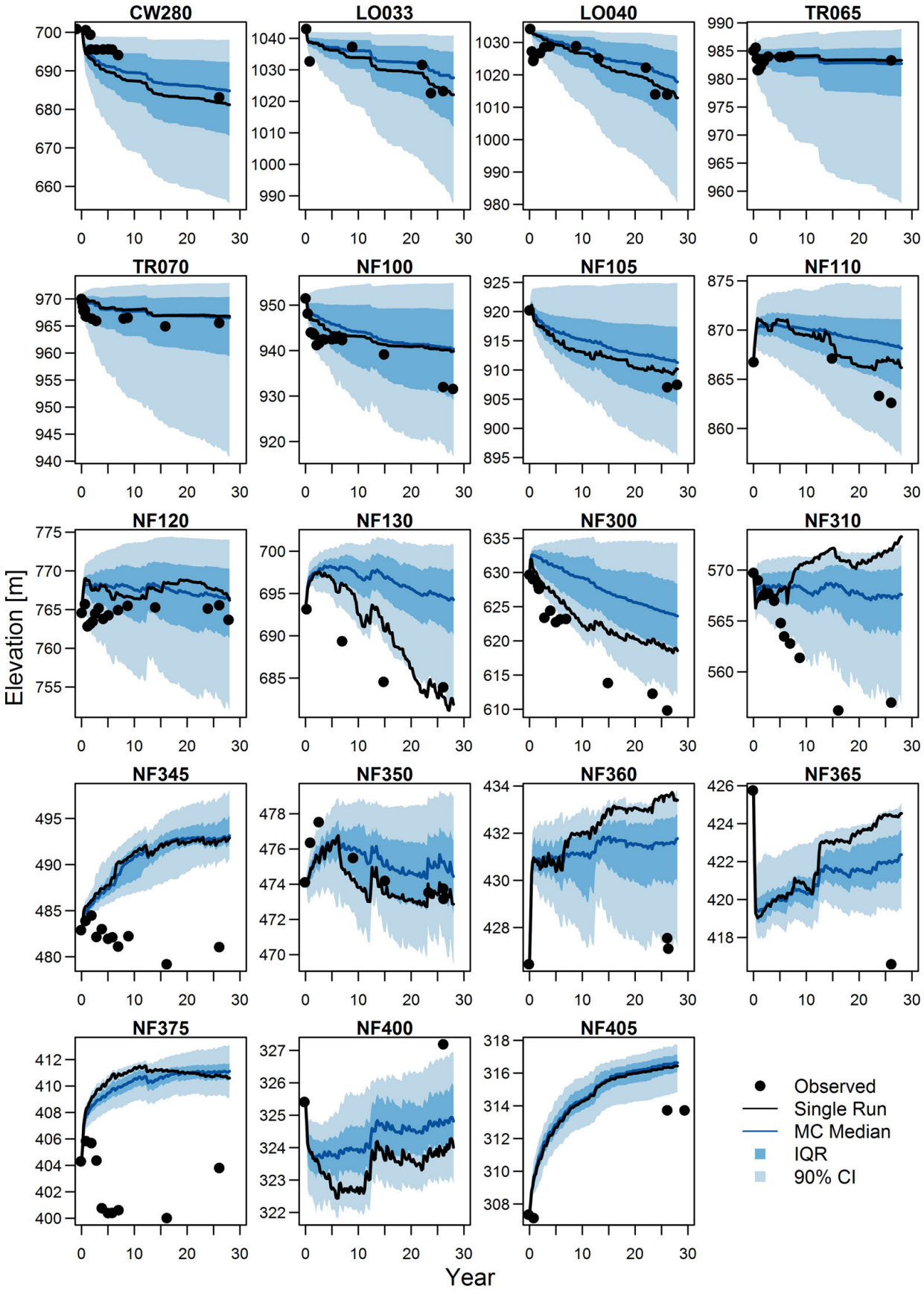
CW280
LO033
LO040
TR065
TR070
NF100
NF105
NF110
NF120
NF130
NF300
NF310
NF345
NF350
NF360
NF365
NF375
NF400
NF405
Elevation [m]
Year
Observed
Single Run
MC Median
IQR
90% CI

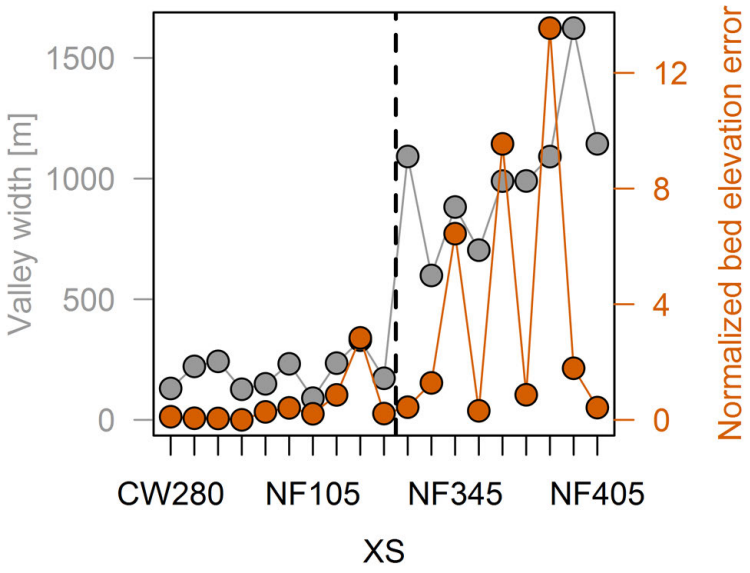

Figure 4.9: Valley width and error in modeled bed elevation for each cross section in the North Fork Toutle River (generally shown in order of upstream to downstream). Errors are generally higher where the valley width becomes significantly wider.

(Figure 4.4). As the upstream channel begins to erode, large amounts of sediment are delivered downstream, causing aggradation. After this upstream sediment supply is cut off (i.e. upstream channel erosion has slowed or stopped), channel incision begins again. This shift between degradation and aggradation depending on sediment delivery from upstream is an important control on channel evolution, as demonstrated in both numerical modeling [*Simon and Darby*, 1997] and field studies [*Simon and Hupp*, 1992]. Downstream aggradation can help stabilize these reaches and allows the channel to more rapidly attain a new stable slope [*Doyle and Harbor*, 2003]. Disrupting this downstream sediment delivery, for example by installing grade control structures, can induce a second round of incision downstream [*Simon and Darby*, 2002], similar to what the modeling showed (Figure 4.4).

Following a disturbance, the channel is expected to adjust rapidly, with the rate of change slowing until the channel reaches some new stable state. This results in an exponential

Figure 4.10 ***(following page)*****:** Observed and modeled initial and final cross sections on the North Fork Toutle River (generally shown in order of upstream to downstream). The year of the initial and final observation data are also shown.

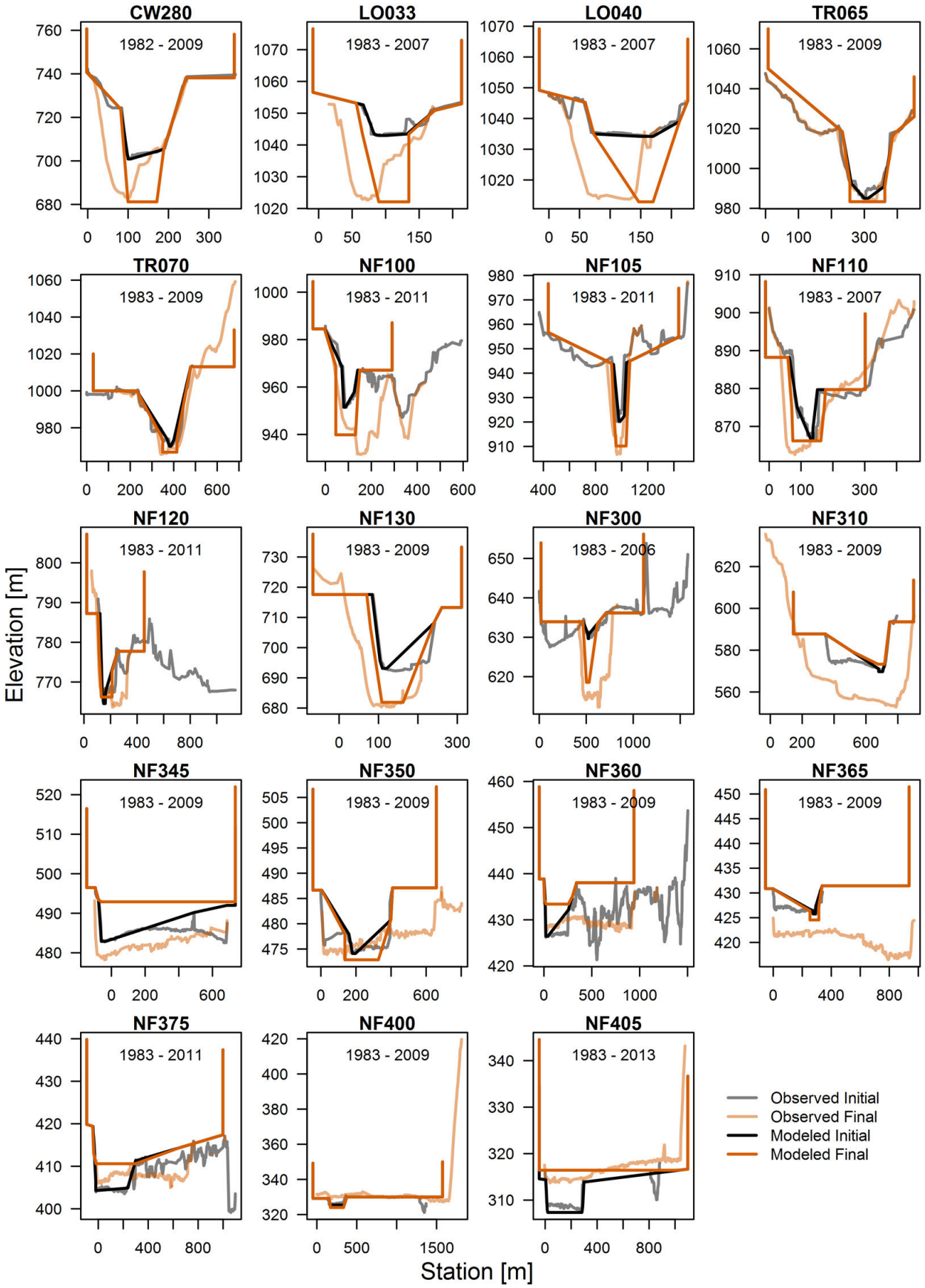
CW280
1982 - 2009
LO033
1983 - 2007
LO040
1983 - 2007
TR065
1983 - 2009
TR070
1983 - 2009
NF100
1983 - 2011
NF105
1983 - 2011
NF110
1983 - 2007
NF120
1983 - 2011
NF130
1983 - 2009
NF300
1983 - 2006
NF310
1983 - 2009
NF345
1983 - 2009
NF350
1983 - 2009
NF360
1983 - 2009
NF365
1983 - 2009
NF375
1983 - 2011
NF400
1983 - 2009
NF405
1983 - 2013
Elevation [m]
Station [m]
Observed Initial
Observed Final
Modeled Initial
Modeled Final

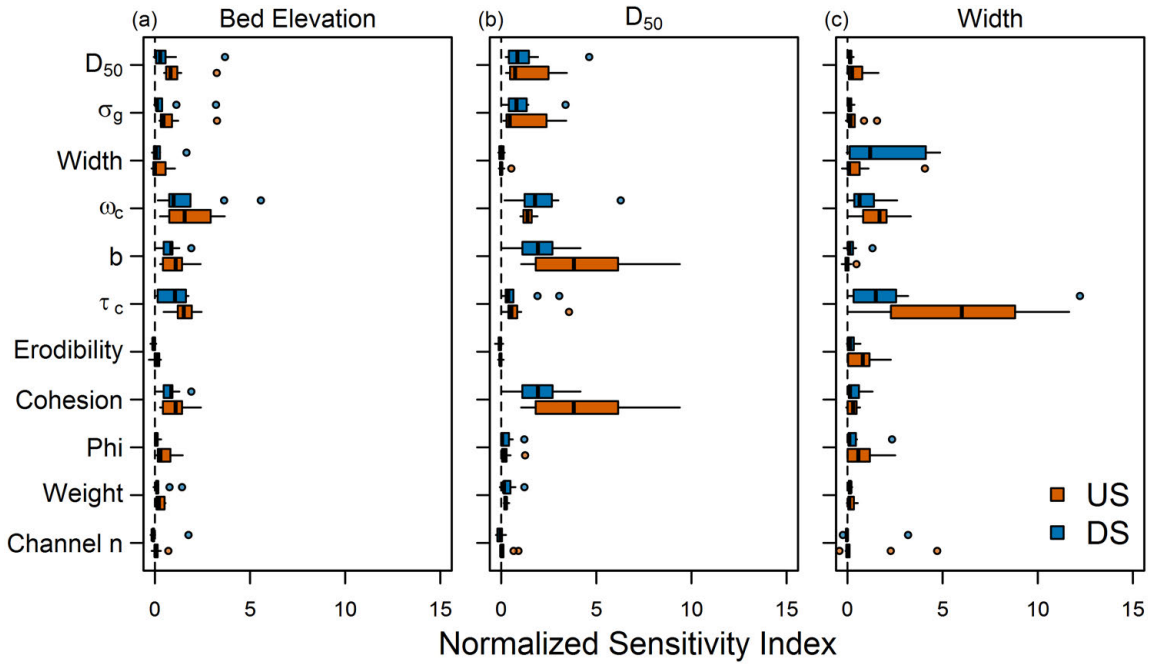

Figure 4.11: Summary of sensitivity results from the North Fork Toutle River modeling for three outputs: (a) bed elevation, (b) D_{50}, and (c) channel width. Sensitivity indices for each input variable were computed separately for each of the 19 cross sections. Boxplots summarize these indices, separated by the upstream channel (upstream of NF130), and downstream channel (NF300 through NF405). This is the same division as the vertical line in Figure 4.9. For clarity, cohesion, phi, and weight results are shown for the higher value of either the bank or bank toe. Vertical dashed line is a normalized sensitivity index of zero (i.e. no influence on model output).

decay in channel variables to some asymptote. These variables may include stream power [*Bull*, 1979], sediment discharge [*Simon*, 1999], or bed elevation [*Begin et al.*, 1981], but all describe a reduction in the rate of energy dissipation [*Simon*, 1992]. Modeling shows these exponential reductions in specific stream power and sediment discharge, and an exponential increase in channel width (Figure 4.4). Bed elevation follows a more complex trajectory, but does decrease towards an asymptote during the second round of incision. Modeled width-depth ratio decreases initially as the bed level drops, but then increases again as the channel widens. None of the cross sections (with the exception of the most downstream one, Figure 4.3) return to their pre-disturbance width-depth ratio. This is consistent with previous modeling on sand bed channels with cohesive banks [*Simon and Darby*, 1997].

Modeling from the NFTR also shows this exponential decrease (or increase) in bed elevation (Figure 4.8), consistent with physical understanding of channel evolution. In the Colorado River modeling, the greatest incision and bed coarsening were seen closest to the dam (the disturbance), with less channel change downstream (data not shown). Furthermore, REM accurately predicts the magnitude of channel incision in this system (bed elevation root mean squared error (RMSE) 0.7 – 1.5 m for all years). Bed material coarsening is also accurately predicted, although there are more variable errors (D_{50} RMSE 0.1 – 5 mm). In the NFTR, REM also accurately predicts channel incision in the upper half of the watershed (CW280 – NF130). This portion of the channel is single thread, while the downstream portion is anastomosing or braided — features that were deliberately not incorporated into REM. Taken together, these three model tests suggest that REM can predict channel evolution in single-thread systems with reasonable accuracy, matching both physical understanding of channel change and adequately predicting evolution in real-world, dynamic fluvial systems.

4.5.2 Model Strengths and Weaknesses

REM's main strength is its parsimony and utility in simulating watershed scale channel evolution processes. Watershed scale assessment is essential because channel evolution is not limited to local disturbances or dynamics. As I and others have shown, changes in both upstream and downstream channel form and sediment delivery affects local channel response [e.g. *Schumm et al.*, 1984; *Simon*, 1992; *Simon and Darby*, 2002]. Both bed and bank erosion processes are especially important in smaller urban watersheds [*Booth*, 1990]. Furthermore, channel hardpoints (i.e. bed and bank armoring) can significantly influence both local channel evolution and adjustment in other parts of the watershed [*Booth and Fischenich*, 2015]. REM accounts for these processes — enabling the user to specify non-erodible cross sections — and may be an important tool for understanding urban channel network evolution. Other numerical models have been developed that include both bed and bank erosion, but these are typically designed for reach-scale application. For example, the Conservational Channel Evolution and Pollutant Transport System (CONCEPTS) model [*Langendoen and Simon*, 2008; *Langendoen and Alonso*, 2008] and *Darby and Thorne* [1996a] model both include more detailed modeling processes than REM, but cannot be easily applied at the watershed scale. Alternatively, the watershed scale Soil and Water Assessment Tool (SWAT) [*Allen et al.*, 1999; *Mittelstet et al.*, 2016; *Arnold et al.*, 1998] has some channel erosion processes, but not to the extent of REM. REM incorporates the most important mechanisms to realistically simulate channel evolution while still keeping data requirements to a minimum.

Another important strength of REM is its capacity to explicitly account for input variable uncertainty. It automates the use of Monte Carlo simulations, allowing users to easily quantify model uncertainty and produce probabilistic estimates of channel change. Quantifying uncertainty can be useful for decision making and assessing reliability of model outputs [e.g. *Pappenberger and Beven*, 2006]. Model field tests illustrate this. In most cases, it appears the median of the Monte Carlo simulations predicts river behavior as well or better than

the single model run (with the exception of NF130 and NF300 from the NFTR, Figure 4.8). This suggests that accounting for uncertainty in the inputs can actually improve model accuracy. This may be especially true in complex systems like the NFTR where model inputs are uncertain and the river is highly sensitive to change.

How much uncertainty is too much is a question that must be answered by the model user because it depends on the question(s) being asked. The model test cases show large uncertainty bounds. This may seem discouraging, but is an inescapable consequence of simulating complex and uncertain systems [*Shreve*, 1975]. By quantifying this uncertainty, I can at least be candid about the confidence in the model's predictions. The widths of the simulated uncertainty bounds are proportional to the magnitude of modeled bed elevation (Figs. 4.5 and 4.8) and grain size (Figure 4.6). This is expected — the larger the change, the greater uncertainty.

REM is only applicable for single-thread rivers. It was therefore not surprising that it could not adequately predict channel evolution in the lower portion of the NFTR. This section of the river migrates across a wide valley bottom and — in the extreme lower reaches of NF405 and NF400 — the channel braids [*Zheng et al.*, 2017]. In reality, much of the channel is 15 – 20 m wide, but may be within a several hundred meter wide valley. The model does not account for the aggressive channel migration observed in the lower portion of the watershed and instead spreads the water out over the unrealistically wide modeled channel bottom. Figure 4.9 illustrates this issue, showing how error in modeled bed elevation increases substantially where the valley widens (just downstream of NF130). REM does include a meandering algorithm, but this is not entirely mechanistic (e.g. no point bar deposition forcing meander migration) and is incorporated to allow single thread meandering channels an additional mode of slope adjustment.

Other limitations are a consequence of REM's relative simplicity. The model assumes uniform flow (bed slope equals friction slope) to calculate specific stream power and relies on new empirical equations to convert stream power to shear stress for cohesive erosion model-

ing. This facilitates network scale analysis without detailed hydraulic modeling but may be a source of error. This also neglects local, complex flow hydraulics which can have an impact on channel change. The model is more suited for larger scale applications because it neglects these local complexities. Also, it cannot simulate flood waves, dam breaks, or other cases where hydraulics change rapidly. Still, REM has a strong physical basis, integrating novel stream power based sediment transport models (Chapter 3) with a well tested bank erosion algorithm (BSTEM; [*Simon et al.*, 2000, 2011]) that underwent systematic sensitivity and uncertainty analyses to identify the most parsimonious representation of essential physical processes [*Lammers et al.*, 2017].

4.5.3 Model Sensitivity

Sensitivity is a function of (1) how much an input influences model output and (2) how much the input varies. Sensitivity analysis can therefore reveal information about model structure and suggest which variables should be most accurately quantified to obtain the most reliable results. The sensitivity analyses largely confirm the validity of the model as important parameters are known to be linked to important channel evolution processes and are consistent with results reported in the literature.

Bed elevation is most controlled by D_{50}, σ_g, width, and floodplain angle (Colorado River, Figure 4.7) plus hiding function parameters and bank τ_c and cohesion (NFTR, Figure 4.11). The size and erodibility of the bed material directly influences the extent of incision. Bank erodibility has a secondary effect by either allowing the channel to widen and reducing incision, or limiting widening and forcing the channel to incise more [*Simon*, 1992]. Other numerical models have shown that bed D_{50} has a significant effect on modeled channel profiles [*El Kadi Abderrezzak et al.*, 2008; *El Kadi Abderrezzak and Paquier*, 2009]; however, *Darby and Thorne* [1996b] found that D_{50} had a minimal effect on modeled channel incision, which was driven primarily by variations in discharge. Sensitivity analysis of the sediment transport equations used by REM show that D_{50} has a small influence on calculated transport rates

compared with discharge or slope (Chapter 3); however, these inputs were not incorporated in the REM sensitivity analyses.

Predicted bed D_{50} was most influenced by initial grain size distribution in the Colorado River case study (Figure 4.7), but the hiding function parameters were equally or more influential for the NFTR (Figure 4.11). Others have also shown that hiding function parameters (in their case, critical shear stress and the hiding factor) controls modeled grain sizes [*Ruark et al.*, 2011; *Hoey and Ferguson*, 1994]. The NFTR results also show that bank τ_c and cohesion had an influence on modeled D_{50}. Sediment from bank erosion has the same grain size distribution of the initial bed sediment. As the bed coarsens, bank erosion therefore becomes a source of finer sediment.

Channel width was controlled most by bank τ_c (Figure 4.11). This suggests that fluvial erosion, not mass failure, was the dominant bank erosion process. *Darby and Thorne* [1996b] also found that τ_c had a much greater influence on channel widening than bank cohesion. The three variables controlling bank failure (cohesion, ϕ', and weight) all had similar relative importance, unlike other sensitivity analyses of bank erosion models that found cohesion was the dominant control on bank stability [*Lammers et al.*, 2017; *Van de Wiel and Darby*, 2007; *Parker et al.*, 2008; *Samadi et al.*, 2009]. These studies, however, did not show that τ_c was important, possibly because they did not model bank erosion over longer periods of time which would incorporate the threshold effect of τ_c determining when erosion occurs.

Different parameters become influential when different channel processes are dominant. For the downstream reaches of the NFTR, bed D_{50} is less influenced by local variability in inputs. Here, aggradation dominated so bed grain size was more controlled by the amount and size of sediment coming from upstream. Similarly, these cross sections widened primarily due to aggradation filling in the channel so bank erodibility was less important than in upstream reaches (Figure 4.11). This change in model sensitivity with dominant channel evolution process was also shown by *Darby and Thorne* [1996b]. They found that bank cohesion had little influence on modeled channel dimensions while the channel was incising.

Only after the banks became unstable and the channel widened did bank strength become important. It is important for model users to recognize the dominant processes at play in their system and tailor their data collection efforts accordingly.

Despite its relative simplicity, REM is dependent on field data which may be difficult to collect; however, the sensitivity results provide guidance on which parameters should be most accurately quantified to yield the best model results. This is especially important for grain size distributions, τ_c, and cohesion which have a strong influence on the model, are subject to considerable uncertainty, and are difficult to measure in the field. Soil erodibility parameters (τ_c and k) are especially variable [*Wynn et al.*, 2008; *Konsoer et al.*, 2016; *Daly et al.*, 2015a] and difficult to predict. An alternative, more mechanistic fluvial erosion model has also been developed [*Wilson*, 1993a, b] which relies on erodibility parameters which may show less variability and therefore contribute less uncertainty to modeled erosion rates [*Enlow et al.*, 2017]. Future work could incorporate the *Wilson* [1993b] model into REM. Regardless, bank τ_c may need to be estimated through model calibration to provide more reliable values than field estimates. Hiding function parameters were also influential but can only be calculated using sediment transport data by grain size — a rare thing to have for most field sites. Since REM relies on a new specific stream power based hiding function, more work is needed to explore variability in these parameters.

4.5.4 Future Improvements and Applications

There are a number of modifications that could improve model predictions. Coupling REM with an upland erosion model would provide more realistic estimates of sediment inputs and channel response [e.g. *Stryker et al.*, 2017]. Furthermore, floodplains can be significant sediment sinks [*Kronvang et al.*, 2007; *Fryirs and Brierley*, 2001]; however, floodplain sedimentation likely has a larger effect on fine sediment delivery [e.g. *Walling et al.*, 1998], than the bed material load that primarily controls channel incision and aggradation. Adding additional processes may improve model predictions, but this additional complexity

also increases data requirements and uncertainty. It is important to balance the need to incorporate relevant processes while retaining the model simplicity that makes REM applicable at the small watershed scale.

REM has a number of potential applications, both in river management and research. For example, channel erosion can be a significant, but difficult to quantify, source of fine sediment and phosphorus pollution in watersheds [*Fox et al.*, 2016]. REM could be used to estimate pollutant loading from channel erosion in a variety of systems. Urban stormwater management (or mismanagement) is a leading cause of channel degradation [*Walsh et al.*, 2016, 2005]. While certain stormwater design standards can help mitigate channel degradation [e.g. *Tillinghast et al.*, 2011], REM may allow a more comprehensive analysis of channel stability when coupled with a stormwater management model. REM also has a number of research applications. The search for an "optimal" or "equilibrium" channel form has intrigued scientists for decades [e.g. *Langbein and Leopold*, 1964; *Yang et al.*, 1981; *Millar*, 2005; *Huang et al.*, 2014]. Tools like REM can be used to explore this concept in more detail, looking beyond the "optimal" channel cross section and examining interactions between parts of a channel network and their influence on watershed scale channel evolution.

4.6 Conclusions

I present a new model for simulating channel evolution at the watershed scale. This model is based on specific stream power and does not require detailed hydraulic modeling. Results from a generic test case of channel response to base level lowering match physical understanding of channel evolution. The model also accurately predicts channel incision and bed coarsening for a reach of the lower Colorado River downstream from Parker Dam. I also modeled vertical and lateral channel change on the North Fork Toutle River. The model accurately predicted channel incision and widening in the upper portion of the watershed where the channel eroded significantly but remained single thread. Model predictions did not match observation in the lower portion of the watershed where the river migrated significantly

across the valley floor — a behavior that REM is not designed to simulate. Results from these case studies suggest the model can provide useful predictions of watershed-scale channel erosion, while recognizing it is limited to single thread channels. Importantly, the model can also account for uncertainty in input variables — allowing for a probabilistic assessment of channel change. More model testing is required to fully understand its capabilities and limitations. For example, REM's ability to simulate cohesive incision, knickpoint migration, or meandering was not tested because of a lack of sufficient field data, so it is still unclear how accurately the model can simulate these processes. Further testing is also warranted on the smaller watersheds (i.e. 10 – 100 km^2) for which REM was designed.

Understanding how and how much rivers may change under future climate and land use variability is an essential question for sustainable management of river ecosystems. Other tools have been developed to estimate watershed sediment dynamics [*Czuba et al.*, 2017; *Schmitt et al.*, 2016; *Czuba and Foufoula-Georgiou*, 2014] and erosion and deposition potential [*Soar et al.*, 2017; *Parker et al.*, 2015]. In smaller, urbanizing watersheds, however, channel changes are driven by both bed and bank erosion processes [*Booth*, 1990] and strongly influenced by channel armoring and other channel "improvements" [*Booth and Fischenich*, 2015]. By accounting for these processes, REM can provide insight into urban stream evolution. Additionally, the model can be used to test different restoration or mitigation strategies; for example, by simulating how the river erodes under different stormwater and/or stream restoration scenarios. Using REM to test different mitigation strategies can support cost effective and successful solutions to address excessive channel erosion.

Chapter 5

Modeling watershed phosphorus and sediment loading from river erosion while accounting for uncertainty

Summary

Phosphorus and fine sediment pollution are primary causes of water quality degradation. The significance of stream channel erosion as a source of these pollutants is increasingly being recognized, but it remains difficult to quantify the magnitude of this loading. I use a new, easily applied, watershed scale model to simulate the potential for future phosphorus and sediment loading from channel erosion in two watersheds: Big Dry Creek, Colorado and Lick Creek, North Carolina. The projected magnitude of loading for phosphorus is about an order of magnitude higher in Big Dry Creek compared to Lick Creek, while sediment loading results are similar. In both watersheds, model results suggest that channel erosion will not be a significant source of phosphorus ($\sim$1 – 4% of historic watershed total) but will of sediment (30 – 100% of historic watershed total). Uncertainty in these estimates is high — similar to what has been reported for other estimates of bank erosion — and is larger than typical uncertainty bounds for other non-point pollution sources. Still, quantifying confidence in projections is important for comparing relative magnitudes of these sources. Importantly, modeling also suggests that loading will not decrease over time in either watershed, suggesting that the channels are not adjusting to a new stable state and erosion will continue to be a pollutant source. Lick Creek model results are sensitive to upstream sediment supply while Big Dry Creek's are not, reinforcing the importance of considering alterations to both the hydrologic and sediment regimes when analyzing potential channel changes — at least in vertically active

channels. This new model is a useful tool for estimating historic and future phosphorus and sediment loading from channel erosion and may enable easier quantification of this potentially potent pollutant source.

5.1 Introduction

Phosphorus and fine sediment are two of the leading sources of water pollution in the United States [*EPA*, 2015] and around the world. River channel erosion can be a significant — but highly variable — source of both of these pollutants [*Fox et al.*, 2016]. For example, bank erosion can contribute from around 10% [*Collins and Walling*, 2007] to greater than 90% [*Kronvang et al.*, 1997] of the watershed suspended sediment load. Even within individual watersheds, there is significant inter-annual variability [*Palmer et al.*, 2014a] and uncertainty [*Thoma et al.*, 2005]. Phosphorus loading from bank erosion is generally lower than suspended sediment — both in absolute terms and as a fraction of the total watershed load — but can still be significant [*Howe et al.*, 2011; *Kronvang et al.*, 1997; *Ishee et al.*, 2015]. Like fine sediment, phosphorus loading from bank erosion is subject to significant uncertainty depending on the methods used to quantify both erosion and bank phosphorus concentrations [*Miller et al.*, 2014; *Purvis et al.*, 2016].

There are a number of ways to measure bank erosion, depending on the scale and resolution of interest. Bank pins or repeat surveys can be used to measure local erosion rates over months to years [e.g *Beck et al.*, 2018]. Aerial or satellite imagery allows rapid quantification of bank retreat over years to decades at large spatial scales [e.g *Miller et al.*, 2014; *Purvis and Fox*, 2016]. Repeated LiDAR surveys can provide high spatial resolution data on bank erosion [*Thoma et al.*, 2005], although they can be expensive to collect.

These direct measurement approaches are useful, but they can only be used to estimate historic and current erosion rates. Alternatively, numerical modeling can be used to forecast channel erosion and associated pollutant loading. Modeling has been used to estimate watershed scale sediment and phosphorus loading [*Stryker et al.*, 2017; *Langendoen et al.*,

2012; *Mittelstet et al.*, 2016], and test the effectiveness of channel stabilization measures [*Langendoen*, 2011; *Enlow et al.*, 2018]. The most commonly used model is the Bank Stability and Toe Erosion Model (BSTEM) [*Simon et al.*, 2000, 2011] which has subsequently been integrated into other, more comprehensive models (e.g. CONCEPTS [*Langendoen and Simon*, 2008], HEC-RAS [*Gibson et al.*, 2015], and others [*Klavon et al.*, 2017]). BSTEM has been used for a variety of purposes [*Klavon et al.*, 2017], although most have examined specific erosion mechanisms [*Midgley et al.*, 2012] or the effect of different stabilization or restoration strategies [*Langendoen et al.*, 2012].

Langendoen et al. [2012] used BSTEM to estimate watershed scale sediment and phosphorus loading in the Missisquoi River, Vermont, and to test the effects of different bank grading and riparian planting strategies. *Stryker et al.* [2017] coupled BSTEM to a hydrologic model to account for the combined effects of upland and in-channel processes on sediment export. These are useful approaches, but do not account for coupled bed and bank erosion. Other models (CONCEPTS and HEC-RAS+BSTEM) do account for these two modes of channel adjustment, but may be better suited for reach scale application because they can be difficult to parameterize and apply at the watershed scale.

The objective of this paper is to expand on these past modeling efforts by using a new physically based yet parsimonious model to simulate future sediment and phosphorus loading from channel erosion. The River Erosion Model (REM) simulates both bed and bank erosion at the watershed scale — accounting for how channel evolution in one part of the watershed can influence sediment dynamics in other reaches. Channels responding to disturbance evolve in complex ways [*Schumm et al.*, 1984; *Simon*, 1989; *Booth and Fischenich*, 2015; *Cluer and Thorne*, 2014] and accounting for the dominant mechanisms of channel evolution is essential for accurately quantifying water quality impacts. Importantly, REM is built to run Monte Carlo simulations — quantifying the uncertainty in model projections.

5.2 Methods

I applied REM to two watersheds: Big Dry Creek in Colorado and Lick Creek in North Carolina. These two examples represent very different climates (semi-arid vs. humid) and history (past vs. recent urbanization), providing illustrative examples of the how REM can be used in diverse landscapes.

5.2.1 Model Description

REM simulates changes in channel bed elevation based on a sediment mass balance: erosion occurs if sediment transport capacity exceeds supply while deposition occurs when supply exceeds capacity. Sediment transport by grain size is modeled using new stream power based bedload and total load transport equations (Chapter 3). Channel incision into cohesive material can also be simulated using an excess shear stress approach [*Partheniades*, 1965]. REM uses a modified version of the Bank Stability and Toe Erosion Model (BSTEM) [*Simon et al.*, 2000, 2011] to simulate both fluvial bank erosion and mass failure. Finally, the model can also account for knickpoint erosion [*Allen et al.*, 2018] and channel meandering. A user-specified fraction of eroded bank, knickpoint, and cohesive bed material is added to the bed material load (sand and coarser). The remainder is assumed to be washload (silt and clay) that is all transported the watershed outlet (i.e. no in-channel or floodplain storage). All model estimates of sediment and phosphorus loading are from this washload material. For a more detailed description of REM see Chapter 4.

5.2.2 Study Watersheds

Big Dry Creek, Colorado

Big Dry Creek is a 280 km^2 watershed located in the northern suburbs of Denver on the Front Range of Colorado. The bed material is primarily sand, but with some gravel in the upper reaches. Streambank material is mostly clay and sandy clay loam. Riparian areas consist of grasses, willows, Russian olive, and some cottonwoods. The upper portion of the

watershed is mostly undeveloped, but with a growing urban area in the middle. Most of the lower third of the watershed is agricultural land (Figure 5.1). A management goal has been set to reduce phosphorus loading from Big Dry Creek as part of a total maximum daily load (TMDL) plan for the Barr-Milton watershed [*Clary*, 2017]. In addition, total phosphorus concentrations in much of Big Dry Creek regularly exceed forthcoming in-stream nutrient standards set by the State of Colorado [*Clary*, 2017].

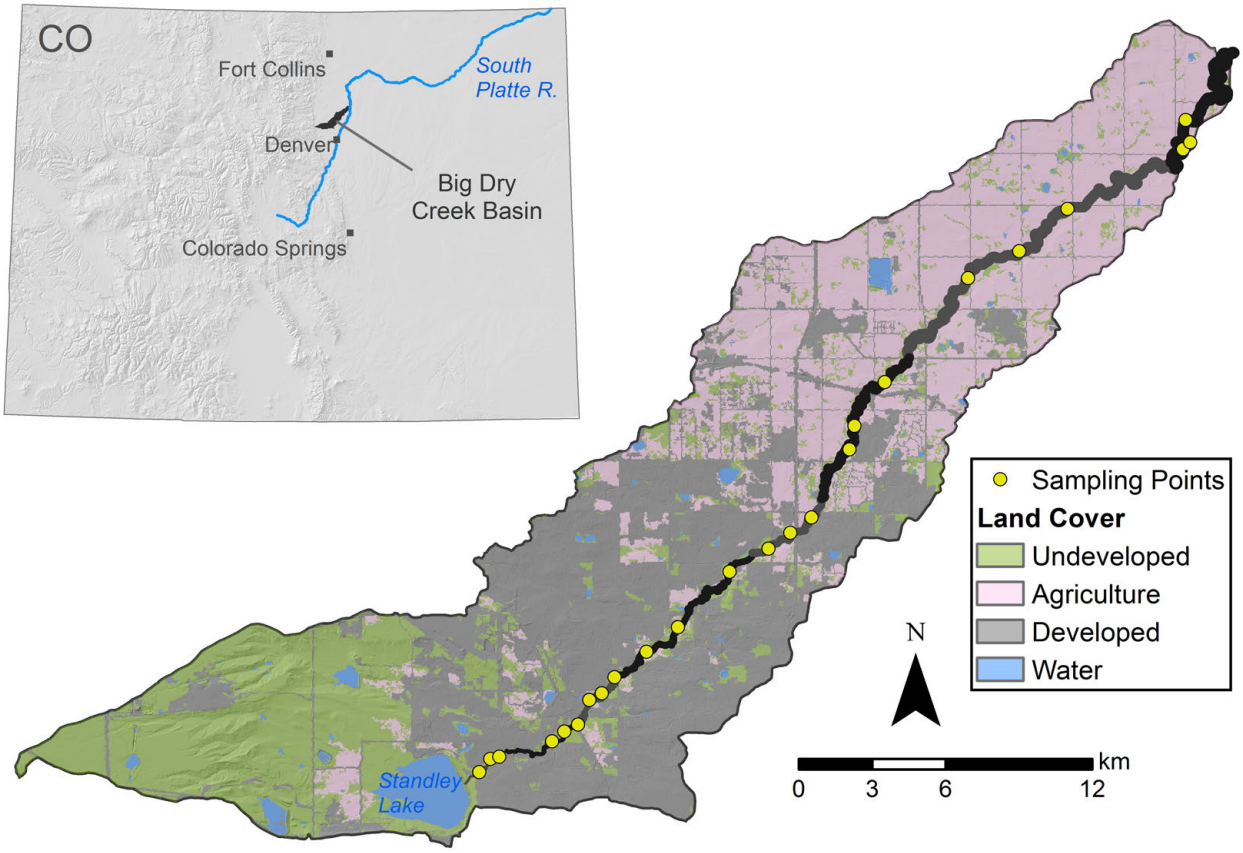

Figure 5.1: Big Dry Creek watershed. Land use is 24% undeveloped, 33% agriculture, 40% developed, and 3% water (NLCD 2011; *Homer et al.* [2015]).

The hydrologic regime of Big Dry Creek has been significantly altered. Standley Lake, a reservoir in the upstream part of the basin, was constructed in 1912 to provide irrigation water to downstream farms. Today, the reservoir also serves as a municipal drinking water source but releases are still highly managed to supply water to downstream users. The

watershed has also seen two population booms — one in the 1970s and the other starting in the 1990s and continuing until today. This rapid development has increased stormwater runoff to the stream. Furthermore, three wastewater treatment plants in the watershed provide a near continuous baseflow to Big Dry Creek. These hydrologic alterations — irrigation releases, increased stormwater runoff, and wastewater treatment effluent – have led to significant channel degradation.

Lick Creek, North Carolina

Lick Creek is a 38 km^2 watershed located on the outskirts of Durham, NC. Land use is primarily forested with small portions of agricultural land and expanding development in the headwaters. Development and agriculture are mostly limited to the uplands while the valley floor is extensively forested (Figure 5.2). The bed material is primarily sand but with some clay and isolated bedrock outcrops. Streambank material is mostly loam, clay loam, and sandy loam. There are also a number of relict and active beaver dams on the tributaries. The lower main stem of Lick Creek has incised and widened. This incision is migrating upstream into the tributaries and I identified two active knickpoints during field data collection. Lick Creek is currently listed as impaired for aquatic life. The creek drains to Falls Lake reservoir, which is subject to a nutrient reduction plan and is currently listed as impaired due to high turbidity [*North Carolina Department of Environmental Quality*, 2016].

5.2.3 Data Collection and Model Application

During summer 2015, I collected field data at 24 sites along Big Dry Creek (Figure 5.1). Prior to the field campaign, the channel was divided into eight reaches that had relatively homogeneous land use and riparian condition. Where possible, reaches were separated at major grade controls (e.g. road crossings, diversion structures, or bed stabilization structures). I measured bank geometries at three sites within each of the eight reaches. Three soil samples per site (from the top, middle, and toe of one bank) were collected and analyzed

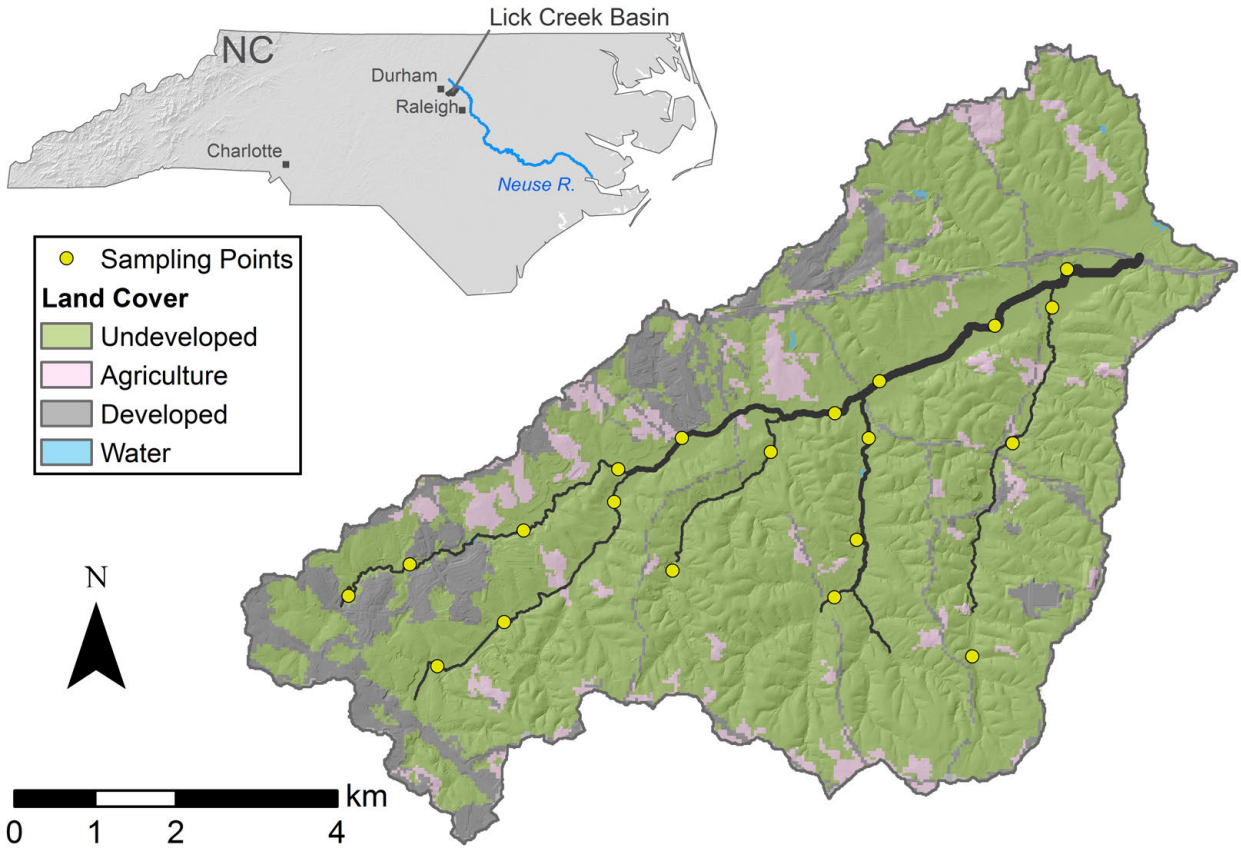

Figure 5.2: Lick Creek watershed. Land use is 80% undeveloped, 7% agriculture, and 13% developed (NLCD 2011; *Homer et al.* [2015]).

for phosphorus content and soil texture. Soil samples were processed by the Soil, Water, and Plant Testing Laboratory at Colorado State University for total phosphorus (TP; EPA Method 3050a), Mehlich-3 P, and water extractable P. Channel longitudinal profiles and channel widths were obtained from a LiDAR-derived DEM (0.75 m resolution) from October 2013 (geodata.co.gov). To estimate historic erosion rates, I delineated the channel banks from 1993 and 2014 aerial imagery [*Google Earth Pro*, 2017b], overlayed the two channel polygons, and calculated eroded areas based on differences in channel position. Based on repeat delineation of the same 3 km reach, average errors were 1.4 – 1.8 m. I therefore only included erosion estimates that were greater than 2 m to incorporate these errors and unknown orthorectification errors. Bank heights, soil bulk densities, and phosphorus

concentrations were then used to estimate sediment and phosphorus loading over this time period.

In spring 2016 I collected field data at 20 sites along Lick Creek and its major tributaries (Figure 5.2), following the same data collection procedure as on Big Dry Creek. Channel longitudinal profiles, channel widths, and floodplain widths and slopes were obtained from a 1 m resolution DEM constructed from LiDAR data collected in early 2015 (sdd.nc.gov/sdd). I delineated the stream network and extracted channel geometry data for both watersheds using the hydro-geomorphological GIS tool developed by *Biron et al.* [2013]. Historic erosion rates for Lick Creek could not be determined using aerial imagery because the narrow stream and dense canopy made it impossible to see the channel banks.

Estimating bank cohesion

Logistic regression analysis of bank heights and angles was used to estimate soil cohesion [*Bledsoe et al.*, 2012]. Logistic regression predicts the probability of bank failure (p) based on bank angle (α) and height (H):

$$\ln \frac{p}{1-p} = \beta_o + \beta_\alpha \ln \alpha + \beta_H \ln H \tag{5.1}$$

where β_o, β_α, and β_H are fitted model coefficients.

This model was fit to field data on bank heights and angles for stable ($p = 0$) and unstable ($p = 1$) banks. The logistic regression model solved for $p = 0.5$ (assumed equal to the critical bank height for failure) was used in conjunction with the Culmann equation for geotechnical slab failure to estimate the effective cohesion of the bank material (c', kPa):

$$c' = \frac{\gamma \left(1 - \cos(\alpha - \phi')\right) \exp\left(\frac{-\beta_o}{\beta_H} - \frac{\beta_\alpha}{\beta_H} \ln \alpha\right)}{4 \sin \alpha \cos \phi'} \tag{5.2}$$

where γ is the unit weight of the soil [kN m^{-3}] and ϕ' is the effective friction angle of the bank material [degrees]. I assumed ϕ' varied uniformly between 11.4° and 32.3°, γ between 16.9 and

19.2 kN m^{-3} [*Simon et al.*, 2011], and α between 40° and 90°. This yielded a mean c' value of 1.4 kPa (standard deviation = 0.4) for Big Dry Creek and 2.1 kPa (standard deviation = 2.0) for Lick Creek (see Appendix C.1.3 for fitted logistic regression models). These cohesion estimates account for a variety of sources of bank strength (including vegetation) and may be considered operational shear strengths [*Bledsoe et al.*, 2012].

Estimating bank critical shear stress

Critical shear stress (τ_c) of bank material in both watersheds was estimated using measured erosion rates and USGS gage data. For Lick Creek, I used erosion data collected by the City of Durham from nearby Ellerbe Creek, located near USGS gage 0208675010. Lick and Ellerbe creeks both have Triassic soils [*Voli et al.*, 2013], so I assumed their bank soils have similar erosion resistance. Specific stream power was calculated using 15 minute flow data and DEM-derived channel slope and width. These stream power values were converted to a wall shear stress using the same empirical equation used by REM. I then found the value of τ_c that best approximated observed erosion rates (Appendix C.1.1). A similar approach was used for Big Dry Creek, using 15 min and hourly flow data from USGS gage 06720820 and bank erosion rates estimated from the aerial imagery analysis. Soil erodibility was calculated by REM from supplied τ_c values using the empirical relationship developed by *Simon et al.* [2010].

Hydrology

For Big Dry Creek, I used daily flow data from two USGS gages, one in the urbanized area of the watershed (06720820) and the other at the watershed outlet (06720990). Peak flows and flashiness have both increased in the watershed over the period of record. Therefore, I used flow data from Jan. 2006 – Dec. 2017 as representative of the future hydrology of the basin. Discharge for each modeled reach was calculated based on drainage area, while accounting for releases from Standley Lake (summer only) and two wastewater treatment plants (year round) as well as withdrawals from five irrigation ditches (summer only). A

41 year flow record (2013 – 2053) was constructed with flow data from 2013 – 2017 (corresponding to initial DEM-derived channel geometry from 2013) plus repeating the 12 years of historic flow data (2006 – 2017) three times.

For Lick Creek, there are no current or historic flow data. Instead, I used daily flow data from Little Lick Creek (USGS 0208700780) which is the watershed directly adjacent. These daily data were available for Oct. 1982 – Sep. 1995. I expected these flow data to be representative of current and future conditions in Lick Creek because the watershed population density is currently increasing at a similar rate as Little Lick Creek did from 1982 – 1995 (Appendix C.2). Flows in each modeled reach were scaled based on drainage area. These 13 years of data were repeated three times to give a total model simulation of 39 years (2015 (year of DEM) through 2053).

Model application

I applied REM to Big Dry Creek using a cross section spacing of 500 m and a time step of 900 s. I ran two simulations with different upstream sediment supply: $Q_s = 0.5$ and 1.0 of transport capacity. The total load sediment transport equation was used to model grain sizes smaller than 4 mm, and the bedload equation for all coarser material. Five grade control structures were included (i.e. putting a non-erodible cohesive bed at these locations) (Table 5.1). Eight reaches with unique channel geometries (but the same bank soil properties) were modeled. Modeled annual sediment and phosphorus loads from channel erosion were compared to historic total annual loads calculated from in-stream water quality data (courtesy of the Big Dry Creek Watershed Association) and flow data from the USGS gage at the watershed outlet.

For Lick Creek, I used a cross section spacing of 200 m, time step of 2,400 s, and uniform grain size of 2 mm (total load transport equation). Four grade controls (roads and bedrock outcrops) were incorporated. For the remaining cross sections, a clay layer was assumed to be 2 m below the alluvium with the same τ_c as the bank material. This was based on field observations of exposed clay bed in incising channels. Two knickpoints were observed during

the field campaign. Knickpoint erodibility coefficients were calibrated to match observed migration rates from 2001 – 2015 (see Appendix C.1.2). Since there is no information on upstream sediment supply, I ran three simulations with different rates: Q_s = 0.5, 0.75, and 1.0 of transport capacity (Table 5.2). Eleven reaches with unique channel geometries (but the same bank soil properties) were modeled. Measured sediment and phosphorus water quality data for Lick Creek were obtained from the City of Durham and Upper Neuse River Basin Association. Since there is no gage on this stream, annual loads could not be calculated. Instead, I converted modeled loads to concentrations (annual load / annual flow volume) to compare to these measured data. For both watersheds, I used measured bank total phosphorus concentrations, as described above. For both watersheds, I ran 1,000 Monte Carlo simulations to quantify uncertainty in model projections. All data analyses were performed in R version 3.4.4 [*R Core Team*, 2018].

5.3 Sensitivity Analysis

Sensitivity analyses of each model output were performed using the *Plischke et al.* [2013] density-based method. These analyses quantify the impact of each input variable on uncertainty in model output from the Monte Carlo simulations. For each simulation, I quantified uncertainty in predicted phosphorus loading, sediment loading, bed elevation, and channel width. To give a single output value for bed elevation and channel width, I summed the absolute value of total change in the variable across all cross sections. For the loading variables, I used the median annual load from each Monte Carlo simulation.

5.4 Results

5.4.1 Historic and Current Erosion

Big Dry Creek

Incision is widespread in Big Dry Creek, as evidenced by the tall vertical banks throughout much of the watershed. However, it appears this incision has slowed or halted because of

Table 5.1: Big Dry Creek model inputs. *Proportion of the eroded bank material that is bed material load (sand and coarser). The remainder is assumed to be washload.

Variable	Value	MC Values	Source
Bed profile	–	–	LiDAR DEM
Bank geometry	0.9 – 2 m; 45° – 90°	±50%	Field measured
Width [m]	5 – 7	±50%	LiDAR DEM
Discharge	–	–	See text
Sediment supply	50% and 100% of transport capacity	–	Assumed
Bank τ_c [Pa]	7.2	±50%	Calibrated
Bank cohesion [kPa]	1.4	normal (mean = 1.4; sd = 0.4)	Calculated from bank geometry
Bank friction angle, ϕ' [deg]	22	±50%	Typical values [*Simon et al.*, 2011]
Bank soil weight [kN/m^3]	18	±50%	Typical values [*Simon et al.*, 2011]
Bank P [mg/kg]	310	normal (mean = 310; sd = 100)	Measured
Bank bedload prop*	38 – 64%	±50%	% Sand from sampled banks
Cohesive bed	5 grade control structures	–	Field observations
GSD	D_{50} = 2 mm; σ_g = 1.5	±50%	Assumed
Floodplain geometry	width: 50 m; slope: 1°	±50%	Assumed
Manning n	chnl: 0.035; fp: 0.06	±50%	Assumed
R_c [m]	35	±50%	Aerial imagery
Sinuosity	1.3 – 2.4	±50%	Aerial imagery

Table 5.2: Lick Creek model inputs. *Proportion of the eroded bank material that is bed material load (sand and coarser). The remainder is assumed to be washload.

Variable	Value	MC Values	Source
Bed profile	–	–	LiDAR DEM
Bank geometry	1 – 2.8 m; 48° – 70°	±50%	Field measured
Width [m]	1.8 – 17.3	±50%	LiDAR DEM
Discharge	–	–	See text
Sediment supply	50% - 100% of transport capacity	–	Assumed
Bank τ_c [Pa]	10.2	±50%	Calibrated
Bank cohesion [kPa]	2.1	lognormal (logmean = 0.44; logsd = 0.78)	Calculated from bank geometry
Bank friction angle, ϕ' [deg]	22	±50%	Typical values [*Simon et al.*, 2011]
Bank soil weight [kN/m^3]	18	±50%	Typical values [*Simon et al.*, 2011]
Bank P [mg/kg]	50	normal (mean = 53; sd = 30)	Measured
Bank bedload prop*	28 – 59%	±50%	% Sand from sampled banks
Cohesive bed	0 – 2 m depth; τ_c = 10.2 Pa	–	Field observations; assumed τ_c = bank
D_{50}	uniform 2 mm	0.5 – 3.5 mm	Assumed
Floodplain geometry	width: 40 – 160 m; slope: 2° – 8°	±50%	LiDAR DEM
Manning n	chnl: 0.045; fp: 0.08	±50%	Assumed
Knickpoints	height: 0.9 – 1.3 m; K_d: 0.219 – 0.253 cm/Pa/hr	–	LiDAR DEM & Field observations

artificial (e.g. rock structures) and natural (e.g. clay soil) grade controls. As the channel is now mostly vertically stable, it has recently adjusted primarily via bank erosion and lateral channel migration. The aerial imagery analysis provided additional evidence of this (Figure 5.3). There was a mix of widening and narrowing along the channel from 1993 – 2014, but the average change in channel width was not significant. Sinuosity, on the other hand, did show a slight but statistically significant increase over this period (median increase of 0.04; $p < 0.0001$; Wilcoxon Signed Rank Test). Much of the upper portion of the watershed is in the later stages of channel evolution (stages IV–V in the *Schumm et al.* [1984] channel evolution model, CEM). The lower half of the watershed has not widened as significantly, and is currently in stage II (incision or arrested incision) or III (widening) of the CEM (Fig. 5.4). Big Dry Creek is still evolving, and it is unclear when it will re-stabilize. Ongoing urbanization will likely continue to alter watershed hydrology, and changes in sediment supply — from upland and in-channel sources — could either hasten or delay the return of the channel to a quasi-equilibrium state.

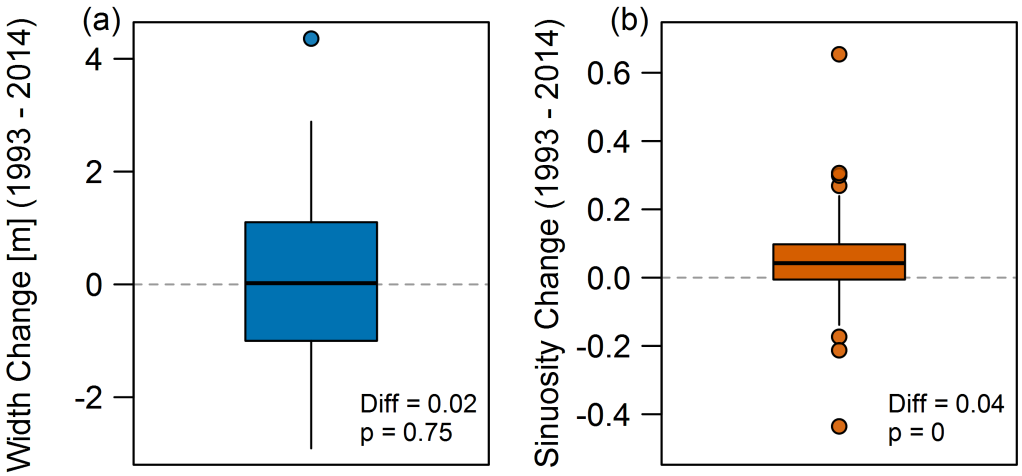

Figure 5.3: Changes in channel width (a) and sinuosity (b) in Big Dry Creek from 1993 – 2014 for the same, 1 km long reaches. Values estimated using digitized stream channels from aerial imagery. The median difference and p-value of a Wilcoxon Signed Rank Test are shown. These tests suggest the width change was not significantly different from zero but that sinuosity showed a statistically significant increase over the observation period.

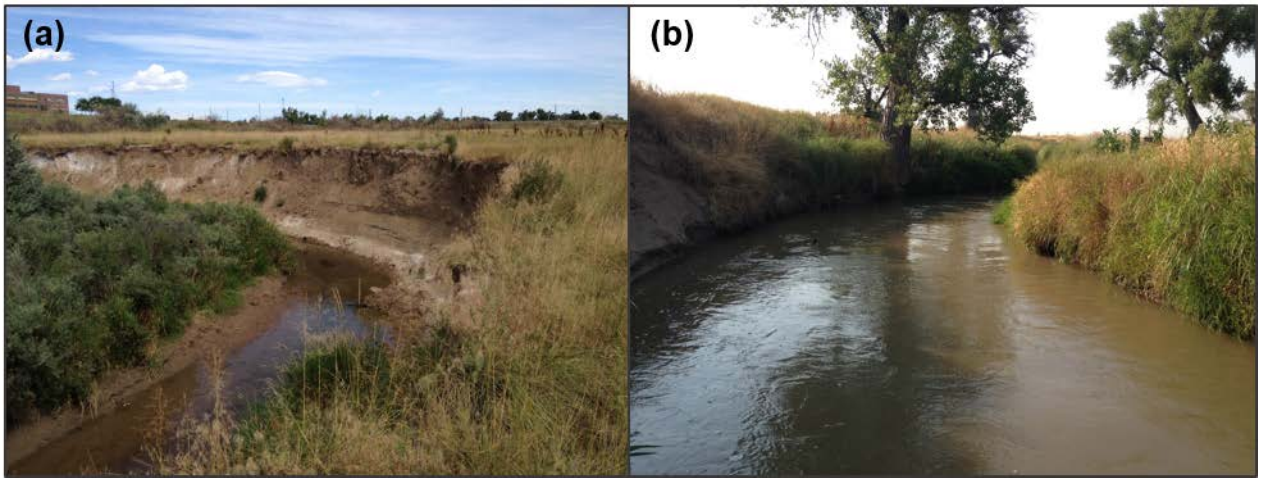

Figure 5.4: Looking upstream at an incised and actively migrating channel in the middle portion of the Big Dry Creek watershed (a); eroding bank height about 5 m. Looking downstream at a less incised and less laterally active portion of the channel near the watershed outlet (b); left bank height about 1.2 m.

Lick Creek

The channels in Lick Creek are actively evolving, presumably in response to changes in runoff and sediment supply caused by ongoing development. Much of the main stem has incised and widened, and this incision is currently migrating up the tributaries (Figure 5.5). There is significant sand deposition in the lower reaches of Lick Creek, probably as a result of high sand loading from upstream bed and bank erosion. These lower aggrading reaches are in stage IV of the CEM (aggrading and widening), while the tributaries are all in stages II–III (incising and widening). Development will likely continue into the future, further destabilizing the stream. There are several bedrock outcrops serving as local grade controls but these may not be sufficient to keep the channels from significantly incising and widening in response to this watershed disturbance.

5.4.2 Bank Phosphorus Concentrations

Figure 5.6 shows bank total phosphorus concentrations from Big Dry Creek and Lick Creek compared to data from 15 other studies. Big Dry Creek's bank phosphorus content is similar to these other data, but Lick Creek has extremely low values (with the exception

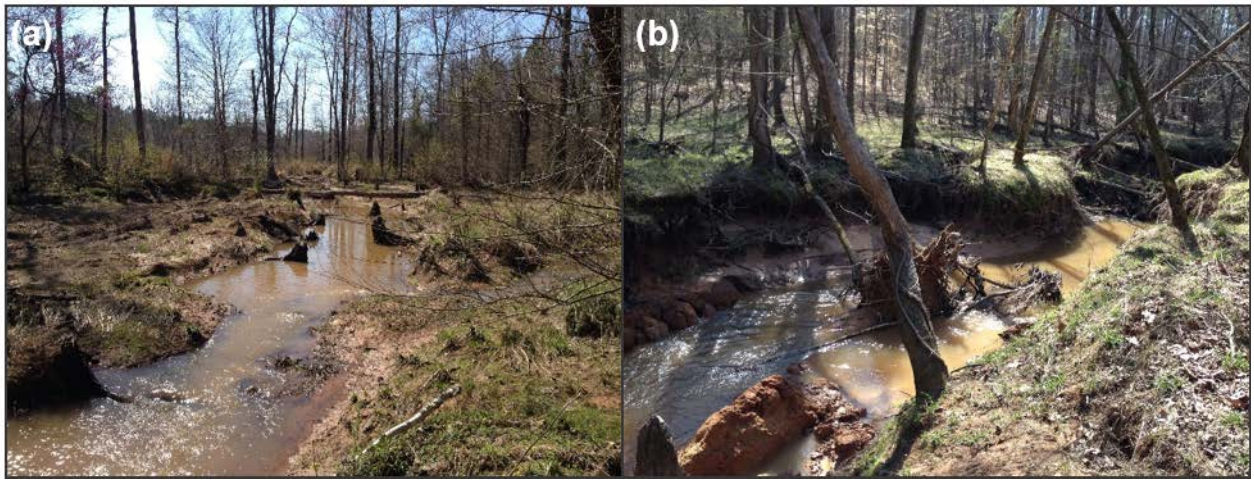

Figure 5.5: A tributary to Lick Creek immediately upstream (a) and downstream (b) of a 1 m high knickpoint. Both photographs are looking upstream.

of one outlier >1,800 mg/kg). For both watersheds, concentrations of Mehlich-3 phosphorus and water extractable phosphorus are about 10% and 5% of total phosphorus concentrations, respectively. These extraction methods may be more representative of bioavailable phosphorus than the TP concentrations shown here; however, I modeled total phosphorus loading to compare with measured data (using total phosphorus loads and concentrations) and because most regulations focus on total phosphorus.

5.4.3 Projected Phosphorus and Sediment Loading from Channel Erosion

Big Dry Creek

Figure 5.7 shows modeled annual phosphorus and sediment loads in Big Dry Creek from channel erosion (2013 – 2053, with uncertainty) from the $Q_s = 0.5$ simulation, compared to measured annual loads at the watershed outlet (1997 – 2017). Bank loading estimates from the aerial analysis (1993 – 2014) are also shown. The results from the single model run and median of the Monte Carlo simulations are essentially identical. There is significant inter-annual variability in projected loads, and the peaks of the uncertainty range do appear

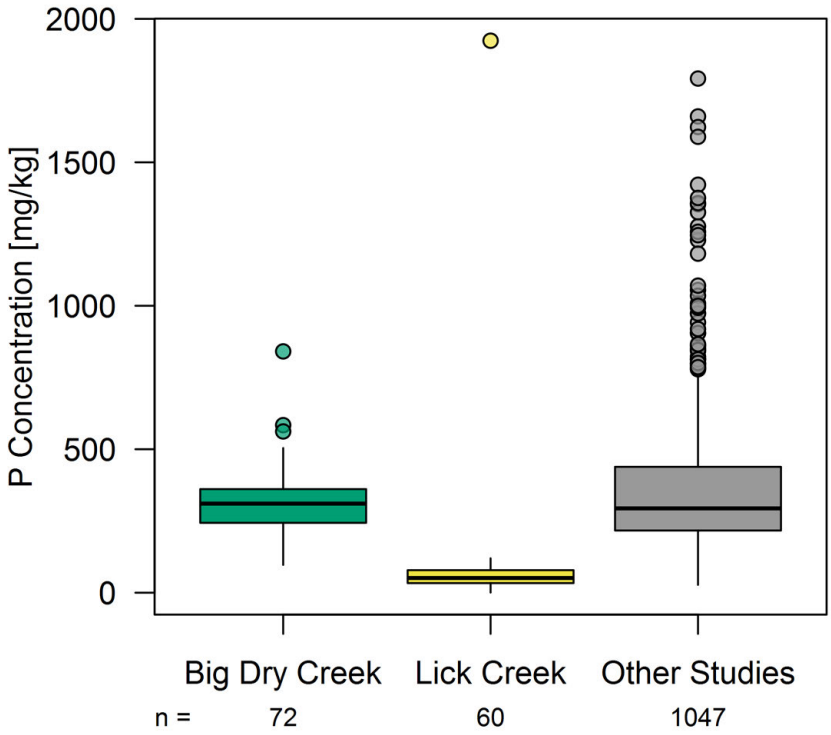

Figure 5.6: Measured bank total phosphorus concentrations for the two study watersheds compared to data from 15 other studies (Chapter 2).

to decrease over time. There is not, however, any statistically significant trend in the median results (Mann-Kendall trend test, p = 0.57 for both $Q_s = 0.5$ and 1.0 simulations).

Figure 5.8 compares distributions of median annual loads from the two model simulations ($Q_s = 0.5$ and $Q_s = 1.0$) with the historic observed watershed load and bank loading estimate from the aerial imagery analysis. The two model simulations show nearly identical results. The modeled median annual phosphorus load (median 0.3 ton/yr; 0.005 – 1.8 ton/yr 90% confidence interval [CI]) was one quarter of the aerial imagery analysis estimate (1.2 ton/yr). Both are significantly less than the historic measured watershed TP load (median 35 ton/yr). Modeled median annual sediment loads (median 950 ton/yr; 17 – 5,600 ton/yr 90% CI) are also less than both the historic watershed load (3,100 ton/yr) and aerial estimate (3,900 ton/yr). These results indicate that future phosphorus loading from channel erosion could be small relative to the historic watershed load (median ∼1%, 0.01 – 5% 90% CI) but that future sediment loading could be significant percentage (median 31%; 0.5 – 180% 90% CI) of

the historic watershed sediment load. Table 5.3 summarizes modeled median annual loadings of both phosphorus and sediment.

Figure 5.9 shows modeled sediment loading rates by reach, with uncertainty ($Q_s = 0.5$ simulation). Sediment loading was relatively consistent throughout the channel network, although the most upstream reach did have consistently higher rates than others. The spatial distribution of phosphorus loading is identical and is therefore not shown. Plots of pollutant loading, channel incision, channel widening, and sensitivity analysis results for both simulations are included in Appendix C.3.

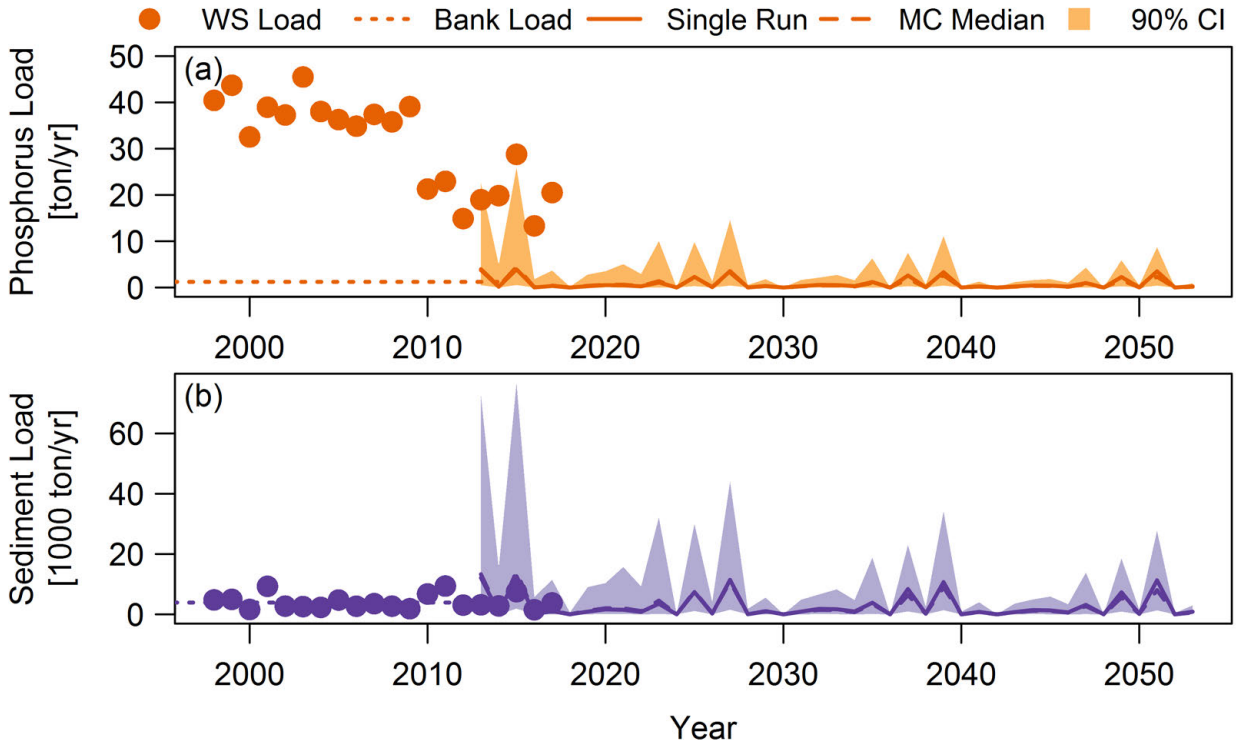

Figure 5.7: Observed and modeled annual loads of phosphorus (a) and sediment (b) for Big Dry Creek. Measured watershed loads are shown as points, bank loading estimates from the aerial photo analysis are shown as a horizontal dotted line, and model results for the single model run (solid line), median of the Monte Carlo simulations (dashed line), and 90% CI are projected through 2053. Model results are from simulations with $Q_s = 0.5$.

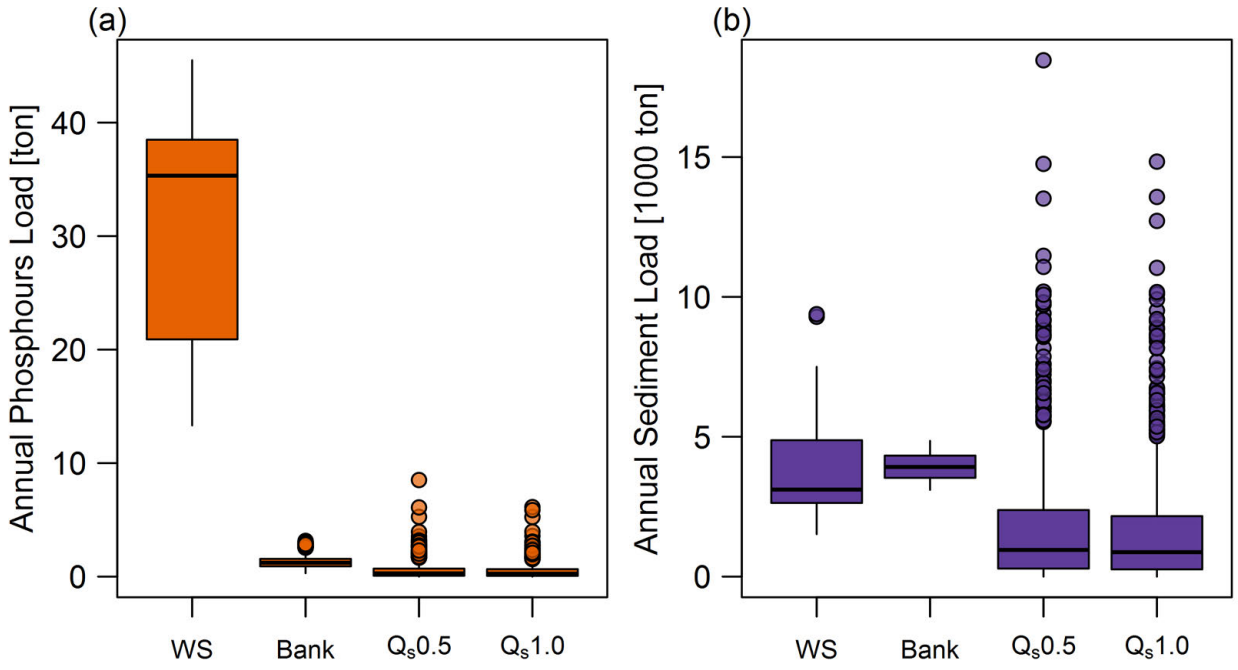

Figure 5.8: Distributions of predicted phosphorus (a) and sediment (b) loads for the two modeled scenarios from Big Dry Creek: $Q_s = 0.5$ and $Q_s = 1.0$. These are compared to estimates of loading from bank erosion from the aerial imagery analysis (Bank) and observed watershed loads from 1998 – 2017.

Lick Creek

Figure 5.10 shows modeled average annual total phosphorus (TP) and total suspended solids (TSS) concentrations in Lick Creek from channel erosion (2015 – 2053, $Q_s = 0.5$ simulation), with uncertainty, compared to historic measured values at the watershed outlet (2004 – 2017). There is some inter-annual variability in modeled concentrations, especially in the peaks of the 90% CI. There is not, however, an obvious increase or decrease in concentrations with time. A Mann-Kendall trend test confirms there is no statistically significant trend for any simulation ($Q_s = 0.5$: p = 0.36; $Q_s = 0.75$: p = 0.96; $Q_s = 1.0$: p = 0.08).

Figure 5.11 compares distributions of modeled TP and TSS concentrations for the three simulations to measured values. Modeled concentrations decrease as upstream sediment supply increases. For all simulations, modeled TSS concentrations are at or above historic observations while TP concentrations are significantly less than measured values. Modeled

Table 5.3: Modeled median annual total phosphorus and sediment loading from channel erosion in Big Dry Creek and Lick Creek. Median values are shown with 90% CI in parentheses.

Simulation	Annual P Load [kg/yr]	Annual P Load [kg/km/yr]	Annual Sed Load [ton/yr]	Annual Sed Load [ton/km/yr]
Big Dry Creek, $Q_s = 0.5$	285 (5 – 1,800)	4.8 (0.1 – 31)	950 (17 – 5,600)	16.2 (0.3 – 95)
Big Dry Creek, $Q_s = 1.0$	255 (4 – 1,770)	4.3 (0.1 – 30)	875 (16 – 5,400)	14.8 (0.3 – 91)
Lick Creek, $Q_s = 0.5$	48 (4 – 140)	1.8 (0.1 – 5.3)	940 (460 – 2,060)	35 (17 – 77)
Lick Creek, $Q_s = 0.75$	42 (3 – 124)	1.6 (0.1 – 4.7)	820 (410 – 1,850)	31 (15 – 69)
Lick Creek, $Q_s = 1.0$	27 (2 – 73)	1.0 (0.1 – 2.7)	520 (270 – 1,100)	19 (10 – 41)

median annual TP concentrations (median 0.003 mg/L; 0.0002 – 0.009 mg/L 90% CI) are an order of magnitude lower than observed values (median 0.08 mg/L). Modeled median annual TSS (median 59 mg/L; 31 – 131 mg/L 90% CI) is higher than observations (median 29 mg/L). These model results for the $Q_s = 0.5$ simulation suggest that future channel erosion could contribute >100% (median 203%; 106 – 450% 90% CI) of the historic fine sediment pollution in Lick Creek, but only ∼4% (0.3 – 11% 90% CI) of the historic phosphorus.

Figure 5.12 shows modeled sediment loading by reach over the course of the simulation ($Q_s = 0.5$). Two reaches had consistently higher loading throughout all the Monte Carlo simulations. Both reaches had actively migrating knickpoints which likely contributed to high modeled sediment loads. The spatial distribution of phosphorus loading is identical, therefore these data are not shown.

The median of the modeled annual phosphorus load ($Q_s = 0.5$ simulation) was 48 kg/yr (4 – 140 kg/yr 90% CI). Median annual sediment loading was 940 ton/yr (460 – 2,060 ton/yr 90% CI). Similar to the concentration data, modeled loads for this simulation were higher than the other two (Table 5.3). Plots of pollutant loading, channel incision, channel widening, and sensitivity analysis results for all three simulations are included in Appendix C.3.

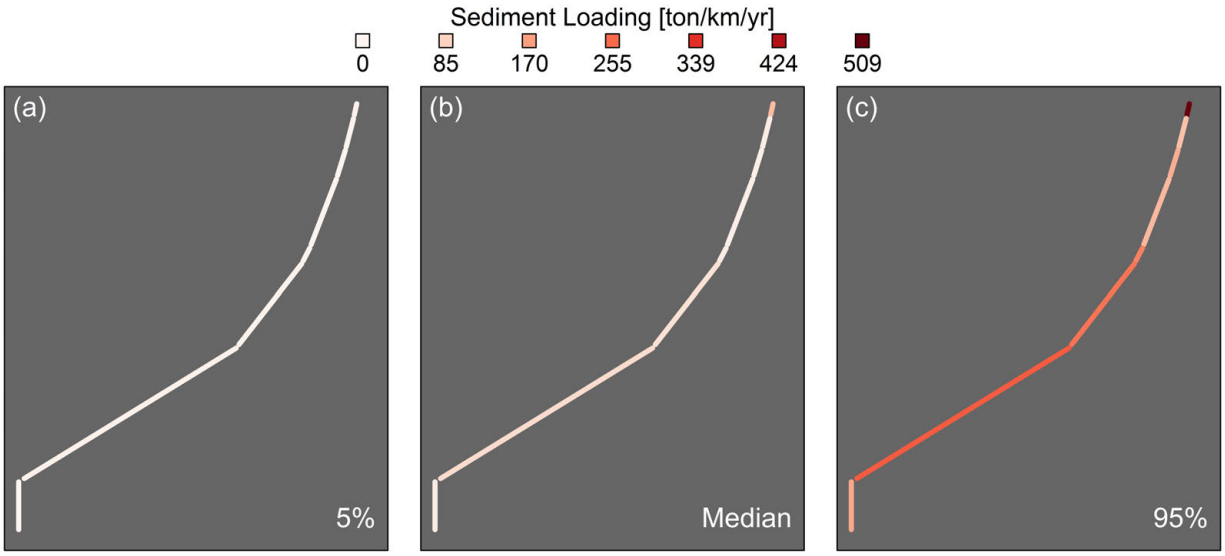

Figure 5.9: Network schematic of Big Dry Creek showing annual sediment loading rates by modeled reach, normalized by reach length, including the uncertainty range (a and c) and the median of the Monte Carlo results (b). Loading rates are larger than reported in Table 5.3 because these are cumulative loads over the simulation rather than median annual loads. Results from simulation with $Q_s = 0.5$.

5.5 Discussion

5.5.1 Significance of Channel Erosion as a Pollutant Source

For both Big Dry Creek and Lick Creek, model simulations suggest channel erosion will be a minor source of phosphorus ($\sim$1 – 4% of historic total watershed load or concentration) but may contribute 30 – 200% as much fine sediment pollution as has been recently observed from all sources in the watershed. This assumes that historic observed loads (Big Dry Creek) and concentrations (Lick Creek) at the watershed outlets are representative of future conditions. The fact that model simulations for Lick Creek are higher than observed TSS concentrations either suggests the model is overpredicting loading from channel erosion or that watershed pollutant loading could increase in the future due to continued channel instability.

The temporal overlap between the beginning of the model simulation and observed data is useful for evaluating model accuracy; however, neither model was calibrated to these measured water quality data and the daily flow record used in the Lick Creek models does not necessarily match actual flows over this time period. The point is instead to assess the

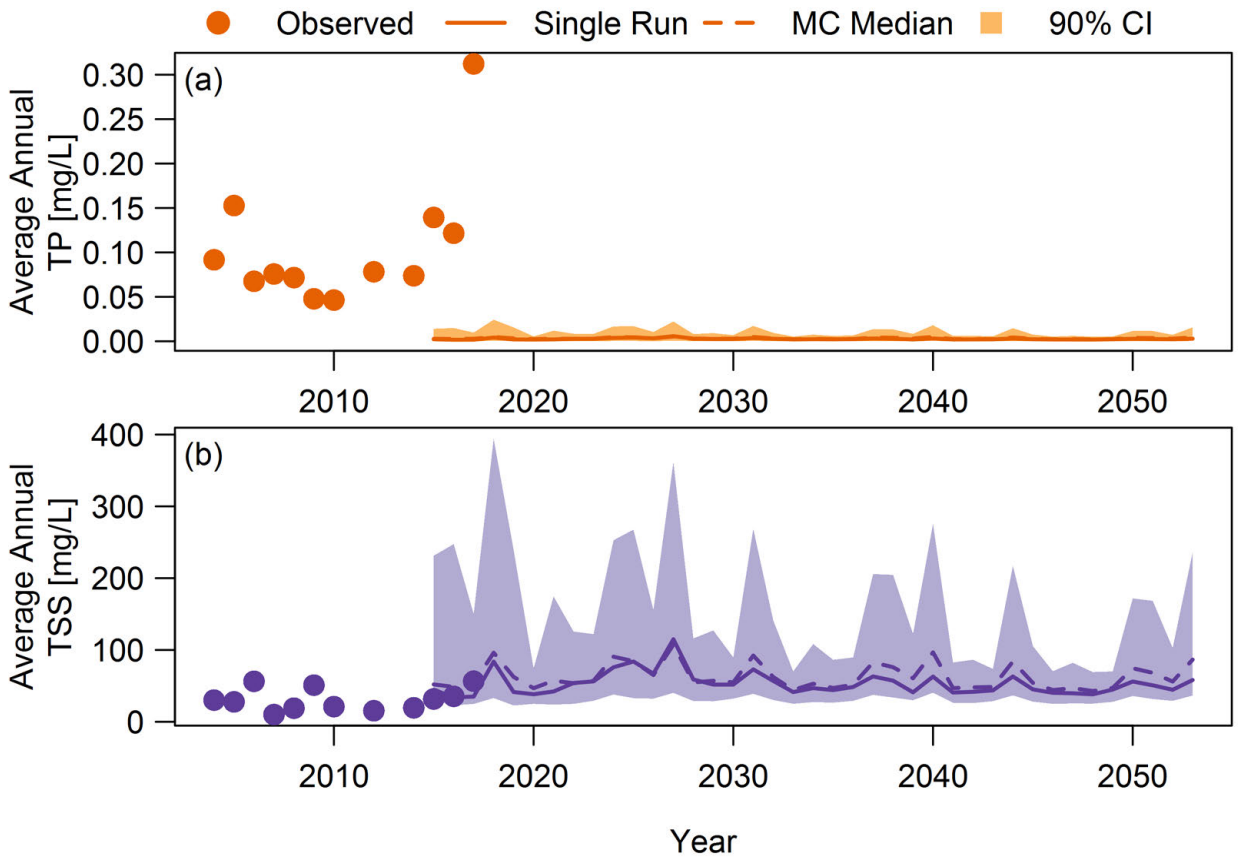

Figure 5.10: Observed and modeled average annual concentrations of TP (a) and TSS (b) for Lick Creek. Measured concentrations at the watershed outlet are shown as points. The model results for the single model run (solid line), median of the Monte Carlo simulations (dashed line), and the 90% CI are projected through 2053. Model results from simulations with $Q_s = 0.5$.

magnitude of modeled loading versus historic values. In Big Dry Creek, the first several years of the simulation show sediment loading that is similar to total watershed sediment loads. These peaks in annual sediment loading are obvious throughout the remainder of the simulation and represent the influence of high discharge years on pollutant loading. Despite these peaks, average annual sediment loading is only about one third of historic total watershed sediment loads. Model predictions for both phosphorus and sediment are less than historic loading estimates from bank erosion from the aerial imagery analysis. This could indicate that future pollutant loading from channel erosion will be less than what has recently been observed.

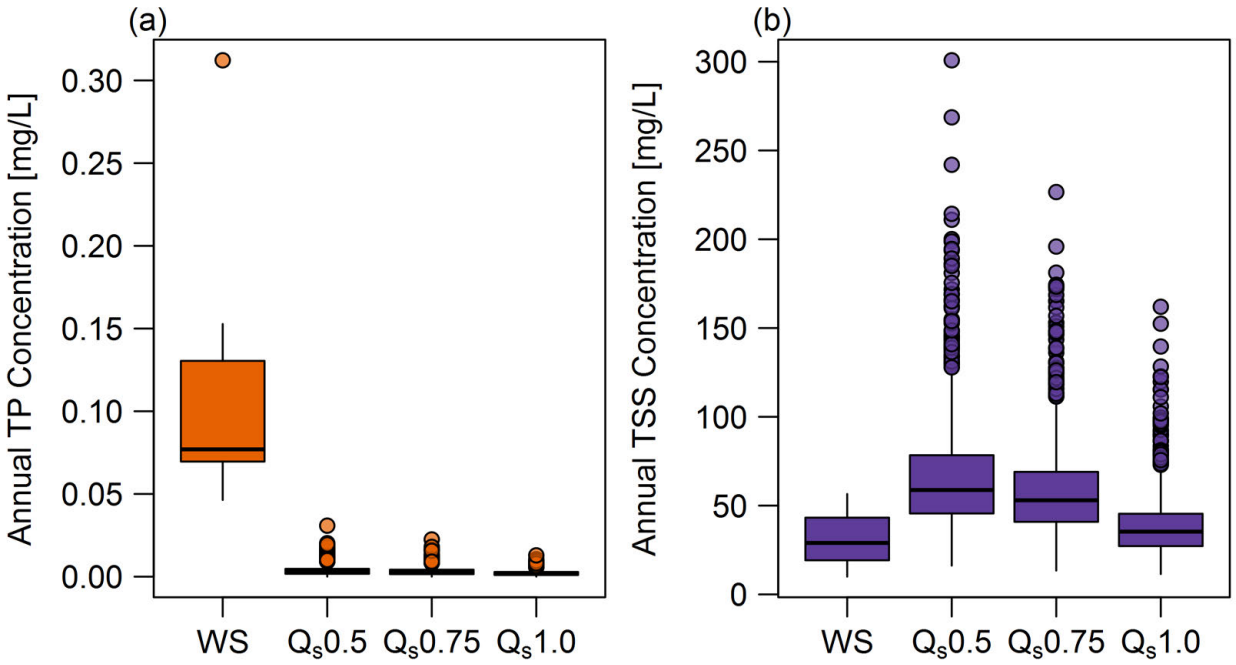

Figure 5.11: Distributions of median predicted TP (a) and TSS (b) concentrations for Lick Creek across the years of the simulation, for the three different modeled scenarios: $Q_s = 0.5$, $Q_s = 0.75$, and $Q_s = 1.0$ of transport capacity. These are compared to the distributions of observed TP and TSS concentrations at the watershed outlet from 2004 – 2017.

Modeling shows little change in bed elevations throughout the watershed — consistent with field observations that the channel is relatively stable vertically (Figure C.4). Modeling does, however, predict slight (1 – 2 m) widening (Figure C.5) and increases in channel sinuosity (median increase ∼0.15). The aerial imagery analysis showed no net change in channel width (Figure 5.3), although 1 – 2 m of widening is certainly within the range of observations. This analysis also showed a general increase in channel sinuosity, although at smaller annual rates (0.002 / year) than what modeling showed (0.0035 / year). Taken together, these results suggest that the channel will continue to adjust via a mix of widening and increased sinuosity, with little bed aggradation or incision.

In Lick Creek, the three years of overlap between the simulations and observed data (2015 – 2017) actually show remarkable agreement between measured and modeled TSS concentrations, and consistently high modeled TSS throughout the simulation. Model results, however, do not take into account other sources of fine sediment pollution. Sediment

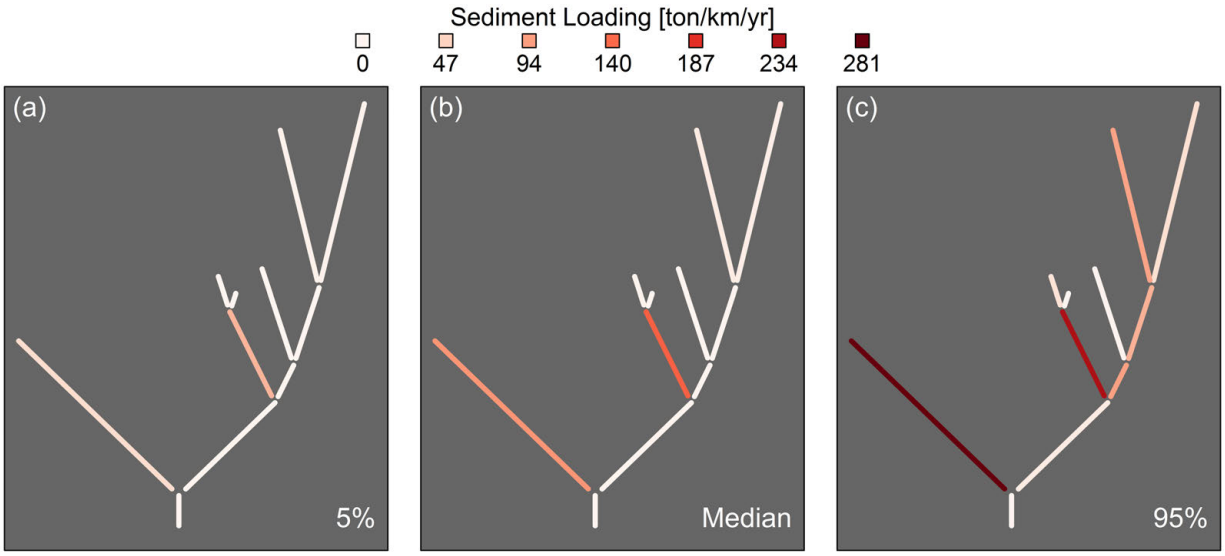

Figure 5.12: Network schematic of Lick Creek showing annual sediment loading rates by modeled reach, normalized by reach length including the uncertainty range (a and c) and the median of the Monte Carlo results (b). The two reaches with highest loading rates both had actively migrating knickpoints. Loading rates are larger than reported in Table 5.3 because these are cumulative loads over the simulation rather than median annual loads. Results from simulation with $Q_s = 0.5$.

fingerprinting from 2011 showed that bank erosion contributed only 25% (11 – 43% $\pm$ 1σ) of the total suspended sediment [*Voli et al.*, 2013] in Lick Creek, with the largest source being construction sites. This suggests the model may be overpredicting sediment contribution from channel erosion. This could indicate my estimate of bank τ_c is too low, the clay bed material in the watershed is not as widespread or easily erodible as I assumed, or the model overestimates knickpoint erosion. Bank erosion contributed <10% of the modeled loading in all three simulations, suggesting that if any source is being overestimated, it is cohesive bed erosion and knickpoint migration. Alternatively, loading estimates may be accurate and the model could be overestimating the proportion that reaches the watershed outlet by neglecting fine sediment storage. Regardless, the simulations indicate that a significant amount of sediment could come from channel erosion, but that this would contribute very little phosphorus to the watershed. Importantly, the simulations do not show a significant decreasing trend in predicted loading, indicating that the channel will not adjust to a new

stable state in the next 40 years and will instead continue to erode and be a source of fine sediment pollution.

Modeled channel changes in Lick Creek are consistent with field observations, with channel incision (with some local aggradation) predicted in the tributaries and aggradation along the mainstem. This indicates that recent channel response will continue into the future. The model also predicts widening generally throughout the watershed, suggesting that even the aggrading lower reaches are still susceptible to bank erosion. These trends are consistent across both the $Q_s = 0.5$ and $Q_s = 0.75$ simulations, while the $Q_s = 1.0$ run shows much more widespread aggradation due to higher upstream sediment supply (see Appendix C.3). Modeled estimates of loading decreased as sediment supply increased (Figure C.12); although, uncertainty within each simulation is large relative to the differences among simulations. The fact that upstream sediment supply has such a pronounced impact on modeled fine sediment loading illustrates the importance of accounting for altered sediment regimes in geomorphic and water quality analyses [*Wohl et al.*, 2015a; *Bledsoe*, 2001]. Still, even the $Q_s = 1.0$ simulation had significant fine sediment loading because knickpoint erosion — which is not impacted by incoming sediment loads — was a major loading source. Modeled loading in watersheds without knickpoints may be more sensitive to supplied bed material from upstream. In reality, large sand and gravel loads could bury a migrating knickpoint; however, REM assumes a constant knickpoint height and therefore would not capture this behavior.

Phosphorus and sediment loading rates per unit stream length in Big Dry Creek (Table 5.3) are on the low end but of similar order of magnitude to eroding streams in Iowa [*Zaimes et al.*, 2008b; *Tufekcioglu*, 2010; *Nellesen et al.*, 2011], Missouri [*Peacher*, 2011], and Denmark [*Kronvang et al.*, 2012]. They are one to two orders of magnitude less than model estimates of loading from Vermont [*Langendoen et al.*, 2012] and Oklahoma [*Miller et al.*, 2014] and from erosion of millpond sediment in Pennsylvania [*Walter et al.*, 2007] (Chapter 2, Table 2.1). This suggests that modeled loading estimates are similar to what has been observed in other

eroding streams of similar size. Lick Creek's normalized sediment loading rates are also similar to these other studies, but predicted phosphorus loading is significantly lower than what has been observed elsewhere. This is expected given the low phosphorus abundance in Lick Creek streambanks.

The relative importance of channel erosion for phosphorus and sediment pollution is consistent for both watersheds, but the reasons for it differ. For Big Dry Creek, two large wastewater treatment plants are likely responsible for most of the watershed phosphorus load, while contributing little or no suspended sediment. In fact, the significant drop in the watershed phosphorus load since 2010 (Figure 5.7) has been attributed to improved phosphorus removal at these facilities [*Clary*, 2017]. In Lick Creek, on the other hand, modeled phosphorus loading is extremely small because of the naturally low abundance of phosphorus in streambank soils.

Low measured bank phosphorus content in Lick Creek was not surprising given that North Carolina — and most of the southeastern coastal plain — has low soil phosphorus abundance [*Smith et al.*, 2013]. Bank phosphorus concentrations for both Lick Creek and Big Dry Creek show significant variability, but there are not any observable trends. Other studies have found that bank phosphorus is correlated with location in the watershed [*Miller et al.*, 2014], position on the bank [*Bledsoe et al.*, 2000; *Purvis et al.*, 2016], soil silt-clay content [*Cooper and Gilliam*, 1987; *Bledsoe et al.*, 2000; *Agudelo et al.*, 2011; *Kerr et al.*, 2011; *Young et al.*, 2012], and land use [*Palmer-Felgate et al.*, 2009; *Haggard et al.*, 2007]. None of these variables were correlated with bank total phosphorus in my study watersheds. Still, uncertainty in bank phosphorus content can introduce significant uncertainty into modeled phosphorus loading. This was the case in Lick Creek where loading was predominately from cohesive bed and knickpoint erosion (Figures C.15, C.20, and C.25). In Big Dry Creek, however, uncertainty in phosphorus loading was driven almost exclusively by bank τ_c — indicating that the magnitude of bank erosion and lateral channel migration was more important for loading than variability in bank phosphorus content (Figures C.6 and C.11).

5.5.2 Uncertainty in Model Projections

Uncertainty in loading estimates were high and it is important to put these results into perspective. Is this magnitude of uncertainty expected for loading estimates from channel erosion? Unfortunately, very few studies have quantified uncertainty in estimated pollutant loading in stream systems. *Purvis et al.* [2016] estimated historic phosphorus loading from bank erosion using aerial imagery and measured bank P content, accounting for uncertainty in these measured values. They estimated historic total P loading averaged 12,000 kg/yr (300 – 50,000 90% CI). The magnitude of loading is higher than model estimates for Big Dry Creek or Lick Creek, but the uncertainty range is similar. The *Purvis et al.* [2016] range was about four times their average estimate, lower than Big Dry Creek (range 6.3 times the median estimate) but higher than Lick Creek (range three times the median). Uncertainty ranges of sediment loading over the same time period were about twice the average value [*Purvis and Fox*, 2016]. Model results also showed the same or lower uncertainty in sediment loading (Big Dry Creek range 5.9 times the median, Lick Creek range 2.7 times the median). This is expected since phosphorus loading results have all the same uncertainty as sediment loading, with the added effect of variable bank phosphorus concentrations. *Klavon et al.* [2017] used aerial imagery and BSTEM to estimate sediment loading over a 10 year period in two streams. The uncertainty ranges for the aerial analysis were significant (10,100 – 80,700 ton/yr and 12,600 – 38,400 ton/yr) but were smaller than their model estimates (303 – 177,000 ton/yr and 494 – 34,000 ton/yr). The aerial imagery uncertainty ranges were about one to one and half times the average, while BSTEM ranges were around twice the average result. While this is a limited set of studies, it indicates that the magnitude of uncertainty in my model estimates is similar to what has been quantified by others for sediment and phosphorus loads from both aerial imagery methods and modeling. A more interesting question remains: how does uncertainty in loading from channel erosion compare to *other* sources of sediment and phosphorus pollution?

Mittelstet and Storm [2016] quantified legacy phosphorus inputs from a variety of sources in a large watershed in Oklahoma and Arkansas. Their estimated annual loading of 3,350 ton P/yr (2,840 – 3,860 ton/yr 90% CI) had a much smaller uncertainty range than my model results (less than one third of their average estimate). Uncertainty in GIS-based loading from non-point sources (median 486 kg P/yr; 250 – 750 kg/yr 90% CI) was similar to uncertainty in measured loads [*Murdoch et al.*, 2005]. Another simple watershed model predicted daily TP concentrations of around 0.3 mg/L (0.2 – 0.4 mg/L 95% CI) [*Smith et al.*, 2005]. Application of the generalized likelihood uncertainty estimation (GLUE) to the integrated catchment model of phosphorus (INCA-P) showed similar uncertainty ranges, on the order of 0.2 mg/L [*Dean et al.*, 2009]. Even models of wastewater treatment facilities can show significant uncertainty in predicted nutrient effluent concentrations [*Sin et al.*, 2011]. Modeled TP concentrations from Lick Creek were low (median 0.003 mg/L) but the uncertainty range was about three times this median value, larger than what was observed in these other studies.

These results suggest that model estimates of pollutant loading — and other studies quantifying loading from bank erosion — have significantly higher uncertainty than estimates from other non-point sources. It is possible that channel erosion is subject to inherently greater uncertainty that other sources of pollution, or simply that I accounted for more contributing factors than these other studies. The magnitude of uncertainty estimates is directly related to how many sources of uncertainty are incorporated into the analysis, and their relative variability. While I did account for uncertainty in many input variables, variability in future hydrology was not considered. This is likely a large — if not the largest — source of uncertainty in modeling future channel erosion [*Darby and Thorne*, 1996b].

5.5.3 Future Research

There are a number of avenues for future research that can both improve REM and improve understanding of the role of channel erosion in sediment and phosphorus pollution.

First, several additional processes could be added to REM that could increase model accuracy. For instance, floodplain sedimentation can be a significant sediment and phosphorus sink [*Kronvang et al.*, 2007]. Incorporating this into REM could reduce modeled loads that reach the watershed outlet. Second, in-stream phosphorus dynamics are complex, with P subject to adsorption-desorption processes, uptake by aquatic organisms, and transformation between organic and inorganic forms [*Hoffman et al.*, 2009; *McDaniel et al.*, 2009; *Records et al.*, 2016]. There is not currently a strong mechanistic foundation for understanding these processes so incorporating them into a model like REM is not feasible at this time. Still, it is important to understand the limitations of all models that estimate P loading to streams because of their inability to simulate these complex dynamics [*Fox et al.*, 2016]. REM incorporates the two mechanisms of bank erosion that typically dominant in watersheds: fluvial erosion and mass failure. Recent research has shown, however, that subaerial processes including freeze-thaw and wetting-drying cycles can significantly influence bank erosion rates and subsequent suspended sediment loading [*Couper and Maddock*, 2001; *Clark and Wynn*, 2007; *Inamdar et al.*, 2018]. The mechanisms controlling these processes are still not clear but future versions of REM could incorporate them empirically (e.g. decreasing bank τ_c with time to simulate freeze-thaw weathering).

REM has a number of potential applications beyond what was examined here. I used REM to simulate sediment and phosphorus loading from bank erosion; however, the model can also be used to estimate loading of many other sediment-bound pollutants. Streambanks can contain high concentrations of lead [*Palumbo-Roe et al.*, 2012] and other metals [*Domínguez et al.*, 2016] or even radioactive contaminants [*Paridaens and Vanmarcke*, 2001]. Furthermore, bank erosion has been shown to contribute significant amounts of mercury [*Rhoades et al.*, 2009] and nitrogen [*Walter et al.*, 2007] to watersheds. Although much of the work on bank erosion as a pollutant source has focused on sediment and phosphorus [*Fox et al.*, 2016], exploring its role in other water quality issues is important for protecting water resources.

Additionally, the model could be an important tool for predicting how different watershed management options (e.g. stormwater controls that reduce discharge) and stream restoration strategies (e.g. bed and bank stabilization) may impact channel evolution and associated pollutant loading. Others have used BSTEM [*Simon et al.*, 2011; *Langendoen et al.*, 2012; *Klavon et al.*, 2017] and CONCEPTS [*Langendoen*, 2011; *Enlow et al.*, 2018] to estimate the relative impact of different channel restoration strategies on bank erosion; however, these two models are usually applied at the reach scale. REM is easily run at the watershed scale and accounts for how restoration in one part of the watershed may impact channel response elsewhere. This also allows identification of locations in the channel network that are projected to be significant pollutant sources and may benefit from targeted restoration or stabilization (Figures 5.9 and 5.12). The importance of incorporating uncertainty into estimates of pollutant loading from channel erosion has been recognized by others [*Klavon et al.*, 2017; *Fox et al.*, 2016]. Monte Carlo simulations of REM can easily be run to estimate this uncertainty. It can even be used to just explore uncertainty in the simplified BSTEM sub-model, something that is currently not built-in to the current version of BSTEM.

5.6 Conclusion

I estimated recent and potential future sediment and phosphorus loading rates from channel erosion using a new watershed scale model (REM) that simulates both channel bed and bank erosion. The model predicted similar rates of median annual sediment loading in Big Dry Creek, CO (median 950 ton/yr) and Lick Creek, NC (940 ton/yr). Phosphorus loading, on the other hand, was significantly higher in Big Dry Creek (median 285 kg/yr) compared to Lick Creek, NC (48 kg/yr). Despite this order of magnitude difference, the potential importance of channel erosion as a phosphorus source was similar for both watersheds (only $\sim$1 – 4% of historic phosphorus load/concentration). Channel erosion may be a significant source of fine sediment pollution, ranging from 30% to >100% of historic sediment loads (Big Dry Creek) and concentrations (Lick Creek). Uncertainty ranges on

these estimates were high — similar in magnitude to other studies of pollutant loading from bank erosion but larger than estimates from other non-point sources. Still, quantifying this uncertainty is essential for effectively comparing relative magnitudes of different pollution sources. Importantly, model simulations show no decreasing trends in pollutant loading in either watershed. This indicates that both Big Dry Creek and Lick Creek will continue to actively evolve over the next 40 years and keep supplying fine sediment to their watersheds. Also, the fact that loading estimates for Lick Creek declined as upstream sediment supply increased underscores the need to consider alterations in both flow and sediment when analyzing channel evolution [*Wohl et al.*, 2015a; *Bledsoe*, 2001] — especially in streams prone to active incision. Upstream sediment supply had little effect on Big Dry Creek simulations because this channel was already vertically stable. This is the first application of REM to project future sediment and phosphorus loading from channel erosion. Channel erosion's importance as a pollutant source is increasing in recognition [*Fox et al.*, 2016], and more studies are attempting to quantify the magnitude of pollutant loading using field measurements [e.g. *Purvis et al.*, 2016; *Beck et al.*, 2018] and modeling approaches [e.g. *Langendoen et al.*, 2012; *Klavon et al.*, 2017; *Stryker et al.*, 2017]. REM can be a powerful new tool to assess the significance of this pollutant source and aid in planning targeted remediation and restoration to reduce loadings and improve water quality.

Chapter 6

Conclusions

Despite the passage of the Clean Water Act nearly 50 years ago, many of our nation's waters fall short of the goal of "swimmable and fishable". Sediment and nutrient pollution in particular continue to degrade water quality. Agencies and local governments are looking beyond the usual culprits — turning their attention to the streams themselves. Degraded and eroding streams (especially in urban areas) can be a source of pollution while limiting the natural nutrient retention capability of river ecosystems. Restoring these channels can, in a stroke, reduce pollutant loading and increase nutrient removal. The question then becomes — how significant are these benefits?

This is the question I have attempted to answer. In Chapter 2 I summarize the current state of the science on using stream restoration to reduce nutrient loading and increase nutrient retention. Results are mixed. There is strong evidence that stream restoration can reduce nutrient loading and improve water quality; however, individual restoration projects are often insufficient to make a noticeable dent in watershed scale pollution issues and it remains unclear how best to target these interventions. Stream restoration cannot solve this problem alone, other strategies are needed that reduce pollution at the source and prevent nutrients from reaching streams in the first place. Nutrient processing in streams is complex and dependent on nutrient sources, chemical and biological conditions in the stream and beneath it, and the time of year. Still, there does seem to be a consensus that some restoration strategies can be effective, even if quantifying these benefits is difficult. For example, riparian buffers can trap nutrients before they reach the stream, but estimating total nutrient removal requires long term, detailed monitoring. Nutrient removal can also be significant in hyporheic zones. Restoring these surface-subsurface exchanges should therefore provide a net benefit, but it is extremely difficult to quantify the magnitude of this exchange

before and after restoration. Bank stabilization, perhaps one of the most common strategies, can rapidly reduce sediment and phosphorus loading. The question remains, however, how significant is this pollutant source and how do we quantify the benefits of restoration?

This question was addressed in the remainder of this dissertation. In Chapter 3, I introduce new sediment transport equations which are easily applied at the watershed scale. These equations — and really the whole model — are built on the seminal work of *Bagnold* [1966, 1980], who formalized the use of stream power to estimate the work done by river channels. My motivation for developing these equations was to use them to model channel incision and aggradation as part of REM. Hopefully, they will also find use outside of this context. Understanding sediment transport throughout river networks is vitally important for effective management, as evidenced by several recent advances in modeling network sediment connectivity [*Schmitt et al.*, 2016, 2018; *Czuba*, 2016]. My new transport equations might be useful for continued growth in this area.

In Chapter 4, I introduce the River Erosion Model to simulate channel evolution and associated pollutant loading. REM accounts for the two dominant modes of channel adjustment: bed and bank erosion. A simple case study demonstrates that the model matches physical understanding of channel evolution. REM is also able to accurately simulate channel incision and bed material coarsening on a reach of the lower Colorado River downstream from Parker Dam. Finally, REM accurately predicts channel incision and widening on the upper portion of the North Fork Toutle River which responded dramatically to the 1980 eruption of Mount St. Helens. The model does a poor job in the lower portion of the watershed where the river migrated significantly across its valley bottom and even braided — processes that were not included in REM.

In Chapter 5 I used REM to estimate future sediment and phosphorus loading from channel erosion in two watersheds: Big Dry Creek, CO and Lick Creek, NC. In both cases, channel erosion is projected to be a significant source of fine sediment, but a relatively small source of phosphorus. Uncertainty in these projections is significant, and may complicate

REM's usefulness for decision makers; however, it is better to be honest about our ability to predict changes in these complex stream systems than to hide behind the false veil of deterministic model results.

The obvious application of REM is to estimate sediment and phosphorus loading from channel erosion in disturbed watersheds. Given its strong mechanistic basis, however, it also has a variety of other potential uses. For example, different stream stabilization or stormwater management approaches could be simulated to understand their effects on channel change and water quality. Alternatively, REM could also be used to explore magnitudes and trajectories of channel change under different climate and land use scenarios. This could improve our understanding of stream morphologic response to these widespread types of disturbances. Finally, REM may be useful for answering other river research questions, including when and where the concept of channel equilibrium is applicable and how processes in different parts of the watershed affect this understanding. It is my hope that both the management and research communities find REM useful. Our rivers deserve to be better managed and understood and REM may be a helpful tool to achieve these goals.

Bibliography

Ackers, P., and W. R. White, 1973, Sediment transport: New approach and analysis, *Journal of the Hydraulics Division*, *99*, 2041–2060.

Agudelo, S. C., N. O. Nelson, P. L. Barnes, T. D. Keane, and G. M. Pierzynski, 2011, Phosphorus adsorption and desorption potential of stream sediments and field soils in agricultural watersheds, *Journal of Environmental Quality*, *40*, 144–152.

Aldridge, K. T., J. D. Brookes, and G. G. Ganf, 2009, Rehabilitation of stream ecosystem functions through the reintroduction of coarse particulate organic matter, *Restoration Ecology*, *17*, 97–106.

Aldridge, K. T., J. D. Brookes, and G. G. Ganf, 2010, Changes in abiotic and biotic phosphorus uptake across a gradient of stream condition, *River Research and Applications*, *26*, 636–649.

Allen, C. R., J. J. Fontaine, K. L. Pope, and A. S. Garmestani, 2011, Adaptive management for a turbulent future, *Journal of Environmental Management*, *92*, 1339–1345.

Allen, P. M., J. G. Arnold, and E. Jakubowski, 1999, Prediction of stream channel erosion potential, *Environmental & Engineering Geoscience*, *5*, 339–351.

Allen, P. M., J. G. Arnold, L. Auguste, J. White, and J. Dunbar, 2018, Application of a simple headcut advance model for gullies, *Earth Surface Processes and Landforms*, *43*, 202–217.

Almedeij, J. H., Bedload transport in gravel-bed streams under a wide range of Shields stresses, Phd dissertation, Virginia Polytechnic Institute., 2002.

Argerich, A., E. Martí, F. Sabater, M. Ribot, D. von Schiller, and J. L. Riera, 2008, Combined effects of leaf litter inputs and a flood on nutrient retention in a Mediterranean mountain stream during fall, *Limnology and Oceanography*, *53*, 631–641.

Army Corps of Engineers, Hydraulic design of flood control channels, *Tech. rep.*, EM 1110-2-1601, Department of the Army, 1970.

Arnold, J. G., R. Srinivasan, R. S. Muttiah, and J. R. Williams, 1998, Large area hydrologic modeling and assessment part I: Model development, *Journal of the American Water Resources Association*, *34*, 73–89.

Ashida, K., and M. Michiue, An investigation of river bed degradation downstream of a dam, in *Proceedings of the 14th IAHR Congress*, pp. 247–255, Paris, 29 August - 3 September, 1971.

Azinheira, D. L., D. T. Scott, W. Hession, and E. T. Hester, 2014, Comparison of effects of inset floodplains and hyporheic exchange induced by in-stream structures on solute retention, *Water Resources Research*, *50*, 6168–6190.

Bacchi, V., A. Recking, N. Eckert, P. Frey, G. Piton, and M. Naaim, 2014, The effects of kinetic sorting on sediment mobility on steep slopes, *Earth Surface Processes and Landforms*, *39*, 1075–1086.

Bagnold, R. A., An approach to the sediment transport problem from general physics, *Tech. rep.*, USGS Professional Paper 422-I., 1966.

Bagnold, R. A., 1973, The nature of saltation and of 'bed-load' transport in water, *Proceedings of the Royal Society of London A: Mathematical, Physical and Engineering Sciences*, *332*, 473–504.

Bagnold, R. A., 1977, Bed load transport by natural rivers, *Water Resources Research*, *13*, 303–312.

Bagnold, R. A., 1980, An empirical correlation of bedload transport rates in flumes and natural rivers, *Proceedings of the Royal Society of London: Series A, Mathematical and Physical Sciences*, *372*, 453–473.

Baker, D. W., B. P. Bledsoe, and J. Mueller Price, 2012, Stream nitrate uptake and transient storage over a gradient of geomorphic complexity, north-central Colorado, USA, *Hydrological Processes*, *26*, 3241–3252.

Bathurst, J. C., Hydraulics of mountain rivers, *Tech. rep.*, Report CER78-79JCB-RML-DBS55. Department of Civil Engineering, Colorado State University, Fort Collins, CO., 1979.

Bathurst, J. C., 2013, Critical conditions for particle motion in coarse bed materials of nonuniform size distribution, *Geomorphology*, *197*, 170–184.

Bathurst, J. C., W. H. Graf, and H. H. Cao, Bed load discharge equations for steep mountain rivers, in *Sediment Transport in Gravel-Bed Rivers*, edited by C. R. Thorne, J. C. Bathurst, and R. D. Hey, pp. 453–492, John Wiley & Sons, Chichester, 1987.

Beck, W., T. Isenhart, P. Moore, K. Schilling, R. Schultz, and M. Tomer, 2018, Streambank alluvial unit contributions to suspended sediment and total phosphorus loads, Walnut Creek, Iowa, USA, *Water*, *10*, 111.

Becker, J. F., T. A. Endreny, and J. D. Robinson, 2013, Natural channel design impacts on reach-scale transient storage, *Ecological Engineering*, *57*, 380–392.

Begin, Z. B., D. F. Meyer, and S. A. Schumm, 1981, Development of longitudinal profiles of alluvial channels in response to base-level lowering, *Earth Surface Processes and Landforms*, *6*, 49–68.

Bernhardt, E. S., and G. E. Likens, 2002, Dissolved organic carbon enrichment alters nitrogen dynamics in a forest stream, *Ecology*, *83*, 1689–1700.

Bernhardt, E. S., and M. A. Palmer, 2007, Restoring streams in an urbanizing world, *Freshwater Biology*, *52*, 738–751.

Bernhardt, E. S., J. R. Blaszczak, C. D. Ficken, M. L. Fork, K. E. Kaiser, and E. C. Seybold, 2017, Control points in ecosystems: Moving beyond the hot spot hot moment concept, *Ecosystems*, *20*, 665–682.

Bernhardt, E. S., et al., 2005, Synthesizing U.S. river restoration efforts, *Science*, *308*, 636–637.

Biron, P. M., G. Choné, T. Buffin-Bélanger, S. Demers, and T. Olsen, 2013, Improvement of streams hydro-geomorphological assessment using LiDAR DEMs, *Earth Surface Processes and Landforms*, *38*, 1808–1821.

Bizzi, S., and D. N. Lerner, 2015, The use of stream power as an indicator of channel sensitivity to erosion and deposition processes, *River Research and Applications*, *31*, 16–27.

Bledsoe, B. P., Relationships of stream responses to hydrologic changes, in *Linking Stormwater BMP Designs and Performance to Receiving Water Impact Mitigation*, edited by B. R. Urbonas, pp. 127–144, American Society of Civil Engineers, 2001.

Bledsoe, B. P., K. A. O'Connor, C. C. Watson, and K. H. Carlson, Phosphorus content of bed, bank and upland sediments: Long Creek and Johnson Creek Watersheds, Mississippi, *Tech. rep.*, Colorado State University: Prepared for USACE, Vicksburg District, 2000.

Bledsoe, B. P., E. D. Stein, R. J. Hawley, and D. Booth, 2012, Framework and tool for rapid assessment of stream susceptibility to hydromodification, *JAWRA Journal of the American Water Resources Association*, *48*, 788–808.

Böhlke, J. K., M. E. O'Connell, and K. L. Prestegaard, 2007, Ground water stratification and delivery of nitrate to an incised stream under varying flow conditions., *Journal of Environmental Quality*, *36*, 664–680.

Böhlke, J. K., R. C. Antweiler, J. W. Harvey, A. E. Laursen, L. K. Smith, R. L. Smith, and M. A. Voytek, 2009, Multi-scale measurements and modeling of denitrification in streams with varying flow and nitrate concentration in the upper Mississippi River basin, USA, *Biogeochemistry*, *93*, 117–141.

Booth, D. B., 1990, Stream-channel incision following drainage-basin urbanization, *Water Resources Bulletin*, *26*, 407–417.

Booth, D. B., and C. J. Fischenich, 2015, A channel evolution model to guide sustainable urban stream restoration, *Area*, *47*, 408–421.

Booth, D. B., D. R. Montgomery, and J. Bethel, Large woody debris in urban streams of the Pacific Northwest, in *Effects of watershed development and management on aquatic ecosystems: Engineering Foundation Conference*, edited by L. A. Roesner, pp. 178–197, Snowbird, Utah, 1996.

Brady, N. C., and R. R. Weil, *The Nature and Properties of Soils*, 13th ed., Prentice Hall, Upper Saddle River, New Jersey, 2002.

Bravo-Espinosa, M., Prediction of bedload discharge for alluvial channels, Ph.d. dissertation, University of Arizona, 1999.

Browning, M., The efficacy of urban stream restorations to improve water quality across a spectrum of design approaches, Master's thesis, George Mason University, 2008.

Brownlie, W. R., Compilation of alluvial channel data: Laboratory and field, *Tech. rep.*, WM Keck Laboratory of Hydraulics and Water Resources, California Institute of Technology, 1981.

Brownlie, W. R., Prediction of flow depth and sediment discharge in open channels, Ph.d. dissertation, California Institute of Technology, 1982.

Bull, W. B., 1979, Threshold of critical power in streams, *Geological Society of America Bulletin*, *90*, 453–464.

Buscombe, D., and D. C. Conley, 2012, Effective shear stress of graded sediments, *Water Resources Research*, *48*, W05,506.

Camenen, B., 2012, Discussion of "Understanding the influence of slope on the threshold of coarse grain motion: Revisiting critical stream power" by C. Parker, N.J. Clifford, and C.R. Thorne Geomorphology, Volume 126, March 2011, Pages 51-65, *Geomorphology*, *139-140*, 34–38.

Carline, R. F., and M. C. Walsh, 2007, Responses to riparian restoration in the Spring Creek watershed, Central Pennsylvania, *Restoration Ecology*, *15*, 731–742.

Charbonneau, R., and V. H. Resh, 1992, Strawberry Creek on the University of California, Berkeley campus: A case history of urban stream restoration, *Aquatic Conservation: Marine and Freshwater Ecosystems*, *2*, 293–307.

Chen, D., and J. D. Duan, 2006, Simulating sine-generated meandering channel evolution with an analytical model, *Journal of Hydraulic Research*, *44*, 363–373.

Clark, L. A., and T. M. Wynn, 2007, Methods for determining streambank critical shear stress and soil erodibility: Implications for erosion rate predictions, *Transactions of the American Society of Agricultural and Biological Engineers*, *50*, 95–106.

Clary, J., Big Dry Creek annual water quality summary for 2016, *Tech. rep.*, Prepared for the Big Dry Creek Watershed Association by Wright Water Engineers, Inc., 2017.

Cluer, B., and C. Thorne, 2014, A stream evolution model integrating habitat and ecosystem benefits, *River Research and Applications*, *30*, 135–154.

Collins, A. L., and D. E. Walling, 2007, Sources of fine sediment recovered from the channel bed of lowland groundwater-fed catchments in the UK, *Geomorphology*, *88*, 120–138.

Collins, K. E., C. Doscher, H. G. Rennie, and J. G. Ross, 2013, The effectiveness of riparian 'restoration' on water quality - A case study of lowland streams in Canterbury, New Zealand, *Restoration Ecology*, *21*, 40–48.

Cooper, J. R., and J. W. Gilliam, 1987, Phosphorus redistribution from cultivated fields into riparian areas, *Soil Science Society of America Journal*, *51*, 1600–1604.

Couper, P. R., and I. Maddock, 2001, Subaerial river bank erosion processes and their interaction with other bank erosion mechanisms on the River Arrow, Warwickshire, UK, *Earth Surface Processes and Landforms*, *26*, 631–646.

Craig, L. S., et al., 2008, Stream restoration strategies for reducing river nitrogen loads, *Frontiers in Ecology and the Environment*, *6*, 529–538.

Crispell, J. K., and T. A. Endreny, 2009, Hyporheic exchange flow around constructed in-channel structures and implications for restoration design, *Hydrological Processes*, *23*, 1158–1168.

Crosato, A., 2007, Effects of smoothing and regridding in numerical meander migration models, *Water Resources Research*, *43*.

Crosland, A. R., F. J. Zhao, S. P. McGrath, and P. W. Lane, 1995, Comparison of aqua regia digestion with sodium carbonate fusion for the determination of total phosphorus in soils by inductively coupled plasma atomic emission spectroscopy (ICP), *Communications in Soil Science and Plant Analysis*, *26*, 1357–1368.

Cruff, R. W., Cross-channel transfer of linear momentum in smooth rectangular channels, *Tech. rep.*, USGS Water-Supply Paper 1592-B, 1965.

Czuba, J. A., A Network-Based Framework for Hydro-Geomorphic Modeling and Decision Support with Application to Space-Time Sediment Dynamics, Identifying Vulnerabilities, and Hotspots of Change, Phd dissertation, University of Minnesota, 2016.

Czuba, J. A., and E. Foufoula-Georgiou, 2014, A network-based framework for identifying potential synchronizations and amplifications of sediment delivery in river basins, *Water Resources Research*, *50*, 3826–3851.

Czuba, J. A., and E. Foufoula-Georgiou, 2015, Dynamic connectivity in a fluvial network for identifying hotspots of geomorphic change, *Water Resources Research*, *51*, 1401–1421.

Czuba, J. A., E. Foufoula-Georgiou, K. B. Gran, P. Belmont, and P. R. Wilcock, 2017, Interplay between spatially-explicit sediment sourcing, hierarchical river-network structure, and in-channel bed-material sediment transport and storage dynamics, *Journal of Geophysical Research: Earth Surface*, *122*, 1090–1120.

Daly, E. R., G. A. Fox, A. S. T. Al-Madhhachi, and D. E. Storm, 2015a, Variability of fluvial erodibility parameters for streambanks on a watershed scale, *Geomorphology*, *231*, 281–291.

Daly, E. R., R. B. Miller, and G. A. Fox, 2015b, Modeling streambank erosion and failure along protected and unprotected composite streambanks, *Advances in Water Resources*, *81*, 114–127.

Daniluk, T. L., L. K. Lautz, R. P. Gordon, and T. A. Endreny, 2013, Surface water-groundwater interaction at restored streams and associated reference reaches, *Hydrological Processes*, *27*, 3730–3746.

Darby, S. E., and C. R. Thorne, 1996a, Numerical simulation of widening and bed deformation of straight sand-bed rivers. I: Model development, *Journal of Hydraulic Engineering*, *122*, 184–193.

Darby, S. E., and C. R. Thorne, 1996b, Modelling the sensitivity of channel adjustments in destabilized sand-bed rivers, *Earth Surface Processes and Landforms*, *21*, 1109–1125.

Darby, S. E., C. R. Thorne, and A. Simon, 1996, Numerical simulation of widening and bed deformation of straight sand-bed rivers. II: Model evaluation, *Journal of Hydraulic Engineering*, *122*, 194–202.

Darby, S. E., A. M. Alabyan, and M. J. Van de Wiel, 2002, Numerical simulation of bank erosion and channel migration in meandering rivers, *Water Resources Research*, *38*, 1163.

Darby, S. E., M. Rinaldi, and S. Dapporto, 2007, Coupled simulations of fluvial erosion and mass wasting for cohesive river banks, *Journal of Geophysical Research*, *112*, F03,022.

Davis, R. T., J. L. Tank, U. H. Mahl, S. G. Winikoff, and S. S. Roley, 2015, The influence of two-stage ditches with constructed floodplains on water column nutrients and sediments in agricultural streams, *Journal of the American Water Resources Association*, *51*, 941–955.

Dean, S., J. Freer, K. Beven, A. J. Wade, and D. Butterfield, 2009, Uncertainty assessment of a process-based integrated catchment model of phosphorus, *Stochastic Environmental Research and Risk Assessment*, *23*, 991–1010.

DeWolfe, M. N., W. C. Hession, and M. C. Watzin, 2004, Sediment and phosphorus loads from streambank erosion in Vermont, USA, *Critical Transitions in Water and Environmental Resources Management*, pp. 1–10.

Dey, S., and U. V. Raju, 2002, Incipient motion of gravel and coal beds, *Sadhana*, *27*, 559–568.

Diamond, J., *Collapse: How societies choose to fail or succeed*, Penguin Books, New York, NY, 2005.

Dick, W. A., and M. A. Tabatabai, 1977, An alkaline oxidation method for determination of total phosphorus in soils, *Soil Science Society of America Journal*, *41*, 511–514.

Dietrich, W. E., Mechanics of flow and sediment transport in river bends, in *River Channels: Environment and Process*, edited by K. Richards, pp. 179–227, Basil Blackwell, Oxford, UK, 1987.

Domínguez, M. T., J. M. Alegre, P. Madejón, E. Madejón, P. Burgos, F. Cabrera, T. Marañón, and J. M. Murillo, 2016, River banks and channels as hotspots of soil pollution after large-scale remediation of a river basin, *Geoderma*, *261*, 133–140.

Downs, P. W., and A. Simon, 2001, Fluvial geomorphological analysis of the recruitment of large woody debris in the Yalobusha river network, Central Mississippi, USA, *Geomorphology*, *37*, 65–91.

Doyle, M. W., and J. M. Harbor, 2003, Modelling the effect of form and profile adjustments on channel equilibrium timescales, *Earth Surface Processes and Landforms*, *28*, 1271–1287.

Doyle, M. W., E. H. Stanley, and J. M. Harbor, 2003, Hydrogeomorphic controls on phosphorus retention in streams, *Water Resources Research*, *39*, 1147.

Drinker, P. A., Boundary shear stresses in curved trapezoidal channels, Phd dissertation, Massachusetts Institute of Technology, 1961.

Eaton, B. C., and M. Church, 2011, A rational sediment transport scaling relation based on dimensionless stream power, *Earth Surface Processes and Landforms*, *36*, 901–910.

Eaton, B. C., and R. G. Millar, 2017, Predicting gravel bed river response to environmental change: the strengths and limitations of a regime-based approach, *Earth Surface Processes and Landforms*, *42*, 994 – 1008.

El Kadi Abderrezzak, K., and A. Paquier, 2009, One-dimensional numerical modeling of sediment transport and bed deformation in open channels, *Water Resources Research*, *45*, 1–20.

El Kadi Abderrezzak, K., A. Paquier, and B. Gay, 2008, One-dimensional numerical modelling of dam-break waves over movable beds: Application to experimental and field cases, *Environmental Fluid Mechanics*, *8*, 169–198.

Elosegi, A., C. Elorriaga, L. Flores, E. Martí, and J. Díez, 2016, Restoration of wood loading has mixed effects on water, nutrient, and leaf retention in Basque mountain streams, *Freshwater Science*, *35*, 41–54.

Elser, J. J., et al., 2007, Global analysis of nitrogen and phosphorus limitation of primary producers in freshwater, marine and terrestrial ecosystems, *Ecology Letters*, *10*, 1–8.

Engelund, F., and E. Hansen, *A Monograph on Sediment Transport in Alluvial Streams*, Teknish Forlag Technical Press, Copenhagen, Denmark, 1967.

Enlow, H. K., G. A. Fox, and L. Guertault, 2017, Watershed variability in streambank erodibility and implications for erosion prediction, *Water*, *9*, 1–16.

Enlow, H. K., G. A. Fox, T. A. Boyer, A. Stoecker, D. E. Storm, P. Starks, and L. Guertault, 2018, A modeling framework for evaluating streambank stabilization practices for reach-scale sediment reduction, *Environmental Modelling and Software*, *100*, 201–212.

Ensign, S. H., and M. W. Doyle, 2005, In-channel transient storage and associated nutrient retention: Evidence from experimental manipulations, *Limnology and Oceanography*, *50*, 1740–1751.

EPA, Watershed Assessment, Tracking & Environmental Results, National Summary of State Information, 2015.

Fanelli, R. M., and L. K. Lautz, 2008, Patterns of water, heat, and solute flux through streambeds around small dams, *Groundwater*, *46*, 671–687.

Ferguson, R., 2007, Flow resistance equations for gravel- and boulder-bed streams, *Water Resources Research*, *43*, W05,427.

Ferguson, R. I., 1986, River loads underestimated by rating curves, *Water Resources Research*, *22*, 74–76.

Ferguson, R. I., 2005, Estimating critical stream power for bedload transport calculations in gravel-bed rivers, *Geomorphology*, *70*, 33–41.

Ferguson, R. I., 2012, River channel slope, flow resistance, and gravel entrainment thresholds, *Water Resources Research*, *48*, W05,517.

Filoso, S., and M. A. Palmer, 2011, Assessing stream restoration effectiveness at reducing nitrogen export to downstream waters, *Ecological Applications*, *21*, 1989–2006.

Fink, D. F., and W. J. Mitsch, 2007, Hydrology and nutrient biogeochemistry in a created river diversion oxbow wetland, *Ecological Engineering*, *30*, 93–102.

Forshay, K. J., and E. H. Stanley, 2005, Rapid nitrate loss and denitrification in a temperate river floodplain, *Biogeochemistry*, *75*, 43–64.

Fox, G. A., R. A. Purvis, and C. J. Penn, 2016, Streambanks: A net source of sediment and phosphorus to streams and rivers, *Journal of Environmental Management*, *181*, 602–614.

Frey, P., and M. Church, 2011, Bedload: A granular phenomenon, *Earth Surface Processes and Landforms*, *36*, 58–69.

Fryirs, K., and G. J. Brierley, 2001, Variability in sediment delivery and storage along river courses in Bega catchment, NSW, Australia: Implications for geomorphic river recovery, *Geomorphology*, *38*, 237–265.

Fryirs, K., G. J. Brierley, and W. D. Erskine, 2012, Use of ergodic reasoning to reconstruct the historical range of variability and evolutionary trajectory of rivers, *Earth Surface Processes and Landforms*, *37*, 763–773.

Garbrecht, J., R. Kuhnle, and C. Alonso, 1995, A sediment transport capacity formulation for application to large channel networks, *Journal of Soil and Water Conservation*, *50*, 527–529.

Ghosh, S. N., and N. Roy, 1970, Boundary shear distribution in open channel flow, *Journal of the Hydraulics Division*, *96*, 967–994.

Gibson, S., A. Simon, E. J. Langendoen, N. Bankhead, and J. Shelley, A physically-based channel-modeling framework integrating HEC- RAS sediment transport capabilities and the USDA-ARS Bank-Stability and Toe-Erosion Model (BSTEM), in *3rd Joint Federal Interagency Sedimentation and Hydrologic Modeling Conference*, p. 12, Reno, NV, 2015.

Gift, D. M., P. M. Groffman, S. S. Kaushal, and P. Mayer, 2010, Denitrification potential, root biomass, and organic matter in degraded and restored urban riparian zones, *Restoration Ecology*, *18*, 113–120.

Gold, A., K. Addy, A. Morrison, and M. Simpson, 2016, Will dam removal increase nitrogen flux to estuaries?, *Water*, *8*, 522.

Gomez, B., and M. Church, A catalogue of equilibrium bedload transport data for coarse sand and gravel-bed channels, *Tech. rep.*, University of British Columbia., 1988.

Gomez, B., and M. Church, 1989, An assessment of bed load sediment transport formulae for gravel bed rivers, *Water Resources Research*, *25*, 1161–1186.

Google Earth Pro, Lower Colorado River near Parker, AZ 34 07'21" 114 21'22" Imagery Date 2017-06-16, 2017a.

Google Earth Pro, Google Earth Imagery, 2017b.

Gooseff, M. N., D. M. McKnight, R. L. Runkel, and J. H. Duff, 2004, Denitrification and hydrologic transient storage in a glacial meltwater stream, McMurdo Dry Valleys, Antarctica, *Limnology and Oceanography*, *49*, 1884–1895.

Gordon, R. P., L. K. Lautz, and T. L. Daniluk, 2013, Spatial patterns of hyporheic exchange and biogeochemical cycling around cross-vane restoration structures: Implications for stream restoration design, *Water Resources Research*, *49*, 2040–2055.

Groffman, P. M., N. J. Boulware, W. C. Zipperer, R. V. Pouyat, L. E. Band, and M. F. Colosimo, 2002, Soil nitrogen cycle processes in urban riparian zones, *Environmental Science & Technology*, *36*, 4547–4552.

Groffman, P. M., D. J. Bain, L. E. Band, K. T. Belt, G. S. Brush, J. P. Grove, R. V. Pouyat, I. C. Yesilonis, and W. C. Zipperer, 2003, Down by the riverside: urban riparian ecology, *Frontiers in Ecology and the Environment*, *1*, 315–321.

Groffman, P. M., A. M. Dorsey, and P. M. Mayer, 2005, N processing within geomorphic structures in urban streams, *Journal of the North American Benthological Society*, *24*, 613–625.

Groffman, P. M., et al., 2006, Methods for measuring denitrification: diverse approaches to a difficult problem, *Ecological Applications*, *16*, 2091–2122.

Habersack, H. M., and J. B. Laronne, 2002, Evaluation and improvement of bed load discharge formulas based on Helley-Smith sampling in an alpine gravel bed river, *Journal of Hydraulic Engineering*, *128*, 484–499.

Hack, J. T., Studies of longitudinal stream profiles in Virginia and Maryland, *Tech. rep.*, United States Geological Survey Professional Paper 294B, 1957.

Haggard, B. E., D. R. Smith, and K. R. Brye, 2007, Variations in stream water and sediment phosphorus among select Ozark catchments, *Journal of Environmental Quality*, *36*, 1725–1734.

Hankin, R. K. S., 2006, Special functions in R: Introducing the gsl package, *R News*, *6*, 24 – 26.

Hanson, G. J., and A. Simon, 2001, Erodibility of cohesive streambeds in the loess area of the midwestern USA, *Hydrological Processes*, *15*, 23–38.

Harrison, M. D., P. M. Groffman, P. Mayer, and S. S. Kaushal, 2012, Microbial biomass and activity in geomorphic features in forested and urban restored and degraded streams, *Ecological Engineering*, *38*, 1–10.

Hawley, R. J., B. P. Bledsoe, E. D. Stein, and B. E. Haines, 2012, Channel evolution model of semiarid stream response to urban-induced hydromodification, *Journal of the American Water Resources Association*, *48*, 722–744.

Hefting, M. M., J.-C. Clément, D. Dowrick, A. C. Cosandey, S. Bernal, C. Cimpian, A. Tatur, T. P. Burt, and G. Pinay, 2004, Water table elevations controls on soil nitrogen cycling in riparian wetlands along a European climatic gradient, *Biogeochemistry*, *67*, 113–134.

Hester, E. T., and E. N. Cranmer, 2014, Variation of hyporheic potential among urban region streams: implications for stream restoration, *Environmental & Engineering Geoscience*, *20*, 287–304.

Hester, E. T., and M. W. Doyle, 2008, In-stream geomorphic structures as drivers of hyporheic exchange, *Water Resources Research*, *44*, W03,417.

Hester, E. T., and M. N. Gooseff, 2010, Moving beyond the banks: Hyporheic restoration is fundamental to restoring ecological services and functions of streams, *Environmental Science and Technology*, *44*, 1521–1525.

Hester, E. T., B. Hammond, and D. T. Scott, 2016, Effects of inset floodplains and hyporheic exchange induced by in-stream structures on nitrate removal in a headwater stream, *Ecological Engineering*, *97*, 452–464.

Hill, A. R., 1996, Nitrate removal in stream riparian zones, *Journal of Environmental Quality*, *25*, 743–755.

Hinton, D., R. Hotchkiss, and D. P. Ames, Sediment transport database HydroServer, 2016.

Hirsch, C., *Numerical Computation of Internal and External Flows*, 2nd ed., Butterworth-Heinmann, Oxford, 2007.

Hoey, T. B., and R. Ferguson, 1994, Numerical simulation of downstream fining by selective transport in gravel bed rivers: Model development and illustration, *Water Resources Research*, *30*, 2251–2260.

Hoffman, A. R., D. E. Armstrong, R. C. Lathrop, and M. R. Penn, 2009, Characteristics and influence of phosphorus accumulated in the bed sediments of a stream located in an agricultural watershed, *Aquatic Geochemistry*, *15*, 371–389.

Hollis, G. E., 1975, The effect of urbanization on floods of different recurrence interval, *Water Resources Research*, *11*, 431–435.

Homer, C. G., et al., 2015, Completion of the 2011 National Land Cover Databse for the conterminous United States - Representing a decade of land cover change information, *Photogrammetric Engineering and Remote Sensing*, *81*, 345–354.

Hongthanat, N., Phosphorus sorption-desorption of soils and sediments in the Rathbun Lake watershed, Master's thesis, Iowa State University, 2010.

Hooke, J. M., Styles of channel change, in *Applied Fluvial Geomorphology for River Engineering and Management*, edited by C. R. Thorne, R. D. Hey, and M. D. Newson, pp. 237–268, John Wiley & Sons, Chichester, 1997.

Hooke, J. M., River meandering, in *Treatise on Geomorphology, vol. 9, Fluvial Geomorphology*, edited by I. Shroder and E. Wohl, pp. 260–288, Academic Press, San Diego, CA, 2013.

Hothorn, T., P. Buehlmann, S. Dudoit, A. Molinaro, and M. Van Der Laan, 2006, Survival ensembles, *Biostatistics*, *7*, 355–373.

Howe, E., M. Winchell, D. Meals, S. Folle, J. Moore, D. Braun, C. DeLeo, K. Budreski, and R. Schiff, Identification of critical source areas of phosphorus within the Vermont sector of the Missisquoi Bay basin, *Tech. rep.*, Stone Environmental Inc, Prepared for Lake Champlain Basin Program, Grand Isle, VT, 2011.

Huang, H. Q., C. Deng, G. C. Nanson, B. Fan, X. Liu, T. Liu, and Y. Ma, 2014, A test of equilibrium theory and a demonstration of its practical application for predicting the morphodynamics of the Yangtze River, *Earth Surface Processes and Landforms*, *39*, 669–675.

Hubbard, L. C., D. S. Biedenharn, and S. L. Ashby, Assessment of environmental and economic benefits associated with streambank stabilization and phosphorus retention, *Tech. rep.*, USACE Research and Development Center, Vicksburg, MS, 2003.

Hupp, C. R., G. B. Noe, E. R. Schenk, and A. J. Benthem, 2013, Recent and historic sediment dynamics along Difficult Run, a suburban Virginia Piedmont stream, *Geomorphology*, *180-181*, 156–169.

Ikeda, H., Experiments on bedload transport, bed forms, and sedimentary structures using fine gravel in the 4-metre-wide flume, *Tech. rep.*, Paper 2. Environmental Research Center, University Tsukuba, Ibaraki, Japan., 1983.

Ikeda, S., 1982, Incipient motion of sand particles on side slopes, *Journal of the Hydraulics Division*, *108*, 95–114.

Inamdar, S., E. Johnson, R. Rowland, D. Warner, R. Walter, and D. Merritts, 2018, Freeze-thaw processes and intense rainfall: the one-two punch for high sediment and nutrient loads from mid-Atlantic watersheds, *Biogeochemistry*, pp. 1–17.

Ishee, E. R., D. S. Ross, K. M. Garvey, R. R. Bourgault, and C. R. Ford, 2015, Phosphorus characterization and contribution from eroding streambank soils of Vermont's Lake Champlain basin, *Journal of Environmental Quality*, *44*, 1745–1753.

Jaeger, K. L., E. Wohl, and A. Simon, 2010, A comparison of average rates of alluvial erosion between the south-western and south-eastern United States, *Earth Surface Processes and Landforms*, *35*, 447–459.

Johnson, J. W., Laboratory investigations on bedload transportation and bed roughness, *Tech. rep.*, Technical Paper 50, United States Agricultural Service, Soil Conservation Service., 1943.

Johnson, L. T., J. L. Tank, and C. P. Arango, 2009, The effect of land use on dissolved organic carbon and nitrogen uptake in streams, *Freshwater Biology*, *54*, 2335–2350.

Jones, C. N., D. T. Scott, C. Guth, E. T. Hester, and W. C. Hession, 2015, Seasonal variation in floodplain biogeochemical processing in a restored headwater stream, *Environmental Science and Technology*, *49*, 13,190–13,198.

Jordan, T. E., D. L. Correll, and D. E. Weller, 1993, Nutrient interception by a riparian forest receiving inputs from adjacent cropland, *Journal of Environmental Quality*, *22*, 467–473.

Kasahara, T., and A. R. Hill, 2006a, Effects of riffle-step restoration on hyporheic zone chemistry in N-rich lowland streams, *Canadian Journal of Fisheries and Aquatic Sciences*, *63*, 120–133.

Kasahara, T., and A. R. Hill, 2006b, Hyporheic exchange flows induced by constructed riffles and steps in lowland streams in southern Ontario, Canada, *Hydrological Processes*, *20*, 4287–4305.

Kaushal, S. S., et al., 2008, Interaction between urbanization and climate variability amplifies watershed nitrate export in Maryland, *Environmental Science and Technology*, *42*, 5872–5878.

Kerr, J. G., M. Burford, J. Olley, and J. Udy, 2011, Phosphorus sorption in soils and sediments: implications for phosphate supply to a subtropical river in southeast Queensland, Australia, *Biogeochemistry*, *102*, 73–85.

Khorashadi Zadeh, F., J. Nossent, F. Sarrazin, F. Pianosi, A. van Griensven, T. Wagener, and W. Bauwens, 2017, Comparison of variance-based and moment-independent global sensitivity analysis approaches by application to the SWAT model, *Environmental Modelling and Software*, *91*, 210–222.

King, J. G., W. W. Emmett, P. J. Whiting, R. P. Kenworthy, and J. J. Barry, Sediment transport data and related information for selected coarse-bed streams and rivers in Idaho, *Tech. rep.*, U.S. Forest Service Report RMRS-GTR-131., 2004.

King, S. E., D. L. Osmond, J. Smith, M. R. Burchell, M. Dukes, R. O. Evans, S. Knies, and S. Kunickis, 2016, Effects of riparian buffer vegetation and width: A 12-year longitudinal study, *Journal of Environmental Quality*, *45*, 1243–1251.

Klavon, K., G. Fox, L. Guertault, E. Langendoen, H. Enlow, R. Miller, and A. Khanal, 2017, Evaluating a process-based model for use in streambank stabilization: insights on the Bank Stability and Toe Erosion Model (BSTEM), *Earth Surface Processes and Landforms*, *42*, 191–213.

Kleinman, P. J. A., A. N. Sharpley, K. Gartley, W. M. Jarrell, S. Kuo, R. G. Menon, R. Myers, K. R. Reddy, and E. O. Skogley, 2001, Interlaboratory comparison of soil phosphorus extracted by various soil test methods, *Communications in Soil Science and Plant Analysis*, *32*, 2325–2345.

Knight, D. W., 1981, Boundary shear in smooth and rough channels, *Journal of the Hydraulics Division*, *107*, 839–851.

Knight, D. W., J. D. Demetriou, and M. E. Hamed, 1984, Boundary shear in smooth rectangular channels, *Journal of Hydraulic Engineering*, *110*, 405–422.

Knighton, A. D., 1999, Downstream variation in stream power, *Geomorphology*, *29*, 293–306.

Knust, A. E., and J. J. Warwick, 2009, Using a fluctuating tracer to estimate hyporheic exchange in restored and unrestored reaches of the Truckee River, Nevada, USA, *Hydrological Processes*, *23*, 1119–1130.

Konsoer, K. M., B. L. Rhoads, E. J. Langendoen, J. L. Best, M. E. Ursic, J. D. Abad, and M. H. Garcia, 2016, Spatial variability in bank resistance to erosion on a large meandering, mixed bedrock-alluvial river, *Geomorphology*, *252*, 80–97.

Kottek, M., J. Grieser, C. Beck, B. Rudolf, and F. Rubel, 2006, World map of the Köppen-Geiger climate classification updated, *Meteorologische Zeitschrift*, *15*, 259–263.

Kronvang, B., R. Grant, and A. Laubel, 1997, Sediment and phosphorus export from a lowland catchment: quantification of sources, *Water, Air, and Soil Pollution*, *99*, 465–476.

Kronvang, B., I. K. Andersen, C. C. Hoffmann, M. L. Pedersen, N. B. Ovesen, and H. E. Andersen, 2007, Water exchange and deposition of sediment and phosphorus during inundation of natural and restored lowland floodplains, *Water, Air, and Soil Pollution*, *181*, 115–121.

Kronvang, B., J. Audet, A. Baattrup-Pedersen, H. S. Jensen, and S. E. Larsen, 2012, Phosphorus load to surface water from bank erosion in a Danish lowland river basin., *Journal of Environmental Quality*, *41*, 304–13.

Kronvang, B., H. E. Andersen, S. E. Larsen, and J. Audet, 2013, Importance of bank erosion for sediment input, storage and export at the catchment scale, *Journal of Soils and Sediments*, *13*, 230–241.

Kuhnle, R. A., Fractional transport rates of bedload on Goodwin Creek, in *Dynamics of Gravel Bed Rivers*, edited by P. Billi, R. D. Hey, C. R. Thorne, and P. Tacconi, chap. 7, pp. 141–155, John Wiley & Sons Ltd, Chichester, 1992.

Lague, D., 2014, The stream power river incision model: Evidence, theory and beyond, *Earth Surface Processes and Landforms*, *39*, 38–61.

Lai, Y. G., R. E. Thomas, Y. Ozeren, A. Simon, B. P. Greimann, and K. Wu, 2015, Modeling of multilayer cohesive bank erosion with a coupled bank stability and mobile-bed model, *Geomorphology*, *243*, 116–129.

Lamb, M. P., W. E. Dietrich, and J. G. Venditti, 2008, Is the critical Shields stress for incipient sediment motion dependent on channel-bed slope?, *Journal of Geophysical Research: Earth Surface*, *113*, F02,008.

Lammers, R. W., Uncertainty and sensitivity in a bank stability model: Implications for estimating phosphorus loading, Master's thesis, Colorado State University, 2015.

Lammers, R. W., B. P. Bledsoe, and E. J. Langendoen, 2017, Uncertainty and sensitivity in a bank stability model: implications for estimating phosphorus loading, *Earth Surface Processes and Landforms*, *42*, 612–623.

Langbein, W. B., and L. B. Leopold, 1964, Quasi-equilibrium states in channel morphology, *American Journal of Science*, *262*, 782–794.

Langbein, W. B., and L. B. Leopold, River meanders - Theory of minimum variance, *Tech. rep.*, United States Geological Survey Professional Paper 422H, 1966.

Langendoen, E. J., 2011, Application of the CONCEPTS channel evolution model in stream restoration strategies, *Geophysical Monograph Series*, pp. 487–502.

Langendoen, E. J., and C. V. Alonso, 2008, Modeling the evolution of incised streams: I. Model formulation and validation of flow and streambed evolution components, *Journal of Hydraulic Engineering*, *134*, 749–762.

Langendoen, E. J., and A. Simon, 2008, Modeling the evolution of incised streams: II. Streambank erosion, *Journal of Hydraulic Engineering*, *134*, 905–915.

Langendoen, E. J., A. Simon, L. Klimetz, N. Bankhead, and M. E. Ursic, Quantifying sediment loadings from streambank erosion in selected agricultural watersheds draining to Lake Champlain, *Tech. Rep. 72*, US Department of Agriculture - Agricultural Research Service National Sedimentation Laboratory Watershed Physical Processes Research Unit, Oxford, MS, 2012.

Larson, M. G., D. B. Booth, and S. A. Morley, 2001, Effectiveness of large woody debris in stream restoration projects in urban basins, *Ecological Engineering*, *18*, 211–226.

Lashkar-Ara, B., and M. Fathi-Moghadam, 2010, Wall and bed shear forces in open channels, *Research Journal of Physics*, *4*, 1–10.

Lave, R., 2009, The controversy over natural channel design: Substantive explanations and potential avenues for resolution, *Journal of the American Water Resources Association*, *45*, 1519–1532.

Law, A., F. Mclean, and N. Willby, 2016, Habitat engineering by beaver benefits aquatic biodiversity and ecosystem processes in agricultural streams, *Freshwater Biology*, *61*, 486–499.

Lazar, J. G., K. Addy, A. J. Gold, P. M. Groffman, R. A. McKinney, and D. Q. Kellogg, 2015, Beaver ponds: Resurgent nitrogen sinks for rural watersheds in the northeastern United States, *Journal of Environment Quality*, *44*, 1684–1693.

Lea, D. M., and C. J. Legleiter, 2016, Mapping spatial patterns of stream power and channel change along a gravel-bed river in northern Yellowstone, *Geomorphology*, *252*, 66–79.

Lee, K. H., T. M. Isenhart, and R. C. Schultz, 2003, Sediment and nutrient removal in an established multi-species riparian buffer, *Journal of Soil and Water Conservation*, *58*, 1–8.

Lefebvre, S., P. Marmonier, and G. Pinay, 2004, Stream regulation and nitrogen dynamics in sediment interstices: Comparison of natural and straightened sectors of a third-order stream, *River Research and Applications*, *20*, 499–512.

Lipman, P. W., and D. R. Mullineaux (Eds.), *The 1980 Eruptions of Mount St. Helens, Washington*, U.S. Geological Survey Professional Paper 1250, Washington, D.C., 1981.

Liu, X., P. Vidon, P. A. Jacinthe, K. Fisher, and M. Baker, 2014, Seasonal and geomorphic controls on N and P removal in riparian zones of the US Midwest, *Biogeochemistry*, *119*, 245–257.

Mahl, U. H., J. L. Tank, S. S. Roley, and R. T. Davis, 2015, Two-stage ditch floodplains enhance N-removal capacity and reduce turbidity and dissolved P in agricultural streams, *Journal of the American Water Resources Association*, *51*, 923–940.

Major, J. J., A. R. Mosbrucker, and K. R. Spicer, Sediment erosion and delivery from Toutle River basin after the 1980 eruption of Mount St. Helens: A 30-year perspective, in *Ecological Responses at Mount St Helens: Revisited 25 years after the 1980 Eruption*, edited by C. M. Crisafulli and V. H. Dale, chap. 2, pp. 19 – 44, Springer Science+Business Media LLC, New York, 2018.

Manson, S., J. Schroeder, D. Van Riper, and S. Ruggles, IPUMS National Historical Geographic Information System: Version 12.0 [Database], 2017.

Maret, T. J., M. Parker, and T. E. Fannin, 1987, The effect of beaver ponds on the nonpoint source water quality of a stream in southwestern Wyoming, *Water Research*, *21*, 263–268.

Markham, A. J., and C. R. Thorne, Geomorphology of gravel-bed river bends, in *Dynamics of Gravel Bed Rivers*, edited by P. Billi, R. D. Hey, C. R. Thorne, and P. Tacconi, pp. 433–456, John Wiley & Sons, Chichester, 1992.

Marsh, G. P., *Man and Nature*, 1st ed., Belknap Press of Harvard University Press, Cambridge, MA, 1864.

Martin, T. L., N. K. Kaushik, J. T. Trevors, and H. R. Whiteley, 1999, Review: Denitrification in temperate climate riparian zones, *Water, Air, and Soil Pollution*, *111*, 171–186.

Martin, Y., 2003, Evaluation of bed load transport formulae using field evidence from the Vedder River, British Columbia, *Geomorphology*, *53*, 75–95.

Martin, Y., and M. Church, 2000, Re-examination of Bagnold's empirical bedload formulae, *Earth Surface Processes and Landforms*, *25*, 1011–1024.

Martin, Y., and D. Ham, 2005, Testing bedload transport formulae using morphologic transport estimates and field data: Lower Fraser River, British Columbia, *Earth Surface Processes and Landforms*, *30*, 1265–1282.

Mayer, P. M., S. K. Reynolds, T. J. Canfield, and M. D. McCutchen, Riparian buffer width, vegetative cover, and nitrogen removal effectiveness: A review of current science and regulations, *Tech. rep.*, U.S. Environmental Protection Agency, Cincinnati, Ohio, 2005.

Mayer, P. M., S. K. Reynolds, M. D. McCutchen, and T. J. Canfield, 2007, Meta-analysis of nitrogen removal in riparian buffers, *Journal of Environmental Quality*, *36*, 1172–1180.

McClain, M. E., et al., 2003, Biogeochemical hot spots and hot moments at the interface of terrestrial and aquatic ecosystems, *Ecosystems*, *6*, 301–312.

McDaniel, M. D., M. B. David, and T. V. Royer, 2009, Relationships between benthic sediments and water column phosphorus in Illinois streams, *Journal of Environmental Quality*, *38*, 607–617.

McDowell, R. W., 2003, Sediment phosphorus chemistry and microbial biomass along a lowland New Zealand stream, *Aquatic Geochemistry*, *9*, 19–40.

McDowell, R. W., and A. N. Sharpley, 2001, A comparison of fluvial sediment phosphorus (P) chemistry in relation to location and potential to influence stream P concentrations, *Aquatic Geochemistry*, *7*, 255–265.

McDowell, R. W., and R. J. Wilcock, 2007, Sources of sediment and phosphorus in stream flow of a highly productive dairy farmed catchment., *Journal of Environmental Quality*, *36*, 540–8.

McDowell, R. W., A. N. Sharpley, and G. Folmar, 2003, Modification of phosphorus export from an eastern USA catchment by fluvial sediment and phosphorus inputs, *Agriculture, Ecosystems & Environment*, *99*, 187–199.

Meals, D. W., 2001, Water quality response to riparian restoration in an agricultural watershed in Vermont, USA, *Water Science and Technology*, *43*, 175–182.

Meals, D. W., S. A. Dressing, and T. E. Davenport, 2010, Lag time in water quality response to best management practices: a review, *Journal of Environmental Quality*, *39*, 85–96.

Merill, L., and D. J. Tonjes, 2014, A review of the hyporheic zone, stream restoration, and means to enhance denitrification, *Critical Reviews in Environmental Science and Technology*, *44*, 2337–2379.

Meyer-Peter, R., and R. Müller, Formulas for bedload transport, in *Proceedings of the 2nd Meeting of the International Association of Hydraulic Research*, pp. 39–64, Stockholm, 1948.

Midgley, T. L., G. A. Fox, and D. M. Heeren, 2012, Evaluation of the bank stability and toe erosion model (BSTEM) for predicting lateral retreat on composite streambanks, *Geomorphology*, *145-146*, 107–114.

Millar, R. G., 2005, Theoretical regime equations for mobile gravel-bed rivers with stable banks, *Geomorphology*, *64*, 207–220.

Miller, J. R., and R. C. Kochel, 2009, Assessment of channel dynamics, in-stream structures and post-project channel adjustments in North Carolina and its implications to effective stream restoration, *Environmental Earth Sciences*, *59*, 1681–1692.

Miller, R. B., G. A. Fox, C. J. Penn, S. Wilson, A. Parnell, R. A. Purvis, and K. Criswell, 2014, Estimating sediment and phosphorus loads from streambanks with and without riparian protection, *Agriculture, Ecosystems & Environment*, *189*, 70–81.

Mittelstet, A., D. Storm, and G. Fox, 2016, Testing of the modified streambank erosion and instream phosphorus routines for the SWAT model, *JAWRA Journal of the American Water Resources Association*, pp. 1–14.

Mittelstet, A. R., and D. E. Storm, 2016, Quantifying legacy phosphorus using a mass balance approach and uncertainty analysis, *Journal of the American Water Resources Association*, *52*, 1297–1310.

Mizuyama, T., Bedload transport in steep channels, Ph.d. dissertation, Kyoto University., 1977.

Montgomery, D. R., *Dirt: The Erosion of Civilizations*, University of California Press, Berkeley and Los Angeles, CA, 2007.

Mosbrucker, A. R., High-resolution digital elevation model of Mount St. Helens crater and upper North Fork Toutle River basin, Washington, based on an airborne lidar survey of September 2009, *Tech. rep.*, U.S. Geological Survey Data Series 904, 2014.

Mosbrucker, A. R., K. R. Spicer, J. J. Major, D. R. Saunders, T. S. Christianson, and C. G. Kingsbury, Digital database of channel cross-section surveys, Mount St. Helens, Washington, *Tech. rep.*, U.S. Geological Survey Data Series 951, 2015.

Mueller Price, J. S., D. W. Baker, and B. P. Bledsoe, 2016, Effects of passive and structural stream restoration approaches on transient storage and nitrate uptake, *River Research and Applications*, *32*, 1542–1554.

Mulholland, P. J., J. D. Newbold, J. W. Elwood, L. A. Ferren, and J. R. Webster, 1985, Phosphorus spiralling in a woodland stream: Seasonal variations, *Ecology*, *66*, 1012–1023.

Mulholland, P. J., et al., 2008, Stream denitrification across biomes and its response to anthropogenic nitrate loading., *Nature*, *452*, 202–5.

Mulholland, P. J., et al., 2009, Nitrate removal in stream ecosystems measured by 15N addition experiments: Denitrification, *Limnology and Oceanography*, *54*, 666–680.

Muller, I., M. Delisle, M. Ollitrault, and I. Bernez, 2016, Responses of riparian plant communities and water quality after 8 years of passive ecological restoration using a BACI design, *Hydrobiologia*, *781*, 67–79.

Murdoch, E. G., M. J. Whelan, and I. C. Grieve, 2005, Incorporating uncertainty into predictions of diffuse-source phosphorus transfers (using readily available data), *Water Science and Technology*, *51*, 339–346.

Nanson, G. C., and E. J. Hickin, 1983, Channel migration and incision on the Beatton River, *Journal of Hydraulic Engineering*, *109*, 327–337.

Nanson, G. C., and E. J. Hickin, 1986, A statistical analysis of bank erosion and channel migration in western Canada, *Geological Society of America Bulletin*, *97*, 497–504.

National Research Council, *Restoration of aquatic ecosystems: science, technology, and public policy*, National Research Council, Committee on Restoration of Aquatic Ecosystems: Science, Technology, and Public Policy, Water and Science Technology Board, Commission of Geosciences, Environment, and Resources. National Academy Press. Washington, DC, 1992.

Nellesen, S. L., J. L. Kovar, M. M. Haan, and J. R. Russell, 2011, Grazing management effects on stream bank erosion and phosphorus delivery to a pasture stream, *Canadian Journal of Soil Science*, *91*, 385–395.

Nelson, P. A., R. R. McDonald, J. M. Nelson, and W. E. Dietrich, 2015, Coevolution of bed surface patchiness and channel morphology: 2. Numerical experiments, *Journal of Geophysical Research: Earth Surface*, *120*, 1708–1723.

Newbold, J. D., S. Herbert, B. W. Sweeney, P. Kiry, and S. J. Alberts, 2010, Water quality functions of a 15 year old riparian forest buffer system, *Journal of the American Water Resources Association*, *46*, 299–310.

Newcomer, T. A., S. S. Kaushal, P. M. Mayer, A. R. Shields, E. A. Canuel, P. M. Groffman, and A. J. Gold, 2012, Influence of natural and novel organic carbon sources on denitrification in forest, degraded urban, and restored streams, *Ecological Monographs*, *82*, 449–466.

Newcomer Johnson, T. A., S. S. Kaushal, P. M. Mayer, R. M. Smith, and G. M. Sivirichi, 2016, Nutrient retention in restored streams and rivers: A global review and synthesis, *Water*, *8*, 116.

Newson, M. D., and C. L. Newson, 2000, Geomorphology, ecology and river channel habitat: Mesoscale approaches to basin-scale challenges, *Progress in Physical Geography*, *24*, 195–217.

Norman, L. M., M. Gishey, L. Gass, B. Yanites, E. Pfeifer, R. Simms, and R. Ahlbrandt, Processed 1938 aerial photography for selected areas of the lower Colorado River, southwestern United States, *Tech. rep.*, U.S. Geological Survey, 2006.

North Carolina Department of Environmental Quality, Draft 2016 Category 5 Assessments EPA Submittal - 303(d) List, 2016.

NRCS, Stream Restoration Design, *Tech. rep.*, U.S. Deaprtment of Agriculture, Natural Resources Conservation Service, National Engineering Handbook, Part 654 210-VI-NEH, 2007.

Orr, H. G., A. R. G. Large, M. D. Newson, and C. L. Walsh, 2008, A predictive typology for characterising hydromorphology, *Geomorphology*, *100*, 32–40.

Orzetti, L. L., R. C. Jones, and R. F. Murphy, 2010, Stream condition in piedmont streams with restored riparian buffers in the Chesapeake Bay watershed, *Journal of the American Water Resources Association*, *46*, 473–485.

Osman, A. M., and C. R. Thorne, 1988, Riverbank stability analysis I: Theory, *Journal of Hydraulic Engineering*, *114*, 134–150.

Owens, P. N., 2005, Conceptual models and budgets for sediment management at the river basin scale, *Journal of Soils and Sediments*, *5*, 201–212.

Paine, A. D. M., Canyon and terrace formation near Mount St. Helens, Washington, Masters thesis, Colorado State University, 1984.

Palmer, J. A., K. E. Schilling, T. M. Isenhart, R. C. Schultz, and M. D. Tomer, 2014a, Streambank erosion rates and loads within a single watershed: Bridging the gap between temporal and spatial scales, *Geomorphology*, *209*, 66–78.

Palmer, M. A., K. L. Hondula, and B. J. Koch, 2014b, Ecological restoration of streams and rivers: shifting strategies and shifting goals, *Annual Review of Ecology, Evolution, and Systematics*, *45*, 247–272.

Palmer, M. A., et al., 2005, Standards for ecologically successful river restoration, *Journal of Applied Ecology*, *42*, 208–217.

Palmer-Felgate, E. J., H. P. Jarvie, P. J. A. Withers, R. J. G. Mortimer, and M. D. Krom, 2009, Stream-bed phosphorus in paired catchments with different agricultural land use intensity, *Agriculture, Ecosystems & Environment*, *134*, 53–66.

Palumbo-Roe, B., J. Wragg, and V. J. Banks, 2012, Lead mobilisation in the hyporheic zone and river bank sediments of a contaminated stream: Contribution to diffuse pollution, *Journal of Soils and Sediments*, *12*, 1633–1640.

Pappenberger, F., and K. J. Beven, 2006, Ignorance is bliss: Or seven reasons not to use uncertainty analysis, *Water Resources Research*, *42*, 1–8.

Pardo, P., G. Rauret, and J. F. López-Sánchez, 2004, Shortened screening method for phosphorus fractionation in sediments: A complementary approach to the standards, measurements and testing harmonised protocol, *Analytica Chimica Acta*, *508*, 201–206.

Paridaens, J., and H. Vanmarcke, 2001, Radium contamination of the banks of the river Laak as a consequence of the phosphate industry in Belgium, *Journal of Environmental Radioactivity*, *54*, 53–60.

Parker, C., Quantifying catchment-scale coarse sediment dynamics in British rivers, Ph.d. dissertation, University of Nottingham, 2010.

Parker, C., A. Simon, and C. R. Thorne, 2008, The effects of variability in bank material properties on riverbank stability: Goodwin Creek, Mississippi, *Geomorphology*, *101*, 533–543.

Parker, C., N. J. Clifford, and C. R. Thorne, 2011, Understanding the influence of slope on the threshold of coarse grain motion: Revisiting critical stream power, *Geomorphology*, *126*, 51–65.

Parker, C., N. J. Clifford, and C. R. Thorne, 2012, Automatic delineation of functional river reach boundaries for river research and applications, *River Research and Applications*, *28*, 1708–1725.

Parker, C., C. R. Thorne, and N. J. Clifford, 2015, Development of ST:REAM: A reach-based stream power balance approach for predicting alluvial river channel adjustment, *Earth Surface Processes and Landforms*, *40*, 403–413.

Parker, G., 1990, Surface-based bedload transport relation for gravel rivers, *Journal of Hydraulic Research*, *28*, 417–436.

Parker, G., Transport of Gravel and Sediment Mixtures, in *Sedimentation Engineering*, edited by V. A. Vanona, chap. 3, American Society of Civil Engineers, 2008.

Parker, G., P. C. Klingeman, and D. G. McLean, 1982, Bedload and size distribution in paved gravel-bed streams, *Journal of the Hydraulics Division, ASCE*, *108*, 544–571.

Partheniades, E., 1965, Erosion and deposition of cohesive soils, *Journal of Hydraulics Division, ASCE*, *91*, 105–139.

Peacher, R., Impacts of land use on stream bank erosion in the Northeast Missouri Claypan Region, Master's thesis, Iowa State University, 2011.

Pennino, M. J., S. S. Kaushal, P. M. Mayer, R. M. Utz, and C. A. Cooper, 2016, Stream restoration and sewers impact sources and fluxes of water, carbon, and nutrients in urban watersheds, *Hydrology and Earth System Sciences*, *20*, 3419–3439.

Peterjohn, W., and D. L. Correll, 1984, Nutrient dynamics in an agricultural watershed: Observations on the role of a riparian forest, *Ecology*, *65*, 1466–1475.

Peterson, B. J., et al., 2001, Control of nitrogen export from watersheds by headwater streams., *Science*, *292*, 86–90.

Phillips, R. T. J., and J. R. Desloges, 2014, Glacially conditioned specific stream powers in low-relief river catchments of the southern Laurentian Great Lakes, *Geomorphology*, *206*, 271–287.

Pianosi, F., and T. Wagener, 2015, A simple and efficient method for global sensitivity analysis based on cumulative distribution functions, *Environmental Modelling & Software*, *67*, 1–11.

Piña-Ochoa, E., and M. Álvarez-Cobelas, 2006, Denitrification in aquatic environments: A cross-system analysis, *Biogeochemistry*, *81*, 111–130.

Pinay, G., L. Roques, and A. Fabre, 1993, Spatial and temporal patterns of denitrification in a riparian forest, *Journal of Applied Ecology*, *30*, 581–591.

Pinay, G., et al., 2007, Patterns of denitrification rates in European alluvial soils under various hydrological regimes, *Freshwater Biology*, *52*, 252–266.

Plischke, E., E. Borgonovo, and C. L. Smith, 2013, Global sensitivity measures from given data, *European Journal of Operational Research*, *226*, 536–550.

Pollock, M. M., T. J. Beechie, J. M. Wheaton, C. E. Jordan, N. Bouwes, N. Weber, and C. Volk, 2014, Using beaver dams to restore incised stream ecosystems, *BioScience*, *64*, 279–290.

Prancevic, J. P., and M. P. Lamb, 2015, Unraveling bed slope from relative roughness in initial sediment motion, *Journal of Geophysical Research: Earth Surface*, *120*, 474–489.

Prancevic, J. P., M. P. Lamb, and B. M. Fuller, 2014, Incipient sediment motion across the river to debris-flow transition, *Geology*, *42*, 191–194.

Purvis, R. A., and G. A. Fox, 2016, Streambank sediment loading rates at the watershed scale and the benefits of riparian protection, *Earth Surface Processes and Landforms*.

Purvis, R. A., G. A. Fox, C. J. Penn, D. E. Storm, and A. Parnell, 2016, Estimating stream-bank phosphorus loads at the watershed scale with uncertainty analysis approach, *Journal of Hydrologic Engineering*, *21*, 04016,028.

Quinn, J., N. Phillips, and S. Parkyn, 2007, Factors influencing retention of coarse particulate organic matter in streams, *Earth Surface Processes and Landforms*, *32*, 1186–1203.

R Core Team, *R: A language and environment for statistical computing*, R Foundation for Statistical Computing, Vienna, Austria., 2018.

Recking, A., 2009, Theoretical development on the effects of changing flow hydraulics on incipient bed load motion, *Water Resources Research*, *45*, W04,401.

Recking, A., 2013, Simple method for calculating reach-averaged bed-load transport, *Journal of Hydraulic Engineering*, *139*, 70–75.

Records, R. M., E. Wohl, and M. Arabi, 2016, Phosphorus in the river corridor, *Earth-Science Reviews*, *158*, 65–88.

Reinfelds, I., T. Cohen, P. Batten, and G. Brierley, 2003, Assessment of downstream trends in channel gradient, total and specific stream power: A GIS approach, *Geomorphology*, *60*, 403–416.

Reisinger, A. J., J. L. Tank, E. J. Rosi-Marshall, R. O. Hall, and M. A. Baker, 2015, The varying role of water column nutrient uptake along river continua in contrasting landscapes, *Biogeochemistry*, *125*, 115–131.

Rhoades, E. L., M. A. O'Neal, and J. E. Pizzuto, 2009, Quantifying bank erosion on the South River from 1937 to 2005, and its importance in assessing Hg contamination, *Applied Geography*, *29*, 125–134.

Rhoads, B. L., 1987, Stream power terminology, *Professional Geographer*, *39*, 189–195.

Rice, S. P., M. T. Greenwood, and C. B. Joyce, 2001, Tributaries, sediment sources, and the longitudinal organisation of macroinvertebrate fauna along river systems, *Canadian Journal of Fisheries and Aquatic Sciences*, *58*, 824–840.

Richardson, C. J., N. E. Flanagan, M. Ho, and J. W. Pahl, 2011, Integrated stream and wetland restoration: A watershed approach to improved water quality on the landscape, *Ecological Engineering*, *37*, 25–39.

Roberts, B. J., P. J. Mulholland, and J. N. Houser, 2007, Effects of upland disturbance and instream restoration on hydrodynamics and ammonium uptake in headwater streams, *Journal of the North American Benthological Society*, *26*, 38–53.

Robertson, W. D., and L. C. Merkley, 2009, In-stream bioreactor for agricultural nitrate treatment, *Journal of Environmental Quality*, *38*, 230–237.

Roley, S. S., J. L. Tank, M. L. Stephen, L. T. Johnson, J. J. Beaulieu, and J. D. Witter, 2012a, Floodplain restoration enhances denitrification and reach-scale nitrogen removal in an agricultural stream, *Ecological Applications*, *22*, 281–297.

Roley, S. S., J. L. Tank, and M. A. Williams, 2012b, Hydrologic connectivity increases denitrification in the hyporheic zone and restored floodplains of an agricultural stream, *Journal of Geophysical Research: Biogeosciences*, *117*, G00N04.

Roni, P., and T. Beechie, *Stream and Watershed Restoration: A Guide to Restoring Riverine Processes and Habitats*, John Wiley & Sons, LTD, 2013.

Rosburg, T. T., P. A. Nelson, and B. P. Bledsoe, 2017, Effects of urbanization on flow duration and stream flashiness: A case study of Puget Sound streams, Western Washington, USA, *Journal of the American Water Resources Association*, *53*, 493–507.

Rosgen, D. L., *Applied River Morphology*, Wildland Hydrology, Colorado, 1996.

Rosgen, D. L., River restoration using a geomorphic approach for natural channel design, in *Proceedings of the Eighth Federal Interagency Sedimentation Conference*, April 2-6, 2006, Reno, NV, 2006.

Ruark, M. D., J. D. Niemann, B. P. Greimann, and M. Arabi, 2011, Method for assessing impacts of parameter uncertainty in sediment transport modeling applications, *Journal of Hydraulic Engineering*, *137*, 623–636.

Rubin, Z., G. Kondolf, and B. Rios-Touma, 2017, Evaluating stream restoration projects: What do we learn from monitoring?, *Water*, *9*, 174.

Saad, M. B. E. A., Critical shear stress of armour coat, in *Sediment Transport Modeling, Proceedings of the International Symposium*, edited by S. S. Y. Wang, pp. 308–313, American Society of Civil Engineers, New York, NY, 1989.

Saltelli, A., P. Annoni, I. Azzini, F. Campolongo, M. Ratto, and S. Tarantola, 2010, Variance based sensitivity analysis of model output. Design and estimator for the total sensitivity index, *Computer Physics Communications*, *181*, 259–270.

Samadi, A., E. Amiri-Tokaldany, and S. E. Darby, 2009, Identifying the effects of parameter uncertainty on the reliability of riverbank stability modelling, *Geomorphology*, *106*, 219–230.

Saunders, D. L., and J. Kalff, 2001, Nitrogen retention in wetlands, lakes and rivers, *Hydrobiologia*, *443*, 205–212.

Schilling, K. E., and P. Jacobson, 2014, Effectiveness of natural riparian buffers to reduce subsurface nutrient losses to incised streams, *Catena*, *114*, 140–148.

Schilling, K. E., and J. Spooner, 2006, Effects of watershed-scale land use change on stream nitrate concentrations, *Journal of Environmental Quality*, *35*, 2132–2145.

Schilling, K. E., J. A. Palmer, E. A. Bettis, P. Jacobson, R. C. Schultz, and T. M. Isenhart, 2009, Vertical distribution of total carbon, nitrogen and phosphorus in riparian soils of Walnut Creek, southern Iowa, *Catena*, *77*, 266–273.

Schmitt, R. J. P., S. Bizzi, and A. Castelletti, 2016, Tracking multiple sediment cascades at the river network scale identifies controls and emerging patterns of sediment connectivity, *Water Resources Research*, *52*, 3941–3965.

Schmitt, R. J. P., S. Bizzi, A. F. Castelletti, and G. M. Kondolf, 2018, Stochastic modeling of sediment connectivity for reconstructing sand fluxes and origins in the unmonitored Se Kong, Se San, and Sre Pok tributaries of the Mekong River, *Journal of Geophysical Research: Earth Surface*, *123*, 2–25.

Schoonover, J. E., and K. W. J. Williard, 2003, Ground water nitrate reduction in giant cane and forest riparian buffer zones, *Journal of the American Water Resources Association*, *39*, 347–354.

Schumm, S. A., M. D. Harvey, and C. C. Watson, *Incised Channels: Morphology, Dynamics and Control*, Water Resources Publications, Littleton, CO, 1984.

Seckin, G., N. Seckin, and R. Yurtal, 2006, Boundary shear stress analysis in smooth rectangular channels, *Canadian Journal of Civil Engineering*, *33*, 336–342.

Segura, C., and D. B. Booth, 2010, Effects of geomorphic setting and urbanization on wood, pools, sediment storage, and bank erosion in Puget Sound streams, *Journal of the American Water Resources Association*, *46*, 972–986.

Seitzinger, S., J. A. Harrison, J. K. Böhlke, A. F. Bouwman, R. Lowrance, B. Peterson, C. Tobias, and G. Van Drecht, 2006, Denitrification across landscapes and waterscapes: A synthesis, *Ecological Applications*, *16*, 2064–2090.

Seitzinger, S. P., 1988, Denitrification in freshwater and coastal marine ecosystems: Ecological and geochemical significance, *Limnology and Oceanography*, *33*, 702–724.

Sekely, A. C., D. J. Mulla, and D. W. Bauer, 2002, Streambank slumping and its contribution to the phosphorus and suspended sediment loads of the Blue Earth River, Minnesota, *Journal of Soil and Water Conservation*, *57*, 243–250.

Selvakumar, A., T. P. O'Connor, and S. D. Struck, 2010, Role of stream restoration on improving benthic macroinvertebrates and in-stream water quality in an urban watershed: case study, *Journal of Environmental Engineering*, *136*, 127–139.

Sheibley, R. W., D. S. Ahearn, and R. A. Dahlgren, 2006, Nitrate loss from a restored floodplain in the Lower Cosumnes River, California, *Hydrobiologia*, *571*, 261–272.

Shields, A., 1936, Awendung der Aehnlichkeitsmechanik und der Turbulenzforschung auf die Geschiebebewegung, *Preussischen Versuchsanst fur Wasserbau*, *26*, 26.

Shreve, R. L., 1975, The probabilistic-topologic approach to drainage-basin geomorphology, *Geology*, *3*, 527–529.

Shvidchenko, A. B., and G. Pender, 2000, Initial motion of streambeds composed of coarse uniform sediments, *Proceedings of the Institution of Civil Engineers-Water Maritime and Energy*, *142*, 217–227.

Shvidchenko, A. B., G. Pender, and T. B. Hoey, 2001, Critical shear stress for incipient motion of sand/gravel streambeds, *Water Resources Research*, *37*, 2273–2283.

Siegel, S., and N. J. Castellan, *Non Parametric Statistics for the Behavioural Sciences*, MacGraw Hill Int., New York, 1988.

Simon, A., 1989, A model of channel response in disturbed alluvial channels, *Earth Surface Processes and Landforms*, *14*, 11–26.

Simon, A., 1992, Energy, time, and channel evolution in catastrophically disturbed fluvial systems, *Geomorphology*, *5*, 345–372.

Simon, A., Channel and drainage-basin response of the Toutle River system in the aftermath of the 1980 eruption of Mount St. Helens, Washington, *Tech. rep.*, USGS Open-File Report 96-633, 1999.

Simon, A., and A. J. Collison, 2002, Quantifying the mechanical and hydrologic effects of riparian vegetation on streambank stability, *Earth Surface Processes and Landforms*, *27*, 527–546.

Simon, A., and S. E. Darby, 1997, Process-form interactions in unstable sand-bed river channels: A numerical modeling approach, *Geomorphology*, *21*, 85–106.

Simon, A., and S. E. Darby, 2002, Effectiveness of grade-control structures in reducing erosion along incised river channels: the case of Hotophia Creek, Mississippi, *Geomorphology*, *42*, 229–254.

Simon, A., and C. R. Hupp, Geomorphic and vegetative recovery processes along modified stream channels of west Tennessee, *Tech. rep.*, U.S. Geological Survey Open File Report 91-502, Nashville, TN, 1992.

Simon, A., and D. Klimetz, Analysis of long-term sediment loadings from the Upper North Fork Toutle River System, Mount St Helens, Washington, *Tech. rep.*, USDA-ARS National Sedimentation Laboratory Technical Report 77, 2012.

Simon, A., and M. Rinaldi, 2006, Disturbance, stream incision, and channel evolution: The roles of excess transport capacity and boundary materials in controlling channel response, *Geomorphology*, *79*, 361–383.

Simon, A., A. Curini, S. E. Darby, and E. J. Langendoen, Streambank mechanics and the role of bank and near-bank processes, in *Incised River Channels*, edited by S. Darby and A. Simon, pp. 123–152, Wiley, Chichester, 1999.

Simon, A., A. Curini, S. E. Darby, and E. J. Langendoen, 2000, Bank and near-bank processes in an incised channel, *Geomorphology*, *35*, 193–217.

Simon, A., M. W. Doyle, M. Kondolf, F. D. Shields Jr, B. Rhoads, and M. McPhillips, 2007, Critical evaluation of how the Rosgen classification and associated 'Natural Channel Design' methods fail to integrate and quantify fluvial processes and channel responses, *Journal of the American Water Resources Association*, *43*, 1117–1131.

Simon, A., R. E. Thomas, and L. Klimetz, 2010, Comparison and experiences with field techniques to measure critical shear stress and erodibility of cohesive deposits, *2nd Joint Federal Interagency Conference, Las Vegas*, *826*.

Simon, A., N. Pollen-Bankhead, and R. E. Thomas, Development and application of a deterministic bank stability and toe erosion model for stream restoration, in *Stream Restoration in Dynamic Fluvial Systems: Scientific Approaches, Analyses, and Tools*, edited by A. Simon, S. Bennett, and J. Castro, pp. 453–474, American Geophysical Union, Washington, D.C., 2011.

Sin, G., K. V. Gernaey, M. B. Neumann, M. C. van Loosdrecht, and W. Gujer, 2011, Global sensitivity analysis in wastewater treatment plant model applications: Prioritizing sources of uncertainty, *Water Research*, *45*, 639–651.

Sivirichi, G. M., S. S. Kaushal, P. M. Mayer, C. Welty, K. T. Belt, T. A. Newcomer, K. D. Newcomb, and M. M. Grese, 2011, Longitudinal variability in streamwater chemistry and carbon and nitrogen fluxes in restored and degraded urban stream networks, *Journal of Environmental Monitoring*, *13*, 288–303.

Smidt, S. J., J. A. Cullin, A. S. Ward, J. Robinson, M. A. Zimmer, L. K. Lautz, and T. A. Endreny, 2014, A comparison of hyporheic transport at a cross-vane structure and natural riffle, *Groundwater*, *53*, 859–871.

Smith, D. B., W. F. Cannon, L. G. Woodruff, F. Solano, J. E. Kilburn, and D. L. Fey, Geochemical and mineralogical data for soils of the conterminous United States, *Tech. rep.*, U.S. Geological Survey Data Series 801, 2013.

Smith, D. G., 1976, Effect of vegetation on lateral migration of anastomosed channels of a glacier meltwater river, *Geological Society of America Bulletin*, *87*, 857–860.

Smith, E. P., and K. A. Rose, 1995, Model goodness-of-fit analysis using regression and related techniques, *Ecological Modelling*, *77*, 49–64.

Smith, R. M., D. J. Evans, and H. S. Wheater, 2005, Evaluation of two hybrid metric-conceptual models for simulating phosphorus transfer from agricultural land in the river enborne, a lowland UK catchment, *Journal of Hydrology*, *304*, 366–380.

Smith, V., 2003, Eutrophication of freshwater and coastal marine ecosystems: A global problem, *Environmental Science and Pollution Research*, *10*, 126–139.

Smith, V. H., G. Tilman, and J. C. Nekola, 1999, Eutrophication: impacts of excess nutrient inputs on freshwater, marine, and terrestrial ecosystems., *Environmental Pollution*, *100*, 179–96.

Soar, P., N. Wallerstein, and C. Thorne, 2017, Quantifying river channel stability at the basin scale, *Water*, *9*, 133.

Sobol', I. M., 1976, Uniformly distributed sequences with an additional uniform property, *USSR Computational Mathematics and Mathematical Physics*, *16*, 236–242.

Society for Ecological Restoration, *The SER International Primer on Ecological Restoration*, Society for Ecological Restoration International, Tucson, 2004.

Soulsby, R. L., *Dynamics of Marine Sands, a Manual for Practical Applications*, Thomas Telford, London, UK, 1997.

Spruill, T. B., 2000, Statistical evaluation of effects of riparian buffers on nitrate and ground water quality, *Journal of Environment Quality*, *29*, 1523–1538.

Stanley, E. H., S. M. Powers, N. R. Lottig, I. Buffam, and J. T. Crawford, 2012, Contemporary changes in dissolved organic carbon (DOC) in human-dominated rivers: Is there a role for DOC management?, *Freshwater Biology*, *57*, 26–42.

Stover, S. C., and D. R. Montgomery, 2001, Channel change and flooding, Skokomish River, Washington, *Journal of Hydrology*, *243*, 272–286.

Strobl, C., A.-L. Boulesteix, A. Zeileis, and T. Hothorn, 2007, Bias in random forest variable importance measures: Illustrations, sources and a solution, *BMC Bioinformatics*, *8*.

Strobl, C., A.-L. Boulesteix, T. Kneib, T. Augustin, and A. Zeileis, 2008, Conditional variable importance for random forests, *BMC Bioinformatics*, *9*.

Stryker, J., B. Wemple, and A. Bomblies, 2017, Modeling sediment mobilization using a distributed hydrological model coupled with a bank stability model, *Water Resources Research*, *53*, 2051–2073.

Sutton, A. J., T. R. Fisher, and A. B. Gustafson, 2010, Effects of restored stream buffers on water quality in non-tidal streams in the Choptank River basin, *Water, Air, and Soil Pollution*, *208*, 101–118.

Taylor, B. D., Temperature effects in alluvial streams, *Tech. rep.*, Report KH-R-27, W.M. Keck Laboratory of Hydraulic and Water Resources, California, Institution Technic., 1971.

Theil, H., *Economic Forecasts and Policy*, North Holland, Amsterdam, Netherlands, 1958.

Theriot, J. M., J. L. Conkle, S. Reza Pezeshki, R. D. DeLaune, and J. R. White, 2013, Will hydrologic restoration of Mississippi River riparian wetlands improve their critical biogeochemical functions?, *Ecological Engineering*, *60*, 192–198.

Therneau, T., B. Atkinson, and B. Ripley, *rpart: recursive partitioning and regression trees*, R package version 4.1-10, http://cran.r-project.org/package=rpart, 2015.

Thoma, D. P., S. C. Gupta, M. E. Bauer, and C. E. Kirchoff, 2005, Airborne laser scanning for riverbank erosion assessment, *Remote Sensing of Environment*, *95*, 493–501.

Thomas, R. E., The dynamics of knickpoint mgiration in the Yalobusha River basin, MS, USA, Bsc(honors), University of Nottingham, 2000.

Thompson, C. A., and A. M. S. McFarland, 2007, Effects of surface and groundwater interactions on phosphorus transport within streambank sediments., *Journal of Environmental Quality*, *39*, 548–557.

Thorne, C. R., Processes and mechanisms of bank erosion, in *Gravel Bed Rivers*, edited by R. Hey, J. Bathurst, and C. Thorne, pp. 227–271, Wiley, Chichester, 1982.

Thornton, C. I., K. S. Sin, P. Sclafani, and S. R. Abt, Boundary shear stress along rigid trapezoidal bends, *Tech. rep.*, Colorado State University, Fort Collins, CO, 2012.

Tillinghast, E. D., W. F. Hunt, and G. D. Jennings, 2011, Stormwater control measure (SCM) design standards to limit stream erosion for Piedmont North Carolina, *Journal of Hydrology*, *411*, 185–196.

Tufekcioglu, M., Stream bank soil and phosphorus losses within grazed pasture stream reaches in the Rathbun Watershed in southern Iowa, Phd dissertation, Iowa State University, 2010.

Tuttle, A. K., S. K. McMillan, A. Gardner, and G. D. Jennings, 2014, Channel complexity and nitrate concentrations drive denitrification rates in urban restored and unrestored streams, *Ecological Engineering*, *73*, 770–777.

Ullah, S., and S. P. Faulkner, 2006, Use of cotton gin trash to enhance denitrification in restored forested wetlands, *Forest Ecology and Management*, *237*, 557–563.

U.S. Army Corps of Engineers, Sediment gradation analysis results, 1980-1988: Mount St. Helens, Washington: Cowlitz River, Toutle River, North Fork Toutle River, *Tech. rep.*, U.S. Army Corps of Engineers, Portland, OR, 1988.

U.S. Bureau of Reclamation, Report of river control work and investigations Lower Colorado River Basin: Calendar years 1946 and 1947, *Tech. rep.*, Boulder City, Nevada, 1948.

U.S. Bureau of Reclamation, Report of river control work and investigations Lower Colorado River Basin: Calendar years 1948 and 1949, *Tech. rep.*, Boulder City, Nevada, 1950.

U.S. EPA, Methods for chemical analysis of water and wastes, *Tech. rep.*, U.S. EPA Rep. 600/4-79-020. U.S. EPA Office Res. Development, Cincinnati, OH, 1983.

U.S. EPA, Method 3051a: Microwave-assisted acid digestion of sediments, sludges, soils and oils, 2007.

Valett, H. M., M. A. Baker, J. A. Morrice, C. S. Crawford, M. C. Molles, C. N. Dahm, D. L. Moyer, J. R. Thibault, and L. M. Ellis, 2005, Biogeochemical and metabolic responses to the flood pulse in a semiarid floodplain, *Ecology*, *86*, 220–234.

Van de Wiel, M. J., and S. E. Darby, 2007, A new model to analyse the impact of woody riparian vegetation on the geotechnical stability of riverbanks, *Earth Surface Processes and Landforms*, *32*, 2185–2198.

Vanoni, V. A., *Sedimentation Engineering*, ASCE Manuals and Reports on Engineering Practice No. 54, 1975.

Vaux, W. G., 1968, Intragravel flow and interchange of water in a stream-bed, *Fisheries Bulletin*, *66*, 479–489.

Vázquez-Tarrío, D., and R. Menéndez-Duarte, 2015, Assessment of bedload equations using data obtained with tracers in two coarse-bed mountain streams (Narcea River basin, NW Spain), *Geomorphology*, *238*, 78–93.

Veihe, A., N. H. Jensen, I. G. Schiøtz, and S. L. Nielsen, 2011, Magnitude and processes of bank erosion at a small stream in Denmark, *Hydrological Processes*, *25*, 1597–1613.

Vidon, P., et al., 2010, Hot spots and hot moments in riparian zones: Potential for improved water quality management, *Journal of the American Water Resources Association*, *46*, 278–298.

Vietz, G. J., I. D. Rutherfurd, T. D. Fletcher, and C. J. Walsh, 2016, Thinking outside the channel: Challenges and opportunities for protection and restoration of stream morphology in urbanizing catchments, *Landscape and Urban Planning*, *145*, 34–44.

Vocal Ferencevic, M., and P. Ashmore, 2012, Creating and evaluating digital elevation model-based stream-power map as a stream assessment tool, *River Research and Applications*, *28*, 1394–1416.

Voight, B., H. Glicken, R. J. Janda, and P. M. Douglass, Catastrophic rockslide avalanche of May 18, in *The 1980 Eruptions of Mount St. Helens, Washington*, edited by P. W. Lipman and D. R. Mullineaux, pp. 347 – 377, U.S. Geological Survey Professional Paper 1250, Washington, D.C., 1981.

Voli, M. T., K. W. Wegmann, D. R. Bohnenstiehl, E. Leithold, C. L. Osburn, and V. Polyakov, 2013, Fingerprinting the sources of suspended sediment delivery to a large municipal drinking water reservoir: Falls Lake, Neuse River, North Carolina, USA, *Journal of Soils and Sediments*, *13*, 1692–1707.

Wallace, J. B., J. R. Webster, and J. L. Meyer, 1995, Influence of log additions on physical and biotic characteristics of a mountain stream, *Canadian Journal of Fisheries and Aquatic Sciences*, *52*, 2120–2137.

Walling, D. E., P. N. Owens, and G. J. Leeks, 1998, The role of channel and floodplain storage in the suspended sediment budget of the River Ouse, Yorkshire, UK, *Geomorphology*, *22*, 225–242.

Walsh, C. J., T. D. Fletcher, and A. R. Ladson, 2005, Stream restoration in urban catchments through redesigning stormwater systems: looking to the catchment to save the stream, *Journal of the North American Benthological Society*, *24*, 690–705.

Walsh, C. J., et al., 2016, Principles for urban stormwater management to protect stream ecosystems, *Journal of Freshwater Science*, *35*, 398–411.

Walter, R., D. Merritts, and M. Rahnis, Estimating volume, nutrient content, and rates of stream bank erosion of legacy sediment in the Piedmont and Valley and Ridge physiographic provinces, *Tech. rep.*, Report to the Pennsylvania Department of Environmental Protection, 2007.

Walters, C., *Adaptive Management of Renewable Resources*, Macmillan Publishing Company, New York, 1986.

Ward, A. S., M. N. Gooseff, and P. A. Johnson, 2011, How can subsurface modifications to hydraulic conductivity be designed as stream restoration structures? Analysis of Vaux's conceptual models to enhance hyporheic exchange, *Water Resources Research*, *47*, W08,512.

Watson, T. K., D. Q. Kellogg, K. Addy, A. J. Gold, M. H. Stolt, S. W. Donohue, and P. M. Groffman, 2010, Groundwater denitrification capacity of riparian zones in suburban and agricultural watersheds, *Journal of the American Water Resources Association*, *46*, 237–245.

Weigelhofer, G., N. Welti, and T. Hein, 2013, Limitations of stream restoration for nitrogen retention in agricultural headwater streams, *Ecological Engineering*, *60*, 224–234.

Wilcock, P. R., and J. C. Crowe, 2003, Surface-based transport model for mixed-size sediment, *Journal of Hydraulic Engineering*, *129*, 120–128.

Willett, J., and J. Singer, 1988, Another cautionary note about R2: Its use in weighted least-squares regression analysis, *The American Statistician*, *42*, 236–238.

Williams, G. P., Flume width and water depth effects in sediment transport experiments, *Tech. rep.*, U.S. Geological Survey Professional Paper 562-H, U.S. Geological Survey Professional Paper 562-H, 1970.

Williams, G. P., and D. L. Rosgen, Measured total sediment loads (suspended loads and bedloads) for 93 United States streams, *Tech. rep.*, U.S. Geological Survey, 1989.

Williams, G. P., and M. G. Wolman, Downstream effects of dams on alluvial rivers, *Tech. rep.*, USGS Professional Paper 1286, 1984.

Wilson, B. N., 1993a, Evaluation of a fundamentally based detachment model, *Transactions of the American Society of Agricultural Engineers*, *36*, 1115–1122.

Wilson, B. N., 1993b, Development of a fundamentally based detachment model, *Transactions of the American Society of Agricultural Engineers*, *36*, 1115–1122.

Wohl, E., P. L. Angermeier, B. P. Bledsoe, G. M. Kondolf, L. MacDonnell, D. M. Merritt, M. A. Palmer, N. L. Poff, and D. Tarboton, 2005, River restoration, *Water Resources Research*, *41*, W10,301.

Wohl, E., B. P. Bledsoe, R. B. Jacobson, N. L. Poff, S. L. Rathburn, D. M. Walters, and A. C. Wilcox, 2015a, The natural sediment regime in rivers: Broadening the foundation for ecosystem management, *BioScience*, *65*, 358–371.

Wohl, E., S. N. Lane, and A. C. Wilcox, 2015b, The science and practice of river restoration, *Water Resources Research*, *51*, 5974–5997.

Wynn, T. M., M. B. Henderson, and D. H. Vaughan, 2008, Changes in streambank erodibility and critical shear stress due to subaerial processes along a headwater stream, southwestern Virginia, USA, *Geomorphology*, *97*, 260–273.

Yang, C. T., 1979, Unit stream power equations for total load, *Journal of Hydrology*, *40*, 123–138.

Yang, C. T., C. C. S. Song, and M. J. Woldenberg, 1981, Hydraulic geometry and minimum rate of energy dissipation, *Water Resources Research*, *17*, 1014–1018.

Yang, S., J. Hu, and X. Wang, 2006, Incipient motion of coarse particles in high gradient rivers, *International Journal of Sediment Research*, *21*, 220–229.

Young, E. O., D. S. Ross, C. Alves, and T. Villars, 2012, Soil and landscape influences on native riparian phosphorus availability in three Lake Champlain Basin stream corridors, *Journal of Soil and Water Conservation*, *67*, 1–7.

Young, E. O., D. S. Ross, B. J. Cade-Menun, and C. W. Liu, 2013, Phosphorus speciation in riparian soils: A phosphorus-31 nuclear magnetic resonance spectroscopy and enzyme hydrolysis study, *Soil Science Society of America Journal*, *77*, 1636–1647.

Zaimes, G. N., R. C. Schultz, and T. M. Isenhart, 2008a, Total phosphorus concentrations and compaction in riparian areas under different riparian land-uses of Iowa, *Agriculture, Ecosystems & Environment*, *127*, 22–30.

Zaimes, G. N., R. C. Schultz, and T. M. Isenhart, 2008b, Streambank soil and phosphorus losses under different riparian land-uses in Iowa, *Journal of the American Water Resources Association*, *44*, 935–947.

Zarnetske, J. P., R. Haggerty, S. M. Wondzell, and M. A. Baker, 2011, Labile dissolved organic carbon supply limits hyporheic denitrification, *Journal of Geophysical Research*, *116*, G04,036.

Zheng, S., B. Wu, C. R. Thorne, and A. Simon, 2014, Morphological evolution of the North Fork Toutle River following the eruption of Mount St. Helens, Washington, *Geomorphology*, *208*, 102–116.

Zheng, S., C. R. Thorne, B. S. Wu, and S. S. Han, 2017, Application of the Stream Evolution Model to a volcanically disturbed river: The North Fork Toutle River, Washington State, USA, *River Research and Applications*, *33*, 937–948.

Appendix A

Eaton and Church [2011] Critical Stream Power Model

Eaton and Church [2011] developed a relatively simple equation for dimensionless critical specific stream power using Shields parameter and a flow resistance parameter:

$$\omega_{c*} = {\theta_c}^{3/2}\mathfrak{R} \tag{A.1}$$

where $\mathfrak{R}$ is the flow resistance value given as the ratio of flow velocity (V) to shear velocity ($u_* = \sqrt{(\tau/\rho)}$). *Eaton and Church* [2011] chose to approximate this value using a power law developed by *Ferguson* [2007]:

$$\mathfrak{R} = \frac{V}{u_*} = a\left[\frac{h}{D_s}\right]^b \tag{A.2}$$

where a and b are empirical parameters that vary with relative submergence (defined as hD_{84}). For "deep" flows, a = 7–8 and $b = 1/6$ but for "shallow" flows a = 1–4 and $b = 1$ [*Ferguson*, 2007]. For the incipient motion analysis, I used measured values of V and u_* to calculate flow resistance which avoided the need to approximate this value using Ferguson's power relationship.

Camenen [2012] Critical Stream Power Model

Camenen [2012] defined a theoretical model for computing critical specific stream power:

$$\omega_c = \frac{2.3\rho}{\kappa}\left[\left(\frac{R_h}{D_s}\right)_{cr}\frac{\theta_{c,S}}{\theta_{c,0}}SgD_s\right]^{3/2}\log\left[\frac{15}{e}\left(\frac{R_h}{D_s}\right)_{cr}\right] \tag{A.3}$$

where $\kappa = 0.4$ is the Von Karman constant and R_h is hydraulic radius. The critical relative flow depth (that is the flow depth at incipient motion) varies non-linearly with channel slope:

$$\left(\frac{R_h}{D_s}\right)_{cr} = \frac{(s-1)\theta_{c,0}}{S}\left(0.5 + 6S^{0.75}\right) \tag{A.4}$$

where the subscript 0 in the critical Shields parameter indicates no slope effects. This value is a function of dimensionless grain size [*Soulsby*, 1997]:

$$\theta_{c,0} = \frac{0.30}{1 + 1.2D_*} + 0.055\left[1 - \exp\left(-0.02D_*\right)\right] \tag{A.5}$$

$$D_* = \left[\frac{(s-1)g}{\nu^2}\right]^{1/3} D_s \tag{A.6}$$

Finally, the effect of slope on decreasing the critical Shields parameter as it approaches the angle of repose can be accounted for [*Ikeda*, 1982]:

$$\frac{\theta_{c,S}}{\theta_{c,0}} = \frac{\sin(\varphi_s - \arctan S)}{\sin(\varphi_s)} = \cos(\arctan S)\left[1 - \frac{S}{\tan(\varphi_s)}\right] \tag{A.7}$$

In this analysis, the angle of repose (φ_s) was assumed to equal 52 degrees [*Ferguson*, 2012].

Ferguson [2012] Critical Stream Power Model

The *Ferguson* [2012] critical stream power model is based on the concept of hiding and protrusion in a streambed with non-uniform grain size. Given this configuration, only a portion of the total shear stress is available to entrain small grains due to the additional grain roughness. The ratio of critical shear stress to the critical stress at a "base resistance conditions" (i.e. no hiding and protrusion) is thus related to the ratio of critical flow depths:

$$\frac{\theta_c}{\theta_c'} = \frac{h_c}{h_c'} \tag{A.8}$$

where $\theta_c{}'$ and $h_c{}'$ are the critical Shields parameter and flow depth at the "base resistance condition". This relationship can also be expressed as a function of grain sorting and relative roughness:

$$\frac{\theta_c}{\theta_c'} = \frac{h_c}{h_c'} = \left(\frac{a_0}{a_1}\right)^{3/2}\left(\frac{D_{84}}{D_{50}}\right)^{1/4}\left[1 + \left(\frac{a_1}{a_2}\right)^2\left(\frac{D_{84}}{h}\right)^{5/3}\right]^{3/4} \tag{A.9}$$

where a_0, a_1 and a_2 are constants (assumed to be 8, 6.5 and 2.5 respectively). Slopes can then be found using the definition of the Shields parameter:

$$S = \frac{(s-1)\theta_c D_{50}}{h_c} = \frac{(s-1)(\theta_c/\theta_c')\theta_c'}{(h_c/D_{84})(D_{84}/D_{50})} \tag{A.10}$$

The effect of slope on the critical Shields parameter can be corrected, using the same approach as the Camenen model (Equation (A.9)). In this case, the critical Shields parameter for a given slope must be solved iteratively using trial values of h_c/D_{84}. Once this critical value has been computed, the critical dimensionless stream power can be calculated using a similar approach as *Eaton and Church* [2011]:

$$\omega_{c*} = {\theta_c}^{3/2}\frac{V}{u_*} \tag{A.11}$$

where Vu_* is computed using the variable-power flow resistance equation:

$$\frac{V}{u_*} = \frac{a_1(h/D_{84})}{\left[(h/D_{84})^{5/3} + (a_1/a_2)^2\right]^{1/2}} \tag{A.12}$$

where V is flow velocity [m s^{-1}], u_* is shear velocity [m s^{-1}], and a_1 and a_2 are constants (defined above).

Ackers and White [1973] Total Load Equation

The Ackers and White total load equation takes the following form:

$$C_w = c\frac{\rho_s}{\rho}\frac{D_{50}}{R_h}\left(\frac{V}{u_*}\right)^n\left[\frac{F_{gr}}{A} - 1\right]^m \tag{A.13}$$

where C_w is the sediment concentration by weight, and F_{gr} is the mobility number defined as:

$$F_{gr} = \frac{{u_*}^n {u_*}'^{1-n}}{\sqrt{gD_{50}\left(\frac{\rho_s-\rho}{\rho}\right)}} \tag{A.14}$$

And $u_*{}'$ is:

$$u_*{}' = \frac{V}{\sqrt{32}\log\left(\frac{10R_h}{D_{50}}\right)} \tag{A.15}$$

The values of n, A, m, and c are functions of D_{gr} which is defined as:

$$D_{gr} = \left[\sqrt{\frac{\rho_s - \rho}{\rho}} R_g\right]^{2/3} \tag{A.16}$$

where R_g is the Reynolds grain number:

$$R_g = \frac{\sqrt{gD_{50}{}^3}}{\nu} \tag{A.17}$$

When D_{gr} ¿ 60, the coefficients are:

$$\begin{aligned} n &= 0.0 \\ A &= 0.17 \\ c &= 0.025 \end{aligned} \tag{A.18}$$

If $60 \geq D_{gr} \geq 1$ then:

$$\begin{aligned} n &= 1 - 0.56\log D_{gr} \\ A &= \frac{0.23}{\sqrt{D_{gr}}} + 0.14 \\ m &= \frac{9.66}{D_{gr}} + 1.34 \\ \log c &= 2.86\log D_{gr} - (\log D_{gr})^2 - 3.53 \end{aligned} \tag{A.19}$$

Engelund and Hansen [1967] Total Load Equation

The Engelund and Hansen (1967) total load equation is:

$$C_w = 0.05\left(\frac{\rho_s}{\rho_s - \rho}\right)\left(\frac{VS}{\sqrt{\left(\frac{\rho_s-\rho}{\rho}\right)gD_{50}}}\right)\theta^{1/2} \tag{A.20}$$

where C_w is sediment concentration by weight and θ is the Shields parameter.

Brownlie [1982] Total Load Equation

The *Brownlie* [1982] total load equation is:

$$C_{ppm} = 7115C_f\left(\frac{V - V_c}{\sqrt{(s-1)gD_{50}}}\right)^{1.978} S^{0.6601}\left(\frac{R_h}{D_{50}}\right)^{-0.3301} \tag{A.21}$$

where C_{ppm} is the sediment concentration in ppm, C_f is a correction factor (1.0 for flume data and 1.268 for field data) and:

$$\begin{aligned}\frac{V_c}{\sqrt{(s-1)gD_{50}}} &= 4.596{\theta_c}^{0.529}S^{-0.1405}{\sigma_g}^{-0.1606}\\ \sigma_g &= \sqrt{\frac{D_{84}}{D_{16}}}\end{aligned} \tag{A.22}$$

Brownlie fit a continuous function to the Shields curve to provide consistent estimates of θ_c:

$$\begin{aligned}\theta_c &= 0.22Y + 0.06 \times 10^{-7.7Y}\\ Y &= \left(\frac{\sqrt{(s-1)g{D_{50}}^3}}{\nu}\right)^{-0.6}\end{aligned} \tag{A.23}$$

Since hydraulic radius and grain size were given in the data used, I did not use Brownlie's depth predictor equations for this analysis.

Appendix B

B.1 Model Details

B.1.1 Hiding Function

Hiding functions account for the different behavior of sediment mixtures versus uniform sediments. Generally, larger sediment grains are harder to move than smaller grains. This relationship, however, is complicated in sediment mixtures. Larger grains become easier to move as they protrude above smaller grains, and smaller grains become more difficult to entrain because they are hidden by larger particles. Hiding functions account for this complex behavior by adjusting the threshold of motion criteria (e.g. critical shear stress) based on the ratio of grain size to the median size of the mixture. These relationships generally follow the form [*Parker*, 2008]:

$$\frac{\tau_{ri}*}{\tau_{r50}*} = \left(\frac{D_i}{D_{50}}\right)^{-b} \tag{B.1}$$

where $\tau_{ri}*$ is the reference Shields stress for the i^{th} grain size, $\tau_{r50}*$ is the reference Shields stress for the median grain size, D_i is the grain size, D_{50} is the median grain size, and b is an exponent that varies between 0 and 1.

If b is zero, this implies size independence mobility, or no hiding effects. If b is one, all size fractions are mobilized at the same critical shear stress (equal threshold). A number of studies have quantified b for flume and field data, generally finding a value > 0.7 [*Shvidchenko et al.*, 2001; *Parker*, 2008]. However, there has been no analysis of a hiding function using critical specific stream power in place of critical shear stress. I used available sediment transport data to create a hiding function of the form:

$$\frac{\omega_{ri}*}{\omega_{r50}*} = \left(\frac{D_i}{D_{50}}\right)^{-b} \tag{B.2}$$

where $\omega_{ri}*$ is the reference dimensionless specific stream power of the i^{th} grain size and $\omega_{r50}*$ is the reference dimensionless specific stream power of the median grain size. Stream power is made dimensionless by:

$$\omega_* = \frac{\omega}{\rho(g(s-1)D_s)^{3/2}} \tag{B.3}$$

where ρ is water density [1000 kg m^{-3}], g is gravity [9.81 m s^{-2}], and s is sediment specific gravity (usually 2.65). In Equation B.2, the exponent b varies from 0 (size independence) to 1.5 (equal threshold). The upper limit is increased from 1 to 1.5 because of the 3/2 exponent on grain size in Equation B.3.

I obtained bedload transport data by size fraction from two databases [*Williams and Rosgen*, 1989; *Hinton et al.*, 2016]. I used the surface based reference method to find the reference dimensionless specific stream power for each size class. Briefly, the Einstein bed load parameter (q^*_{bi}) was plotted versus dimensionless specific stream power for each size class, where q^*_{bi} is:

$$q^*_{bi} = \frac{q_{bi}}{\rho_s\sqrt{(s-1)gD_i^3}} \tag{B.4}$$

where q_{bi} is the bedload transport rate of the i^{th} grain size [kg m^{-1} s^{-1}] and ρ_s is the density of sediment [2650 kg m^{-3}]. The value of dimensionless specific stream power where best fit lines to these data intersected $q^*_{bi} = 0.0001$ was taken to be the reference value for incipient motion. An additional data set was obtained from *Kuhnle* [1992], for Goodwin Creek, MS. Values of W^*_i and τ^*_i were obtained from Figure 7.6 of Kuhnle's work (p. 149). Dimensionless transport rate was calculated as:

$$q^*_{bi} = W^*_i \tau_i^{*3/2} \tag{B.5}$$

where W^*_i is a dimensionless sediment transport parameter [*Parker et al.*, 1982].

Using the full Goodwin Creek transport dataset [*Almedeij*, 2002], I calculated the average ω_* value for each given value of τ^*_i. For each site, I then used linear regression of the log-10 transformed data to fit values of $\omega_{r50}*$ and b from Equation B.2. I adjusted the value of $\omega_{r50}*$ for transformation bias after *Ferguson* [1986]. Sites with poor fits or insufficient data were

excluded, based on expert judgment. Additionally, I only included sites which had D_i/D_{50} ratios spanning above and below one. This yielded a total of five sites (Table B.1).

Figure B.1 shows fitted hiding functions for the five field sites, along with a combined hiding function fit to data from all sites. Exponents vary between sites (from 0.44 – 0.84), and no single value of b sufficiently describes the data (Table B.1). The variability in the fitted exponents is not surprising. Others have shown similar variability and suggested that this can be explained by median grain size, sorting of the bed mixture, and shear velocity [*Shvidchenko et al.*, 2001; *Buscombe and Conley*, 2012]

Table B.1: Summary of hiding function fits.

Source	**Site**	ω_{r50*}	b	D_i/D_{50}	D_{50} [mm]
Hinton et al. [2016]	Annie Creek	0.12	0.65	0.02 – 2.51	9
Williams and Rosgen [1989]	Muddy Creek	0.16	0.44	0.11 – 7.07	0.8
Williams and Rosgen [1989]	Pony Creek	0.24	0.8	0.04 – 5.39	2.1
Hinton et al. [2016]	Sycan River above Marsh	0.07	0.76	0.01 – 1.41	16
Kuhnle [1992]	Goodwin Creek	0.11	0.84	0.03 – 3.87	11.7

The mean value of 0.70 is lower than exponents from shear stress-based hiding functions [*Parker*, 2008]. For the stream power based hiding function, however, the exponent ranges from 0 – 1.5. This means that the average b value of 0.70 found in this analysis is equivalent to an exponent of ~ 0.47 if using a shear stress approach, which is significantly lower than what has been found by others [*Shvidchenko et al.*, 2001; *Parker*, 2008]. Of the datasets used in this analysis, only the Goodwin Creek data have been used previously to develop a shear stress-based hiding function [*Kuhnle*, 1992]. In that analysis, the value of b was calculated as 0.805, which is higher than my equivalent b value (0.84 / 1.5 = 0.56). This is partially due to my analysis using $q^*_{bi} = 0.0001$ as a threshold for calculating ω^*_{ri} whereas *Kuhnle* [1992] used $W^*_i = 0.002$. Rerunning this analysis using the W^*_i threshold yielded a b value of 1.15 (or ~ 0.76 as a shear stress equivalent, closer to Kuhnle's value of 0.805).

Fitted values of ω^*_{r50} also vary between sites but they are within the range of critical dimensionless specific stream power values for a variety of field sites (including some the same sites included in this analysis; see Chapter 3). Based on these results, I use default model values of $b = 0.8$ and $\omega^*_{r50} = 0.1$, which is the average value found by *Parker et al.* [2011] and in Chapter 3.

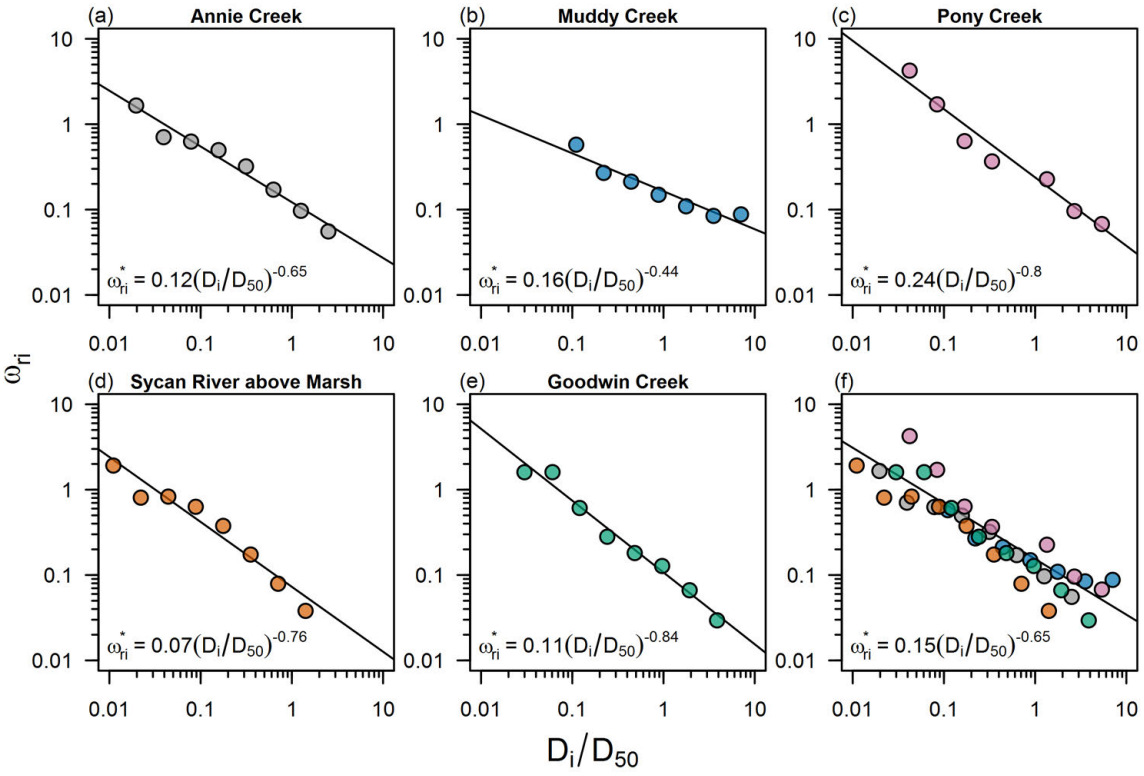

Figure B.1: Fitted hiding functions for five analyzed field sites (a–e) and a hiding function fit to the combined data (f).

B.1.2 Stream Power - Shear Stress Relationship

Assuming a rectangular channel, specific stream power can be calculated as the product of shear stress and velocity:

$$\omega = \tau V \tag{B.6}$$

Since REM does not calculate flow hydraulics, however, I do not know flow velocity and therefore can't use this approach to compute τ from ω. I instead opted for a purely empirical approach.

I used hydraulic data available in a previous compilation of bedload and total load sediment transport data (Chapter 3). I was not interested in the sediment transport data for this analysis but it provided a convenient set of hydraulic data (including specific stream power and shear stress) from a wide range of rivers and flumes. I fit a simple power relationship between ω and τ:

$$\tau = 1.96\omega^{0.72} \tag{B.7}$$

Figure B.2 shows predicted versus observed shear stress values (where observed values were calculated as $\tau = \gamma hS$). Points are colored according to velocity, and show that this equation tends to overpredict τ for higher velocities and underpredict τ for lower velocities.

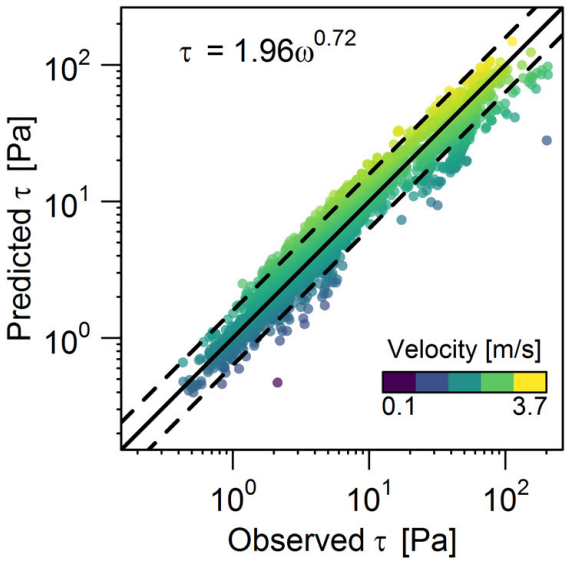

Figure B.2: Predicted versus observed average boundary shear stress using an empirical power equation fit using a large database of hydraulic data from rivers and flumes (Chapter 3). The 1:1 line (solid) and lines of twice and half the actual value (dashed) are shown. Points are colored based on velocity.

As an alternative approach, I also considered assuming rectangular channel geometry and calculating flow depth by iteratively solving the Manning equation (given discharge, slope, and width). This calculated depth value would then be used to estimate τ. This approach, however, was sensitive to the selection of a roughness coefficient and could not predict values of τ as accurately as Equation B.7.

B.1.3 Stream Power - Wall Shear Stress Relationship

To model fluvial bank erosion, like cohesive incision, I need to develop a relationship between stream power and shear stress. Here, I am interested in the shear *at the bank*, also called the wall shear stress. There are two potential approaches to achieving this: (1) relate shear stress and specific stream power using a flow resistance formula or (2) developing a direct empirical relationship between specific stream power and wall shear stress. The first approach is physically based but requires assumptions of channel roughness and an empirical relationship to relate bed shear stress to wall shear stress [e.g. *Knight et al.*, 1984]. I instead chose option (2), which is much simpler and had very similar accuracy to option (1) (data not shown).

I collected published data on average wall shear stress from six flume studies (Table B.2). These data showed a clear nonlinear relationship between ω and τ_w, suggesting a power relationship may be most appropriate. I fit a power relationship using data from smooth and rough rectangular and trapezoidal flumes:

$$\tau_w = 0.83\omega^{0.65} \tag{B.8}$$

This equation performed well and I found no difference in accuracy based on channel geometry or roughness (Figure B.3).

Table B.2: Summary of flume studies with measured wall shear stress.

Study	N	Slope [x 10^{-3}]	Q [m^3 s^{-1}]	ω [W m^{-2}]	w/h	Manning's n	τ_w [Pa]
Cruff [1965]	25	0.41 - 29.82	11.3 - 207.4	0.04 - 25.49	4.7 - 38	0.005 - 0.014	0.09 - 6.84
Ghosh and Roy [1970]	36	3.02 - 4.35	5 - 33	0.74 - 5.44	1.1 - 7.1	0.009 - 0.031	0.62 - 2.92
Knight [1981]	50	0.96	3 - 113.6	0.06 - 2.32	1.5 - 15	0.009 - 0.023	0.12 - 1.23
Knight et al. [1984]	25	0.97	2 - 28.7	0.1 - 0.66	0.3 - 19.1	0.009 - 0.011	0.21 - 0.65
Lashkar-Ara and Fathi-Moghadam [2010]	14	1.95	18.3 - 69.6	0.44 - 1.66	7.9 - 18.6	0.009 - 0.01	0.48 - 1.24
Seckin et al. [2006]	9	2.02	3.9 - 14.9	0.2 - 0.75	6.6 - 14.8	0.009 - 0.01	0.32 - 0.73

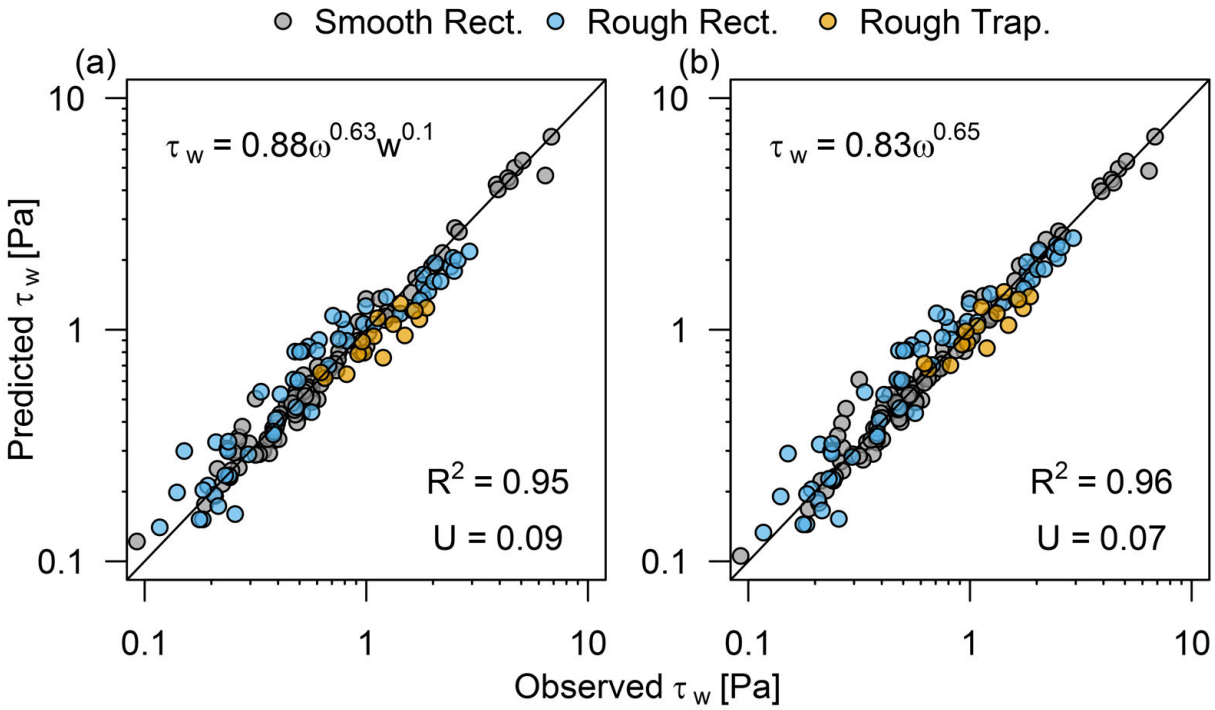

Figure B.3: Predicted versus observed wall shear stress using an empirical power equation fit using only data from smooth rectangular flumes (a) and fit using data from smooth and rough rectangular and trapezoidal flumes (b). Equations are tested using all rough and smooth flume data. R^2 is the coefficient of determination (modified for log10 transformed data) and U is the *Theil* [1958] measure of association [*Smith and Rose*, 1995]. High values of R^2 and low values of U indicate a good model fit.

B.1.4 Coupled Bank Erosion

Figures B.4 and B.5 show how coupled fluvial bank erosion and mass failure are modeled.

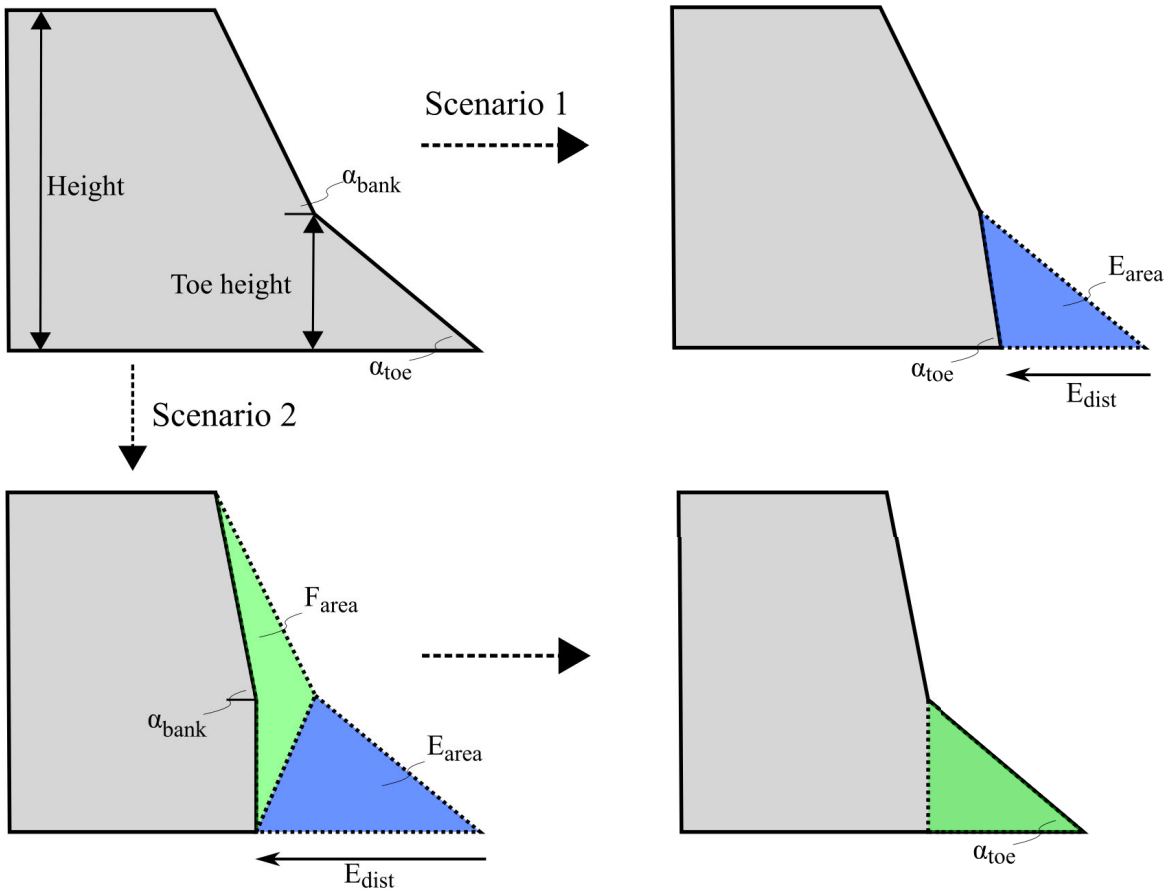

Figure B.4: Drawing of the model procedure for updating bank geometry after fluvial erosion. If the eroded distance (E_{dist}) is small (Scenario 1), α_{toe} is updated and the eroded bank material is added to the sediment mass balance for the reach. If E_{dist} is large (Scenario 2) and leads to an undercut bank, the bank fails and the bank angle (α_{bank}) is updated. The toe area eroded from fluvial erosion is added to the bed material sediment mass balance (blue area, E_{area}) while the failed soil block (green area, F_{area}) is deposited at the bank toe and α_{toe} is updated.

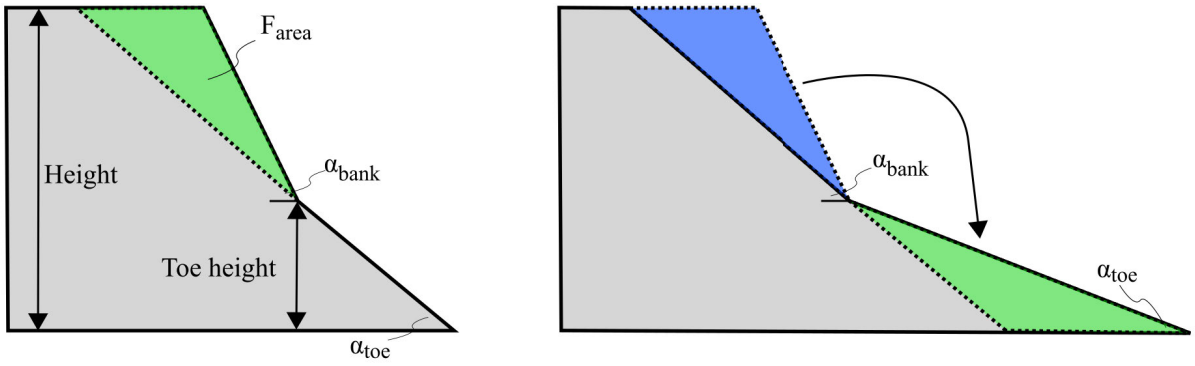

Figure B.5: Drawing of the model procedure for updating bank geometry after a mass failure. The area of the failed soil block (blue) is deposited on the bank toe (green), conserving total soil mass. Both α_{bank} and α_{toe} are updated based on the new bank geometry. A similar procedure is used if the failure plane intersects the base of the toe, rather than the top of the toe as shown in this figure.

B.1.5 Meander Dynamics

To simulate meander dynamics, the model requires a value for radius of curvature, sinuosity, and cross section spacing (dx). The model makes an initial guess of the number of bends in the reach to calculate the length of each bend (reach length divided by the number of bends). Using this, the angle of each bend is calculated:

$$\alpha_{bend} = \frac{s}{R_c} \tag{B.9}$$

where α_{bend} is the bend angle [radians], s is the bend arc length [m], and R_c is radius of curvature [m]. The total reach valley length is then calculated as the product of the length of the circular segment formed by the bend (a) and the number of bends in the reach:

$$a = 2R_c \sin\left(\frac{\alpha_{bend}}{2}\right) \tag{B.10}$$

$$L_v = a \times \#bends \tag{B.11}$$

where L_v is the total valley length [m]. The sinuosity of the reach is then calculated $P = L_v/dx$ and compared to the user supplied sinuosity. The number of bends is adjusted until these two sinuosity values converge.

Based on the migration distance of the channel centerline, a new value of R_c is calculated. First, a is calculated from Equation B.10. I assume the length of this circular segment does not change as the bend evolves. The bend height (h) is calculated:

$$h = R_c - 0.5 * \sqrt{4 * R_c^2 - a^2} \tag{B.12}$$

The erosion distance of the bend is then added to this value to obtain the height of the new bend (Figure B.7). The new R_c of this bend is calculated using this adjusted value of h:

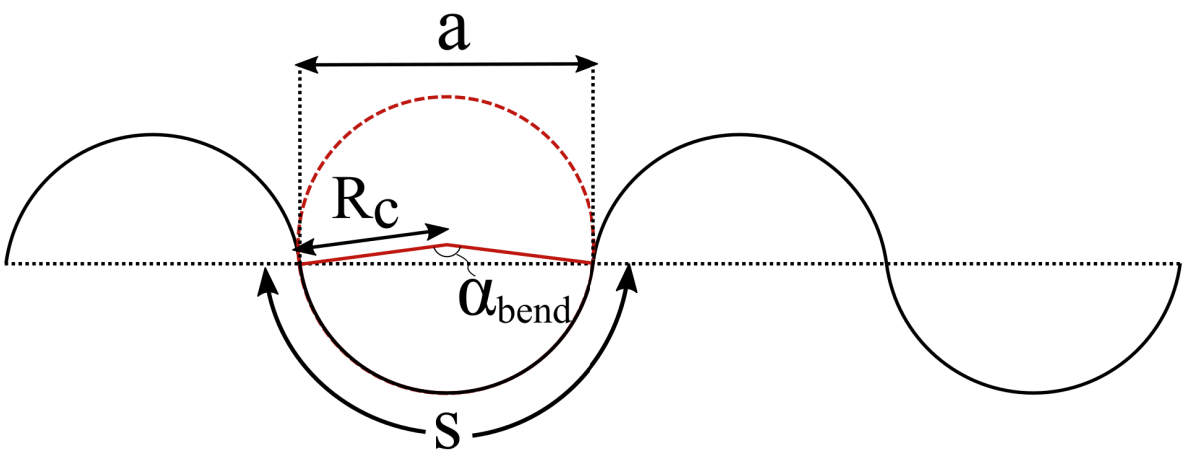

Figure B.6: Diagram showing how the model handles channel meandering. The channel is described by the black curve. Bends are conceptualized as arc segments of circles with a radius R_c and total bend length s. These values, and the bend angle α are used to calculate the length of the circular segment (a). The total valley length is a times the number of bends (four in this drawing).

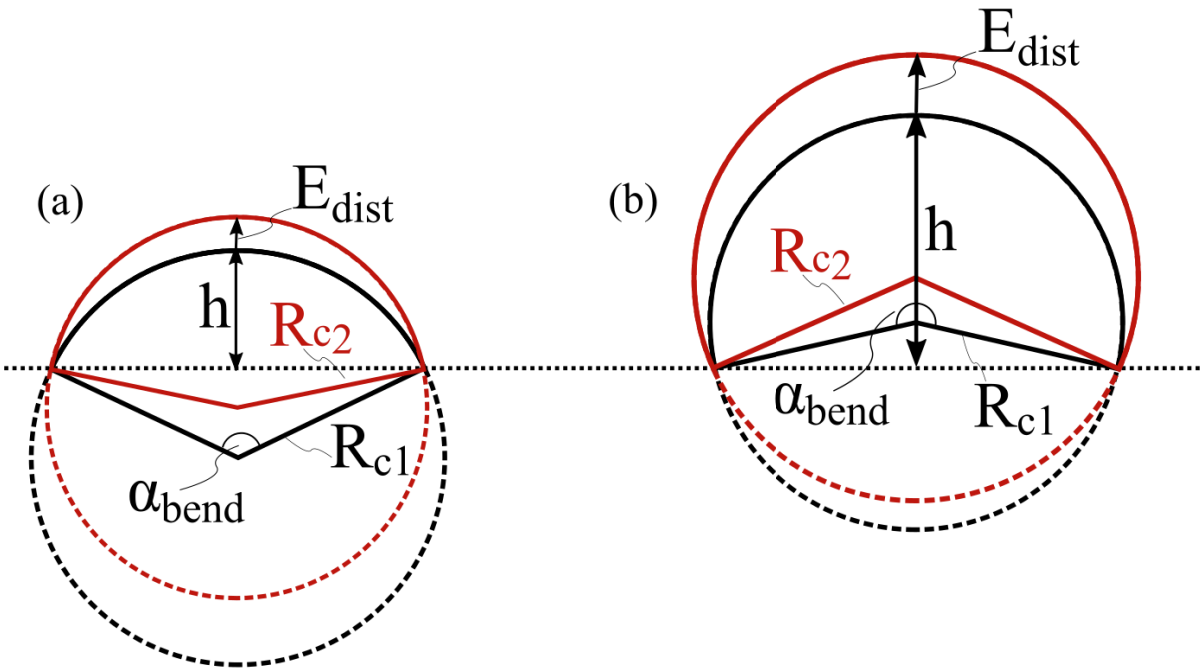

Figure B.7: Diagram showing how the model updates bend R_c. Black circles indicate original bend geometry and red is the post-migration geometry. h is the bend height, E_{dist} is the eroded distance of the channel centerline, and R_{c1} and R_{c2} are the original and new radii of curvature, respectively. If $\alpha_{bend} < 180°$, lateral migration tightens the bend ($R_{c2} < R_{c1}$) (a). If, however, $\alpha_{bend} > 180°$, lateral migration reduces bend curvature ($R_{c2} > R_{c1}$) (b).

$$R_c = \frac{4h^2 + a^2}{8h} \tag{B.13}$$

Next, the new bend angle is calculated:

$$\alpha_{bend} = 2 \arcsin\left(\frac{a}{2R_c}\right) \tag{B.14}$$

α_{bend} and R_c are used to calculate the new arc length (s) using Equation B.9. This is used to update the dx value for the selected cross section. At the end of each time step, the new sinuosity of the entire reach is calculated.

This is a simple approach to modeling meander growth and sinuosity change in rivers. It allows the channel to adjust its slope via lateral migration but it fails to account for many processes relevant in meander bend migration and evolution. For example, the model assumes circular, symmetrical bend geometry, rather than using a sine-generated curve [*Langbein and Leopold*, 1966] which may describe bend shape more accurately. Furthermore, this assumption of circular bends fails to account for the formation of complex bends which are ubiquitous features in natural meandering streams [*Hooke*, 2013]. Finally, the model only incorporates bend elongation, rather than down-valley bend migration. Modeling suggests that down-valley migration dominates in low-sinuosity streams while tighter bends migrate laterally [*Chen and Duan*, 2006].

B.1.6 Knickpoint Model Validation

The empirical knickpoint erosion model I use was built for and tested on ephemeral gullies in agricultural fields [*Allen et al.*, 2018], rather than the perennial streams REM will likely be applied to. I therefore explored this knickpoint model in more detail to test its applicability in these situations. Using data from *Downs and Simon* [2001] and *Thomas* [2000] on knickpoint retreat in the Yalobusha River basin of central Mississippi, I calibrated the *Allen et al.* [2018] model to find values of soil erodibility, K_d (Equations 4.20 and 4.21). I used daily flow data from USGS gages 07282000 and 07282100 for the period the knickpoint

data were collected (1997 – 1999). Missing flow data from gage 07282100 were replaced with data from 07282000, scaled by drainage area. I scaled all flows by drainage area to estimate daily discharge at each knickpoint.

Calibrated values of K_d varied across a relatively narrow range (0.19 – 0.22 cm Pa^{-1} hr^{-1}). Despite this, a single calibrated value for all sites failed to give accurate predictions of knickpoint retreat rates (Figure B.8). Values of K_d are strongly correlated with observed knickpoint retreat rates, normalized by drainage area (Figure B.9). This analysis suggests that the knickpoint retreat model is sensitive to small changes in K_d, even between streams in the same watershed. Figure B.10 shows calculated knickpoint retreat rates versus K_d for a 1 m knickpoint with four different discharges. This again emphasizes that predicted retreat rates can vary significantly over small ranges of K_d. Based on these results, I suggest direct calibration of the K_d values for any site that will be modeled using REM.

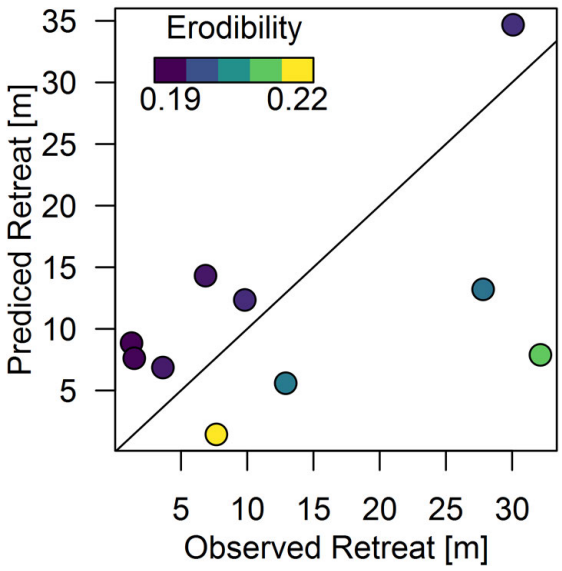

Figure B.8: Predicted versus observed knickpoint retreat using a single value of K_d for all sites. Points are colored based on their site-specific calibrated soil erodibility. Generally, retreat rates were underpredicted for sites with higher values of K_d and overpredicted for sites with low K_d.

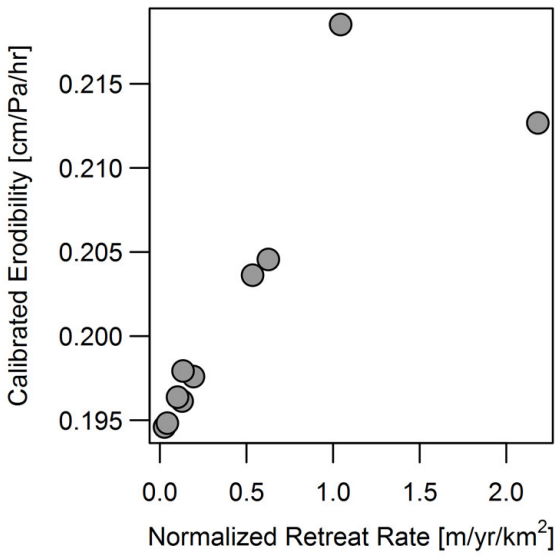

Figure B.9: Calibrated values of K_d versus observed knickpoint retreat rate, normalized by watershed area.

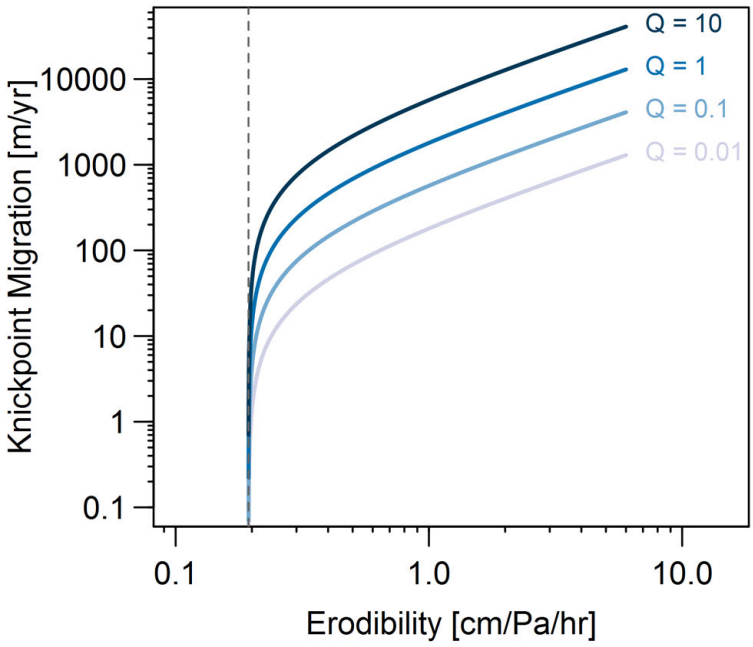

Figure B.10: Calculated migration rates versus K_d for a 1 m tall knickpoint at four different discharges [m^3 s^{-1}]. Note the log-log scale. Calculated erosion rates asymptotically approach zero as K_d approaches $3.2/16.5 \approx 0.194$.

B.2 Summary of Model Inputs

Table B.3: Model inputs for the generic model test case. [a]Values are lowest for each tributary and increase moving downstream. [b]Proportion of the eroded bank material that is added to the bed material load (sand and coarser). Remaining material is washload.

Variable	**Value**
Sediment supply	Initial transport capacity
Discharge [m^3 s^{-1}][a]	1 – 3
Width [m][a]	10 – 30
Slope [m m^{-1}]	0.003
D_{50} [mm]	2
Bank height [m]	2
Bank toe height [m]	1
Bank angle	90°
Bank toe angle	45°
Bank τ_c [Pa]	2.5
Bank erodibility [m^3 N^{-1} s^{-1}]	Calculated by REM
Bank cohesion [kPa]	1.3
Bank ϕ'	30°
Bank soil unit weight [kN m^{-3}]	18
Bank bedload proportion[b]	0.8
Floodplain width [m]	20
Floodplain angle	0°
Channel roughness (n)	0.03
Floodplain roughness (n)	0.06
Knickpoint height [m]	1.5
XS spacing [m]	200
Time step [s]	4,800

Table B.4: A summary of all inputs used by the model. Variables under the "Main Model" heading are required. The rest are only required if those specific sub-models are being run.

Variable	Description
	Main Model
Discharge [m^3 s^{-1}]	Discharge for each reach at user-specific time step (e.g. daily, hourly, 15-min)
Sediment supply [m^3 m^{-1} s^{-1}]	Sediment transport rate for each reach at same time step as discharge. Can also be set to a fraction of the transport capacity.
Bed elevations [m]	Upstream bed elevation per reach (uniform slope) or individual values for each cross section.
XS spacing [m]	Length of each reach (uniform slope) or unique distance between each XS
Width [m]	Channel bottom width by reach
Grain size distribution	One set of grain sizes but unique initial bed surface fractions by reach
Bank height [m]	Unique by reach for left and right banks (total height, including toe)
Bank toe height [m]	Unique by reach for left and right banks (must be less than bank height)
Bank angle [degrees]	Unique by reach for left and right banks (max 90°)
Bank toe angle [degrees]	Unique by reach for left and right banks (max 90°)
Floodplain width [m]	Unique by reach for left and right floodplain
Floodplain angle [degrees]	Unique value per reach
Channel roughness (n)	Manning's n value for the main channel, unique value by reach
Floodplain roughness (n)	Manning's n value for the floodplain, unique value by reach
Hiding function coefficient (ω_{c*})	Single value, defaults to 0.1
Hiding function exponent (b)	Single value, defaults to 0.8
Link	Matrix describing layout of the channel network (i.e. connection of reaches)
Sediment transport type	Bedload or total load transport (or both depending on grain size)
Bank erosion type	None, mass failure, fluvial erosion, or both
	Bank Erosion
Bank τ_c [Pa]	Critical shear stress of the bank material
Bank erodibility [m^3 N^{-1} s^{-1}]	Erodibility of the bank material (calculated by REM if not supplied)
Bank cohesion [kPa]	Cohesion of the bank material (can be different for main bank and toe)
Bank ϕ'	Friction angle of the bank material (can be different for main bank and toe)
Bank soil unit weight [kN m^{-3}]	Saturated weight of the bank soil (can be different for main bank and toe)
Bank bedload proportion	Proportion of the eroded bank material that will be added to the bank material load (sand and coarser)
Bed bedload proportion	Proportion of the eroded bed material (cohesive erosion) that will be added to the bank material load (sand and coarser)
Soil pollutant concentration [mg kg^{-1}]	Concentration of pollutant (e.g. phosphorus) in the eroded bank and cohesive bed material (unique values for each)
	Cohesive Bed Erosion
Depth to cohesive layer [m]	Depth below initial bed elevation to cohesive material. Unique value by reach (uniform slope) or by XS.
Bed τ_c [Pa]	Critical shear stress of cohesive bed material — can be set to high value (e.g. 999) to simulate non-erodible bed
	Meandering
Sinuosity	Channel sinuosity by reach
R_c [m]	Average bend radius of curvature by reach
	Knickpoint Migration
Location	Reach in which the knickpoint is initially
Distance DS [m]	Initial location downstream from beginning of reach
Elevation [m]	Elevation of the top of the knickpoint
Height [m]	Knickpoint height
K_d [cm Pa^{-1} h^{-1}]	Knickpoint soil erodibility (see Appendix B.1.6)

B.3 Additional Model Results

B.3.1 Full NFTR Sensitivity Results

Figures B.11, B.12, and B.13 show full sensitivity results for each cross section of the NFTR. The relative importance of different inputs can vary considerably between cross sections. This is due in part to different ranges of each of these inputs, and the different dominant channel response at each cross section. For example, NF 375 widened primarily through aggradation filling up the channel, rather than through bank erosion. This results in changes in channel width being largely controlled by initial channel width, rather than other parameters like bank τ_c.

Table B.5 shows input values for all reaches in the NFTR modeling.

B.3.2 Recommendations for Sensitivity Analyses

The accuracy and stability of the sensitivity analysis method [*Plischke et al.*, 2013] is dependent on the number of model runs used to feed it. Figure B.14 shows how the calculated sensitivity indices for various input variables converges as the number of model runs increases. Most of the variables seem to have reaches stable values by about 3000 iterations, although the values for the dummy variable and other less-important inputs continue to decrease. Bootstrapping the sensitivity analysis (not done for Figure B.14) helps reduce this issue, removed bias, and provides confidence bounds for the sensitivity estimate. This allows accurate sensitivity results even for a smaller number of model iterations.

Figure B.11 ***(following page)*****:** Full Toutle River sensitivity results by cross section for the bed elevation output.

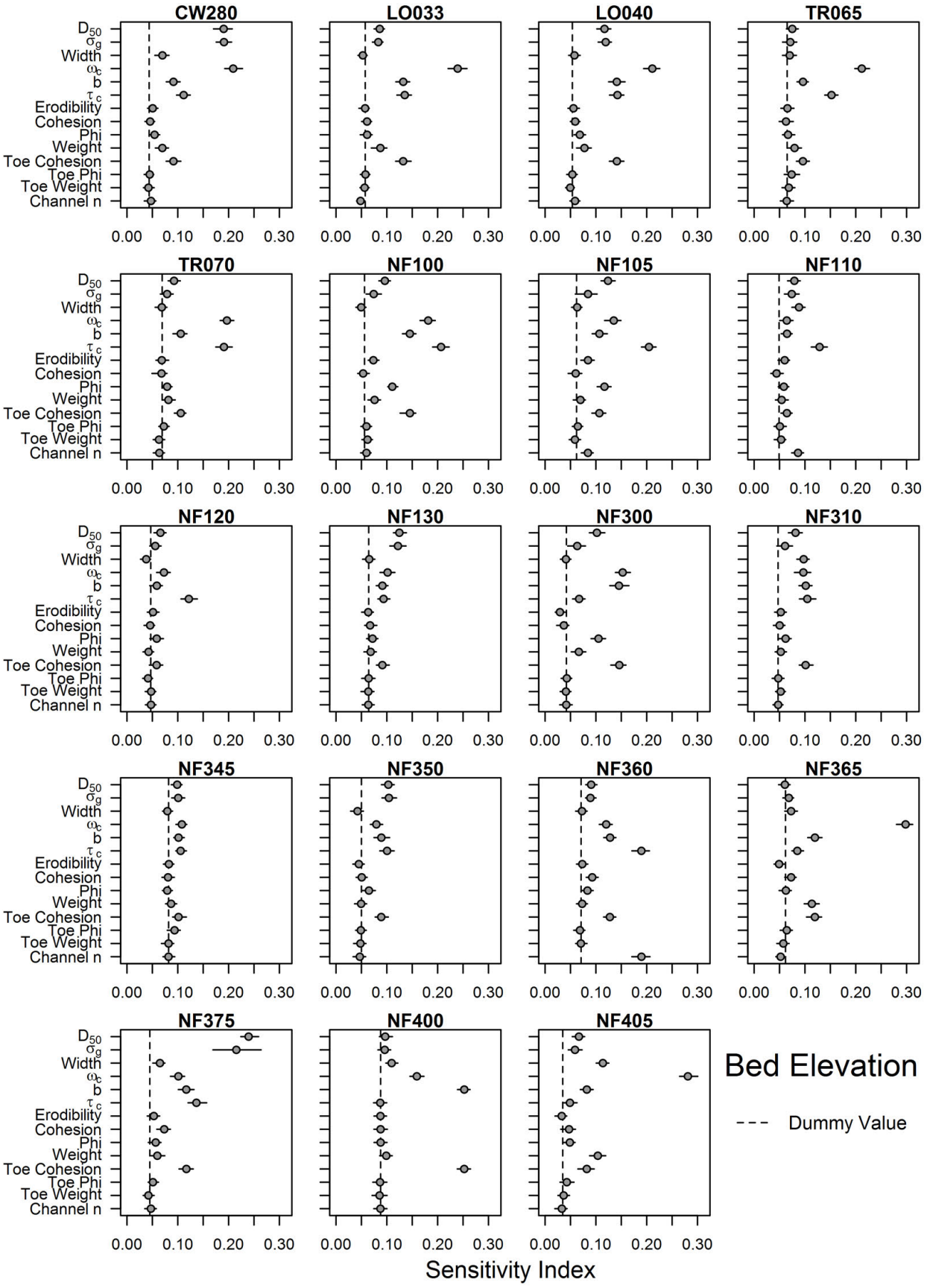
CW280
LO033
LO040
TR065
TR070
NF100
NF105
NF110
NF120
NF130
NF300
NF310
NF345
NF350
NF360
NF365
NF375
NF400
NF405
D50
σg
Width
ωc
b
τc
Erodibility
Cohesion
Phi
Weight
Toe Cohesion
Toe Phi
Toe Weight
Channel n
0.00
0.10
0.20
0.30
Sensitivity Index
Bed Elevation
Dummy Value

Figure B.12 ***(following page)*****:** Full Toutle River sensitivity results by cross section for the bed D_{50} output.

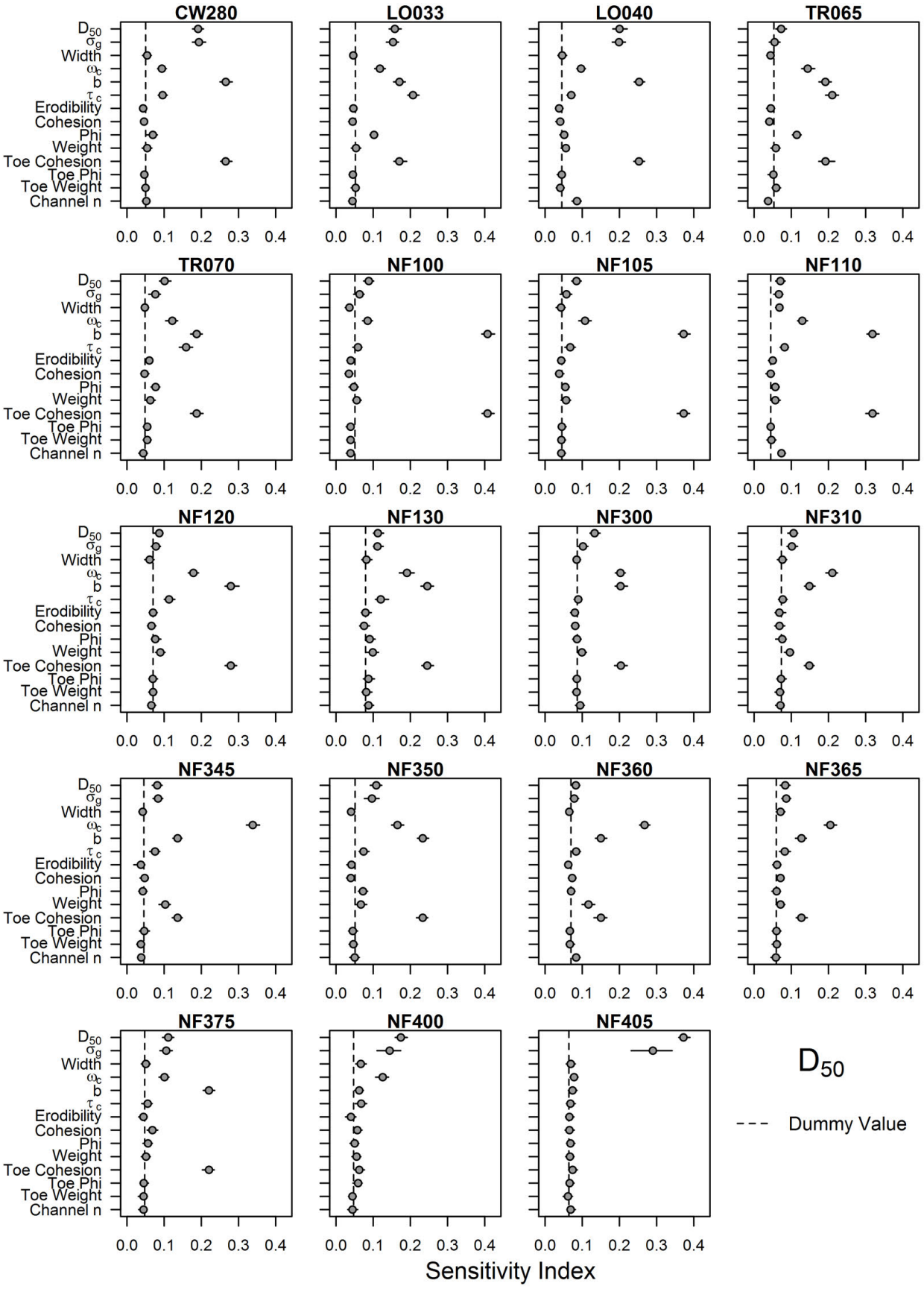
CW280
LO033
LO040
TR065
TR070
NF100
NF105
NF110
NF120
NF130
NF300
NF310
NF345
NF350
NF360
NF365
NF375
NF400
NF405
D50
σg
Width
ωc
b
τc
Erodibility
Cohesion
Phi
Weight
Toe Cohesion
Toe Phi
Toe Weight
Channel n
0.0 0.1 0.2 0.3 0.4
Sensitivity Index
D50
Dummy Value

Figure B.13 ***(following page)*:** Full Toutle River sensitivity results by cross section for the channel width output.

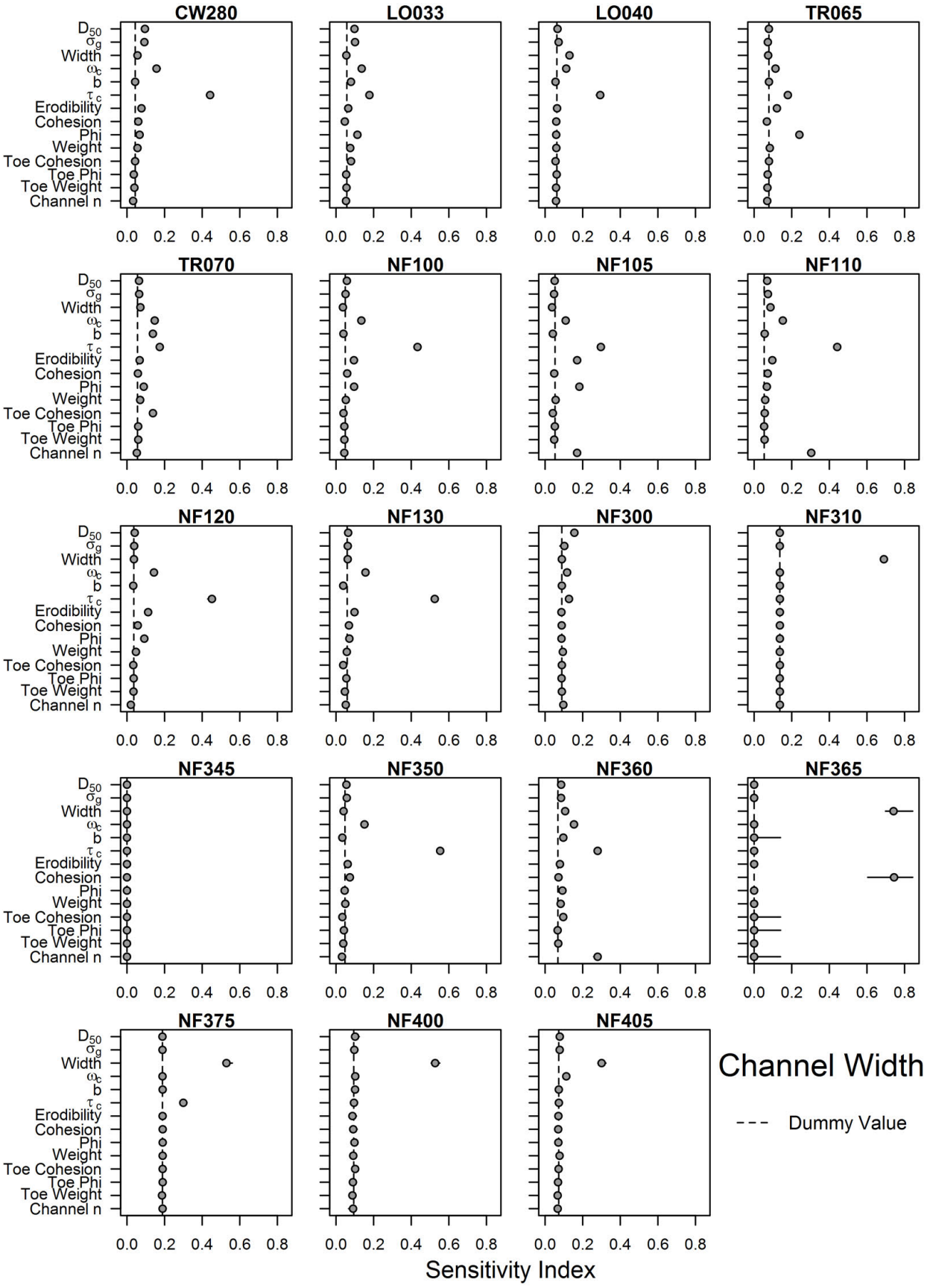
CW280
LO033
LO040
TR065
TR070
NF100
NF105
NF110
NF120
NF130
NF300
NF310
NF345
NF350
NF360
NF365
NF375
NF400
NF405
D50
σg
Width
ωc
b
τc
Erodibility
Cohesion
Phi
Weight
Toe Cohesion
Toe Phi
Toe Weight
Channel n
0.0
0.2
0.4
0.6
0.8
Sensitivity Index
Channel Width
Dummy Value

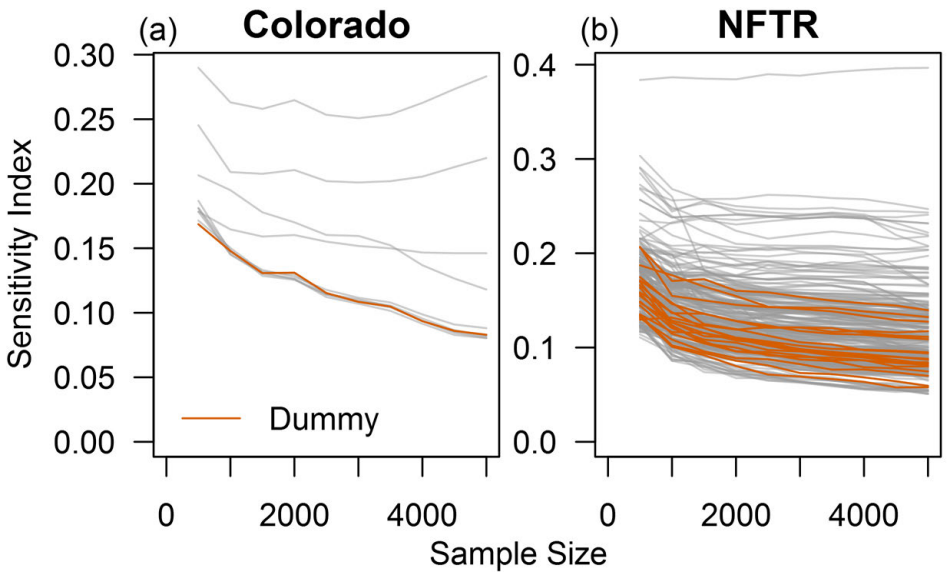

Figure B.14: Convergence of calculated sensitivity indices as sample size increases for (a) the Colorado River modeling and (b) the North Fork Toutle River modeling. The index for the dummy variable is colored to show how this value decreases as sample size increases.

Table B.5: Summary of inputs for all reaches of the North Fork Toutle River.

Reach	Variable	Single Run Value	Monte Carlo Range
CW280	Width [m]	5.8	2.9 – 8.8
	D_{50} [mm]	1.14	0.24 – 2.89
	σ_g [mm]	7.4	6 – 8.6
	τ_c [Pa]	6.7	3.4 – 10
	Erodibility [m^3 N^{-1} s^{-1}]	3.90E-07	1.9e-07 – 5.8e-07
	Cohesion [kPa]	0	0 – 1
	ϕ' [degrees]	34	17 – 51
	Soil unit weight [kN m^{-3}]	19.5	9.8 – 29.2
	Channel roughness (n)	0.035	0.018 – 0.035
LO033	Width [m]	10.9	5.5 – 16.4
	D_{50} [mm]	1.14	0.24 – 2.89
	σ_g [mm]	7.4	6 – 8.6
	τ_c [Pa]	5.5	2.8 – 8.3
	Erodibility [m^3 N^{-1} s^{-1}]	3.90E-07	1.9e-07 – 5.8e-07
	Cohesion [kPa]	0	0 – 1
	ϕ' [degrees]	31.3	15.7 – 46.9
	Soil unit weight [kN m^{-3}]	19.3	9.7 – 29
	Channel roughness (n)	0.065	0.033 – 0.065
LO040	Width [m]	20.2	10.1 – 30.3
	D_{50} [mm]	1.14	0.24 – 2.89
	σ_g [mm]	7.4	6 – 8.6
	τ_c [Pa]	12.2	6.1 – 18.2
	Erodibility [m^3 N^{-1} s^{-1}]	2.00E-07	1e-07 – 3e-07
	Cohesion [kPa]	0	0 – 1
	ϕ' [degrees]	30	15 – 45
	Soil unit weight [kN m^{-3}]	19.1	9.5 – 28.6
	Channel roughness (n)	0.03	0.015 – 0.03
TR065	Width [m]	11.6	5.8 – 17.4
	D_{50} [mm]	2.84	1.44 – 4.3
	σ_g [mm]	6.4	6.1 – 6.6
	τ_c [Pa]	8	4 – 11.9
	Erodibility [m^3 N^{-1} s^{-1}]	2.90E-07	1.4e-07 – 4.3e-07
	Cohesion [kPa]	0	0 – 1
	ϕ' [degrees]	33	16.5 – 49.5
	Soil unit weight [kN m^{-3}]	19.7	9.8 – 29.5
	Channel roughness (n)	0.055	0.028 – 0.055
TR070	Width [m]	6.6	3.3 – 9.9
	D_{50} [mm]	2.84	1.44 – 4.3
	σ_g [mm]	6.4	6.1 – 6.6
	τ_c [Pa]	8	4 – 11.9
	Erodibility [m^3 N^{-1} s^{-1}]	2.90E-07	1.4e-07 – 4.3e-07
	Cohesion [kPa]	0	0 – 1
	ϕ' [degrees]	33	16.5 – 49.5
	Soil unit weight [kN m^{-3}]	19.7	9.8 – 29.5
	Channel roughness (n)	0.055	0.028 – 0.055

Table B.5: Summary of inputs for all reaches of the North Fork Toutle River.

Reach	Variable	Single Run Value	Monte Carlo Range
NF100	Width [m]	7.6	3.8 – 11.4
	D_{50} [mm]	2.84	1.44 – 4.3
	σ_g [mm]	6.4	6.1 – 6.6
	τ_c [Pa]	10.2	5.1 – 15.3
	Erodibility [m^3 N^{-1} s^{-1}]	2.40E-07	1.2e-07 – 3.5e-07
	Cohesion [kPa]	0	0 – 1
	ϕ' [degrees]	33	16.5 – 49.5
	Soil unit weight [kN m^{-3}]	19.7	9.8 – 29.5
	Channel roughness (n)	0.065	0.033 – 0.065
NF105	Width [m]	7.5	3.7 – 11.2
	D_{50} [mm]	2.84	1.44 – 4.3
	σ_g [mm]	6.4	6.1 – 6.6
	τ_c [Pa]	10.2	5.1 – 15.3
	Erodibility [m^3 N^{-1} s^{-1}]	2.40E-07	1.2e-07 – 3.5e-07
	Cohesion [kPa]	0	0 – 1
	ϕ' [degrees]	33	16.5 – 49.5
	Soil unit weight [kN m^{-3}]	19.7	9.8 – 29.5
	Channel roughness (n)	0.065	0.033 – 0.065
NF110	Width [m]	7.1	3.6 – 10.7
	D_{50} [mm]	2.84	1.44 – 4.3
	σ_g [mm]	6.4	6.1 – 6.6
	τ_c [Pa]	10.2	5.1 – 15.3
	Erodibility [m^3 N^{-1} s^{-1}]	2.40E-07	1.2e-07 – 3.5e-07
	Cohesion [kPa]	0	0 – 1
	ϕ' [degrees]	32.1	16.1 – 48.2
	Soil unit weight [kN m^{-3}]	19.1	9.6 – 28.6
	Channel roughness (n)	0.055	0.028 – 0.055
NF120	Width [m]	10.3	5.2 – 15.5
	D_{50} [mm]	2.84	1.44 – 4.3
	σ_g [mm]	6.4	6.1 – 6.6
	τ_c [Pa]	12	6 – 18
	Erodibility [m^3 N^{-1} s^{-1}]	1.90E-07	1e-07 – 2.8e-07
	Cohesion [kPa]	0	0 – 1
	ϕ' [degrees]	34	17 – 51
	Soil unit weight [kN m^{-3}]	19.8	9.9 – 29.7
	Channel roughness (n)	0.055	0.028 – 0.055
NF130	Width [m]	11.4	5.7 – 17.1
	D_{50} [mm]	1.51	0.81 – 2.93
	σ_g [mm]	7.4	6.8 – 7.9
	τ_c [Pa]	15.1	7.5 – 22.6
	Erodibility [m^3 N^{-1} s^{-1}]	1.90E-07	1e-07 – 2.8e-07
	Cohesion [kPa]	0	0 – 1
	ϕ' [degrees]	34	17 – 51
	Soil unit weight [kN m^{-3}]	19.8	9.9 – 29.7
	Channel roughness (n)	0.045	0.023 – 0.045

Table B.5: Summary of inputs for all reaches of the North Fork Toutle River.

Reach	Variable	Single Run Value	Monte Carlo Range
NF300	Width [m]	4	2 – 6
	D_{50} [mm]	2.04	1.37 – 7.2
	σ_g [mm]	8.5	8.2 – 9.3
	τ_c [Pa]	32.1	16 – 48.1
	Erodibility [m^3 N^{-1} s^{-1}]	9.00E-08	5e-08 – 1.4e-07
	Cohesion [kPa]	0	0 – 1
	ϕ' [degrees]	25.2	12.6 – 37.8
	Soil unit weight [kN m^{-3}]	19.5	9.8 – 29.2
	Channel roughness (n)	0.045	0.023 – 0.045
NF310	Width [m]	24.9	12.4 – 37.3
	D_{50} [mm]	2.12	1.5 – 2.59
	σ_g [mm]	7	7.2 – 7.7
	τ_c [Pa]	32.1	16 – 48.1
	Erodibility [m^3 N^{-1} s^{-1}]	9.00E-08	5e-08 – 1.4e-07
	Cohesion [kPa]	0	0 – 1
	ϕ' [degrees]	25.2	12.6 – 37.8
	Soil unit weight [kN m^{-3}]	18.4	9.2 – 27.6
	Channel roughness (n)	0.03	0.015 – 0.03
NF345	Width [m]	25.7	12.8 – 38.5
	D_{50} [mm]	1.08	0.63 – 1.81
	σ_g [mm]	7.3	6.6 – 7.7
	τ_c [Pa]	32.1	16 – 48.1
	Erodibility [m^3 N^{-1} s^{-1}]	9.00E-08	5e-08 – 1.4e-07
	Cohesion [kPa]	0	0 – 1
	ϕ' [degrees]	25.2	12.6 – 37.8
	Soil unit weight [kN m^{-3}]	19	9.5 – 28.5
	Channel roughness (n)	0.04	0.02 – 0.04
NF350	Width [m]	17	8.5 – 25.5
	D_{50} [mm]	1.53	0.87 – 3.53
	σ_g [mm]	7.1	6.3 – 7.3
	τ_c [Pa]	7.6	3.8 – 11.4
	Erodibility [m^3 N^{-1} s^{-1}]	3.00E-07	1.5e-07 – 4.5e-07
	Cohesion [kPa]	0	0 – 1
	ϕ' [degrees]	25.2	12.6 – 37.8
	Soil unit weight [kN m^{-3}]	19	9.5 – 28.5
	Channel roughness (n)	0.04	0.02 – 0.04
NF360	Width [m]	21.2	10.6 – 31.7
	D_{50} [mm]	0.79	0.45 – 1.14
	σ_g [mm]	8.2	7.5 – 8.6
	τ_c [Pa]	13.7	6.9 – 20.5
	Erodibility [m^3 N^{-1} s^{-1}]	1.80E-07	9e-08 – 2.7e-07
	Cohesion [kPa]	0	0 – 1
	ϕ' [degrees]	25.2	12.6 – 37.8
	Soil unit weight [kN m^{-3}]	19	9.5 – 28.5
	Channel roughness (n)	0.04	0.02 – 0.04

Table B.5: Summary of inputs for all reaches of the North Fork Toutle River.

Reach	Variable	Single Run Value	Monte Carlo Range
NF365	Width [m]	16.2	8.1 – 24.3
	D_{50} [mm]	2.95	1.3 – 5.1
	σ_g [mm]	10.1	8 – 9.1
	τ_c [Pa]	13.7	6.9 – 20.5
	Erodibility [m^3 N^{-1} s^{-1}]	1.80E-07	9e-08 – 2.7e-07
	Cohesion [kPa]	0	0 – 1
	ϕ' [degrees]	25.2	12.6 – 37.8
	Soil unit weight [kN m^{-3}]	18.1	9.1 – 27.1
	Channel roughness (n)	0.03	0.015 – 0.03
NF375	Width [m]	13.1	6.6 – 19.6
	D_{50} [mm]	2.26	0.8 – 6.07
	σ_g [mm]	7	6.9 – 8
	τ_c [Pa]	7.6	3.8 – 11.4
	Erodibility [m^3 N^{-1} s^{-1}]	3.00E-07	1.5e-07 – 4.5e-07
	Cohesion [kPa]	0	0 – 1
	ϕ' [degrees]	25.2	12.6 – 37.8
	Soil unit weight [kN m^{-3}]	18.1	9.1 – 27.1
	Channel roughness (n)	0.03	0.015 – 0.03
NF400	Width [m]	164.9	82.5 – 247.3
	D_{50} [mm]	2.26	0.8 – 6.07
	σ_g [mm]	7	6.9 – 8
	τ_c [Pa]	32.1	16 – 48.1
	Erodibility [m^3 N^{-1} s^{-1}]	9.00E-08	5e-08 – 1.4e-07
	Cohesion [kPa]	0	0 – 1
	ϕ' [degrees]	25.2	12.6 – 37.8
	Soil unit weight [kN m^{-3}]	18.1	9.1 – 27.1
	Channel roughness (n)	0.03	0.015 – 0.03
NF405	Width [m]	263.1	131.6 – 394.6
	D_{50} [mm]	2.26	0.8 – 6.07
	σ_g [mm]	7	6.9 – 8
	τ_c [Pa]	32.1	16 – 48.1
	Erodibility [m^3 N^{-1} s^{-1}]	9.00E-08	5e-08 – 1.4e-07
	Cohesion [kPa]	0	0 – 1
	ϕ' [degrees]	25.2	12.6 – 37.8
	Soil unit weight [kN m^{-3}]	18.1	9.1 – 27.1
	Channel roughness (n)	0.03	0.015 – 0.03

Appendix C

C.1 Model Calibration

C.1.1 Critical Shear Stress Calibration

I calibrated critical shear stress values for bank material using measured historic erosion rates and estimates of applied stream power over the period of observation. I calculated stream power using 15-min and hourly gage data (whichever was available) and converted them to a bank or wall shear stress using the same empirical equation used by REM:

$$\tau_w = 0.83\omega^{0.65} \tag{C.1}$$

where τ_w is the shear stress acting on the channel bank [Pa] and ω is specific stream power [W m^{-2}]. I then calculated fluvial erosion using the excess shear stress equation:

$$E = k\Delta t(\tau - \tau_c) \tag{C.2}$$

where E is eroded distance [m], Δt is the time step, τ_c is the critical shear stress of the bank material [Pa], and k is the erodibility of the bank material [m^3 N^{-1} s^{-1}] which was calculated as [*Simon et al.*, 2010]:

$$k = 1.6 \times 10^{-6}\tau_c^{-0.826} \tag{C.3}$$

I calculated the value of τ_c that resulted in the best match between measured and calculated erosion rates (Figure C.1). For Big Dry Creek, all erosion measurements were located on channel bends. Therefore, I adjusted the value of τ_w to account for higher shear stress on the outside of bends [*Army Corps of Engineers*, 1970]:

$$\tau_{max} = 2.65\tau_w \left(\frac{R_c}{w}\right)^{-1/2} \tag{C.4}$$

where R_c is the bend radius of curvature [m] (estimated from aerial imagery) and w is channel width.

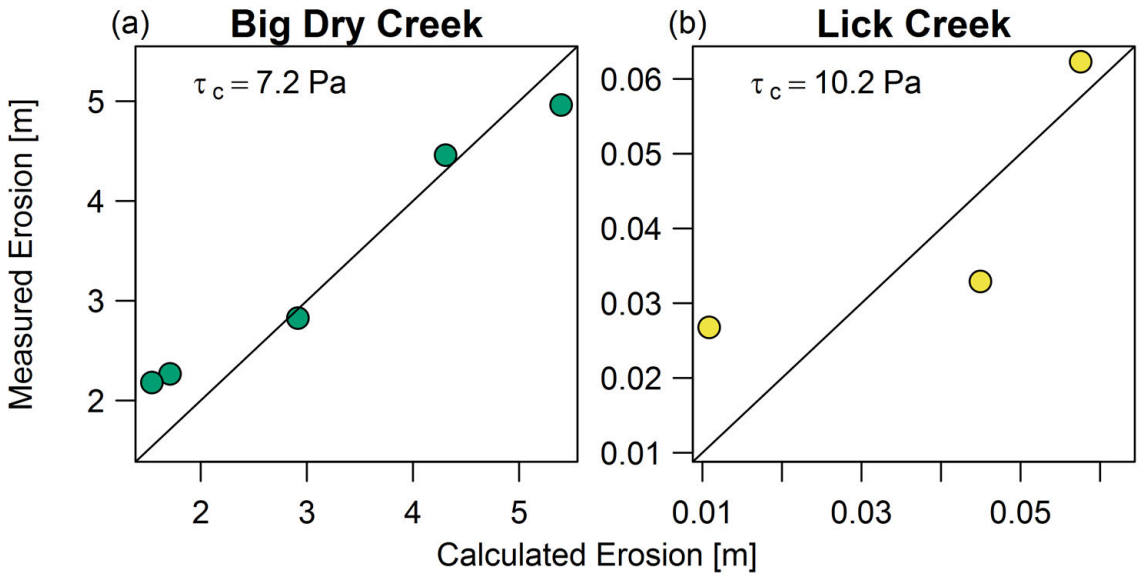

Figure C.1: Measured versus predicted erosion distance for the calibrated value of τ_c for Big Dry Creek (a) and Lick Creek (b). The Big Dry Creek data are from five different locations over the same time period (1993 – 2014). The Lick Creek data are actually from nearby Ellerbe Creek at one location for three time periods (annually from 2014 – 2017).

C.1.2 Knickpoint Calibration

During the field data collection in Lick Creek, I identified two active knickpoints. These knickpoints were later located on the 2015 DEM and a 10 ft resolution DEM from 2001. I calculated a value of K_d from the knickpoint migration model that matched the observed migration rate over this time period. Calibrated values of K_d were 0.253 cm/Pa/s and 0.219 cm/Pa/s. Observed migration rates of the two knickpoints were 26.8 m/yr and 10.1 m/yr. Normalized to their watershed area gives rates of 4.12 m/km^2/yr and 1.64 m/km^2/yr, respectively. These normalized rates are within the ranges observed in Mississippi streams (median 0.83, range 0.03 – 5.43 m/km^2/yr) [*Jaeger et al.*, 2010].

C.1.3 Bank Cohesion Calibration

Figure C.2 shows the data and fitted logistic regression model for predicting bank stability in Big Dry Creek and Lick Creek.

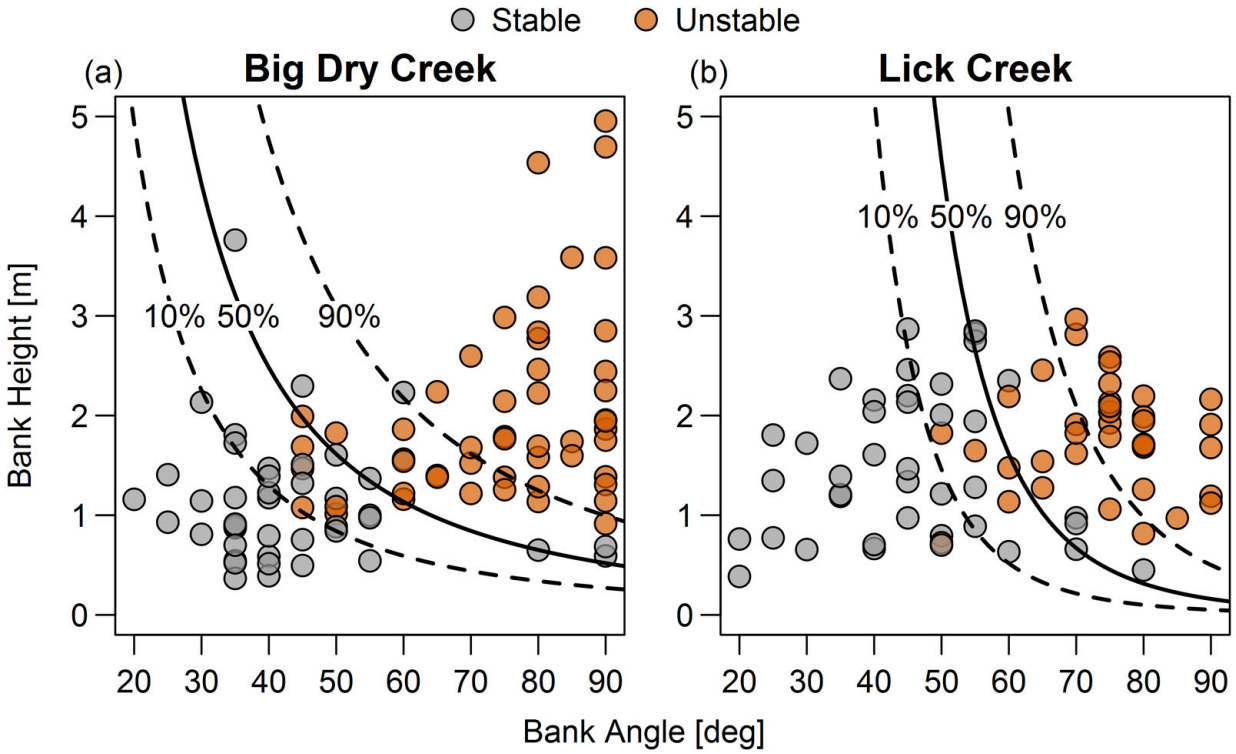

Figure C.2: Measured bank heights and angles for stable and unstable banks and fitted logistic regression for predicting bank stability for Big Dry Creek (a) and Lick Creek (b).

C.2 Watershed Population Estimates

Historic population densities for Big Dry Creek and Lick Creek (and its adjacent watershed, Little Lick Creek) were estimated from census block population data [*Manson et al.*, 2017]. These population data were scaled based on the proportion of each census block within the watershed boundary [*Rosburg et al.*, 2017]. The population of Big Dry Creek has increased steadily since 1970 (Figure C.3). Recent population growth in Lick Creek mirrors growth in Little Lick Creek from 1980 – 1990, the period for which discharge data from Little Lick Creek were available.

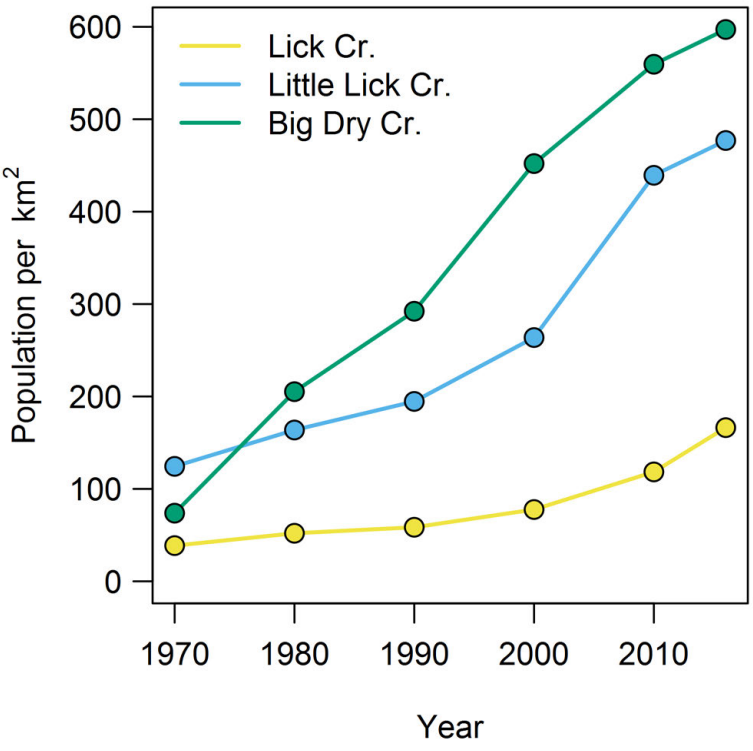

Figure C.3: Population density estimates for the three watersheds from 1970 – 2016.

C.3 Additional Model Results

C.3.1 Big Dry Creek, $Q_s = 0.5$

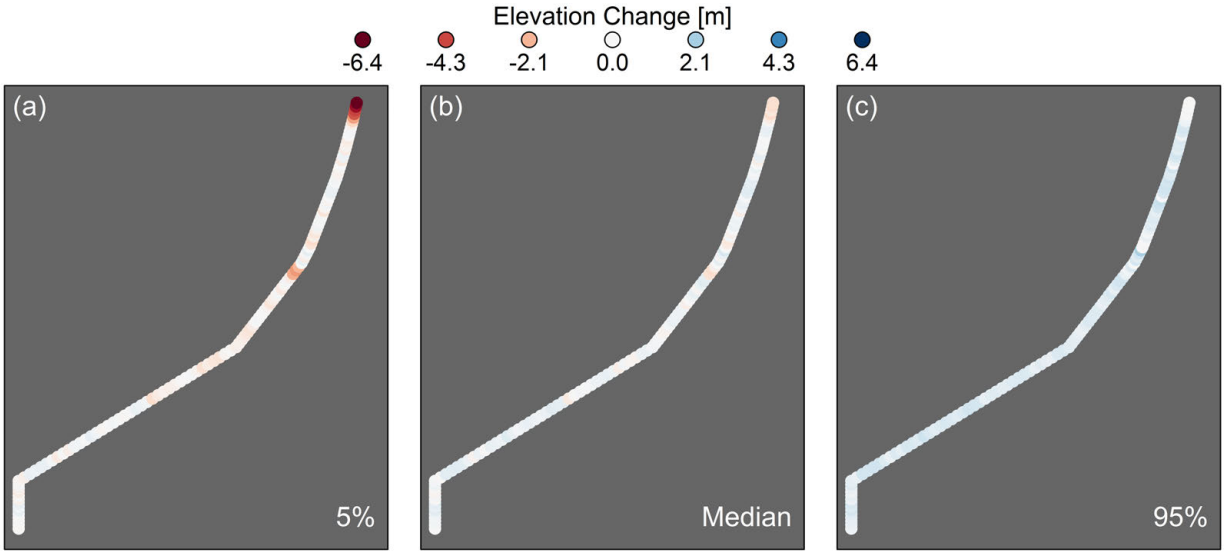

Figure C.4: Changes in bed elevation throughout the Big Dry Creek drainage basin, including the median results and 5^{th} and 95^{th} percentiles. Model runs with $Q_s = 0.5$ transport capacity.

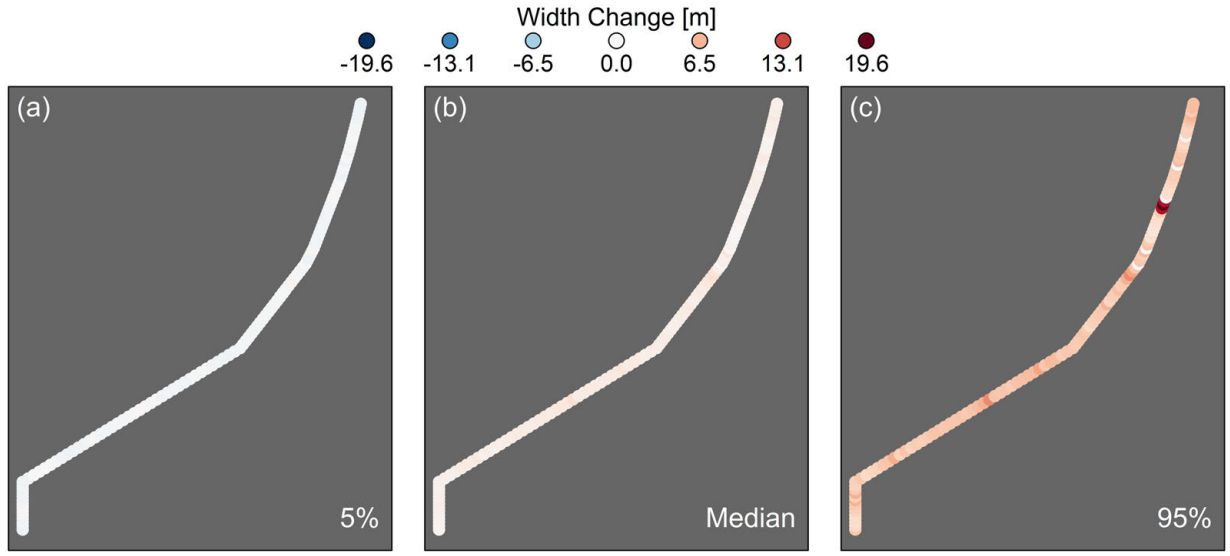

Figure C.5: Changes in channel width throughout the Big Dry Creek drainage basin, including the median results and 5^{th} and 95^{th} percentiles. Model runs with $Q_s = 0.5$ transport capacity.

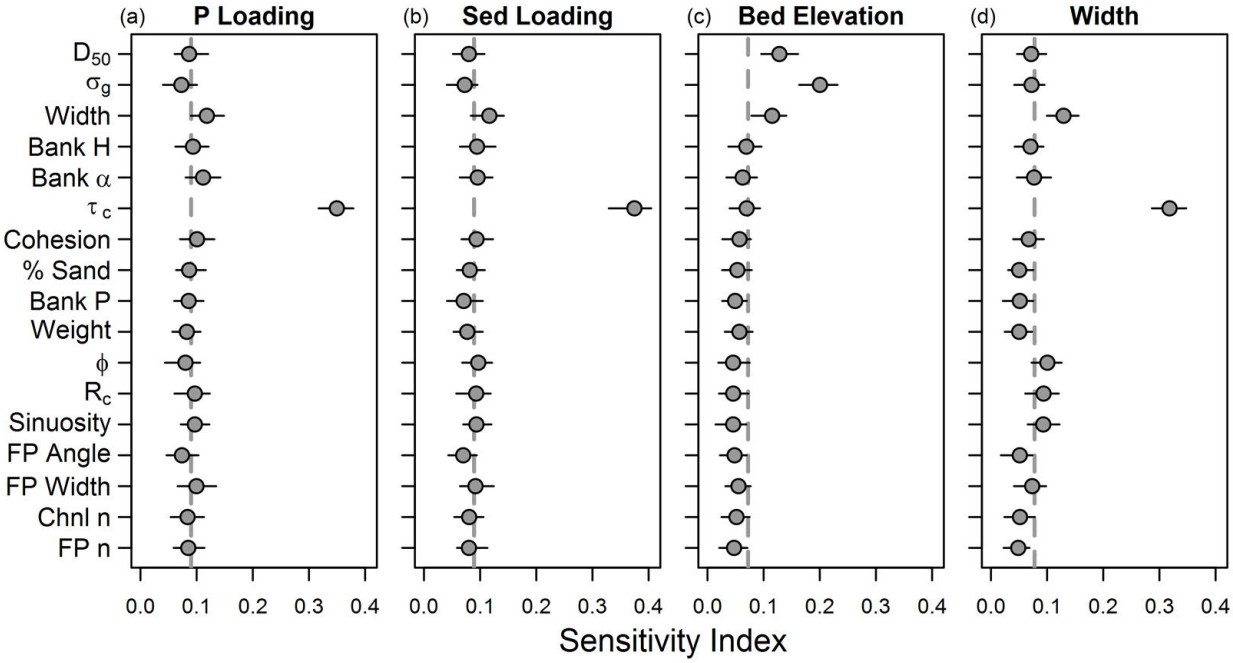

Figure C.6: Big Dry Creek sensitivity analysis results for four different model outputs: phosphorus loading (a), sediment loading (b), bed elevation (c), and channel width (d). Points show bias-corrected sensitivity indices with ranges of estimates from bootstrapping. Points below the vertical dashed line had no influence on model output. Results from model runs with $Q_s = 0.5$ transport capacity.

C.3.2 Big Dry Creek, $Q_s = 1.0$

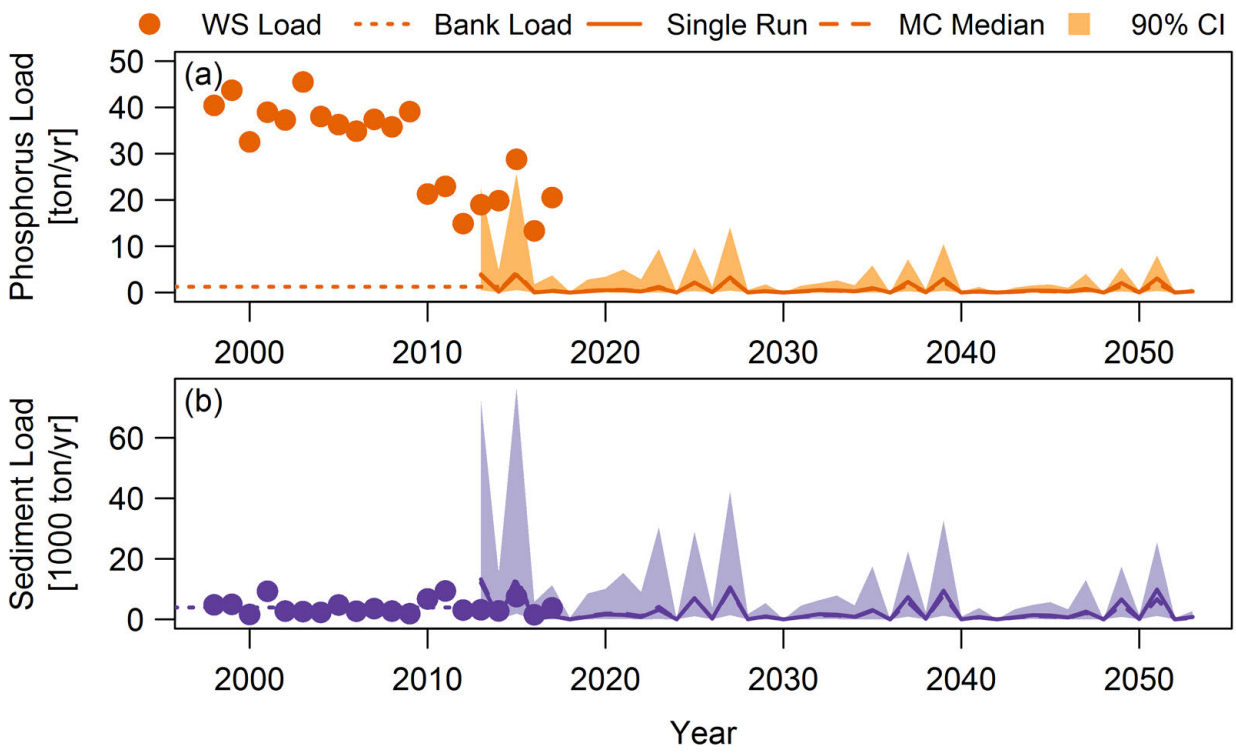

Figure C.7: Observed and modeled average annual loads of phosphorus (a) and sediment (b) in Big Dry Creek. Measured watershed loads are shown as points, bank loading estimates from the aerial photo analysis are shown as a horizontal dotted line, and model results for the single model run (solid line), median of the Monte Carlo simulations (dashed line), and 90% CI are projected through 2053. Model results are from simulations with $Q_s = 1.0$ transport capacity.

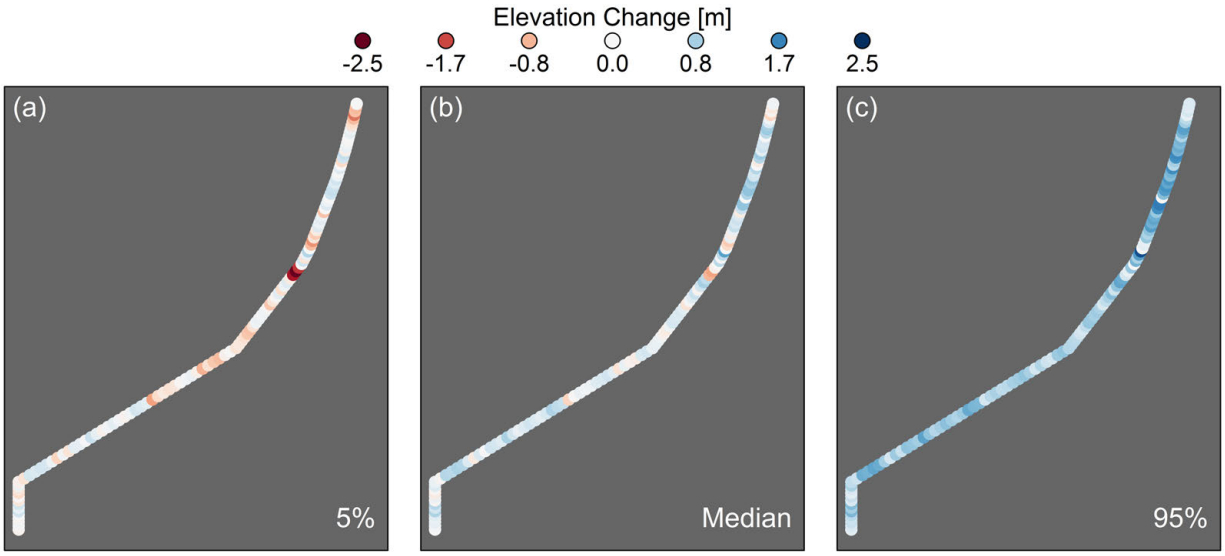

Figure C.8: Changes in bed elevation throughout the Big Dry Creek drainage basin, including the median results and 5^{th} and 95^{th} percentiles. Model runs with $Q_s = 1.0$ transport capacity.

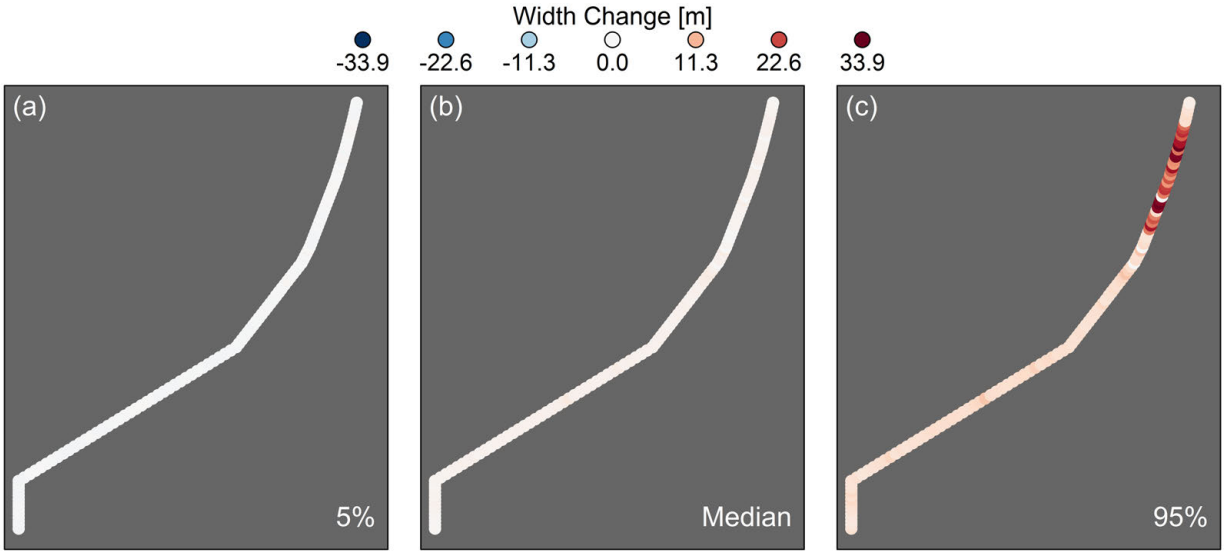

Figure C.9: Changes in channel width throughout the Big Dry Creek drainage basin, including the median results and 5^{th} and 95^{th} percentiles. Model runs with $Q_s = 1.0$ transport capacity.

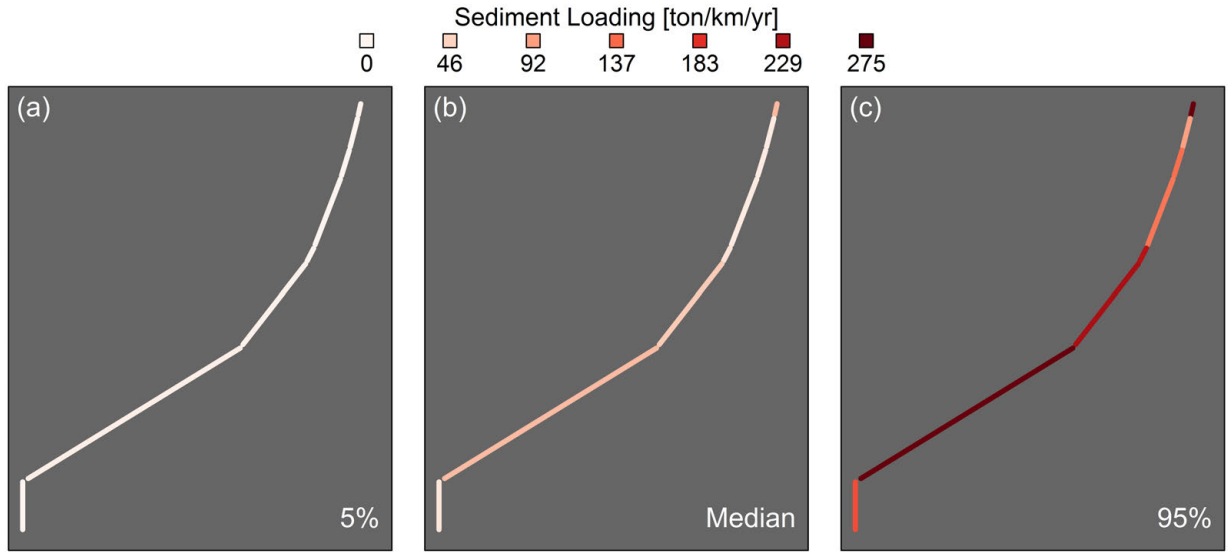

Figure C.10: Network schematic of Big Dry Creek showing annual sediment loading rates by modeled reach, normalized by reach length, including the uncertainty range (a and c) and the median of the Monte Carlo results (b). Loading rates are larger than reported in Table 5.3 because these are cumulative loads over the simulation rather than median annual loads. Results from simulation with $Q_s = 1.0$ transport capacity.

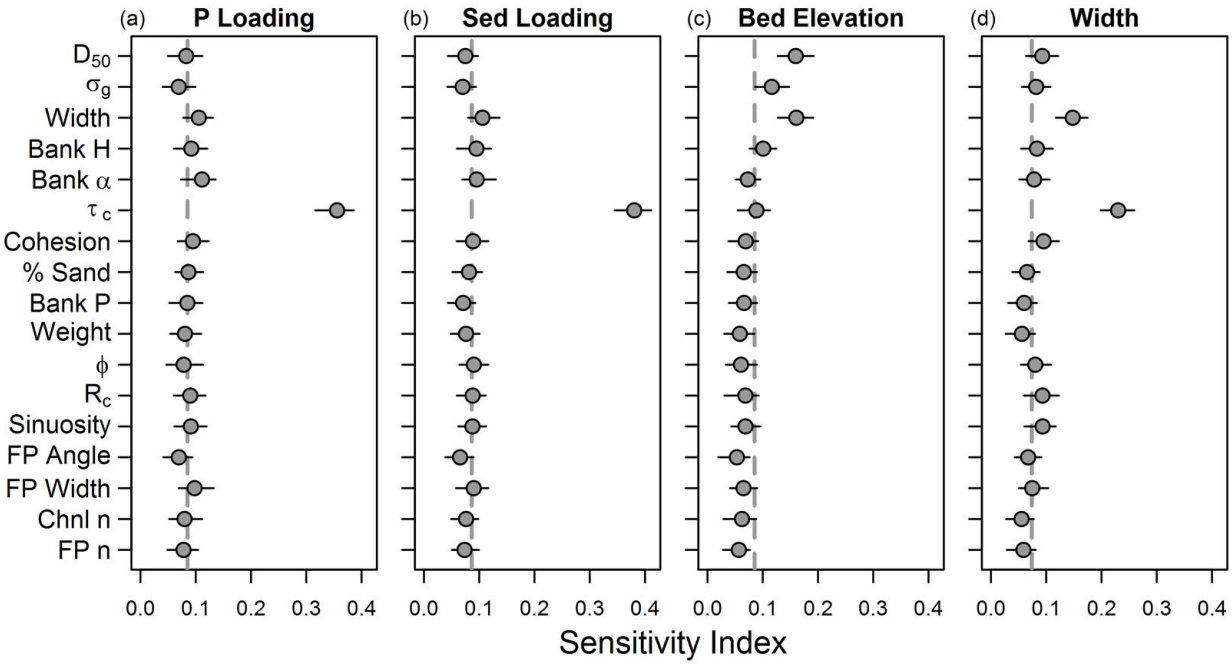

Figure C.11: Big Dry Creek sensitivity analysis results for four different model outputs: phosphorus loading (a), sediment loading (b), bed elevation (c), and channel width (d). Points show bias-corrected sensitivity indices with ranges of estimates from bootstrapping. Points below the vertical dashed line had no influence on model output. Results from model runs with $Q_s = 1.0$ transport capacity.

C.3.3 Lick Creek, Loading Results

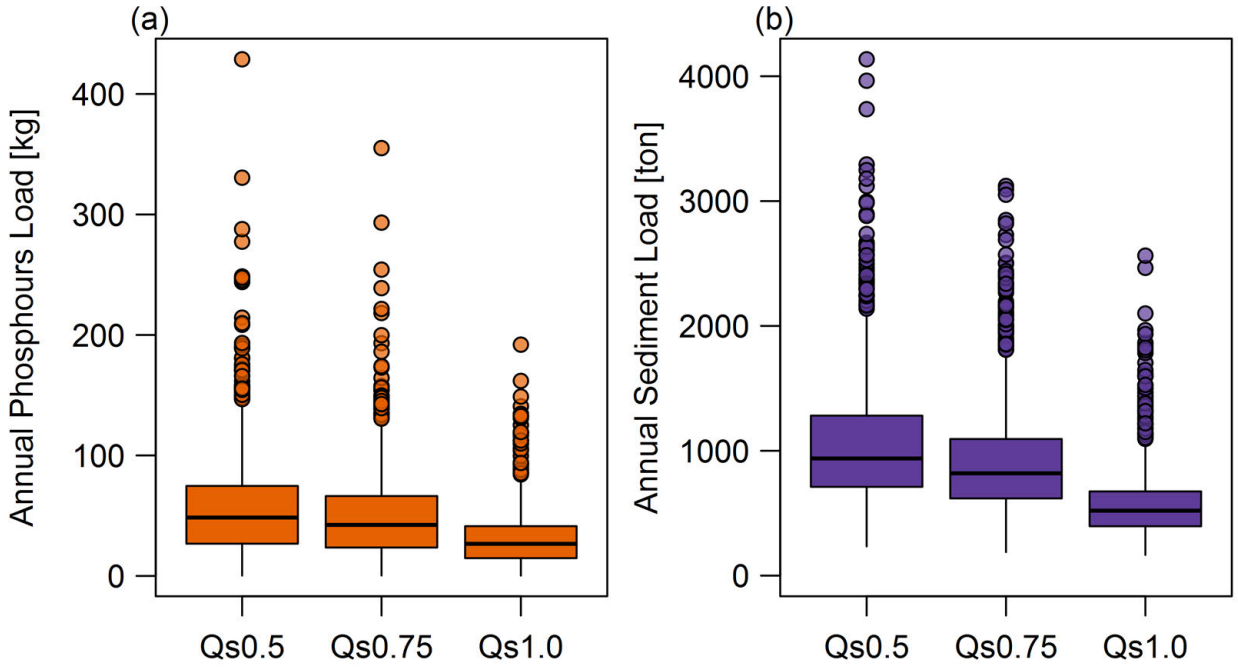

Figure C.12: Distributions of median annual phosphorus (a) and sediment (b) loads in Lick Creek across the years of the simulation, for the three different modeled scenarios: $Q_s = 0.5$, $Q_s = 0.75$, and $Q_s = 1.0$ of transport capacity.

C.3.4 Lick Creek, $Q_s = 0.5$

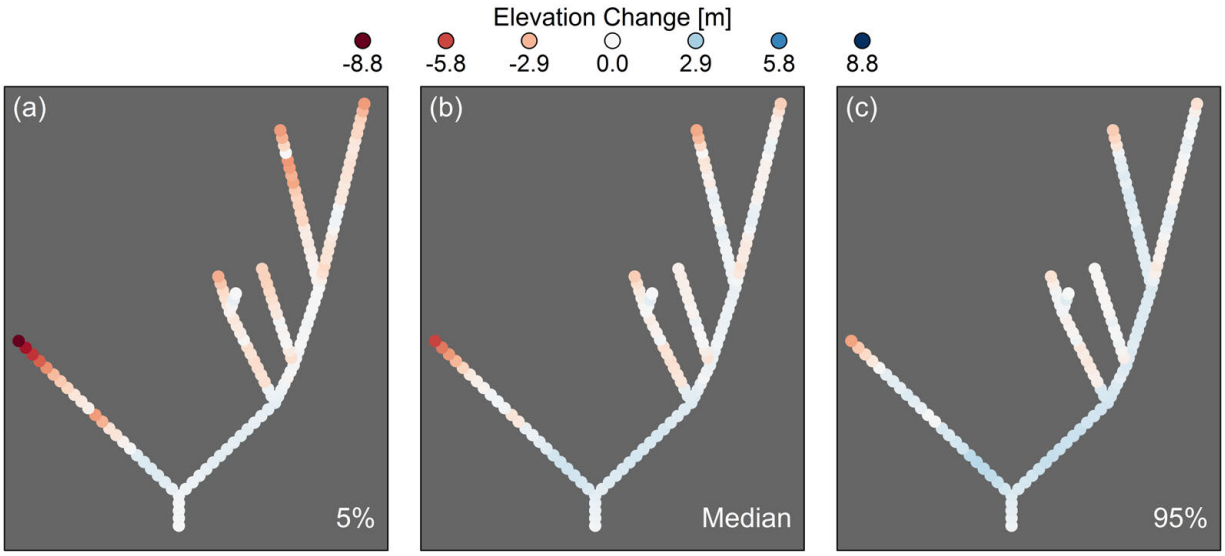

Figure C.13: Changes in bed elevation throughout the Lick Creek watershed, including the median results and 5^{th} and 95^{th} percentiles. Model runs from $Q_s = 0.5$ transport capacity.

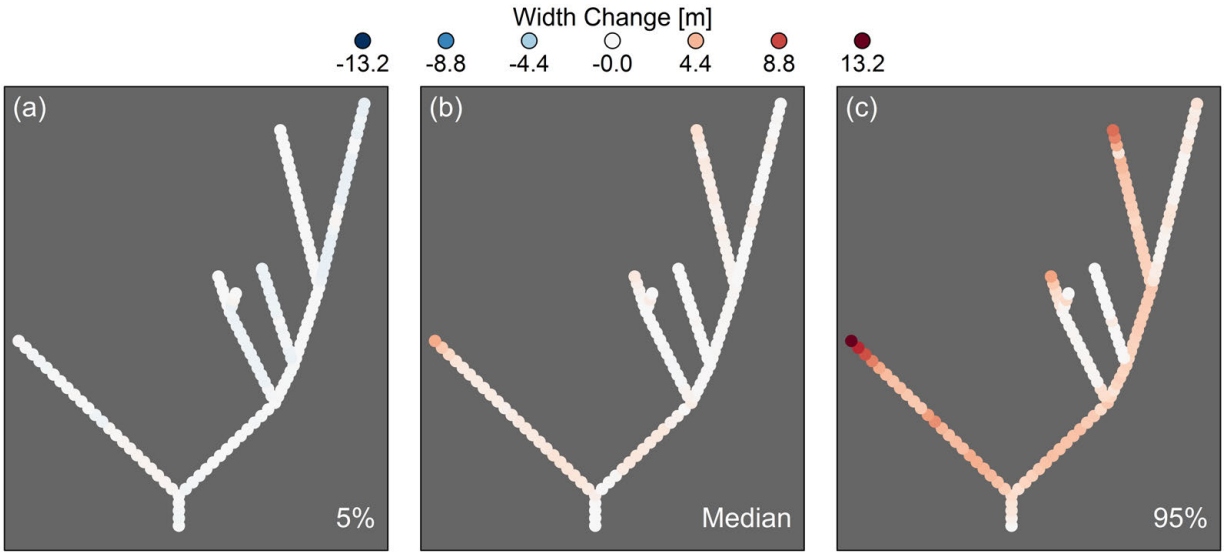

Figure C.14: Changes in channel width throughout the Lick Creek watershed, including the median results and 5^{th} and 95^{th} percentiles. Model runs from $Q_s = 0.5$ transport capacity.

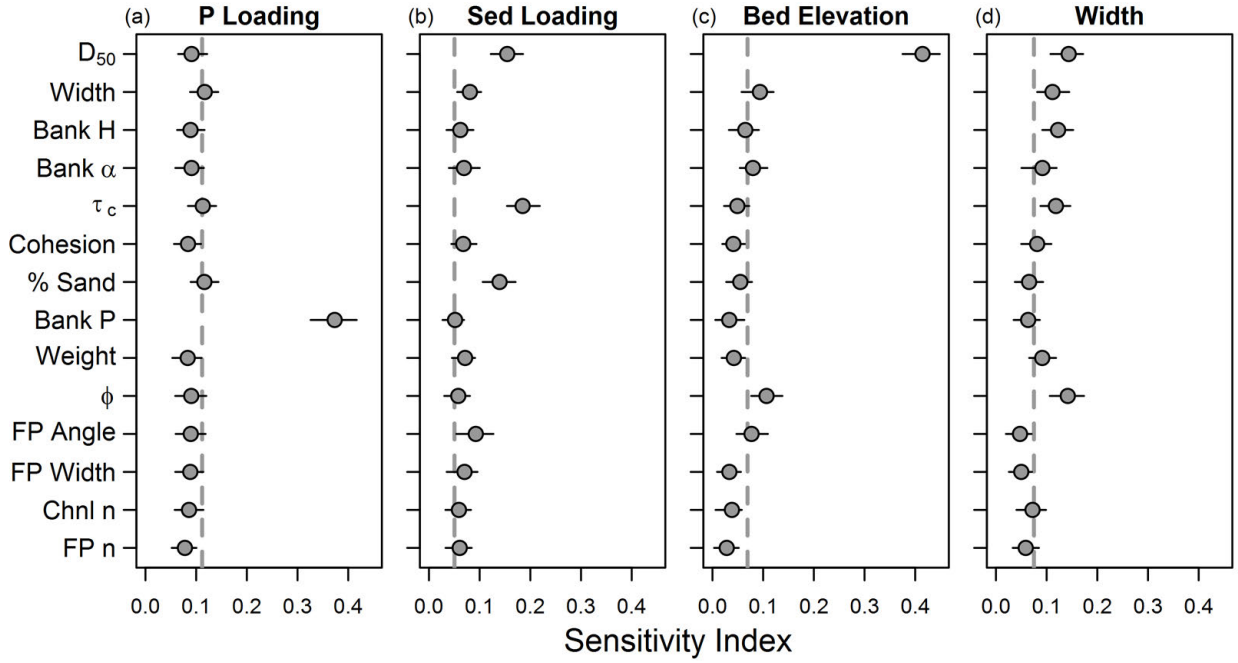

Figure C.15: Lick Creek sensitivity analysis results for four different model outputs: phosphorus loading, sediment loading, bed elevation, and channel width. Points show bias-corrected sensitivity indices with ranges of estimates from bootstrapping. Points below the vertical dashed line had no influence on model output. Results from model runs where $Q_s = 0.5$ transport capacity.

C.3.5 Lick Creek, $Q_s = 0.75$

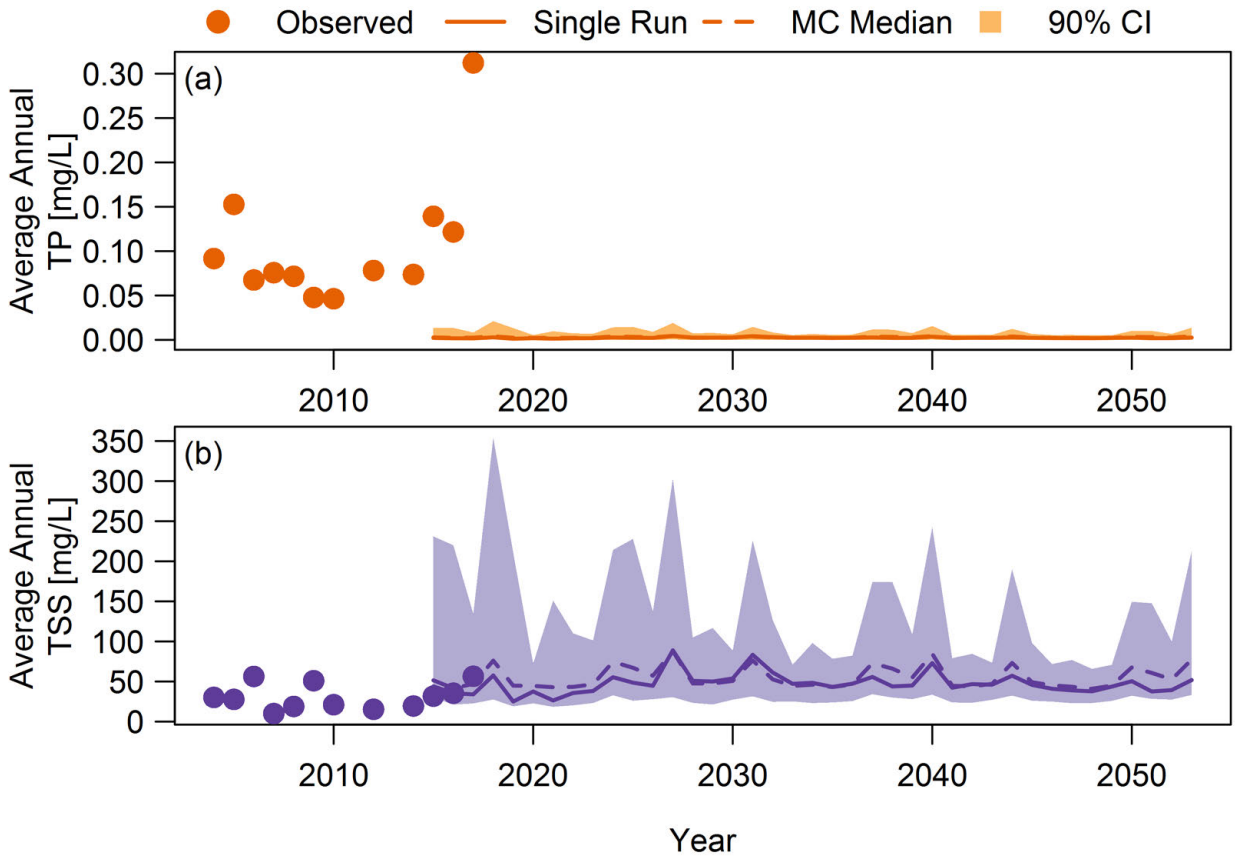

Figure C.16: Measured TP and TSS concentrations in Lick Creek at the watershed outlet, along with modeled projections for the single run and median and 90% CI for the Monte Carlo simulations. Model runs from $Q_s = 0.75$ transport capacity.

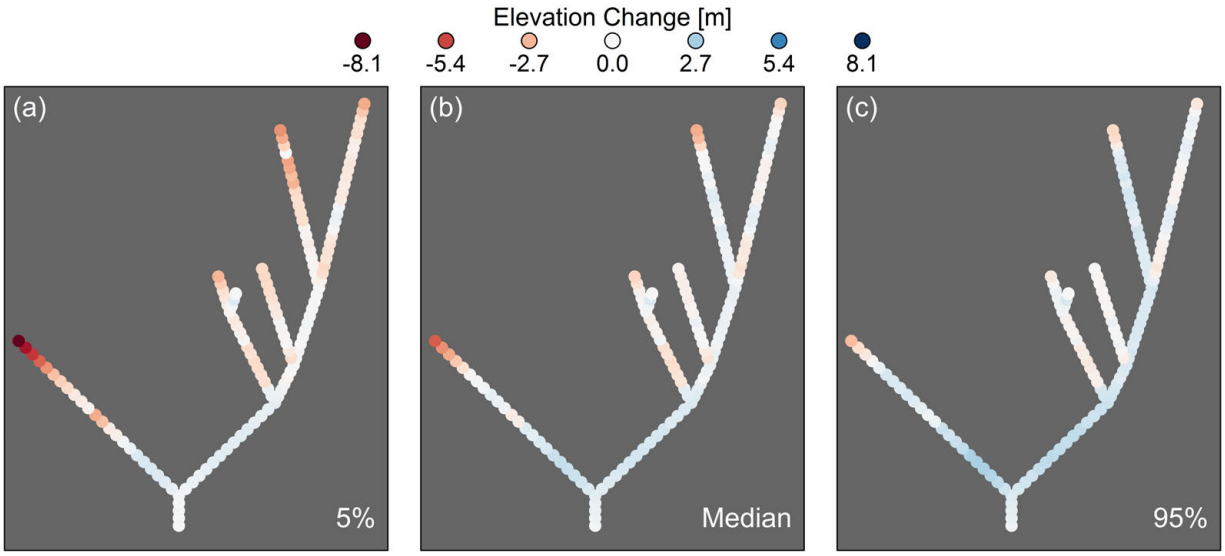

Figure C.17: Changes in bed elevation throughout the Lick Creek watershed, including the median results and 5^{th} and 95^{th} percentiles. Model runs from $Q_s = 0.75$ transport capacity.

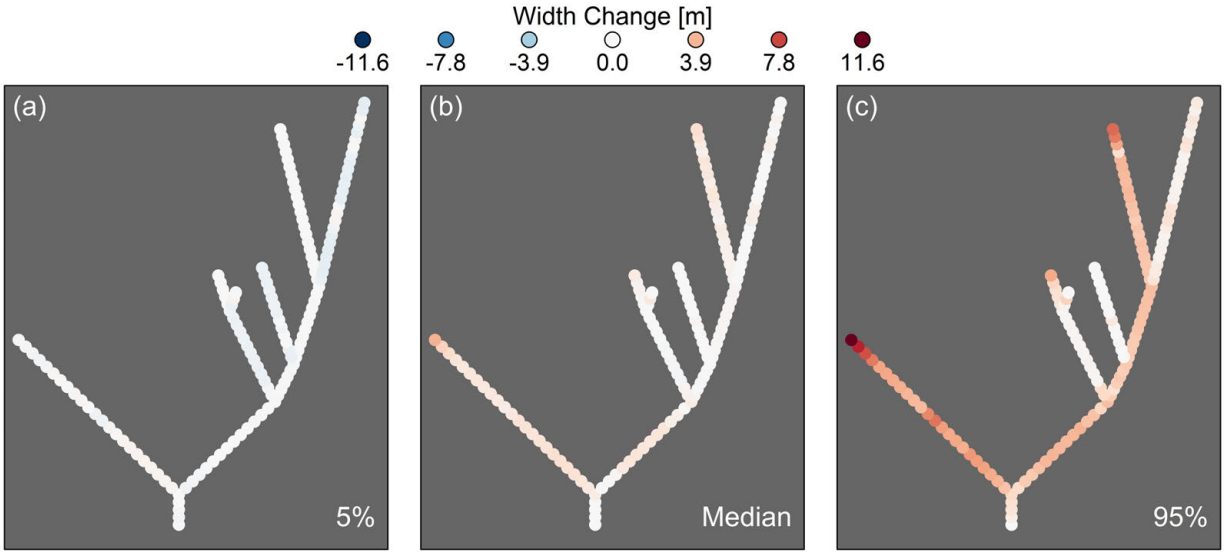

Figure C.18: Changes in channel width throughout the Lick Creek watershed, including the median results and 5^{th} and 95^{th} percentiles. Model runs from $Q_s = 0.75$ transport capacity.

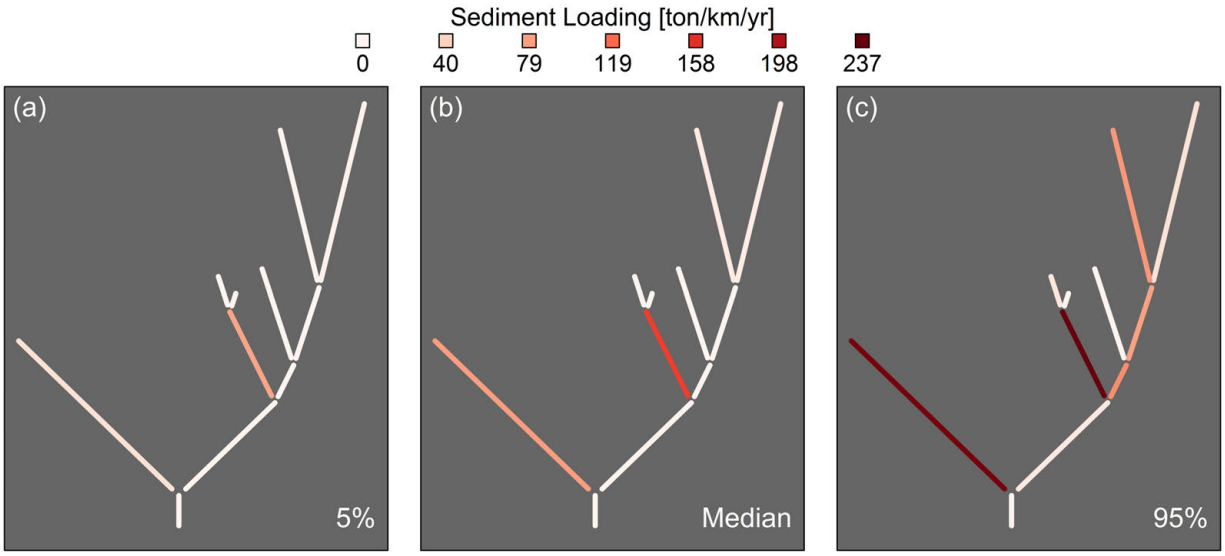

Figure C.19: Network schematic of Lick Creek showing annual sediment loading rates by modeled reach, normalized by reach length including the uncertainty range (a and c) and the median of the Monte Carlo results (b). The two reaches with highest loading rates both had actively migrating knickpoints. Loading rates are larger than reported in Table 5.3 because these are cumulative loads over the simulation rather than median annual loads. Results from simulation with Q_s = 0.75 transport capacity.

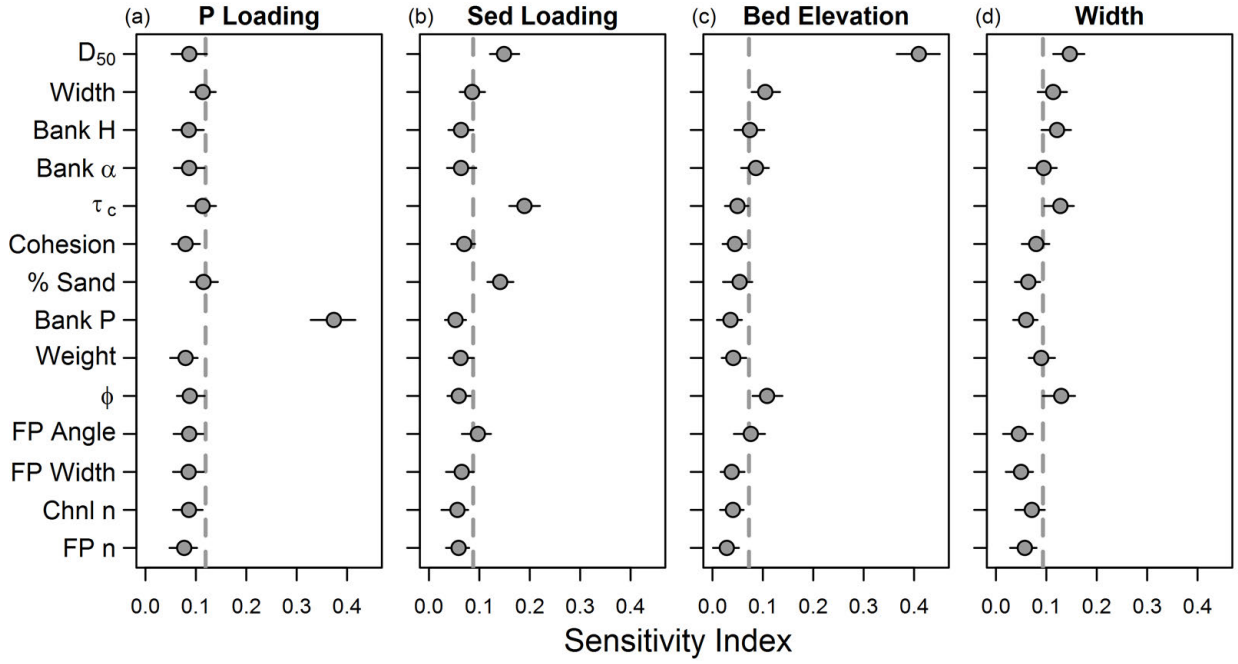

Figure C.20: Lick Creek sensitivity analysis results for four different model outputs: phosphorus loading, sediment loading, bed elevation, and channel width. Points show bias-corrected sensitivity indices with ranges of estimates from bootstrapping. Points below the vertical dashed line had no influence on model output. Results from model runs where $Q_s = 0.75$ transport capacity.

C.3.6 Lick Creek, $Q_s = 1.0$

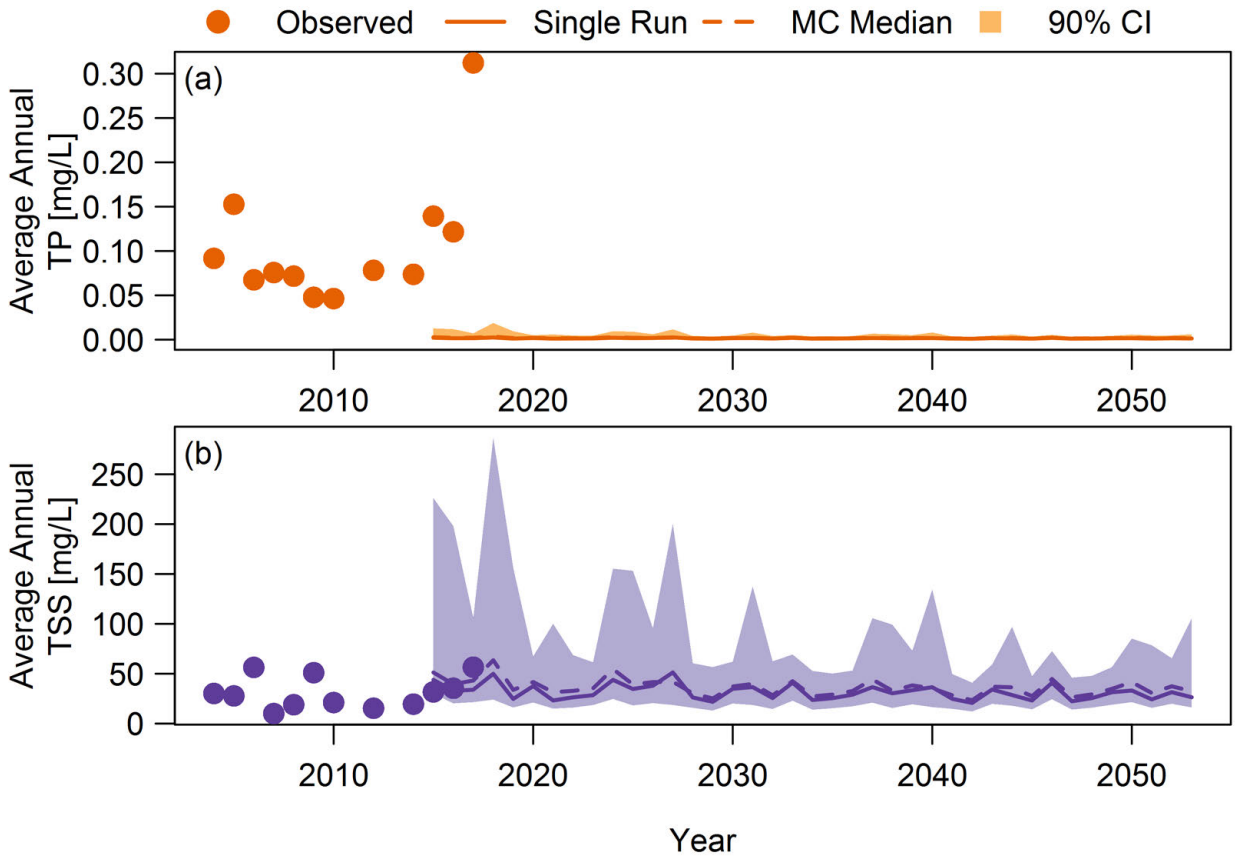

Figure C.21: Measured TP and TSS concentrations in Lick Creek at the watershed outlet, along with modeled projections for the single run and median and 90% CI for the Monte Carlo simulations. Model runs from $Q_s = 1.0$ transport capacity.

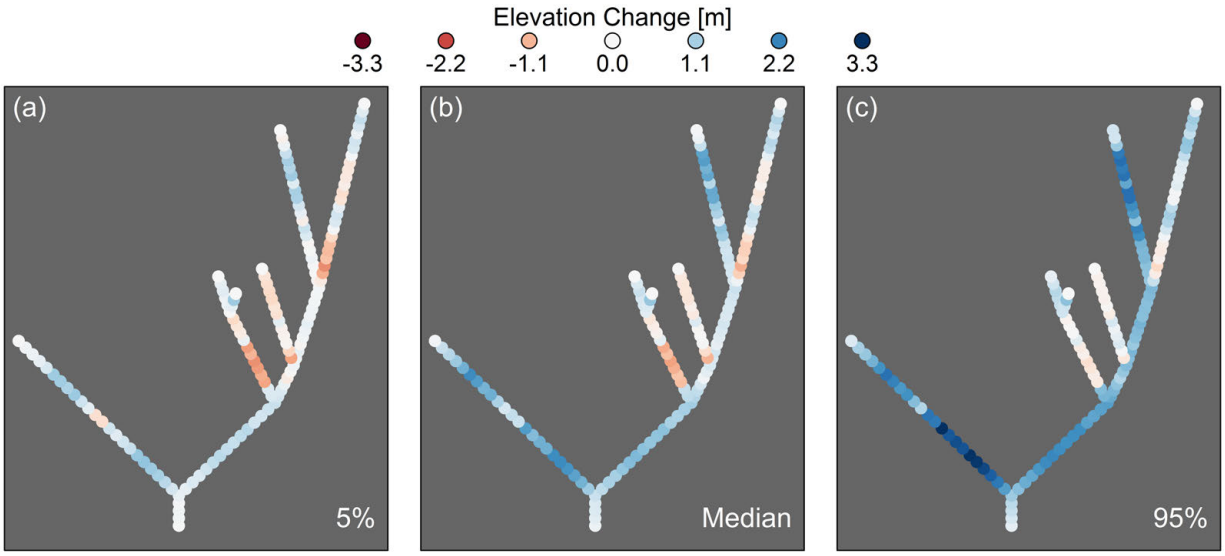

Figure C.22: Changes in bed elevation throughout the Lick Creek watershed, including the median results and 5^{th} and 95^{th} percentiles. Model runs from $Q_s = 1.0$ transport capacity.

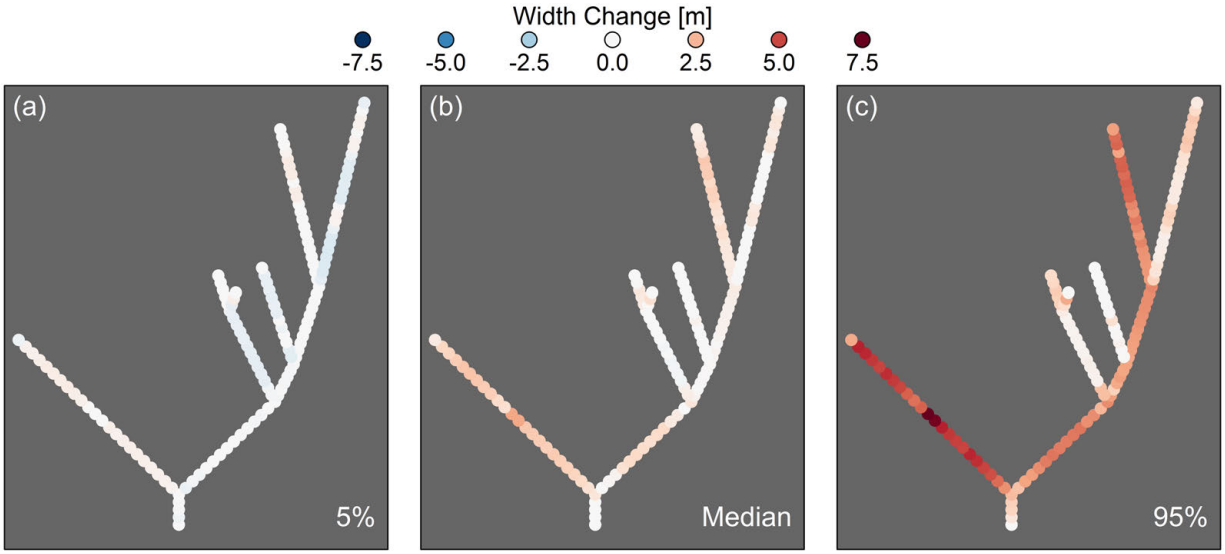

Figure C.23: Changes in channel width throughout the Lick Creek watershed, including the median results and 5^{th} and 95^{th} percentiles. Model runs from $Q_s = 1.0$ transport capacity.

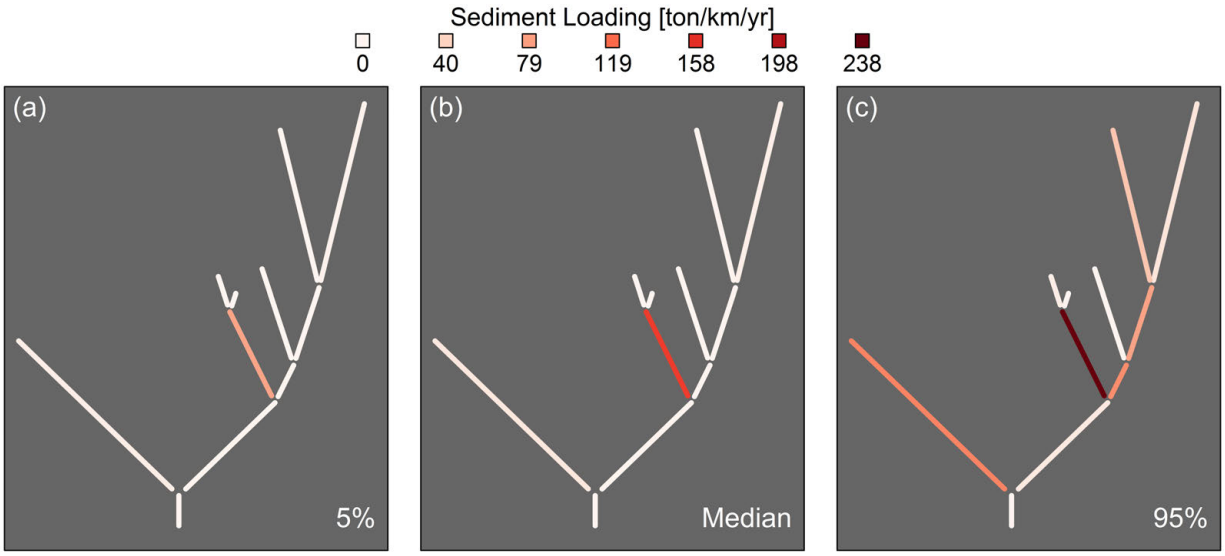

Figure C.24: Network schematic of Lick Creek showing annual sediment loading rates by modeled reach, normalized by reach length including the uncertainty range (a and c) and the median of the Monte Carlo results (b). The two reaches with highest loading rates both had actively migrating knickpoints. Loading rates are larger than reported in Table 5.3 because these are cumulative loads over the simulation rather than median annual loads. Results from simulation with $Q_s = 1.0$ transport capacity.

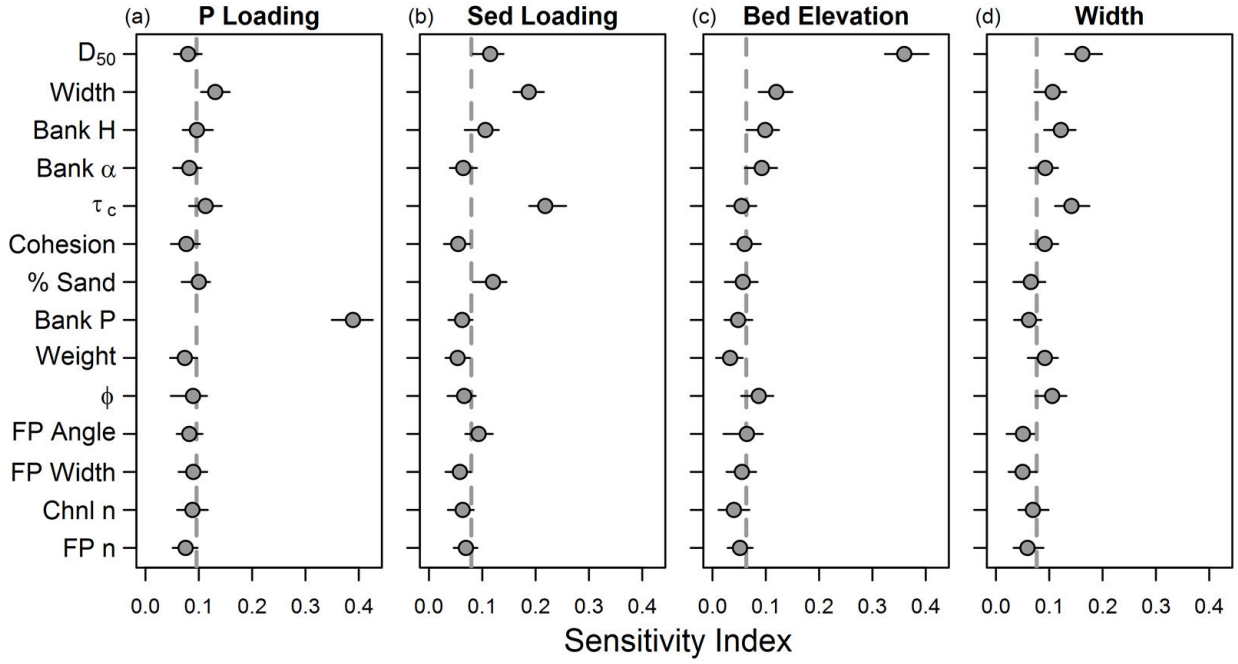

Figure C.25: Lick Creek sensitivity analysis results for four different model outputs: phosphorus loading, sediment loading, bed elevation, and channel width. Points show bias-corrected sensitivity indices with ranges of estimates from bootstrapping. Points below the vertical dashed line had no influence on model output. Results from model runs where $Q_s = 1.0$ transport capacity.